Trayana Stoykova Tankova

STABILITY DESIGN OF STEEL COLUMNS, BEAMS AND BEAM-COLUMNS: BEHAVIOUR, GENERAL FORMULATION AND RELIABILITY

Abril, 2018

· U C ·

UNIVERSIDADE DE COIMBRA

STABILITY DESIGN OF STEEL COLUMNS, BEAMS AND BEAM-COLUMNS: BEHAVIOUR, GENERAL FORMULATION AND RELIABILITY

DIMENSIONAMENTO À ENCURVADURA DE COLUNAS, VIGAS E VIGAS-COLUNA: COMPORTAMENTO, FORMULAÇÃO GERAL E FIABILIDADE

Dissertação científica na especialidade de Construção Metálica e Mista

Autor

Trayana Stoykova Tankova

Orientador

Prof. Luís Alberto Proença Simões da Silva

Coorientadora

Dr. Liliana Raquel Simões Marques

ABSTRACT

The European stability design rules for prismatic steel columns and beams are classically based on the buckling curve approach, whereas the verification of beam-columns combines the resistances of a column and a beam through interaction factors. For generic single members, built-up or not, uniform or not, with complex support conditions or not, the available possibilities for such cases are the General Method given in clause 6.3.4 of Eurocode 3 (2005) or advanced numerical simulations. The applicability of the General Method, however, is limited and in some aspects inconsistent *Simões da Silva et al.* (2010). For instance, when applied to non-uniform members, the choice of the imperfection factors is not straight-forward and their definition may lead to either unsafe or over conservative solutions. As an alternative to the General Method, the stability of non-uniform members can be analysed using numerical GMNIA which, again, requires the definition of the correct imperfection shape and magnitude, but it is also a time-consuming procedure; and the output and its reliability are highly dependent on the experience of the user.

On the other hand, the safety of design rules in the Eurocodes is based on the limit state design, where relevant design situations are distinguished by the use of partial factors accounting for the uncertainties related to loading and resistance. Hence, the design rules and their accuracy depend on the scatter of the basic variables such as material properties, geometric properties and imperfections. It is therefore required to appropriately characterize the statistical distributions of these basic variables in order to comply with the (semi-) probabilistic safety level assessment of design rules. The buckling curves rely on the calibration of imperfection factors in order to estimate the maximum resistance which gives the flexibility of adjusting imperfection factors according to the cross-section shape, steel grade and other relevant

parameters. This feature allows the adoption of the Ayrton-Perry design philosophy for more general applications.

In this thesis, a novel general formulation for stability design of steel columns, beams and beam-columns with variable geometry, loads and supports covering any buckling mode is proposed. The verification is based on the buckling mode as shape of the initial imperfection with an amplitude previously calibrated for the standard prismatic simply-supported columns and beams in Eurocode 3. In order to ensure its reliability, safety assessment of the Eurocode 3-1-1 stability design rules for prismatic columns, beams and beam-columns are assessed using statistical data which reflects the steel production nowadays.

This general formulation is transparent and consistent with the Eurocode 3-1-1 design rules. It avoids the calibration of additional factors because it is applied as an interaction equation and the first and second order contributions to the longitudinal stress utilization are added for each cross-section along the member length. To promote its ease of use, several aspects regarding the member behaviour in the context of a specific buckling mode are discussed. Finally, validation of the approach is carried out based on large number of numerical simulations calibrated to experimental tests. The results confirm its consistency and accuracy.

ii |

RESUMO

As regras Europeias de dimensionamento de estabilidade para colunas e vigas de aço prismáticos são classicamente baseadas na abordagem da curva de encurvadura, enquanto a verificação de vigas-coluna combina as resistências de uma coluna e uma viga através de fatores de interação. Para elementos separados e genéricos, soldados ou não, uniformes ou não, com condições de suporte complexas ou não, as opções disponíveis para tais casos são o Método Geral dado na cláusula 6.3.4 do Eurocódigo 3 (2005) ou o recurso a métodos computacionais avançados (FEM). A aplicabilidade do Método Geral, entretanto, é limitada e, em alguns aspetos, inconsistente *Simões da Silva et al.* (2010). Por exemplo, quando aplicada a elementos não uniformes, a escolha dos fatores de imperfeição não é direta e sua definição pode levar a soluções inseguras ou conservadoras. Como uma alternativa ao Método Geral, a estabilidade de membros não uniformes pode ser analisada usando analise numérica avançada que, por sua vez, requer a definição da forma e magnitude correta da imperfeição inicial, que é um procedimento computacionalmente exigente sendo o resultado altamente dependente da experiência do utilizador.

Por outro lado, a segurança das regras de dimensionamento nos Eurocódigos baseia-se na verificação de estado limite, em que as situações de dimensionamento relevantes são distinguidas pela utilização de fatores parciais responsáveis pelas incertezas relacionadas com o carregamento e a resistência. Assim, as regras de dimensionamento e sua precisão dependem da dispersão das variáveis básicas, como propriedades do material, propriedades geométricas e imperfeições. Portanto, é necessário caracterizar apropriadamente as distribuições estatísticas dessas variáveis básicas, a fim de cumprir a avaliação (semi-) probabilística do nível de segurança das regras de dimensionamento. As curvas de encurvadura baseiam-se na calibração

dos fatores de imperfeição para estimar a resistência máxima, o que dá a flexibilidade de ajustar os fatores de imperfeição de acordo com a forma da seção transversal, grau de aço e outros parâmetros relevantes. Esse recurso permite a adoção da filosofia de dimensionamento Ayrton-Perry para aplicações mais gerais.

Nesta tese, uma nova formulação geral para análise de estabilidade de colunas, vigas e vigas-colunas de aço com geometria variável, cargas e condições de fronteira para qualquer modo de encurvadura é proposta. A verificação é baseada no modo de encurvadura como forma da imperfeição inicial com uma amplitude previamente calibrada para as colunas e vigas simples prismáticas padrão no Eurocódigo 3. Para garantir sua fiabilidade, a avaliação de segurança do Eurocode 3-1-1, as regras de dimensionamento de estabilidade para colunas, vigas e vigas-coluna prismáticas são avaliadas usando dados estatísticos que refletem a produção de aço atualmente.

Esta formulação geral é transparente e consistente com as regras de dimensionamento no Eurocódigo 3-1-1. Evita a calibração de fatores adicionais porque é aplicada como uma equação de interação e as contribuições de primeira e segunda ordem para a utilização de tensão longitudinal são adicionadas para cada seção transversal ao longo do comprimento do elemento. Para promover a sua facilidade de uso, vários aspetos relacionados como comportamento do elemento no contexto de um modo específico de encurvadura são discutidos. Finalmente, a validação desta abordagem inovadora foi realizada através de um extenso estudo numérico paramétrico, baseado em modelos previamente calibrados por ensaios experimentais. Os resultados confirmam sua consistência e precisão.

Palavras-chave: estabilidade, aço, formulação geral, fiabilidade

ACKNOWLEDGEMENTS

This has been an interesting journey and many people contributed to its successful end. In the following lines I would like to express my gratitude to those who took part of it.

First and most, I would like express my deepest gratitude to my supervisor, Professor Luís Simões da Silva, for his guidance, encouragement and thrust. He provided me with excellent working conditions; always made sure that I was following the right direction and offered me a broader vision of the world. He gave me the opportunity to participate in the European project SAFEBRICTILE, several ECCS TC8 meetings and numerous international conferences, where I could see the value of my work.

Big thanks are also due to my co-supervisor, Dr. Liliana Marques. She has always been supportive, even when away, with a pinch of humour and sarcasm. I am very glad we had the opportunity to work together, but even more that I found a great friend.

Special thanks to the SAFEBRICTILE project partners for the interesting discussions and suggestions for improving my work during the project meetings; and also for their patience when I was making my first steps as part of an European project.

I am very grateful to the colleagues and friends from ISISE, for making the daily life easier, funnier and many times putting a smile on my face; for all discussions we had that improved my work; and for helping me in difficult moments (especially Manuela and Rui).

I would also like to thank to all of my friends from *Coimbra Toastmasters Club*, for helping me to become a better speaker (especially in Portuguese) and for encouraging me to never stop improving myself in whatever I do.

Heartfelt thanks to my friends, for being able to distract me and show me that there are more things in life besides work; for maintaining our friendship even though we do not spend as much time nowadays.

Nothing of this would have been possible without the unconditional support of my family. They were always present to cheer me up when I was feeling down and to share my happiness even when I was away from home for a long time. Благодаря ви.

Finally, big thanks to my very special person, for all the passion and affection that he brought into my life; for encouraging me and making me believe in myself; for showing me how to embrace life as he does every day. It is to him that I dedicate this thesis.

Contents

1 INTRODUCTION

1.1 Motivation and objectives

The development of structural design codes is guided by the need to provide practical design rules that cover recurring design situations with an appropriate level of safety and ease of use. These are also the aims of the Structural Eurocodes between the member states in the EU, i.e. reduction of the National Determined Parameters (*Kuhlmann & Rasche*, 2017).

Since the release of part 1-1 of Eurocode 3 (CEN, 2005) a lot of research work has been done at the European and global levels, aiming at the improvement of the design rules. Within the ongoing revision of the Structural Eurocodes, these efforts led to the final draft of prEN 1993-1-1 (CEN/TC250, 2017) that includes many of the modifications and extensions proposed over the last years.

The Eurocode 3 procedures, existing and new proposals, have been calibrated to safety levels which are not necessarily uniform: within the design rule and/or in comparison with other design rules. This results in lack of consistency and different safety levels which can compromise the design. In the past, several reliability assessments were carried out, e.g. in the research projects *Partial safety factors for resistance of steel elements to EC3 and EC4 - Calibration for various steels products and failure criteria* (*Chabrolin et al.*, 2002) and *PROQUA – Probabilistic quantification of safety of a steel structure highlighting the potential of steel versus other materials (Cajot et al., 2005)*, which aimed at the justification of the partial factors used in Eurocode 3. Generally, there is a broad agreement on the partial factor γ_{M0}, which is not the case regarding the stability design rules and γ_{M1}. This partial factor deviates from the recommended value in several member states (Germany, Austria, Denmark) while

some authors claim that it is different for the different stability phenomena, i.e. for the interaction between bending and axial force (*Chabrolin et al.*, 2002) and it could also be non-uniform within the same rule *Taras* (2010).

Nevertheless, even though the stability design of members is a classical topic, the extensions, corrections and improvements that evolved over time since the beginning of the development of the column buckling curves in the 1960's and 70's were not very often assessed under the same assumptions, resulting in scatter of the safety level across the range of cases covered by the design formulas.

In addition, there is a continuous development of new structural steels with largely improved mechanical properties that, combined with the stricter quality control procedures for the geometrical dimensions of steelwork, also contribute to the need for reassessment of the safety levels in order to keep the competitiveness of the steel construction.

Regarding the basic variables that are required in a reliability assessment, a considerable advantage for the standardization, application and economy of design rules can be achieved by maintaining a database of statistical variation of all relevant basic input parameters (*Simões da Silva et al.,* 2009), (*Rebelo et al.,* 2009). Such collection can serve for the critical assessment and comparison in future versions of Eurocode 3, but also for the evaluation of new design rules on the same basis as the calibration of the existing ones.

From a methodological point of view, the verification of columns, beams and beam-columns based on the generalized imperfection approach leads to good agreement with experimental results, with a good balance between accuracy and economy. However, their scope is still limited to uniform members effectively braced at the ends only. The more general case of single members, built-up or not, uniform or not, with complex support conditions or not, is not directly covered by the generalized imperfection approach. Hence, Eurocode 3-1-1 proposes an alternative method, denoted general method to address such cases. However, recent research work shows the wide scatter of the method varying from -50% (unsafe) up to 70% (safe), when applied to frames (*Naumes*, 2009). Additionally, in *Simões da Silva et al.* (2010) and *Marques* (2012) this was also confirmed, probably because of the lack of mechanical background. In *Marques* (2012), the (analytically backed) account for a design location was provided for flexural and lateral-torsional buckling or web-tapered columns and beams respectively and applied to beam-columns based on interaction formulae approach. However, a general solution is still missing.

Finally, nowadays the available computational resources together with programming techniques and symbolic mathematical manipulation permit a higher level of accuracy in the prediction of the stability behaviour, thus allowing for a new generation of design codes based on numerical analyses using FEM (finite element method). All these improvements are the tools to be used in the future structural design where the classical analysis and design of individual members (extracted from the real structure) will be replaced by the analysis and design of sub-structures and/or entire structures.

All these points yielded as a motivation for this research with the main focus of the dissertation on the stability design of steel members, keeping a strong relation to their respective safety levels.

Therefore, the goal of this work is to contribute towards safer yet economic stability design rules, which are general, but mechanically consistent.

The goal was achieved through the completion of the following objectives:

- **Data collection for basic variables**: these were essential for the outcome of the safety assessment since the statistical analysis is always performed in the basis of assumed distributions. It was aimed to collect data and to understand the distributions which reflect the steel production nowadays.

- **Safety assessment of design rules**: it was necessary to assess to what extent the existing rules comply with the target reliability in the Eurocode 3. It was also useful in order to understand the background of these rules.

- **General stability design methodology**: The third objective was the development of a methodology which is capable of dealing with various aspects regarding the stability design of members. Since the use of computer calculations has become the standard practice, it was aimed to incorporate it to some extent in the design process, yet keeping simplicity and mechanical consistency. For the complete validation of this approach, experiments on web-tapered members were carried out; the test results helped to confirm and validate the numerical model usually adopted for the validation of stability design rules. The experimental programme also contributed towards additional knowledge for the member imperfections, namely the residual stresses and initial out-of-straightness.

A part of this research was performed in line with the European RFCS project RFSR-CT-2013-00023 SAFEBRICTILE. In the project the main objective was the harmonization of the reliability level of design rules for steel structures covering modes driven by ductility, stability and fracture. The project provided an objective safety assessment procedure which was applied to the studied failure modes using statistical data collected throughout the project reflecting the current steel market. Another part of the thesis was carried out in line with the objective of the nationally funded project TAPERSTEEL PTDC/ECM-EST/1970/2012. In TaperSteel, the main objective was to develop design rules for web tapered steel members. Hence, following the research goals this work comprises safety of the existing design rules and makes the necessary towards the development of consistent design rules for the design of non-uniform members.

1.2 Scope

The dissertation covers the stability design of steel members with a strong emphasis on the accuracy of the adopted design approaches. The steel members included by this work are uniform and non-uniform in geometry and/or loading and/or boundary conditions/restraints. Their assessment and proposed design approaches are based on analytical, experimental and numerical approaches.

From analytical point of view, it was aimed to keep consistency with the mechanical background of the studied phenomena as well as with the existing Eurocode 3 design rules. For that, it was necessary, firstly, to study the basic and uniform cases for the various buckling modes.

The experimental work carried out in the scope of the TAPERSTEEL project aimed to supply experimental evidence of the buckling behaviour of non-uniform members. It was used as a reference for validation of advanced numerical model.

The numerical approaches were employed for generation of large number of numerical "experiments" using the validated advanced numerical model. These results were used for the reliability assessment of the existing design rules and for the validation of the novel procedures.

A great attention was paid to the data collection. Data for the material and geometrical properties were collected in European database of steel properties from the partner institutions in the SAFEBRICTILE, from university laboratories, and literature. Data on the material and

geometrical imperfections was collected mainly from the literature since it is hardly accessible from the industry.

The studies covered in this thesis extend to steel grade S460. It is generally limited to the application of H and I sections fabricated by welding of hot-rolled plates or hot-rolled profiles.

1.3 Outline of the dissertation

The research objectives are described in the seven chapters of this dissertation. Following the general introduction in Chapter 1, Chapter 2 presents a general state-of-the-art for the stability and safety of steel members. It gives a brief overview of the existing stability design rules for uniform and non-uniform members. It focuses on their evolution and on the future trends for steel member design. Regarding the safety of these design rules, in Chapter 2, a summary of the basis of design according to the Eurocodes is also described.

In Chapter 3, the experimental programme carried out in the scope of the research project TAPERSTEEL is presented. Firstly, a review of previous experimental campaigns on non-uniform members, as well as available sources with measurements on residual stresses and geometrical imperfections is carried out. In a second step, the experimental layouts for the buckling tests and the supplementary tests (residual stress measurements, material characterization and geometrical imperfections) are described in detail. Finally, a summary of the test results is offered. These results were then used for validation of an advanced numerical model. The model and its validation are described in Chapter 4.

In Chapter 5, following the Eurocode objective of harmonization and to extend the stability design rules to non-uniform members, it was necessary to assess the reliability of the existing design rules. This task was carried out in the scope of the SAFEBRICTILE project. The assessment was performed on the basis of the safety assessment procedure developed within the project and using the statistical distributions of basic variables also recommended by the project. In this chapter, firstly, a brief overview of the underlying theoretical basis is given. Secondly, adopted methodologies and parametric studies for columns, beams and beam-columns are presented. Then, the results are presented and discussed and the necessary conclusions are highlighted.

The general formulation is presented in Chapter 6. It relies on an interaction equation of linear stress utilization that includes: (i) normal stresses due to applied forces; and (ii) normal stresses due to second order forces. The procedure is easily applicable to members with varying geometry, loading and support conditions. Firstly, the theoretical background of the new methodology is summarized, it is then followed by its validation for: i) flexural buckling of columns and beam-columns with non-uniform sections and/or non-uniform compression; ii) lateral-torsional buckling of beams and beam-columns with non-uniform sections and/or non-uniform loading;

Finally, in Chapter 7 the general conclusions of this work are summarized. It also gives recommendations for future developments.

2 STABILITY DESIGN: BACKGROUND AND EXISTING DESIGN RULES

2.1 Introduction

Owing to the high strength of the material, a common problem in the steel construction is its stability due to the high slenderness of the structural components. The design of steel structures requires the appropriate consideration of the various stability phenomena that may cause structural failure. The very beginning of the stability theory is the Euler's derivation of the elastic critical load of a pin-ended strut in 1744 (*Euler*, 1744). Since then, researchers pursue the quest for a thorough understanding of the buckling behaviour of steel members.

The first attempts for the consideration of the behaviour of columns in the inelastic range may be tracked to the *Considère-Engesser* theory (1889, 1895) who introduced the double modulus concept that was further developed by *von Karman* (1910). The milestone in the understanding of the post-buckling behaviour of inelastic columns was achieved by *Shanley* (1947) who explained the paradox between the tangent and the reduced modulus theories. At the same time, the behaviour of imperfect columns also attracted the attention of researchers. The classical work in this direction is the work by *Ayrton & Perry* (1886), whereby the resistance of the member is defined as the first yield of the most compressed fibre is reached, calculated using second order forces. The Ayrton-Perry model was validated experimentally by Robertson in 1925 (*Robertson,* 1925). This model is in the origin of the European buckling curves which were established in the 1970's, based on an extensive experimental programme carried out by the European Convention for Constructional Steelwork (ECCS) (*Sfintensco,* 1970), on theoretical developments by thorough analysis of the experimental programme (*Beer & Schulz,* 1970) and on reliability assessment by Monte Carlo simulations *Strating & Vos* (1973). In this

way, the column buckling curves account for the member geometry and its deviations, as well as different material properties and residual stresses. Similar approaches were adopted by design codes around the world, i.e. in the United States and Canada column buckling resistance is based on the SSRC curves. (*Ziemian*, 2010).

The elastic lateral-torsional buckling of beams was intensively studied since the middle of the twentieth century. However, the first important work is by *Saint-Venant* (1855) on uniform torsion, which set the beginning of a reliable description of the twisting behaviour of members in torsion. *Michell* (1899) and *Prandtl* (1899) explored flexural torsional buckling, precisely lateral buckling of a beam with narrow rectangular cross-section. Warping torsion was firstly considered by *Timoshenko* (1905). Further research by *Wagner* (1936) led to the development of a general theory for lateral-torsional buckling (*Timoshenko* 1953, *Vlasov,* 1961). Closed-form solutions for the elastic critical moment are available only for the simplest cases. The most trivial case is a prismatic beam with "fork" support conditions subject to constant bending moment (*Timoshenko & Gere,* 1961). Numerical solutions for beams under variable moments are available by *Massonet* (1947), *Horne* (1954), *Salvadori* (1955, 1956) and *Kirby & Nethercot* (1974) among others. The lateral buckling of beams with bracings was studied by *Kitipornchai & Richter* (1978), *Hancock & Trahair* (1979). Lateral buckling of beams with mono-symmetric sections can be found in *Galambos* (1968), *Kitipornchai & Trahair* (1980). *Clark & Hill* (1960) developed a 3-factor formula, which accounts for the destabilizing effect of the load, mono-symmetry, support conditions and non-uniform bending moment distributions. Nowadays, simple specific computer programs for the calculation of the elastic critical moment of beams under generic conditions are available (LTBeamN, 2015). *Nethercot & Trahair* (1976) and *Dux & Kitipornchai* (1984) developed inelastic solutions of beams. At present, the inelastic buckling behaviour of beams is accounted for by the buckling curve approach adopted in Europe with a normalized slenderness calculated using the value of the elastic critical moment and assuming that the columns and beams have similar behaviour regarding their buckling resistance.

Furthermore, extending to more complex case of beam-columns, a summary of the available analytical solutions and approximations is provided by *Chen & Atsuta* (1977) for in- and out-of-plane buckling. Due to the complexity of the problem, it is common to separate the behaviour into both planes for design purposes and add calibrated factors which account for the joint behaviour of the applied forces and their second order contributions. These are the approaches adopted by Eurocode 3, the north American standard AISC (2010), the Canadian CSA-S16-09 (CSA, 2009) and the Australian AS-4100-1998 codes.

Finally, all these members are part of a global structure. The structural analysis shall take into account the global second order effect (P-Δ) and member second order effects (P-δ) (*Simões da Silva et al.*, 2014). Modern design codes like Eurocode 3 and AISC (2010) provide clear specifications on the type on analysis and the subsequent verification checks to be performed with these results. Currently, the preferred practical approach is to carry out a 2nd order analysis incorporating global (P-Δ) effects followed by the verification of the buckling resistance of individual member using the buckling curve approach. Alternatively, even though the codes provide guidance on how to perform second order analysis with imperfections, these are still too complex for daily applications at the design office, because they are time-consuming, require correct definition of the initial imperfections in shape and magnitude, and their reliability is questionable since it depends on the experience of the user.

This chapter aims at summarizing the necessary background of the analytical expressions and current design rules, so that it can be used to extend it towards the achievement of the objectives of the thesis. It also offers a short summary of the basis of design in order to facilitate the understanding of the reliability background of the Eurocode. Finally, the recent developments in the stability design by other authors are summarized.

2.2 Buckling of members

2.2.1 Basic equations

In this section the equations governing beam-column behaviour are presented in their general form. They are used as a reference for further discussions in this section.

Without loss of generality, when the analysed member is perfect (without any initial imperfections) the differential equilibrium equations are given by:

$$EI_y \frac{d^2w(x)}{dx^2} + Nw(x) + M_y + M_z\theta(x) = 0$$

$$EI_z \frac{d^2v(x)}{dx^2} + M_y\theta(x) + Nv(x) + M_z = 0 \tag{2.1}$$

$$EI_w \frac{d^3\theta(x)}{dx^3} - GI_t \frac{d\theta(x)}{dx} + M_y \frac{dv(x)}{dx} + M_z \frac{dw(x)}{dx} + r_0^2 N \frac{d\theta(x)}{dx} = 0$$
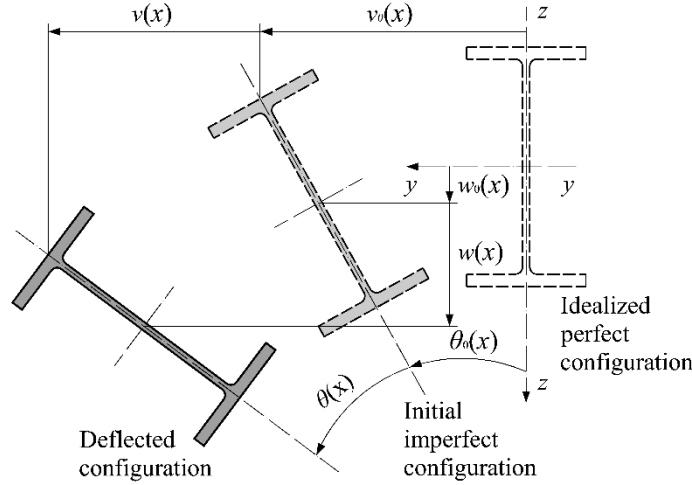
Figure 2.1 - Coordinate system and cross-sectional displacements

In these equations, $v(x)$ and $w(x)$ are the transverse displacements (along y and z, respectively), $\theta(x)$ is the twist rotation (positive according to the right-hand rule). Moreover, EI_y is the in-plane bending stiffness, EI_z is the out-of-plane bending stiffness, EI_w is the warping stiffness, GI_t is the Saint-Venant torsional stiffness and r_0 is the polar radius of gyration.

For simply supported members loaded with uniform axial force and bending moments, the system of differential equations is solved by half sine waves as functions for the displacements and rotations.

$$w(x) = \overline{w} \sin \frac{\pi x}{L}$$

$$v(x) = \overline{v} \sin \frac{\pi x}{L} \tag{2.2}$$

$$\theta(x) = \overline{\theta} \sin \frac{\pi x}{L}$$

Furthermore, if the member is considered with an initial imperfection, there are additional terms and the system of equations is transformed to Eq. (2.3).

$$EI_y \frac{d^2 w(x)}{dx^2} + Nw(x) + M_y + M_z \theta(x) = -Nw_0(x) - M_z \theta_0(x)$$

$$\tag{2.3}$$

$$EI_z \frac{d^2 v(x)}{dx^2} + M_y \theta(x) + Nv(x) = -M_y \theta_0(x) - Nv_0(x)$$

$$EI_w \frac{d^3\theta(x)}{dx^3} - GI_t \frac{d\theta(x)}{dx} + M_y \frac{dv(x)}{dx} + M_z \frac{dw(x)}{dx} + r_0^2 N \frac{d\theta(x)}{dx}$$

$$= -M_y \frac{dv_0(x)}{dx} - r_0^2 N \frac{d\theta_0(x)}{dx} - M_z \frac{dw_0(x)}{dx}$$

v_0 (x), w_0 (x), θ_0 (x) represent the initial deviation from a perfectly straight member, as shown in *Figure 2.1*.

2.2.2 Critical forces and amplification relationships

2.2.2.1 Flexural buckling of columns

In view of its fundamental character as a guideline for subsequent developments, the out-of-plane behaviour of a column ($M_y = M_z = 0$) with an initial imperfection (see *Figure 2.2*) is briefly addressed here. It is common to assume that the initial imperfection has the same shape as the lateral displacement:

$$v_0(x) = \bar{v}_0 sin \frac{\pi x}{L} \tag{2.4}$$

In these circumstances, the differential equation (2.3), together with the boundary conditions $v(0) = v(L) = 0$, yields

$$v(x) = \frac{N}{N_{cr,z} - N} \bar{v}_0 sin \frac{\pi x}{L} = \bar{v} sin \frac{\pi x}{L} \tag{2.5}$$

where $N_{cr,z} = \frac{EI_z \pi^2}{L^2}$ is the elastic critical load. The following amplification relationship can thus be established:

$$\bar{v}_{tot} = \bar{v} + \bar{v}_0 = \frac{1}{1 - N/N_{cr,z}} \bar{v}_0 \tag{2.6}$$
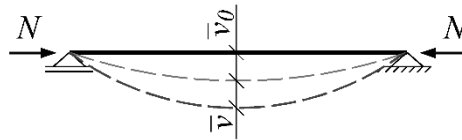
Figure 2.2 – Compressed column with initial imperfections

In-plane flexural buckling is described with identical equations and relationships, the only change is that the critical force $N_{cr,z}$ becomes $N_{cr,y}$, the displacement $v(x)$ - $w(x)$ and the initial imperfection $\bar{v}_0$ - $\bar{w}_0$, respectively.

2.2.2.2 Flexural buckling of beam-columns

The case of flexural buckling of a beam-column under bending moment and axial force is addressed here. This problem has a closed-form solution; however, it is problem dependent. Solutions for various bending moment distributions can be found in the literature *Chen & Lui* (1987).

In this section, the case of a beam-column loaded with uniform bending moment is considered, as shown in *Figure 2.3*.
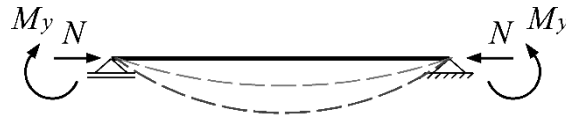
Figure 2.3 – Prismatic beam-column loaded with uniform axial force and bending moment

If the column in consideration is loaded with major axis bending moment and axial force, the solution for the in-plane displacement is given by:

$$w(x) = \frac{M_y}{EI_y k^2}\left[\cos kx - \frac{\cos kL - 1}{\sin kL}\sin kx - 1\right] \tag{2.7}$$

in which $k = N/EI_y$.

The displacement function can be used to determine the maximum second order bending moment, which in this case occurs at mid-span:

$$M_{y,max}{}^{II} = M_y \frac{1}{\cos k\frac{L}{2}} = M_y \frac{1}{\cos \frac{\pi}{2}\sqrt{N/N_{cr}}} \approx M_y \frac{1}{1 - N/N_{cr}} \tag{2.8}$$
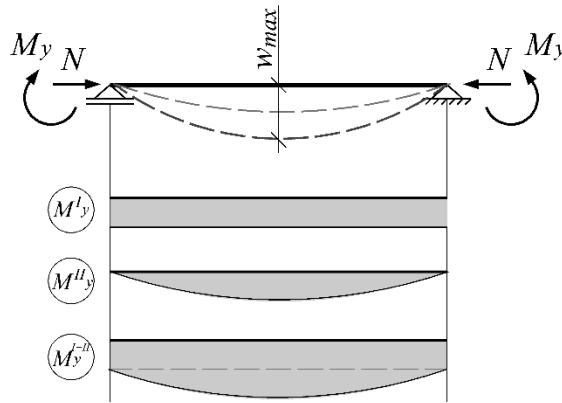
Figure 2.4 – Second order bending moment

Eq. (2.8) gives the maximum second order bending moment that consists of the primary moment M_y acting on the member and the second order component caused by the axial force N_{Ed} magnified by the maximum displacement w_{max} as shown in *Figure 2.4*.

2.2.2.3 Lateral-torsional buckling of beams

Considering the standard case of a simply-supported beam with fork supports ($v(0) = v(L) = 0$, $\theta(0) = \theta(L) = 0$ and $\frac{d^2\theta}{dx^2}(0) = \frac{d^2\theta}{dx^2}(L) = 0$) subject to a uniform bending moment (*Figure 4*),
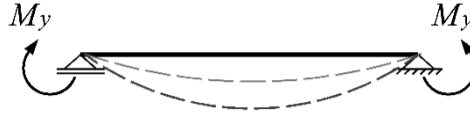
Figure 2.5 - Simply supported beam subject to uniform bending

it can be verified *Chen & Atsuta* (1977) that the amplitudes of the first buckling mode shapes of the perfect system Eq.(2.2) are related by

$$\frac{\bar{v}}{\bar{\theta}} = \frac{M_{cr}}{N_{cr,z}} = r_0\sqrt{\frac{N_{cr,x}}{N_{cr,z}}} \tag{2.9}$$

In Eq. (2.9), M_{cr} is the elastic critical bending moment and $N_{cr,x}$ is the pure torsional buckling force:

$$M_{cr} = r_0\sqrt{N_{cr,x}N_{cr,z}} \tag{2.10}$$

$$N_{cr,x} = \frac{1}{r_0^2}\left(\frac{EI_w\pi^2}{L^2} + GI_t\right). \tag{2.11}$$

2.2.2.4 Lateral-torsional buckling of beam-columns

Consider the standard case of a simply-supported beam-column with fork supports ($v(0) = v(L) = 0$, $\theta(0) = \theta(L) = 0$ and $\frac{d^2\theta}{dx^2}(0) = \frac{d^2\theta}{dx^2}(L) = 0$) subject to a uniform bending moment and axial force *Figure 2.3*, but in this time exhibiting lateral-torsional buckling. Then Eq. (2.1) leads to the following relationships between the critical forces:

$$\left(\frac{M_{cr,NM}}{M_{cr}}\right)^2 = \left(1 - \frac{N_{cr,NM}}{N_{cr,z}}\right)\left(1 - \frac{N_{cr,NM}}{N_{cr,x}}\right) \tag{2.12}$$

and between the amplitudes of the lateral displacement and rotation:

$$\frac{\bar{v}}{\bar{\theta}} = \frac{M_{cr,NM}}{N_{cr,z}-N_{cr,NM}}$$

(2.13)

If a beam-column with initial imperfections is subjected to an axial force and bending moment, it is again assumed that the relationship between the lateral imperfection and the rotation amplitudes is the same as in Eq.(2.13):

$$\frac{\bar{v}_0}{\bar{\theta}_0} = \frac{M_{cr,NM}}{N_{cr,z}-N_{cr,NM}}$$

(2.14)

Furthermore, considering that the axial force and bending moment are increased proportionally, that is, the ratio between the applied forces is equal to the ratio between the critical forces:

$$\frac{M_{cr,NM}}{N_{cr,NM}} = \frac{M_y}{N}$$

(2.15)

using expressions (2.14) and (2.15) in the system of equations (2.3), it is possible to obtain the following amplification of the amplitudes of the initial imperfections:

$$\begin{bmatrix}\bar{v}_{tot} \\ \bar{\theta}_{tot}\end{bmatrix} = \frac{1}{1-1/\alpha_{cr}} \times \begin{bmatrix}\bar{v}_0 \\ \bar{\theta}_0\end{bmatrix}$$

(2.16)

in which α_{cr} is the critical load multiplier.

2.3 The Eurocode 3 stability design rules

At present the stability design of members in Eurocode 3-1-1 is based on the buckling curve approach for uniform columns and beams; and on an interaction approach for the design of members loaded in bending and compression. For non-standard cases, the code offers a Merchant-Rankine type of empirical interaction expression denoted general method.

2.3.1   Members in compression

2.3.1.1   Flexural buckling

Regarding the resistance of uniform members in compression are given in clause 6.3.1 of Eurocode 3. According to the code, the buckling resistance of members is verified using:

$$\frac{N_{Ed}}{\chi N_{Rd}} \leq 1.0 \tag{2.17}$$

where N_{Ed} is the design axial force, N_{Rd} is the plastic resistance in compression and χ is the reduction factor for the relevant buckling mode.

$$\chi = \frac{1}{\phi + \sqrt{\phi^2 - \bar{\lambda}^2}} \leq 1.0 \tag{2.18}$$

$$\phi = 0.5\left(1 + \alpha(\bar{\lambda} - 0.2) + \bar{\lambda}^2\right) \tag{2.19}$$
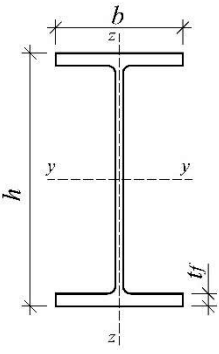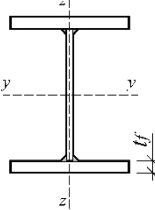
where $\bar{\lambda} = \sqrt{\frac{Af_y}{N_{cr}}}$ is the normalized slenderness and α is the imperfection factor (see *Table 2.1*).

Table 2.1 – Imperfection factor for buckling curves

Buckling curve	a_0	a	b	c	d
Imperfection factor α	0.13	0.21	0.34	0.49	0.76

The buckling curves for I-section are chosen according to *Table 2.2*.

Table 2.2 – Selection of buckling curve for a section

Fabrication		Limits		Axis	EC3-1-1	
					S235 S355	S460
Rolled profiles	h/b>1.2	$t_f \leq 40$ mm		y-y	a	a_0
				z-z	b	a_0
		40 mm<$t_f \leq$ 100 mm		y-y	b	a
				z-z	c	a
	h/b≤1.2	$t_f \leq 100$ mm		y-y	b	a
				z-z	c	a
		$t_f > 100$ mm		y-y	d	c
				z-z	d	c
Welded profiles		$t_f \leq 40$ mm		y-y	b	b
				z-z	c	c
		$t_f > 40$ mm		y-y	c	c
				z-z	d	d

2.3.1.2 Torsional and Flexural-torsional buckling

For open sections, the code endorses the verification of the possibility of torsional or flexural-torsional buckling, using Eq. (2.18) with the non-dimensional slenderness $\bar{\lambda}_T$ for torsional or flexural-torsional buckling calculated with $N_{cr}=N_{cr,FT}$ or $N_{cr,T}$. The imperfection factors used in this verification are the ones relative to minor axis flexural buckling with the corresponding cross-section type.

The new version of Eurocode 3, prEN 1993-1-1 (CEN/TC250, 2017), contains additional rule for double-symmetric I- and H- section members in compression with continuous or discrete intermediate lateral restraints, failing in torsional or torsional-flexural buckling. The buckling reduction factor is calculated as follows:

$$\chi_{TF} = \frac{1}{\phi_{TF} + \sqrt{{\phi_{TF}}^2 - {\bar{\lambda}_{TF}}^2}} \leq 1.0 \tag{2.20}$$

$$\phi_{TF} = 0.5\left(1 + \frac{{\bar{\lambda}_{TF}}^2}{{\bar{\lambda}_z}^2}\,\alpha_{TF}(\bar{\lambda}_z - 0.2) + {\bar{\lambda}_{TF}}^2\right) \tag{2.21}$$

where the imperfection factor is given by

$$\alpha_{TF} = \alpha_z \sqrt{\frac{Af_y\left(i_p^2 + d^2\right)}{6.25GI_t}} \tag{2.22}$$

with $i_p^2 = \frac{I_z + I_y}{A}$ and d is the distance of the intermediate restraint from the shear centre.

2.3.2 Members in bending

The stability of members in bending is verified using the design recommendations from clause 6.3.2 of Eurocode 3. There are two approaches currently available: the General case and the Special case given in clauses 6.3.2.2 and 6.3.2.3, respectively. Both of them make use of the buckling curve approach, thus assuming that the columns and beams have similar behaviour regarding their buckling resistance.

Recent research by *Taras & Greiner* (2008) has resulted in a new Ayrton-Perry design rule, which is based on mechanically consistent analytical derivation and imperfection factors calibrated based on an extensive numerical parametric study. The method is already included

in the final draft of the new Eurocode 3 prEN 1993-1-1 (CEN/TC250, 2017) and it is included in the summary of this section. It is henceforth referred to as New EC3 method or nEC3.

2.3.2.1   General case

The buckling resistance of members is verified using:

$$\frac{M_{y,Ed}}{\chi_{LT} M_{y,Rd}} \leq 1.0 \tag{2.23}$$

where $M_{y,Ed}$ is the design major axis bending moment, $M_{y,Rd}$ is the plastic resistance for cross-section classes 1 and 2, the elastic resistance for cross-section class 3 and the effective resistance for slender sections; χ_{LT} is reduction factor for lateral-torsional buckling.

$$\chi_{LT} = \frac{1}{\phi_{LT} + \sqrt{\phi_{LT}^2 - \bar{\lambda}_{LT}^2}} \leq 1.0 \tag{2.24}$$

$$\phi_{LT} = 0.5\big(1 + \alpha_{LT}(\bar{\lambda}_{LT} - 0.2) + \bar{\lambda}_{LT}^2\big) \tag{2.25}$$

where $\bar{\lambda}_{LT} = \sqrt{\frac{W_y f_y}{M_{cr}}}$ is the normalized slenderness and α_{LT} is the imperfection factor depending on the buckling curve. The buckling curves are chosen according to the member geometry according to *Table 2.3* with imperfection factors as given in *Table 2.4*.

Table 2.3 – Buckling curve selection

Cross-section	Limits	Buckling curve (GC)	Buckling curve (SC)
Rolled I-section	h/b≤2	a	b
	h/b>2	b	c
Welded I-section	h/b≤2	c	c
	h/b>2	d	d
Other section	-	d	-

Table 2.4 – Imperfection factor for buckling curves

Buckling curve	a	b	c	d
Imperfection factor α	0.21	0.34	0.49	0.76

2.3.2.2 Special case

The Special case is intended for the verification of rolled sections or equivalent welded sections. The buckling reduction factor is determined from:

$$\chi_{LT} = \frac{1}{\phi_{LT} + \sqrt{\phi_{LT}^2 - \beta\bar{\lambda}_{LT}^2}} \leq \begin{cases} 1.0 \\ \dfrac{1}{\bar{\lambda}_{LT}^2} \end{cases} \tag{2.26}$$

$$\phi_{LT} = 0.5\left(1 + \alpha_{LT}\left(\bar{\lambda}_{LT} - \bar{\lambda}_{LT,0}\right) + \beta\bar{\lambda}_{LT}^2\right) \tag{2.27}$$

the additional parameters $\bar{\lambda}_{LT,0}$ and β are a choice of the National Annex, the recommended values are: $\bar{\lambda}_{LT,0}$=0.4 and $\beta = 0.75$. The method is applied with the buckling curves from *Table 2.3*.

For a variable bending moment, the method allows a correction in the reduction factor:

$$\chi_{LT,mod} = \frac{\chi_{LT}}{f} \leq 1.0 \tag{2.28}$$
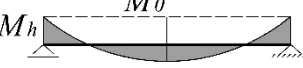
The factor *f* depends on the bending moment diagram

$$f = 1 - 0.5(1 - k_c)\left[1 - 2\left(\bar{\lambda}_{LT} - 0.8\right)^2\right] \leq 1.0 \tag{2.29}$$

The k_c is the correction factor chosen depending on the bending moment distribution (see *Table 2.5*).

Table 2.5 Correction factors k_c and f_m

Moment distribution	k_c	f_M
	1.0	1.0
	$\dfrac{1}{1.33 - 0.33\psi}$ ≤ 1.0	$1.25 - 0.1\psi - 0.15\psi^2$
	0.94	1.05
	0.90 0.91	$\dfrac{M_0}{M_h} < 2\colon 1.0 + 1.35\dfrac{M_0}{M_h} - 0.33\left(\dfrac{M_0}{M_h}\right)^3$ $\dfrac{M_0}{M_h} \geq 2\colon 1.05$
	0.86	1.10
	0.77 0.82	$\dfrac{M_0}{M_h} < 1.47\colon 1.25 + 1.5\left(\dfrac{M_0}{M_h}\right)^2 - 0.275\left(\dfrac{M_0}{M_h}\right)^4$ $\dfrac{M_0}{M_h} \geq 1.47\colon 1.05$

2.3.2.3 New EC3 method
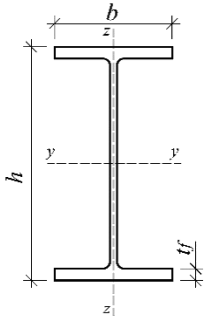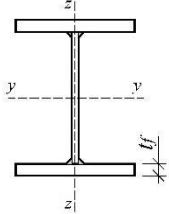
The new version of Eurocode 3 prEN 1993-1-1 (CEN/TC250, 2017) has a new method for the verification of the lateral-torsional buckling resistance of H- and I- sections between discrete lateral restraints on both flanges, for which the buckling reduction factor is calculated from the following:

$$\chi_{LT} = \frac{f_M}{\phi_{LT} + \sqrt{\phi_{LT}^2 - f_M \bar{\lambda}_{LT}^2}} \leq 1.0 \tag{2.30}$$

$$\phi_{LT} = 0.5\left(1 + f_M\left(\frac{\bar{\lambda}_{LT}^2}{\bar{\lambda}_z^2}\alpha_{LT}(\bar{\lambda}_{LT} - 0.2) + \bar{\lambda}_{LT}^2\right)\right) \tag{2.31}$$

The imperfection factor α_{LT} is selected from *Table 2.6*. The factor f_M is chosen according to *Table 2.5*.

Table 2.6 – Selection of buckling curve for a section

Cross-section			Limits	α_{LT}
Rolled profiles		$h/b>1.2$	$t_f \leq 40$ mm	$0.12 \sqrt{\dfrac{W_{el,y}}{W_{el,z}}} \leq 0.34$
			$t_f > 40$ mm	$0.16 \sqrt{\dfrac{W_{el,y}}{W_{el,z}}} \leq 0.49$
		$h/b \leq 1.2$	-	$0.16 \sqrt{\dfrac{W_{el,y}}{W_{el,z}}} \leq 0.49$
Welded profiles			$t_f \leq 40$ mm	$0.21 \sqrt{\dfrac{W_{el,y}}{W_{el,z}}} \leq 0.64$
			$t_f > 40$ mm	$0.25 \sqrt{\dfrac{W_{el,y}}{W_{el,z}}} \leq 0.76$

2.3.3 Members in bending and compression

The stability of members in bending and compression is verified according to clause 6.3.3. The general interaction format is given by the equations:

$$\frac{N_{Ed}}{\chi_y N_{Rd}} + k_{yy} \frac{M_{y,Ed} + \Delta M_{y,Ed}}{\chi_{LT} M_{y,Rd}} + k_{yz} \frac{M_{z,Ed} + \Delta M_{z,Ed}}{M_{z,Rd}} \leq 1.0 \qquad (2.32)$$

$$\frac{N_{Ed}}{\chi_z N_{Rd}} + k_{zy} \frac{M_{y,Ed} + \Delta M_{y,Ed}}{\chi_{LT} M_{y,Rd}} + k_{zz} \frac{M_{z,Ed} + \Delta M_{z,Ed}}{M_{z,Rd}} \leq 1.0 \qquad (2.33)$$

where N_{Ed}, $M_{y,Ed}$ and $M_{z,Ed}$ are the design values of the axial force and the maximum bending moments about y-y and z-z axes, respectively; N_{Rd}, $M_{y,Rd}$ and $M_{z,Rd}$ are the design resistances and k_{ii} and k_{ij} are the interaction factors.

The interaction factors for Method 1 are given in *Table 2.7*. The additional coefficients used with the interaction coefficients for Method 1 are given by equations (2.34)-(2.46).

$$\mu_y = \frac{1 - N_{Ed}/N_{cr,y}}{1 - \chi_y N_{Ed}/N_{cr,y}} \qquad (2.34)$$

$$\mu_z = \frac{1 - N_{Ed}/N_{cr,z}}{1 - \chi_z N_{Ed}/N_{cr,z}} \qquad (2.35)$$

$$w_y = \frac{W_{pl,y}}{W_{el,y}} \leq 1.5 \qquad (2.36)$$

$$w_z = \frac{W_{pl,z}}{W_{el,z}} \leq 1.5 \qquad (2.37)$$

Table 2.7 - Method 1: Interaction factors

Int. factor	Design assumptions	
	Elastic cross-sectional properties Class 3 and 4	Plastic cross-sectional properties Class1 and 2
k_{yy}	$C_{my}C_{mLT}\dfrac{\mu_y}{1 - N_{Ed}/N_{cr,y}}$	$C_{my}C_{mLT}\dfrac{\mu_y}{1 - N_{Ed}/N_{cr,y}}\dfrac{1}{C_{yy}}$
k_{yz}	$C_{mz}\dfrac{\mu_y}{1 - N_{Ed}/N_{cr,z}}$	$C_{mz}\dfrac{\mu_y}{1 - N_{Ed}/N_{cr,z}}\dfrac{1}{C_{yz}}0.6\sqrt{\dfrac{w_z}{w_y}}$
k_{zy}	$C_{my}C_{mLT}\dfrac{\mu_z}{1 - N_{Ed}/N_{cr,y}}$	$C_{my}C_{mLT}\dfrac{\mu_z}{1 - N_{Ed}/N_{cr,y}}\dfrac{1}{C_{zy}}0.6\sqrt{\dfrac{w_y}{w_z}}$
k_{zz}	$C_{mz}\dfrac{\mu_z}{1 - N_{Ed}/N_{cr,z}}$	$C_{mz}\dfrac{\mu_z}{1 - N_{Ed}/N_{cr,z}}\dfrac{1}{C_{zz}}$

For Class 3 and 4 $w_z=w_y=1$.

$$C_{yy} = 1 + (w_y - 1)\left[\left(2 - \frac{1.6}{w_y}C_{my}{}^2\left(\bar{\lambda}_{max} + \bar{\lambda}_{max}{}^2\right)\right)\frac{N_{Ed}}{N_{Rk}/\gamma_{M1}} - b_{LT}\right] \geq \frac{W_{el,y}}{W_{pl,y}} \qquad (2.38)$$

$$C_{yz} = 1 + (w_z - 1)\left[\left(2 - 14\frac{C_{mz}{}^2\bar{\lambda}_{max}{}^2}{w_z{}^5}\right)\frac{N_{Ed}}{N_{Rk}/\gamma_{M1}} - c_{LT}\right] \geq 0.6\sqrt{\frac{w_z}{w_y}}\frac{W_{el,z}}{W_{pl,z}} \qquad (2.39)$$

$$C_{zy} = 1 + (w_y - 1)\left[\left(2 - 14\frac{C_{my}{}^2\bar{\lambda}_{max}{}^2}{w_y{}^5}\right)\frac{N_{Ed}}{N_{Rk}/\gamma_{M1}} - d_{LT}\right] \geq 0.6\sqrt{\frac{w_y}{w_z}}\frac{W_{el,y}}{W_{pl,y}} \qquad (2.40)$$

$$C_{zz} = 1 + (w_z - 1)\left[\left(2 - \frac{1.6}{w_z}C_{mz}{}^2\left(\bar{\lambda}_{max} + \bar{\lambda}_{max}{}^2\right)\right) - e_{LT}\right]\frac{N_{Ed}}{N_{Rk}/\gamma_{M1}} \geq \frac{W_{el,z}}{W_{pl,z}} \qquad (2.41)$$

$\bar{\lambda}_{max}$ is the highest member slenderness.

$$a_{LT} = 1 - \frac{I_t}{I_y} \geq 0 \tag{2.42}$$

$$b_{LT} = 0.5 a_{LT} \bar{\lambda}_0^{\,2} \frac{M_{y,Ed}}{\chi_{LT} M_{pl,y,Rd}} \frac{M_{z,Ed}}{M_{pl,z,Rd}} \geq 0 \tag{2.43}$$
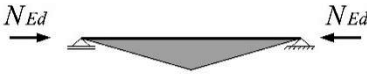
$$c_{LT} = 10 a_{LT} \frac{\bar{\lambda}_0^{\,2}}{5 + \bar{\lambda}_z^{\,4}} \frac{M_{y,Ed}}{C_{my} \chi_{LT} M_{pl,y,Rd}} \geq 0 \tag{2.44}$$

$$d_{LT} = 2 a_{LT} \frac{\bar{\lambda}_0}{0.1 + \bar{\lambda}_z^{\,4}} \frac{M_{y,Ed}}{C_{my} \chi_{LT} M_{pl,y,Rd}} \frac{M_{z,Ed}}{C_{mz} M_{pl,z,Rd}} \geq 0 \tag{2.45}$$

$$e_{LT} = 1.7 a_{LT} \frac{\bar{\lambda}_0}{0.1 + \bar{\lambda}_z^{\,4}} \frac{M_{y,Ed}}{C_{my} \chi_{LT} M_{pl,y,Rd}} \geq 0 \tag{2.46}$$

The equivalent moment factors are used as specified in *Table 2.8* and *Table 2.9*.

<div align="center">

Table 2.8 – Method 1: Equivalent moment factors $C_{mi,0}$

</div>

Moment diagram	$C_{mi,0}$
	$C_{mi,0} = 0.79 + 0.21\psi_i + 0.36(\psi_i - 0.33)\dfrac{N_{Ed}}{N_{cr,i}}$
	$C_{mi,0} = 1 + \left(\dfrac{\pi^2 E I_i |\delta_x|}{L^2 |M_{i,Ed}(x)|} - 1\right)\dfrac{N_{Ed}}{N_{cr,i}}$ $M_{i,Ed}(x)$ is the maximum moment $M_{y,Ed}$ or $M_{z,Ed}$ $|\delta_x|$ is the maximum displacement along the member
	$C_{mi,0} = 1 - 0.18\dfrac{N_{Ed}}{N_{cr,i}}$
	$C_{mi,0} = 1 + 0.03\dfrac{N_{Ed}}{N_{cr,i}}$

$$\varepsilon_y = \frac{M_{y,Ed}}{N_{Ed}} \frac{A}{W_y} \geq 0 \tag{2.47}$$

Table 2.9 – Method 1: Equivalent moment factors $C_{mi,0}$

No torsional deformation $\bar{\lambda}_0 \leq \bar{\lambda}_{limit}$	Possible torsional deformation $\bar{\lambda}_0 > \bar{\lambda}_{limit}$
$C_{my} = C_{my,0}$	$C_{my} = C_{my,0} + (1 - C_{my,0}) \dfrac{a_{LT}\sqrt{\varepsilon_y}}{1 + a_{LT}\sqrt{\varepsilon_y}}$
$C_{mz} = C_{mz,0}$	$C_{mz} = C_{mz,0}$
$k_{LT} = 1.0$	$k_{LT} = \dfrac{C_{my}{}^2 a_{LT}}{\sqrt{(1 - N_{Ed}/N_{cr,z})(1 - N_{Ed}/N_{cr,T})}}$

The interaction factors for Method 2 are given in *Table 2.10* and *Table 2.11*.

$$n_y = \frac{N_{Ed}}{\chi_y N_{Rk}/\gamma_{M1}} \tag{2.48}$$

$$n_z = \frac{N_{Ed}}{\chi_z N_{Rk}/\gamma_{M1}} \tag{2.49}$$

The equivalent moment factors are chosen according to *Table 2.12*.
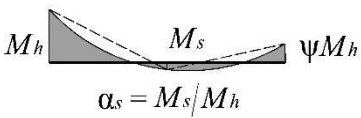
Table 2.10 – Method 2: Interaction factors for members susceptible to lateral-torsional buckling

Int. factor	CS	Design assumptions	
		Elastic cross-sectional properties Class 3 and 4	Plastic cross-sectional properties Class1 and 2
k_{yy}	I, RHS	$C_{my}[1 + 0.6\bar{\lambda}_y n_y] \leq C_{my}[1 + 0.6n_y]$	$C_{my}[1 + (\bar{\lambda}_y - 0.2)n_y] \leq C_{my}[1 + 0.8n_y]$
k_{yz}	I, RHS	k_{zz}	$0.6\,k_{zz}$
k_{zy}	I, RHS	$0.8k_{yy}$	$0.6k_{yy}$
k_{zz}	I	$C_{mz}[1 + 0.6\bar{\lambda}_z n_z] \leq C_{mz}[1 + 0.6n_z]$	$C_{mz}[1 + (2\bar{\lambda}_z + 0.6)n_z] \leq C_{my}[1 + 1.4n_z]$
	RHS		$C_{mz}[1 + (\bar{\lambda}_z - 0.2)n_z] \leq C_{mz}[1 + 0.8n_z]$

Table 2.11 - Method 2: Interaction factors for members susceptible to lateral-torsional buckling

Int. factor	Design assumptions	
	Elastic cross-sectional properties Class 3 and 4	Plastic cross-sectional properties Class3 and 4
k_{yy}	k_{yy} from *Table 2.10*	k_{yy} from *Table 2.10*
k_{yz}	k_{yz} from *Table 2.10*	k_{yz} from *Table 2.10*
k_{zy}	$\left[1 - \dfrac{0.05\bar{\lambda}_z}{C_{mLT}-0.25}n_z\right] \geq \left[1 - \dfrac{0.05}{C_{mLT}-0.25}n_z\right]$	$\left[1 - \dfrac{0.1\bar{\lambda}_z}{C_{mLT}-0.25}n_z\right] \geq \left[1 - \dfrac{0.1}{C_{mLT}-0.25}n_z\right]$ For $\bar{\lambda}_z < 04$ $k_{zy} = 0.6 + \bar{\lambda}_z \leq \left[1 - \dfrac{0.1\bar{\lambda}_z}{C_{mLT}-0.25}n_z\right]$
k_{zz}	k_{zz} from *Table 2.10*	k_{zz} from *Table 2.10*

Table 2.12 – Method 2: Equivalent moment factors C_m

Moment diagram	Range		C_{my} and C_{mz} and C_{mLT}	
			Uniform load	Concentrated load
M_y ⟍ ψM_y	$-1 \leq \psi \leq 1$		$0.6 + 0.4\psi \geq 0.4$	
M_h ⟍ M_s ⟍ ψM_h $\alpha_s = M_s/M_h$	$0 \leq \alpha_s \leq 1$	$-1 \leq \psi \leq 1$	$0.2 + 0.8\alpha_s \geq 0.4$	
	$-1 \leq \alpha_s < 0$	$0 \leq \psi \leq 1$	$0.1 - 0.8\alpha_s \geq 0.4$	$-0.8\alpha_s \geq 0.4$
		$-1 \leq \psi < 0$	$0.1(1-\psi) - 0.8\alpha_s \geq 0.4$	$0.2(-\psi) - 0.8\alpha_s \geq 0.4$
M_s M_h ⟍ ψM_h $\alpha_h = M_h/M_s$	$0 \leq \alpha_h \leq 1$	$-1 \leq \psi \leq 1$	$0.95 + 0.05\alpha_h$	$0.90 + 0.10\alpha_h$
	$-1 \leq \alpha_h < 0$	$0 \leq \psi \leq 1$	$0.95 + 0.05\alpha_h$	$0.90 + 0.10\alpha_h$
		$-1 \leq \psi < 0$	$0.95 + 0.05\alpha_h(1 + 2\psi)$	$0.95 + 0.10\alpha_h(1 + 2\psi)$

For members with sway mode the equivalent uniform moment factor should be taken C_{my}=0.9 or C_{mz}=0.9, respectively.

C_{my},C_{mz} and C_{mLT} shall be obtained according to the bending moment diagram between the relevant braced points.

2.3.4 General method for lateral and lateral-torsional buckling of structural components

The method is used where the rules, given in the previous sections, do not apply. It targets the verification for the resistance to lateral and lateral-torsional buckling of single members, built-up or not, uniform or not, with complex support conditions or not or plane frames or sub-frames composed of such members.

The overall resistance of the structural component is verified using:

$$\frac{\chi_{op}\alpha_{ult,k}}{\gamma_{M1}} \geq 1.0 \tag{2.50}$$

where $\alpha_{ult,k}$ is the minimum load amplifier of the design loads to reach the characteristic resistance of the most critical cross-section of the structural component, considering its in-plane behaviour without taking lateral or lateral-torsional buckling into account however for all effects due to in-plane geometrical deformation and imperfections, global and local, where relevant;

χ_{op} is the reduction factor for the non-dimensional slenderness $\bar{\lambda}_{op}$ which is determined accounting for lateral or lateral-torsional buckling as given in Eq. (2.18)

| 25

$$\bar{\lambda}_{op} = \sqrt{\frac{\alpha_{ult,k}}{\alpha_{cr,op}}} \tag{2.51}$$

where $\alpha_{cr,op}$ is the minimum amplifier for the in-plane loads to reach the elastic critical resistance of the structural component with regards, to latera or lateral-torsional buckling without accounting for in-plane flexural buckling.

The reduction factor χ_{op} is then determined as the minimum of χ according to clause 6.3.1 or χ_{LT} according to clause 6.3.2 or interpolated value between both.

Although it claims generality, the reliability of the method was questioned several times, e.g. *Simões da Silva et al.* (2010), *Taras* (2010), *Marques* (2012), SAFEBRICTILE final report *Simões da Silva et al.* (2017) and it was shown that due to lack of mechanical background it may lead to either over-conservative or unsafe estimates of the design resistance. In the following it will not be further discussed.

2.4 Background of the European design rules

2.4.1 Introduction

This section is dedicated to the background of the design rules for columns, beams and beam-columns presented in the previous section. This summary aims at identifying a consistent way of extending them to a general approach applicable to any kind of member and buckling mode. It also addresses inconsistencies associated with the application of these rules which have been identified by other researches. It follows the organization of the previous section.

2.4.2 Members in compression

The verification format for the flexural buckling of columns is directly derived from the differential equations (2.3) for a column with an initial imperfection. It is achieved by applying a first yield criterion at mid-span for a simply-supported column (*i.e.*, equating the normal stress at the most compressed fibre to f_y):

$$\frac{\sigma}{f_y} = \frac{N}{Af_y} + \frac{M_i^{II}}{W_i f_y} = 1.0 \tag{2.52}$$

where the second order moment due to the initial imperfection is obtained using the amplification relationship derived in Eq.(2.6),

$$\frac{N}{Af_y} + \frac{N\bar{v}_0}{W_i f_y} \frac{1}{1 - \dfrac{N}{N_{cr,z}}} = 1.0 \tag{2.53}$$

which is transformed to

$$\chi + \frac{\chi}{1 - \chi\bar{\lambda}^2}\eta = 1.0 \tag{2.54}$$

where $\bar{\lambda} = \sqrt{\dfrac{Af_y}{N_{cr}}}$ is the normalized slenderness, $\chi = \dfrac{N}{Af_y}$ is the buckling reduction factor and $\eta = \bar{e}_0\dfrac{A}{W}$ is the generalized imperfection factor (accounting for out-of-straightness and residual stresses), with W denoting the elastic section modulus relative to the buckling axis. Eq.(2.54) is the buckling curve equation where the only unknown is the amplitude of the imperfection $\bar{e}_0$. This advantage of the Ayrton-Perry representation of the problem was used in the calibration of the European design rules.

The buckling curves were established in the 1970's, and their development was based on an extensive experimental programme carried out by the *European Convention for Constructional Steelwork* (ECCS) in several European countries; on theoretical developments by thorough analysis of the experimental programme; and on reliability assessment by a Monte Carlo simulation.

The experimental programme was summarized by *Sfintesco* (1970) comprising a total of 1067 column tests. It covered a variety of cross-sections (I and H, hollow and T sections); fabrication procedures (welded and rolled sections). In the scope of the experimental programme, the material and geometrical properties (cross-section dimensions and out-of-straightness) of each column were evaluated and carefully documented.

Furthermore, *Beer & Schulz* (1970) carried out a thorough analysis of the ECCS experimental programme, assessing various parameters that can possibly occur and affect the resistance of compressed members. Special attention was paid to the member imperfections, focussing on: i) initial out-of-straightness; ii) load eccentricity; and iii) residual stresses;
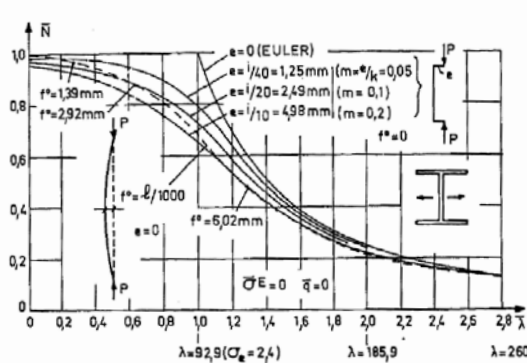
a) Load eccentricity and out-of-straightness   *b) Residual stresses and out-of-straightness*
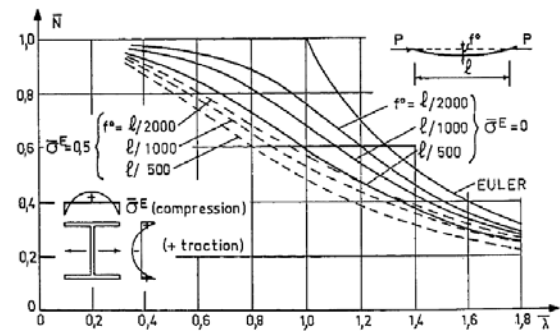
Figure 2.6 – Sensitivity to imperfections Beer & Schulz (1970)

The geometrical imperfections (initial out-of-straightness and load eccentricity) were measured in the experimental programme, providing plausible estimations of their distributions. It was shown in *Beer & Schulz* (1970) that the limit of $L/1000$ as initial out-of-straightness could cover load eccentricities up to 5mm as shown in *Figure 2.6a*. It was also noticed that the unintentional eccentricity can only have a noticeable effect in the low slenderness range, but it was assumed that it could be compensated by the fact that the strain hardening was neglected in the calculations.

There was a certain difficulty in the adoption of magnitude of the residual stresses due to the lack of available data and the high variability of the available measurements. In order to assess the influence of the residual stresses and the geometrical imperfection, a comparison was performed for three levels of geometrical imperfections (L/2000; L/1000 and L/500), with or without considering the residual stresses as shown in *Figure 2.6b*. It was concluded that the influence of the geometrical imperfection reduces with increasing residual stresses. It was possible to show that the curvature effect reaches its maximum at a normalized slenderness λ between 1.0 and 1.3, depending on the level of residual stresses.

Later, the safety of one of the curves was evaluated by Monte Carlo simulation by *Strating & Vos* (1973), accounting for the variability of various parameters such as residual stresses, out-of-straightness, load eccentricity, geometrical and material properties. The adopted distributions are summarized in *Table 2.13*.

Table 2.13 - *Distributions for basic variables in Strating & Vos* (1973)

Basic variable	Gamma distribution		Normal distribution	
	λ	k	mean	st.dev
Load eccentricity	2.798	1.663	-	.
Out-of-straightness	-	-	0.00085L	0.0002L
Area (mm^2)	-	-	2047.33	81.15
Yield stress (MPa)	-	-	314.8	26.5
Residual stresses	-	-	$0.2\sigma_E$	$0.05\sigma_E$

A general assumption was that reasonable safety is achieved by using twice the standard deviation as upper or lower limit. It was applied to all of the variables, except for the yield stress in certain cases. The distributions for all basic variables were considered with Normal distribution, except for the load eccentricity which was considered with Gamma distribution.

Even though the distributions of some of the basic variables in *Table 2.13* have very high variability and not very high mean-to-nominal ratios, it was concluded that the curve is sufficiently reliable.

Finally, *Maquoi & Rondal* (1978) derived the analytical Ayrton-Perry format of the design verification and the curves were put into equation.

At present the code proposes 5 buckling curves, as shown in *Figure 2.7*. Curves a to d were originally calibrated on the basis of the experimental programme. The most relaxed curve a_0, was added later to account for the most favourable properties of high strength steels (HSS). It is worth pointing out that there is an inconsistency regarding the curves for steel grades higher than S460: in *Table 2.2*, the buckling curve selection for the different buckling axes is always more favourable for in-plane buckling than out-of-plane. This is very logical, since the usual residual stress distribution (welded and rolled) is more unfavourable for a member bent about its minor axis. For steel grades higher than S460, however, this fact is not reflected in the buckling curve selection. In Chapter 5, this issue will be discussed on the basis of the reliability assessment.
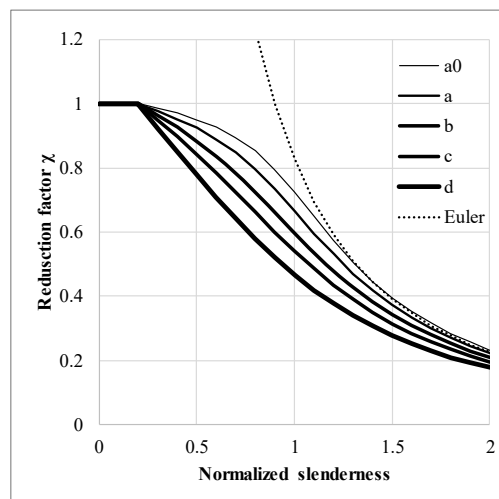
Figure 2.7 - The European buckling curves

2.4.3 Members in bending

2.4.3.1 Existing methods

It was shown already that in the current version of Eurocode 3, there are two possibilities for the verification of the lateral-torsional buckling resistance of beams. The first approach, the General case, assumes that columns and beam act alike, i.e. the compression flange is supposed to act like an equivalent column, and therefore, the same imperfection factors were assumed for the method. It does, however, adopt a different split according to the cross-section geometry, accounting for their different torsional rigidity. According to *ECCS No. 119*, these curves are

meant to be used with deep and slender sections which are outside of the scope of rolled sections. The method has been criticized for being over conservative when applied to members with variable bending moment diagram *Rebelo et al.* (2009), *Taras* (2010).

As an alternative for rolled and equivalent welded sections, Eurocode 3 has another set of buckling curves, denoted as the Special case. The method was calibrated on the basis of extensive numerical studies in the Research Project *Lateral-torsional buckling of steel and composite beams* (1993) and *Salzgeber* (2000). Additional calibration was carried out by *Grainer & Kaim* (2001) on the basis of experimental results by *Janss & Maquoi.* In order to justify, the plateau at 0.4, experimental results by *Byfield & Nethercot* (1998) were used in the assessment according to Annex Z of ENV 1993-1-1:1992. However, the method was shown to be unconservative when compared to numerical results *Snijder & Hoenderkamp* (2007), *Rebelo et al.* (2009).

2.4.3.2 New LT-buckling curves

The new version of Eurocode 3 prEN 1993-1-1 (CEN/TC250, 2017), includes a new method for lateral-torsional buckling of beams with H- and I- sections. The method was developed by *Taras & Greiner* (2008) and it has mechanically consistent analytical background with imperfection factors calibrated on the basis of advanced numerical simulations and assessed using Monte Carlo simulations.

The analytical derivation is performed directly from the differential equations (2.3) for a beam with initial imperfection. It is achieved by applying a first yield criterion at mid-span as it was done for flexural buckling of columns, but in this case, there is an additional second order term that appears in the equation due to warping:

$$\frac{\sigma(x)}{f_y} = \frac{M_y(x)}{W_y(x)f_y} + \frac{M_z^{II}(x)}{W_z(x)f_y} + \frac{M_w^{II}(x)}{W_w(x)f_y} \tag{2.55}$$

where W_y, W_z and W_w denote the elastic section moduli.

Assuming now that the initial imperfections have the same shape as the first buckling mode, that is,

$$v_0(x) = \hat{v}_0 \sin\frac{\pi x}{L} \qquad \theta_0(x) = \hat{\theta}_0 \sin\frac{\pi x}{L} \qquad \frac{\hat{v}_0}{\hat{\theta}_0} = \frac{M_{cr}}{N_{cr,z}} = r_0\sqrt{\frac{N_{cr,x}}{N_{cr,z}}} \tag{2.56}$$

and enforcing a first yield limit condition eventually leads to the Ayrton-Perry equation

$$\frac{M_y}{W_y f_y} + \frac{M_y}{W_i f_y} \frac{\bar{e}_0}{1 - \frac{M_y}{M_{cr}}} \frac{N_{cr,z}}{M_{cr}} = 1.0 \tag{2.57}$$

which is transformed to

$$\chi_{LT} + \frac{\chi_{LT}}{1 - \chi_{LT} \bar{\lambda}_{LT}^2} \eta_{LT} = 1.0 \tag{2.58}$$

with the buckling reduction factor and the normalized slenderness given by:

$$\chi_{LT} = \frac{M_y}{f_y W_y} \qquad \bar{\lambda}_{LT} = \sqrt{\frac{f_y W_y}{M_{cr}}} \tag{2.59}$$

A similar transformation was also performed by *Szalai & Papp* (2010), however without further calibration of the respective imperfection factors.

For design purposes, the generalized imperfection factor in Eq. (2.58) required further calibration:

$$\eta_{LT} = \frac{A \bar{e}_0}{W_z} \frac{\bar{\lambda}_{LT}^2}{\bar{\lambda}_z^2} \tag{2.60}$$
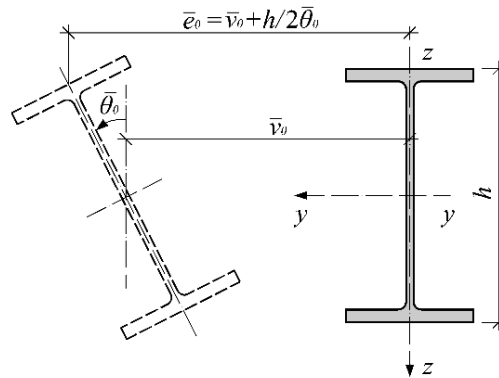
Figure 2.8 – Amplitudes of the geometrical imperfections

The meaning of the geometrical parameter $\bar{e}_0$ appearing in the above definition of η_{LT} is indicated in *Figure 2.8*.

The calibration was performed for the term $\frac{A\bar{e}_0}{W_z}$ from Eq. (2.60) and the two following options were considered:

$$\eta_I = \alpha(\bar{\lambda}_z - 0.2) \tag{2.61}$$

$$\eta_{II} = \alpha(\bar{\lambda}_{LT} - 0.2). \tag{2.62}$$

These options were compared with the numerical estimate η_{num}. It was shown that the imperfection proportional to $\bar{\lambda}_z$ adjusts better to the numerical curve up to a certain point where the geometrical imperfections, which are length dependent, become more relevant ($\bar{\lambda}_z$ approximately 3.0 corresponding to $\bar{\lambda}_{LT} = 1.0$). Hence new imperfection factors α_{LT} were developed, see *Table 2.6*. They use the same limits as the column buckling curves for rolled sections and their magnitude is bound by the imperfection factors for minor axis flexural buckling.

The effect of non-uniform bending moment distributions was included by the calibration of an additional factor f_M, given in *Table 2.5*.

2.4.4   Members in bending and compression

For prismatic members loaded in bending and compression, Eurocode 3 provides an interaction formula. It is based on linear interaction between the axial force and the bending moments, which are combined through interaction factors accounting for the non-linear effects in the beam-column behaviour. In the development of the interaction formula there were two teams: the "French-Belgian" team which was responsible for the interaction coefficients in Method 1 and the "Austrian-German" team responsible for the development of the coefficients associated with Method 2. The main difference between the two methods is the way of considering the various effects which affect the beam-column behaviour. The interaction coefficients associated with Method 1 were developed aiming to distinguish each structural effect in the interaction coefficient, therefore laying the ground for any further modifications, if necessary, and to directly identify the impact of each physical phenomenon. Method 2, aimed at easier practical implementation, combines the non-linearities into global interaction factors k_{ii} and k_{ij} calibrated on the basis of an extensive numerical programme.

In Section 2.2.2.1 it was shown that the in-plane behaviour of beam-columns is associated with the presence of a second order bending moment which arises from the additional lever arm to

the axial force N_{Ed} causing amplification of the deflection and of the bending moment. In the same section, it was also shown that for uniform bending moment, the location where this moment has a maximum is at mid-span.

For non-uniform bending moment distributions, this location varies and to avoid its determination, both methods consider the equivalent moment concept. It is illustrated in *Figure 2.9*, the bending moment M_{Ed} is replaced with $C_m M_{Ed}$, with a sinusoidal bending moment distribution and results in the same second order moment. Then the second order elastic check at the most loaded cross section is given by:

$$\frac{N_{Ed}}{N_{Rd}} + \frac{1}{1 - N_{Ed}/N_{cr}}\frac{N_{Ed}\bar{e}_0}{M_{Rd}} + \frac{1}{1 - N_{Ed}/N_{cr}}\frac{C_m M_{Ed,max}}{M_{Rd}} \leq 1.0 \qquad (2.63)$$

For Method 1, the C_m factors are chosen with more correct expressions that depend on the axial force, see *Table 2.8*. Method 2 uses the Austin formula, which relates to a beam subject to uniform bending moment and does not depend on the axial force,

Table 2.12.
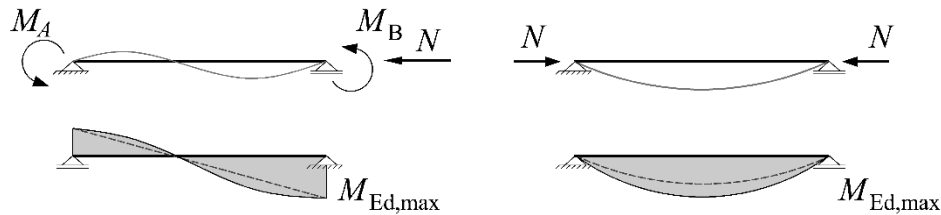
Figure 2.9 - Equivalent moment concept

At low slenderness, the in-plane behaviour of a beam-column may exhibit plastic behaviour. For that reason in Method 1, $M_{el,Rd}$ is replaced with $CM_{pl,Rd}$ in M_{Rd}:

$$\frac{N_{Ed}}{N_{Rd}} + \frac{M_{Ed}}{CM_{pl,Rd}} \leq 1.0 \qquad (2.64)$$

The factor C is found as a function of the member slenderness, applied axial force, the equivalent moment factor C_m and the ratio between the plastic and elastic moduli. It was calibrated in order to achieve continuity with the cross-section resistance. The expressions for C_{ii} and C_{ij}, as given by Eq. (2.38)-(2.41) were calibrated with a lower bound at $M_{el,Rd}$. They also consider the biaxial bending interaction.

For Method 2, the equivalent sinusoidal moment concept was kept; however, the inclusion of plasticity was considered directly in the k-factors, therefore not allowing to split the amplification terms from the plasticity effects at low slenderness.

Regarding lateral-torsional buckling, Method 1 has it incorporated implicitly in the formulation of the interaction coefficients. Method 2 offers a separate set of interaction coefficients to verify the lateral-torsional buckling resistance and therefore distinguish the members as susceptible or not to lateral-torsional deformations, see *Table 2.10* and *Table 2.11*.

Both methods were assessed on the basis of the same set of advanced numerical simulations (*Boissonnade et al.*,2006).

In the present version of Eurocode 3, both sets of interaction coefficients are given in Annex A and Annex B, respectively. In the new version or Eurocode 3 prEN 1993-1-1 (CEN/TC250, 2017) only Method 2 is specified and the interaction coefficients are included in the main text of the code, while Method 1 is included in a technical specification CEN/TC 250 prCEN/TC 1993-1-101:2016.

2.5 Buckling resistance outside Europe

2.5.1 Introduction

Up to this point, the presented design formats were only focused on European standards. In this section, the design recommendations of the north American AISC, (2010) code are summarized.

2.5.2 Design of members in compression

The nominal resistance of members with non-slender members is given by:

$$P_n = F_{cr} A_g \tag{2.65}$$

in which A_g is the cross-section area and F_{cr} is the critical stress determined from:

$$\frac{KL}{r} \leq 4.71 \sqrt{\frac{E}{F_y}} \qquad\qquad F_{cr} = \left[0.658^{\frac{F_y}{F_e}} \right] F_y \tag{2.66}$$

$$\frac{KL}{r} > 4.71\sqrt{\frac{E}{F_y}} \qquad\qquad F_{cr} = 0.877F_e \qquad\qquad (2.67)$$

F_e is the elastic critical buckling stress.

$$F_e = \frac{\pi^2 E}{\left(\dfrac{KL}{r}\right)^2} \qquad\qquad (2.68)$$

The verification is also based on the buckling curve approach. However, unlike the 5 buckling curves of Eurocode 3, the AISC (2010) verification is based on a single buckling curve. It is exactly the same as the SSRC curve 2P (*Ziemian,* 2010), even though it has a different representation.

2.5.3   Design of members in bending

The lateral-torsional buckling resistance is verified according to Section F2 of AISC, (2010). In this case, the curve is divided into three regions: a plastic, inelastic and purely elastic.

$$L_b \leq L_p \qquad\qquad M_n = M_p = Z_x F_y$$

$$L_p \leq L_b \leq L_r \qquad M_n = C_b\left[M_p - (M_p - 0.75S_x F_y)\left(\frac{L_b - L_p}{L_r - L_p}\right)\right] \leq M_p \qquad (2.69)$$

$$L_b > L_r \qquad\qquad M_n = S_x F_{cr} \leq M_p$$

L_b is the distance between the points braced against lateral displacement. F_{cr} is the critical stress:

$$F_{cr} = \frac{C_b \pi^2 E}{\left(\dfrac{L_b}{r_{ts}}\right)^2}\sqrt{1 + 0.078\frac{Jc}{S_x h_0}\left(\frac{L_b}{r_{ts}}\right)^2} \qquad\qquad (2.70)$$

The length limits are defined as:

$$L_p = 1.76 r_y \sqrt{\frac{E}{F_y}} \qquad\qquad (2.71)$$

$$L_r = 1.95 r_{ts} \frac{E}{0.7F_y} \sqrt{\frac{Jc}{S_x h_0} + \sqrt{\left(\frac{Jc}{S_x h_0}\right)^2 + 6.76\left(\frac{0.7F_y}{E}\right)^2}} \qquad (2.72)$$

The verification assumes the transition of the elastic to inelastic region to happen at $0.7F_y$. This format has been recently criticized by *Subramanian & White* (2017), who claimed it is unsafe in the inelastic region due to the incorrect consideration of the buckling length and the typically high magnitudes of the imperfections adopted in numerical simulations.

2.5.4   Design of members under bending and axial force

The design of members in bending and compression is performed by using an interaction approach. For members prone to flexural buckling, AISC (2010) gives the following equations:

$$\frac{P_r}{P_c} \geq 0.2 \qquad\qquad \frac{P_r}{P_c} + \frac{8}{9}\left(\frac{M_{rx}}{M_{cx}} + \frac{M_{ry}}{M_{cy}}\right) \leq 1.0$$

$$\frac{P_r}{P_c} < 0.2 \qquad\qquad \frac{P_r}{2P_c} + \left(\frac{M_{rx}}{M_{cx}} + \frac{M_{ry}}{M_{cy}}\right) \leq 1.0 \qquad (2.73)$$

The lateral-torsional buckling stability of members in bending and compression is verified using a separate formula:

$$\frac{P_r}{P_{cy}}\left(1.5 - 0.5\frac{P_r}{P_{cy}}\right) + \left(\frac{M_{rx}}{C_b M_{cx}}\right)^2 \leq 1.0^* \qquad (2.74)$$

Both verifications are linked to the member resistances obtained separately as in Section 2.5.2 for members in compression and Section 2.5.3 for members in bending.

2.6 Structural design and code verification

The structural design codes provide the link from theory to practice. Their aim is to ensure that design principles and application rules lead to appropriate safety levels. The safety margin directly reflects the risk society is willing to accept yet that maximises economical design. The family of Eurocodes, EN 1990 to EN 1999, are based on the limit state design philosophy, and the use of partial factors. It is often applied since it incorporates the variability in the design code and offers a clear guidance to the engineer. The American code offers two possibilities for

design: the Load and Resistance Factor Design (LRFD) which is a limit state approach, or the allowable stress design as a tradition from the past.

The basic document of the Eurocodes is EN 1990 – *Basis of structural design.* It establishes principles and requirements for the safety assessment of structures; it describes the basis of their design and provides guidelines for structural reliability.

The limit state design method recognizes relevant design situations, where the design values are established by use of partial factors. These safety factors are used on load and on the resistance sides and the design is considered adequate whenever the appropriate limit states are verified:

$$E_d \leq R_d \tag{2.75}$$

where E_d is the design value of the actions; R_d is the design value of the resistance.

The safety factors are established based on a statistical evaluation of experimental data; or based on a calibration to experience derived from a long building tradition. They should be calibrated such that the reliability level is as close as possible to the target reliability. The calibration of safety factors can be performed based on full probabilistic methods, or on First Order Reliability Methods. The full probabilistic approach is often not possible to use due to the lack of sufficient statistical data. *Vrouwenvelder* (2002) reports that the analysis can be based on the Bayesian interpretation of probabilities, where the probabilities are evaluated using available data and previous knowledge.

Figure 2.10 illustrates the various possible reliability methods according to EN 1990.

The level of safety in EN 1990 is chosen according to Consequence classes (CC) defined in Annex B. The consequence classes establish the reliability differentiation of the code by considering the consequence of failure or malfunction of the structure. The Consequence Classes (CC) correspond to Reliability classes (RC), which define the target reliability level though the reliability index β. This index defines the probability of failure, given by:

$$P_f = \Phi(-\beta) \tag{2.76}$$

where Φ is the cumulative distribution function (CDF) for the standard normal distribution.
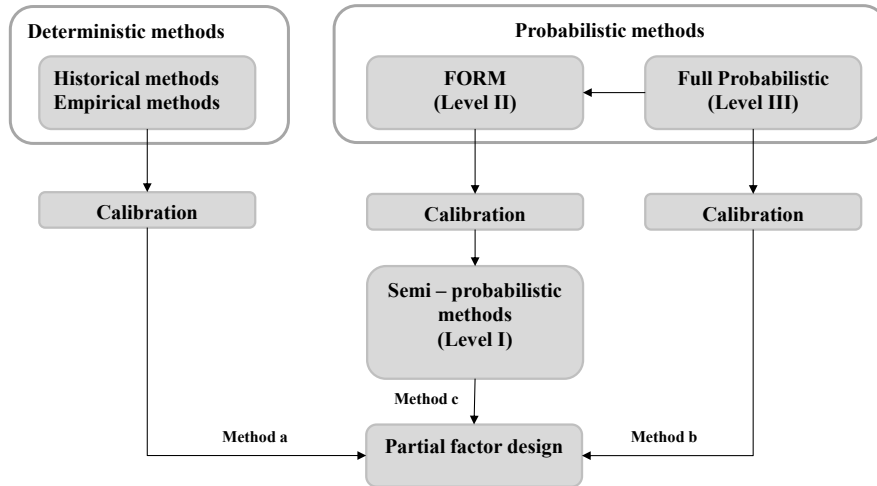
Figure 2.10 Possible Reliability methods

The reliability index covers the scatter on both resistance and action sides. It can be expressed in terms of number of standard deviations as shown on *Figure 2.11*.
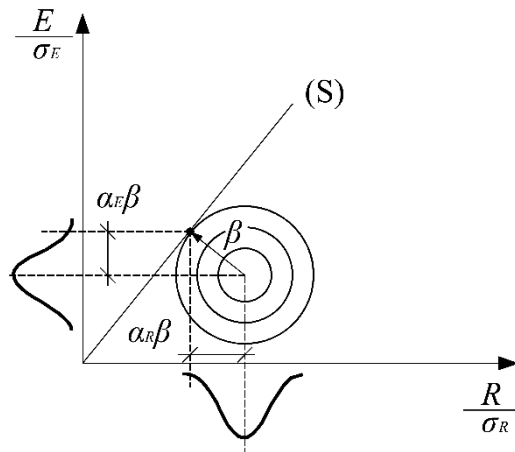
Figure 2.11 Reliability index β

According to *Gulvanessian et al.* (2002), "*the target reliability index or the target failure probability is the minimum requirement for human safety from the individual or societal point of view when the expected number of fatalities is taken into account. It starts from an accepted lethal accident rate of 10^{-6} per year, corresponding to a reliability index $\beta_1 = 4.7$*". The reference period (the design life) depends on the Reliability class, i.e. for most of the structures it is 50 years which leads to *β=3.8*.

The probability of failure as expressed in Eq. (2.76) includes the loading and the resistance parts. EN 1990 allows to separate the scatter due to loading and resistance in terms of coefficients α_E and α_R, respectively (see *Figure 2.11*), where:

$$\sqrt{\alpha_R^2 + \alpha_E^2} \approx 1.0 \qquad (2.77)$$

The partial factors related to the resistance are determined based on the following expression:

$$P(r \leq r_d) = \Phi(-\alpha_R \beta) \qquad (2.78)$$

where r stands for resistance and r_d is the design resistance. The factor α_R may be assumed to have a fixed value of 0.8 in case the standard deviation of the load effect and the resistance do not deviate very much ($0.16<\sigma_E/\sigma_R<7.6$). This simplification is *crucial* for a standardized determination of the partial factors for the resistance side without the need to simultaneously consider the action side.

The LRFD in AISC (2010), for example, does not allow such split and the reliability index β is calibrated for Live-to-Dead load ratio of 3 and it is approximately 2.6 for members and 4.0 for connections. This imposed reliability assessment which is load dependent and more laborious to perform.

The partial factors used in EN 1990 are:

- γ_F – Partial factor for actions, also accounting for model uncertainties and dimensional variations;
- γ_f – Partial factor for actions, which takes account of the possibility of unfavorable deviations of the action values from the representative values;
- γ_{Sd} - Partial factor associated with the uncertainty of the action and/or action effect model;
- γ_M – Partial safety factor for a material property also accounting for model uncertainties and model variations;
- γ_m – Partial factor for a material property;
- γ_{Rd} – Partial factor associated with the uncertainty of the resistance model;

The relation between individual partial factors in the Eurocodes is schematically shown in *Figure 2.12*:
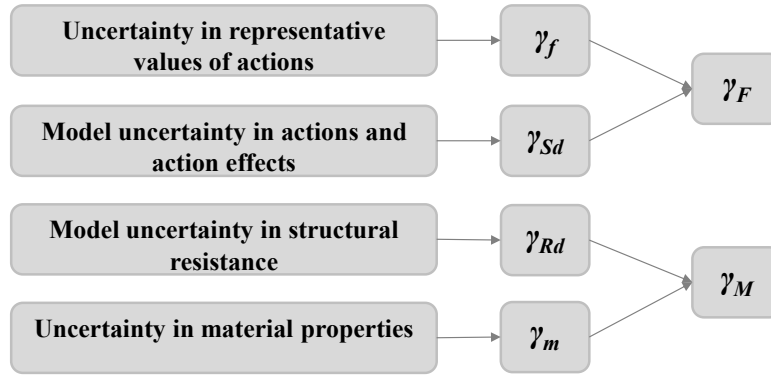
Figure 2.12 - Relation between individual partial factors

Since Eurocode 3 allows the split between the load and the resistance side, henceforth only the resistance part will be discussed and the partial factor γ_M related to it.

Regarding the design resistance, in Section 6 of EN 1990, three different alternatives for its evaluation are proposed, for steel structures, Eurocode 3 recommends the use of Method 2 (clause 6.3.5(3)): the design resistance may be obtained directly from the characteristic value of product or material resistance, without explicit determination of the design values for individual basic variables:

$$R_d = \frac{R_d}{\gamma_M} \tag{2.79}$$

The latter is applicable to products or members made of a single material and it is also used in connection with Annex D of EN 1990.

Furthermore, in Eurocode 3, depending on the type of design rule in consideration there are different partial factors γ_{Mi}:

- – Resistance of cross-sections whatever the class is γ_{M0};
- – Resistance of members to instability assessed by member checks γ_{M1};
- – Resistance of cross-sections in tension to fracture γ_{M2};

2.7 Recent advances

2.7.1 Introduction

Even though the stability design rules presented in this section were based on extensive research, the stability problem continues to attract the attention of researchers due to the

enhanced material properties, new cross-section geometries and the possibility of computer aided design. In this section, the recent developments in the scope of the European design rules are summarized. There are several works which build upon the Ayrton-Perry format for flexural buckling of columns, extending it to beam-columns, non-uniform members and members subject to arbitrary loading. It was shown that this concept is relatively easily extended to flexural-torsional and lateral-torsional buckling once the correct analytical behaviour is considered *Taras* (2010). In *Naumes* (2009), the equilibrium equation for the flexural buckling of tapered members was also established; in this derivation, the shape of the initial imperfection was considered eigenmode conform. It was shown that the Ayrton-Perry design format can be adopted for the design of non-uniform members. However, the proposed expressions are not applicable for practical design verification due to lack of recommendations for the determination of the design location. Furthermore, *Taras* (2010) offers the same type of model for flexural buckling of beam-columns. *Marques* (2012) provided design equations for flexural buckling of web-tapered columns and lateral-torsional buckling of web-tapered beams in the same Ayrton-Perry format. An approximate verification format for beam-columns is proposed by *Hoglund* (2014): aiming for simplicity, the stress utilizations due to axial force and bending moments are specified as power functions. The method claims to provide better representation of the transition between Class 2 and Class 3 sections, which however are already implemented in the final draft of prEN 1993-1-1 (CEN/TC250, 2017) following the recommendations of the European project SEMICOMP+ (*Greiner et al.*, 2011). It is incorporated in Eurocode 9 for verification of aluminium beam-columns. Recent research by *Szalai* (2017) shows the extension of the Ayrton-Perry equation to prismatic simply supported members subject to arbitrary loading. The author does not provide calibration of the corresponding imperfection factors but shows that it is theoretically possible to achieve this format for various buckling modes. Based on this development, *Szalai & Papp* (2017) built their proposal for reformulation of the General method, by putting it into the derived Ayrton-Perry proposal for prismatic simply supported members subject to arbitrary loading, which is its major flaw, being unable to capture the specific aspects of non-uniform members.

Furthermore, there are a few developments supporting the design by use of numerical analyses. Their proposals were mainly focused on the definition of the equivalent geometrical imperfection to be considered in the design *Chladný & Stujberová* (2013a,b), *Aguero et al.* (2015a,b), *Papp* (2016) and a mixture between LBA conform imperfection and a reduction factor calculation *Badari & Papp* (2015).

The methods can be separated according to the type of members they can deal with in the following table:

Table 2.14 – Recent advances

Author	Members in compression	Members in bending	Members in bending and compression
Taras (2010)			x
Marques et al. (2012), (2013), (2014)	x	x	x
Chladný & Stujberová (2013a,b)	x		
Aguero et al. (2015a,b)	x	x	
Badari & Papp (2015)		x	
Papp (2016)	x	x	x

In this section, these recent methods are briefly summarized.

2.7.2   Members in compression

2.7.2.1   Tapered columns

For the verification of linearly web tapered columns, an Ayrton-Perry analytical model was built by *Marques et al.* (2012), based on an equivalent simply-supported segment between effective restraints. The verification format is established on a linear interaction between the first order forces and second order bending moments utilizations, leading to a maximum utilization (and, consequently, to the ultimate load factor) at a certain location, denoted as the second order failure location. The utilization ratio of any section is given by the quotient of applied and resistant forces. It is also the inverse of the load multiplier $\alpha_{ult,k}$. *Figure 2.13* illustrates this aspect over the length L of a tapered column buckling about its major axis.
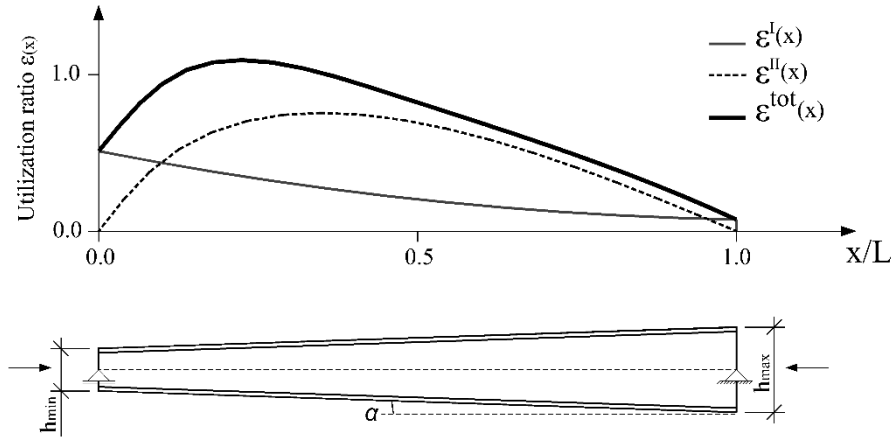
Figure 2.13 Determination of the failure location

In this model for tapered members, eigenmode conform imperfections were considered for the second order forces shape, leading to similar equations as those presented in EC3-1-1 for the stability verification of prismatic columns. As a result, as long as a second order failure location is known and an additional imperfection factor is considered to account for the non-uniformity either of the loading or of the cross section, the verification may be performed analogously to the rules for prismatic columns. The utilization ratio is given by Eq. (2.80) for flexural buckling of columns

$$\varepsilon(x_c^{II}) = \chi(x_c^{II}) + \frac{\chi(x_c^{II})}{1 - \bar{\lambda}^2(x_c^{II})\chi(x_c^{II})}\left[e_0 \frac{N_R(x_c^{II})}{M_R(x_c^{II})}\right]\left[\frac{EI(x_c^{II})(-\delta_{cr}''(x_c^{II}))}{\alpha_{cr}N_{Ed}(x_c^{II})}\right] \qquad (2.80)$$

It was shown that this second order failure location and additional imperfection factor may be replaced by an "over-strength" factor φ which accounts for the relation between the ultimate resistance multiplier of the second order location, $\alpha_{ult,k}(x_c^{II})$ and the first order location, $\alpha_{ult,k}(x_c^I)$, such that if the φ-factor is determined, the verification is always based on x_c^I. φ is given by

$$\varphi = \frac{N_{Rk}(x_c^{II})/N_{Ed}(x_c^{II})}{N_{Rk}(x_c^I)/N_{Ed}(x_c^I)} = \frac{\alpha_{ult,k}(x_c^{II})}{\alpha_{ult,k}(x_c^I)} \qquad (2.81)$$

2.7.2.2 Frames with unique local and global imperfection

Chladný & Stujberová (2013) show the principles of the application of EN 1993-1-1 section 5.3.2(11), where the amplitude of the imperfection is defined on the basis of flexural buckling of prismatic columns and the shape is adopted according to the relevant buckling mode.

$$e_{0,d} = \alpha(\bar{\lambda} - 0.2)\frac{W_{el}}{A}\frac{1 - \dfrac{1 - \bar{\lambda}_m^2\chi}{\gamma_{M1}}}{1 - \bar{\lambda}_m^2\chi} \tag{2.82}$$

Even though it is put in the context of a frame, the imperfection is derived for "*frame structure with axially loaded members*" whose resistance "*shall be equal to the flexural buckling resistance of the equivalent member*". This equivalent member is simply supported, its cross-section and axial force are equal to the critical cross-section of the frame and its length is such that it equals the axial force at the critical section for the critical loading (*Chladný & Stujberová* (2013)). Following this fundamental requirement and establishing the utilization along the member as a sum of the first and second order stresses:

$$U(x) = \frac{N_{Ed}(x)}{N_{Rd}(x)} + \frac{M_{\eta_{init,m}}^{II}(x)}{M_{Rd}(x)} \tag{2.83}$$

they derived the following expression for the imperfection by equalising the imperfections for the equivalent and real member at the critical cross–section:

$$\eta_{init,m}(x) = e_{0,d}\frac{\alpha_{cr}N_{Ed,m}}{EI_m|\eta''_{cr,m}|}\eta_{cr}(x) \tag{2.84}$$

in which the index *m* stands for the critical cross-section.

The procedure is intended for direct use in second order analysis; however, some applications (for members) are possible using direct calculation. In any case, the definition of the critical location for the determination of the magnitude of the imperfection requires an iterative process.

2.7.2.3 *Equivalent geometrical imperfection in steel structures sensitive to flexural and/or torsional buckling due to compression*

Aguero et al. (2015a) extended the concept presented in the previous section to members in compression sensitive to flexural and/or torsional buckling. Their method also finds its basis in section 5.3.2(11) of EN 1993-1-1. *Aguero et al.* (2015a) use the same assumptions as *Chladný & Stujberová* (2013). However, in this case, *Aguero et al.* (2015a) propose two different expressions for the initial imperfection for Class 2 and Class 3 cross-sections which are used to amplify the second order forces obtained from LBA.

$$e_c(x_{cr}) = \alpha\big(\bar{\lambda} - 0.2\big)\frac{1 - \dfrac{1 - \bar{\lambda}_m^{\,2}\chi}{\gamma_{M1}}}{1 - \bar{\lambda}_m^{\,2}\chi}\frac{1}{E\left(\dfrac{I_z}{M_{pl,z,Rd}}\eta''_{\,v} + \dfrac{I_y}{M_{pl,y,Rd}}\eta''_{\,w} + \dfrac{I_w}{M_{pl,w,Rd}}\eta''_{\,\theta}\right)} \qquad (2.85)$$

where $\eta''_{\,v}$, $\eta''_{\,w}$, $\eta''_{\,\theta}$ are the second derivatives of the mode shape translations in y, z directions and twist rotation about x-axis.

This method is also applied using an *iterative* procedure to find the critical location along the member for which the magnitude of the imperfection is calculated.

2.7.3 Members in bending

2.7.3.1 Tapered beams

Similarly to the model for web-tapered columns, an Ayrton-Perry analytical model was built by *Marques et al.* (2013) for the verification of linearly web tapered beams. It is also based on an equivalent simply-supported segment between effective restraints. The verification format is based on a linear interaction between the first and second order bending moment utilizations, leading to a maximum utilization. The utilization ratio is given by:

$$\varepsilon(x_c^{II}) = \chi_{LT}(x_c^{II}) + \frac{\chi_{LT}(x_c^{II})}{1 - \bar{\lambda}_{LT}^{\,2}(x_c^{II})\chi_{LT}(x_c^{II})} \times$$

$$\times\,\alpha_{LT}\big(\bar{\lambda}_z(x_c^{II}) - 0.2\big)\frac{\bar{\lambda}_{LT}^{\,2}(x_c^{II})}{\bar{\lambda}_z^{\,2}(x_c^{II})}\frac{EI_z(x_c^{II})\big({-}\delta_{cr}''(x_c^{II})\big)\xi}{N_{cr,z,Tap}} \times \qquad (2.86)$$

$$\times\,\frac{1 + \dfrac{N_{cr,z,Tap}}{M_{cr,Tap}}\dfrac{h(x_c^{II})}{2}}{1 + \dfrac{N_{cr,z,Tap}}{M_{cr,Tap}}\dfrac{h_{min}}{2}}$$

This theoretical utilization ratio was used for the calibration of "over-strength" factors as it was done for the columns.

2.7.3.2 Equivalent geometrical imperfection in steel structures sensitive to flexural and/or torsional buckling due to compression

Aguero et al. (2015b) extended their concept presented in *Aguero et al.* (2015a) to members in bending sensitive to lateral-torsional buckling. Using the same assumptions as described in section 2.7.2.3, the amplitude of the imperfection is given by:

$$e_M(x_{cr}) = \frac{\alpha_{LT}(\bar{\lambda}_{LT} - \bar{\lambda}_{LT,0})}{\bar{\lambda}_{LT}^{2}} \frac{1 - \dfrac{1 - \bar{\lambda}_{LT}^{2} \chi_{LT}}{\gamma_{M1}}}{1 - \beta \lambda_{LT}^{2} \chi_{LT}} \frac{1}{E\left(\dfrac{I_z}{M_{pl,z,Rd}}\eta''_v + \dfrac{I_w}{M_{pl,w,Rd}}\eta''_\theta\right)} \tag{2.87}$$

2.7.3.3 Lateral-torsional buckling of prismatic beams

Badari & Papp (2015) proposed new buckling curves for lateral-torsional buckling based on the analytical derivation by *Szalai & Papp* (2010). The imperfection factors for the LT-curves were calibrated on the basis of advanced numerical simulations.

They also propose a verification which is performed in terms of a reduction factor χ calculation for various locations along the beam by using the buckling mode and the actual load distribution. The normalized slenderness is calculated at location i along the beam as a ratio between the ultimate load multiplier for the section and the critical load multiplier:

$$\bar{\lambda}_{LT,i} = \sqrt{\frac{\alpha_{ult,k,i}}{\alpha_{cr}}} \tag{2.88}$$

and the generalized imperfection at each section is taken as a part of the maximum

$$\eta_{LT,i} = \eta_{LT} \frac{v_i}{v_{max}} \tag{2.89}$$

Then the bending moment resistance of each cross-section is obtained as:

$$M_{b,Rd,i} = W_{pl,y} f_y \frac{\chi_{LT}}{\gamma_{M1}} \frac{M_{y,Ed}}{M_{y,Ed,i}} \tag{2.90}$$

2.7.4 Members in bending and compression

2.7.4.1 Ayrton-Perry formulation for in-plane flexural buckling of beam-columns

Taras (2010) proposed an Ayrton-Perry equation for in-plane flexural buckling on prismatic beam-columns. The verification format is derived in two alternative forms as a reduction factor applied to the axial force and taking into account the bending moment,

$$\frac{N_{Ed}}{\chi_{y,\eta 0} N_{Rd}} \leq 1.0 \tag{2.91}$$

or as a global in-plane reduction factor which multiplies both axial force and bending moment aiming towards the definition of an overall concept for beam-columns.

$$\chi_{ip} = \frac{c_0}{\phi_{ip} + \sqrt{\phi_{ip}^2 - k_{ni}^* c_0 \bar{\lambda}_{ip}^2}} \leq 1.0 \tag{2.92}$$

$$\phi_{ip} = 0.5 \left(k_{ni}^* + \eta_{tot} + c_0 \bar{\lambda}_{ip}^2 \right) \tag{2.93}$$

$$\eta_{tot} = k_{ni}^* C_{mS} \eta_0 + \eta_{imp,EC3} \tag{2.94}$$

The generalized imperfection, given by Eq.(2.94), has two terms - due to initial imperfection amplified by the axial force and by the second order bending moment.

As mentioned earlier, the in-plane behaviour of beam-columns is highly influenced by plasticity at low slenderness, which led to the calibration of additional plasticity factors in the interaction formula, as described in Section 2.4.4. In the developed Ayrton-Perry equation, since it is based on a first yield criterion, it was also necessary to develop additional factors. They are given by Eq. (2.95) and (2.96). *Taras* (2010) adopted a "split" approach, a multiplier for the moment and the axial force.

$$k_{ni}^* = k_{ni} + (1 - k_{ni}) \rho C_{mS} \bar{\lambda}_{ip} \leq 1.0 \tag{2.95}$$

$$k_{mi}^* = k_{ni} + (w - k_{ni}) \rho C_{mS} \bar{\lambda}_{ip} \leq w \tag{2.96}$$

where

$$k_{n1} = 1.0 \quad k_{m1} = 1.0 - 0.5a \geq 0.75 \quad \eta_{SC1} = \frac{0.8}{1 - 0.8 k_{m1}} \tag{2.97}$$

$$k_{n2} = \frac{0.2}{1-0.8k_{m1}} \quad k_{m2} = 1.0 \quad \eta_{SC2} = \infty \tag{2.98}$$

Similar factors were calibrated for minor axis flexural buckling of I-sections, hollow circular and rectangular cross-sections.

2.7.4.2 Tapered beam-columns

In *Marques et al.* (2014) the design rules for tapered columns and beams developed by the same authors were used to propose a verification format for the stability verification of web-tapered beam-columns. The verification uses the Eurocode 3 interaction approach and adjusted values for k_{yy} and k_{zy} interaction factors. The interaction formula applied at the first order failure location (Eqs. (2.99) and (2.100)), with the reduction factors χ calibrated for tapered columns and beams; and the interaction factors according to *Table 2.15*.

$$\frac{N_{Ed}(x_{c,N}^I)}{\chi_y(x_{c,N}^I)N_{Rd}(x_{c,N}^I)} + k_{yy}\frac{M_{y,Ed}(x_{c,M}^I)}{\chi_{LT}(x_{c,M}^I)M_{y,Rd}(x_{c,M}^I)} \leq 1.0 \tag{2.99}$$

$$\frac{N_{Ed}(x_{c,N}^I)}{\chi_z(x_{c,N}^I)N_{Rd}(x_{c,N}^I)} + k_{zy}\frac{M_{y,Ed}(x_{c,M}^I)}{\chi_{LT}(x_{c,M}^I)M_{y,Rd}(x_{c,M}^I)} \leq 1.0 \tag{2.100}$$

In *Table 2.15, n_y* and *n_z* are obtained using Eqs. (2.48) and (2.49) for the first order failure location.

Table 2.15 - Method 2: Interaction factors for members susceptible to lateral-torsional buckling

Int. factor	Design assumption Plastic cross-sectional properties Class1 and 2
k_{yy}	$C_{my}\left[1 + \left(\bar{\lambda}_y(x_{c,N}^{II}) - 0.2\right)n_y\right] \leq C_{my}\left[1 + 0.8n_y\right]$
k_{zy}	$\left[1 - \frac{0.1\bar{\lambda}_z(x_{c,N}^{II})}{C_{mLT}-0.25}n_z\right] \geq \left[1 - \frac{0.1}{C_{mLT}-0.25}n_z\right]$ For $\bar{\lambda}_z(x_{c,N}^{II}) < 0.4$ $k_{zy} = 0.6 + \bar{\lambda}_z(x_{c,N}^{II}) \leq \left[1 - \frac{0.1\bar{\lambda}_z(x_{c,N}^{II})}{C_{mLT}-0.25}n_z\right]$

2.7.4.3 Overall imperfection method

Finally, *Papp* (2016) proposed an innovative general methodology for the calculation of the buckling resistances of columns, beams and beam-columns. The method avoids the iterations in the previous ones, it transforms the calculation to an equivalent simply-supported member.

The procedure is applied in the following sequence:

- LBA is performed to obtain the critical load multiplier α_{cr} and the elastic buckling shape $v_{cr}(\mathrm{x})$

- In a second step, a second order stress analysis with $v_{cr}(\mathrm{x})$ as initial imperfection is carried out, which gives the defined reference location where the second order stress has maximum - x_{ref}

- The amplitude of the imperfection is then calculated for the reference member, which has cross-section properties of the member at location x_{ref} and the length is calculated so that the reference member has the same critical forces as the designed member at the reference location.

- Once the amplitude is obtained, a second order analysis with the calculated amplitude is carried out.

- Finally, the verification is performed as a cross-section check of the designed member.

2.7.5 Summary

This section summarized the recent developments in the scope of the European stability design. New design methods based on an extension of the Ayrton-Perry concept were proposed, namely for flexural buckling of prismatic beam-columns by *Taras* (2010) and for web-tapered columns and beams by *Marques* (2012). These methods rely on the inevitable calibration of factors to account for the over-strength due to the variation of the failure location.

The second group of methods, that would eventually avoid the additional calibration of factors accounting for the failure location, are the methods which establish the shape of the initial imperfection as the buckling shape of the member. Several developments were presented in this direction as well. *Chladný & Stujberová* (2013a,b) covered the flexural buckling of members and *Aguero et al.* (2015a,b) extended the concept to flexural-torsional and lateral-torsional buckling. In terms of practical application, the major drawback of these methods is the iterative

process in the determination of the critical location. The method by *Papp* (2016) resolves the issue with the critical location by setting a criterion for its evaluation. However, the determination of the amplitude of the initial imperfection is not found very practical (especially for application in a design office) since it requires a two-step procedure: i) second-order stress analysis with random amplitude of the buckling shape to determine the reference location and ii) transformation of the real member to an equivalent at this reference location.

In the following chapters, as a part of the research objectives, it was aimed to develop a method that overcomes the mentioned issues, a method that is general, reliable and consistent with the existing rules.

3 EXPERIMENTAL BUCKLING BEHAVIOUR OF NON-UNIFORM STEEL MEMBERS

3.1 Introduction

The stability design rules for prismatic members presented in the previous chapter were developed on a sound analytical background, validated with experimental, numerical and statistical work. Due to the possible economic advantages, the buckling behaviour of non-uniform members has attracted the interest of the researchers since the very beginning of the last century. Initially, the contributions were focused on analytical solutions for the elastic critical behaviour of non-uniform members. *Timoshenko & Gere* (1961) propose numerical solutions for the critical loads of stepped columns and bars with linearly varying cross-section. *Lee et al.* (1972) presented an equivalent member approach for the critical loads of linearly-web-tapered columns. *Hirt & Crisinel* (2001) established an expression for the determination of an equivalent moment of inertia for tapered columns, which is used in the Euler formula for the calculation of the critical buckling force. *Marques* (2012) derived closed form expressions for the critical load of web-tapered columns based on the Rayleigh-Ritz method. Regarding lateral-torsional buckling, the first studies on the torsional behaviour of non-uniform members are found in *Lee* (1956) and *Lee & Szabo* (1967). Their developments were later used by *Kitipornchai & Trahair* (1972) who provided the theoretical basis for the lateral-torsional buckling of tapered beams. Later, *Brown* (1981) proposed solutions using finite differences for the determination of the critical loads for simply-supported beams and cantilevers with tapered sections. Other approaches for the elastic critical moment of web-tapered beams are available

by *Gálea* (1986) for non-uniform beam under constant bending moment and for web-tapered beams subject to a linear bending moment distributions and cantilevers by *Andrade et al.* (2007).

Furthermore, using the finite element method, theoretical developments were performed by *Yang & Yau* (1987); *Bradford & Cuk* (1988) proposed a solution for mono-symmetric tapered beams; *Bradford* (1988) treated the behaviour of web-tapered beam-columns with restraints; *Rajasekaran* (1993a,b) developed a formulation for tapered thin-walled members with a generic section; *Gupta et al.* (1996) addressed on the behaviour of continuous tapered beams. *Lei & Shu* (2008) presented a new theoretical formulation that correctly accounts for the effects of tapering by incorporating second-order taper effects in the strain-displacement equations

In most common structural applications, however, the real stability behaviour of steel members includes imperfections and nonlinear material behaviour. Accounting for these, design methods for tapered columns were proposed by *Baptista & Muzeau* (1998) adjusting the Eurocode 3 design rule for flexural buckling of prismatic columns by adding a numerically calibrated coefficient *k* to account for the extra resistance. *Raftoyiannis & Ermopoulos* (2005) proposed a verification format based on a first yield criterion which was validated with numerical simulations. *Kim* (2010) adjusted the AISC (2010) expressions for prismatic columns and beams to tapered, using the equivalent member concept. As mentioned earlier, Marques (2012) developed Ayrton-Perry equations for tapered columns and beams. Unlike the design rules for prismatic members, these design methods were validated only numerically, and even though, nowadays, the laboratory experiments are often substituted with advanced numerical simulations, due to the added complexity the experimental evidence is essential in order to evaluate the member response in terms of characterization of the real behaviour and member imperfections.

Therefore, the objective of the present chapter is to provide the experimental background for the development of design rules for non-uniform members. For that, firstly, the existing experimental tests on non-uniform columns, beams and beam-columns were collected. Furthermore, the results from an experimental programme carried-out at the University of Coimbra are presented. These results were then used in the validation of the numerical model in Chapter 4.

3.2 Experiments by others

3.2.1 Experiments on tapered members

There are a few experimental programmes carried out in the past and summarized hereby. Only a brief overview of each is given, in order to provide an idea of the scope of the existing experimental results.

Krefeld et al. (1959) performed experimental tests on cantilevered I-section tapered steel beams, analysing the critical stress for different taper ratios and member lengths. The experimental programme consisted of 16 built-up I and C section beams. The maximum member length was about 5 m and the largest cross-section tested had about 450 mm height, flange width of 220 mm, flange and web thicknesses of about 10 mm and 6 mm, respectively. Based on the results obtained, the authors proposed a method for estimation of the elastic bending stress for non-uniform cantilevered beams, which is built on a comparison of the experimental results for tapered and uniform members and by setting up additional reduction factors depending on the cross-section dimensions, supports and taper angle.

Butler & Anderson (1963) carried out experimental tests on the elastic stability of tapered I members loaded in compression and a combination of bending and compression. The experimental programme covered 14 different specimens, web and/or flange tapered. The maximum cross-section height was about 500 mm, flange width 120 mm and flange and web thicknesses of 8 and 6 mm respectively. The results obtained led to the conclusion that the pure compression tests are in excellent agreement with the analytical solution of the problem; the combined loading revealed interaction dependency on the taper ratio.

Later *Butler* (1966), carried out experiments on elastic buckling of lateral and torsional bracing of beams. The tested specimens were tapered I steel tip-loaded cantilevers. The beam dimensions were chosen to be similar to the previous study *Butler & Anderson* (1963). The conclusions of the paper reveal that end bracing is most effective on the tension flange; the most efficient bracing configuration is tip and mid-span bracing at the tension and compression flanges, respectively. A tension bracing at mid-span would have no influence on the lateral-torsional buckling capacity.

As a continuation of the work by *Butler*, *Prawel et al.* (1974) performed an experimental study where fifteen tapered I-section members were tested in bending and in a combination of bending and compression. The tested members were chosen to fail in the inelastic range. The experiments covered three beams and twelve beam-columns. The members had identical shallow sections (approximately 152x152x6x3 mm). The taper was varied using three different taper ratios (2, 2.67 and 3) and also covering prismatic members. The tapered members were fabricated by welding of the flanges to one side of the web. The study also assessed the effects of oxygen and shear cuts plates. The nominal yield stress was 42 ksi (approximately 290 MPa) and the yield stress determined from the experiments was 52 ksi (approximately 360 MPa). Based on the measurements carried out, the authors proposed a pattern of residual stresses. The maximum tensile stress in both flanges and web is set equal to the yield stress. The tension spreads over 1/3 of the flanges. Regarding the compressive stresses, in the flanges the maximum compression at the flange tips is suggested as $0.5f_y$ which decreases to $0.3f_y$ before the stress changes sign.

Shiomi & Kurata (1980) report on an experimental programme on tapered beam-columns which aimed at the characterization of the structural behaviour of such members for the development of a design formulation. The experimental programme covered 24 full-scale beam-columns with and without lateral restraints and discrete measurements of the residual stresses for three members. The nominal yield stress of the steel was 235 MPa. Before testing the initial out-of-straightness was measured for all members. It was found that for flanges and web taper members, a decrease of the residual compression stress of the flange and an increase in the residual compression stress of the web as the web depth and flange width decreased was noted. The authors also report that the constant width flanges did not exhibit any dependence on the change of the web height.

Experiments and design method for tapered and haunched beams were reported by *Horne et al.* (1979), focussed on the development of plastic design rules for pitched-roof portal frames. Hence, to reflect the realistic case of inclined rafters under gravity loading, the test specimens were supported at intervals along the tension flange. The objective of the experimental programme was to verify their ability to undergo plastic deformation without major loss in the bending moment resistance. The experimental programme consisted of eight haunched beams subject to equal end bending moments and three tapered beams subject to moment gradient such that the plastic moment at the shallow end was achieved and the deeper end was close to yielding. The maximum height of the profiles considered was about 300 mm. The material

properties were characterized by tensile tests, the measured yield stress was around 300 MPa and the actual plastic bending moment resistance was obtained from two control tests. The resulting design procedure led to the definition of a stable length (*Simões da Silva et al.,* 2014) but it was too specific for general application to tapered members. It was also emphasized that the compressive residual stresses induce premature yielding and local buckling of the compression flange.

Salter et al. (1980) carried out tests on web-tapered steel columns. The specimens were loaded in axial compression and major axis bending moment. In total, eight tests were performed. In three of the tests, lateral restraint was provided to one flange at mid-height. The specimens were about half to one third of their full size. The shallow section dimensions were approximately h_s=125 mm or h_s=100 mm, the flange width and b=100 mm or b=90 mm; the flange thickness was t_f=6.4 mm or t_f=4.7 mm; and the web thickness was t_w=4.7 mm. The members were designed using four different taper ratios: 2, 2.2, 2.4 and 2.5. The material properties were determined after testing of the main specimens. The measured yield stress varied between 315 and 335 MPa. The initial out-of-straightness was measured only for the minor column axis. The imperfections were very high: only 1 of 8 measurements was lower than the tolerance of L/750 in EN1090-2 (2011). The residual stresses were measured. However, the paper only reports only on the conclusions. *Salter et al.* (1980) have adopted the pattern proposed in *Young & Robinson* (1975). The test results were compared with numerical non-linear analyses for which good agreement was reported. Regarding the code estimations for the resistance of such columns, the authors conclude that they are safe sided with possibility for improvement.

In the scope of the European project *Lateral-torsional Buckling in Steel and Composite Beams* (2002) on the lateral-torsional buckling of steel and composite beams, seven tests on web-tapered steel beams were carried out. They have measured the sweep on both flanges of the tapered beams. The beams were executed by welding of steel plates in steel grade S355. The material properties were determined by tensile coupon tests for all members. The tested specimens had two tapering ratios 2 and 3, with the same shallow section, a built-up I 300x180x10x8. The tests are well-documented and reported in the project deliverable. The experimental results were then used for the validation of design rules.

3.2.2 Member imperfections

In this section, similar studies on the member imperfections for welded prismatic members are summarized.

Avent & Wells (1982) carried out an experimental programme on seven welded prismatic columns. The columns were tested under axial compression; prior to the main tests, residual stresses (seven measurements), initial geometrical imperfections and material properties were determined. The tested specimens ranged from 229 to 610 mm depths, the flange widths were 127, 152 or 205 mm, the flange thicknesses were 5.6, 6.4 or 9.5 mm and the web thicknesses 3.2 or 4.8 mm. The nominal yield stress was 50 ksi (345 MPa equivalent), with the tensile tests revealing a lower grade for the flanges of 2 columns. For the material imperfections, it is reported that the value of the flange tip compressive residual stress could be approximated with $f_y/2$. It is also proposed that the change in the compressive region occurs approximately at 0.15 of the flange width at $f_y/3$, identical to the pattern proposed by *Prawel et al.* (1974).

Fukumoto & Itoh (1981) summarized a statistical assessment of experiments performed on prismatic welded beams. The study aimed at the characterization of the lateral-torsional buckling stability of these beams as a follow-up to a similar study on rolled beams. It covered 34 tests on residual stresses of welded beams with I cross-section (250x100x6x8 mm). The material properties were determined for the web and flanges separately for the steel with a nominal yield stress of 235 MPa, resulting in $f_{yw,m}$=337.7 MPa and $f_{yf,m}$=283.5 MPa, respectively. The results are reported as statistical indicators. They also performed a statistical characterization of the geometrical imperfection of 68 welded prismatic beams. *Fukumoto & Itoh* (1981) report only on statistical parameters and distribution, the individual results are not presented. The statistics are provided for both major and minor axis out-of-straightness as well as for the twist. The mean values obtained for the major and minor axis are 0.000125(1/8000) and 0.000296 (1/3378) respectively with coefficients of variation of 92% and 81%. The goodness-of-fit was verified by χ^2 and Kolmogorov-Smirnov for Weibull model are of close fit with the measured values by the authors.

Chernenko & Kennedy (1991) carried out a numerical assessment on the buckling behaviour of welded wide flange columns. Their assessment was based on statistical data collected from earlier studies. They proposed a residual stress pattern which has the maximum tensile stress in the flange-to-web junction, varying from 80 % to 100 % of the yield stress while the tension at the flange tips varies from 50 % to 82 % of the yield stress. Regarding the compressive stresses,

their variation in the flanges is between 28 % and 40 %. The out-of-straightness is also discussed in the paper. Furthermore, *Chernenko & Kennedy* (1991) provide statistics on the out-of-straightness based on measurements collected during a site visit at Algoma Steel in Sault Site. Marie, Ontario and also from the company's quality assurance files. Regarding the camber, the mean value was 0.00053 (1/1890) with coefficient of variation of 30.7%. They collected data on the sweep as well, total of 11 measurements with a mean value of 0.000293 (1/3413) and a coefficient of variation of 52.5%. *Chernenko & Kennedy* (1991) point out that no measurements below the tolerance of L/1000 are rarely recorded, because of the additional straightening of the members which develop excessive camber. The camber is reported to be more severe than the sweep of these columns. The large coefficient of variation of the samples is explained by the order of the imperfections (very small). The authors did not recommend suitable distribution that fits the measured data.

3.3 Experimental programme

3.3.1 Scope

The experiments were performed in the framework of the research project TAPERSTEEL PTDC/ECM-EST/1970/2012. Its objective was to study the stability behaviour of non-uniform steel members. The experimental programme covered flexural buckling of columns under uniform compression, lateral-torsional buckling of non-uniform beams under linearly varying bending moment and lateral-torsional buckling of beam-columns loaded with major axis bending moment and uniform compressive force.

All specimens were web-tapered, with different tapering ratios, and two different shape configurations were used: i) different inclination of each flange with respect to the centroid of the beam (shape L Figure 3.1*a*); ii) the equal flange inclination with respect to its centroidal axis (shape V Figure 3.1*b*). The nominal dimensions of the tested members are summarized in *Table 3.1*. The test specimens were fabricated by welding of hot-rolled steel plates fabricated according to EN 10025-2:2004. The steel grade of these steel plates is S355 and the steel quality is JR. The steel grade of all additional plates used to fabricate the hinges is the same or higher and the steel used for the pins and bolts (M30, Grade A, EN 15048-1 and EN ISO 4017) is high strength steel, class 8.8. The nuts and washers required for the bolts are also Grade A, in accordance with the standards EN ISO 4032 and EN ISO 7089, respectively.

Table 3.1. Experimental programme

Member	γ_h	Shape	h_{min}	h_{max}	b	t_w	t_f	L
-	-		mm	mm	mm	mm	mm	m
C1	4	V	120	480	100	12	12	6
C2	2	V	185	370	110	6	12	6
C3	3	L	120	360	100	10	16	6
B1	4	L	250	1000	200	15	16	4
B2	4	L	250	1000	200	6	16	4
BC	3	L	120	360	100	10	16	6

Figure 3.1– a) "L"-shape tapered member; b) "V"-shape tapered member

All member dimensions were measured prior to the tests. The material properties were determined by tensile coupon tests, six coupons were milled from each specimen. The geometrical imperfections (out-of straightness) were measured for all members, for B1 and B2 advanced laser measurement was used, as for C1-C3 and BC the imperfections were measured manually. The residual stresses were measured for specimens C1, C2, C3 and BC using the sectioning method.

The experimental part related to the beams was also part of the Master thesis of *Rodrigues* (2016).

In the following sections, firstly the test set-ups by member type are presented, then the loading conditions are explained and finally a brief summary of the results recorded during each test is presented.

3.3.2   Column tests

The column specimens were designed aiming for the assessment of their in-plane flexural buckling resistance; as a second objective, it was intended to study different variations of the cross-section class along the member length. *Table 3.2* and *Figure 3.4* summarize the variation of the cross-section class along the member length (L) for the three specimens. For C1 approximately 18% of the member was in class 4, for C2 86% and 5% for C3, respectively.

Table 3.2 Cross-section classification of column members.

Cross-section class	Column 1	Column 2	Column 3
1	[0; 0.59L]	-	[0; 0.67L]
2	(0.59L; 0.71L]	[0; 0.05L]	(0.67L; 0.83L]
3	(0.71L; 0.82L]	(0.05L; 0.14L]	(0.83L; 0.95L]
4	(0.82L; L]	(0.14L; L]	(0.95L; L]
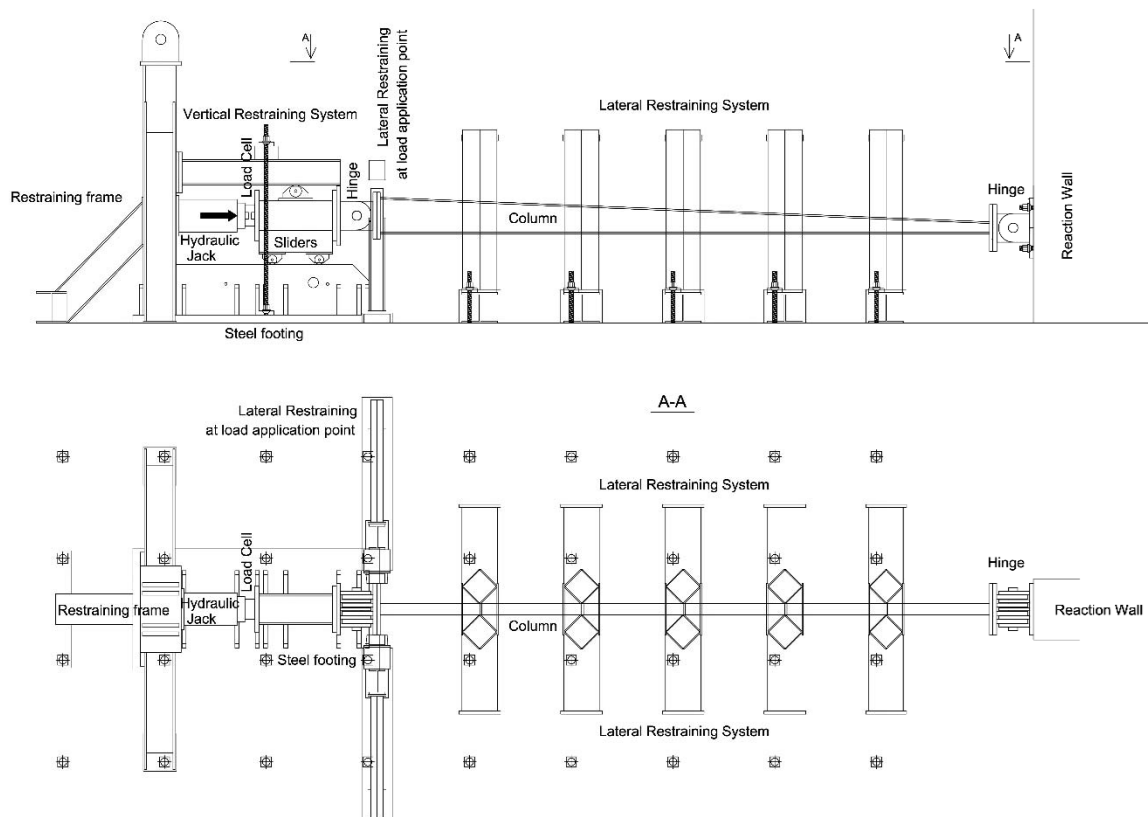
Figure 3.2 - Test layout, Column 3 (and identical for the other columns)

The tested specimens had different taper ratios (2, 3 and 4, respectively), but the same length of 6 m. The three columns were tested using the layout shown in *Figure 3.2*. They were simply supported at both ends using pinned connections (*Figure 3.3a)*, which allowed the free rotation in the plane of the column. At the point of load application, the vertical and transversal movements of the columns were restrained (*Figure 3.3b)*. The global out-of-plane buckling was prevented by the implementation of lateral restraints at each meter length of the column (5 in total), *Figure 3.3c*.

The lateral restraints along each member were implemented using vertical SHS 250x10 profiles rotated by 45º with the edge aligned with the members' top and bottom flanges (*Figure 3.3c*). The SHS 250x10 profiles are connected at their bases to a horizontal profile attached to the strong floor and at their top welded to a plate connecting both sides.

| Pinned connection | b) Lateral bracing at support | c) Lateral restraints |

Figure 3.3 Supports

Strains were measured using strain-gauges type FLA-6-11 glued to the web and the flanges. On the web, they were positioned along vertical lines (3 or 4 at each cross-section), and three strain gauges on each flange (top and bottom). For the measurement of vertical and lateral displacements during the experiment, LVDTs (linear variable differential transducers) were installed at several locations along the columns, their position for the three column specimens is shown in *Figure 3.4*. The positions of measurement of vertical displacements are marked with *V* and the horizontal with *H*, respectively.
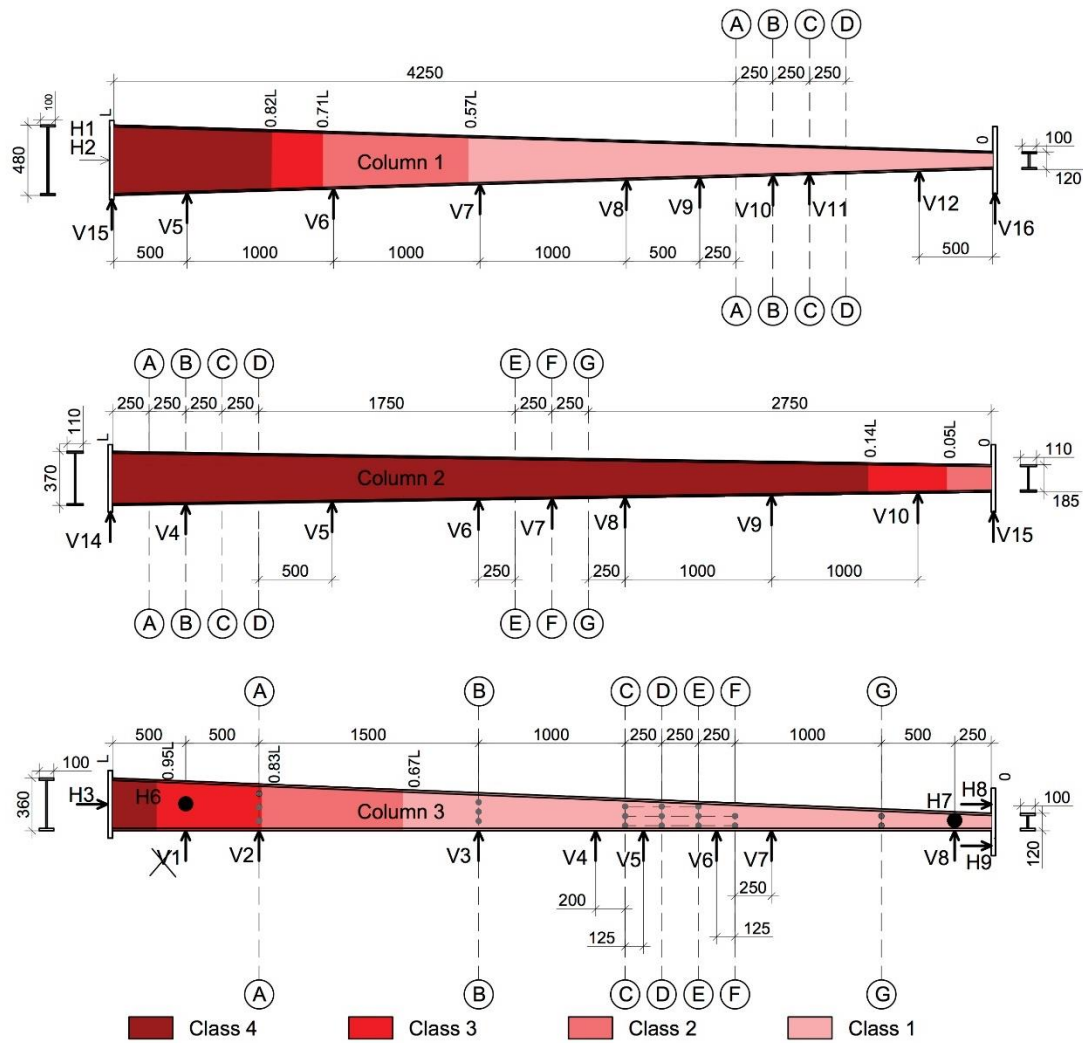
Figure 3.4 - Plan of LVDTs and strain gauges

3.3.3   Beam tests

Two beam tests were performed. Their shape was chosen to resemble part of a simply supported tapered beam, having the shorter flange in compression. Real examples are shown in *Figure 3.5*.

The test set-up is shown on *Figure 3.6,* where the tested non-uniform specimens were fabricated with an uniform cantilever segment, which served for load application. The bending moment at the deepest cross-section was achieved through a concentrated force applied at the end of the cantilever part (*Figure 3.6*). Hence, the beams were designed with variable cross-section in their first 4 meters of length and 1.8 meters of uniform cantilever section serving for the load application, *Figure 3.6*.

Bullring Shopping Centre, Birmingham

http://www.newsteelconstruction.com/wp/the-new-bullring-shopping-centre/
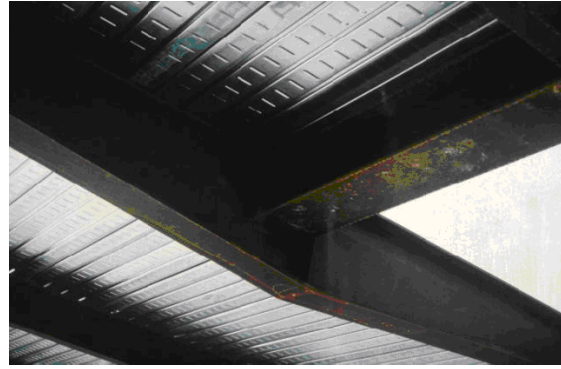
Tapered girder supporting steel decking

http://www.steelconstruction.info/Long-span_beams

Figure 3.5 – Web-tapered steel girders

The two specimens have identical cross-section with respect to depth, flange widths and flange thickness. The web thickness varies from 15 mm for Beam 1 (B1) and 6 mm for Beam 2 (B2) (see *Table 3.1*). The ratio between the deep and shallow sections for both beams is defined by a taper ratio of y_h=4.

In addition, the cantilever uniform segment of B2 was reinforced with transverse web-stiffeners in order to avoid local cross-section effects in this part of the beam aimed exclusively for load application.
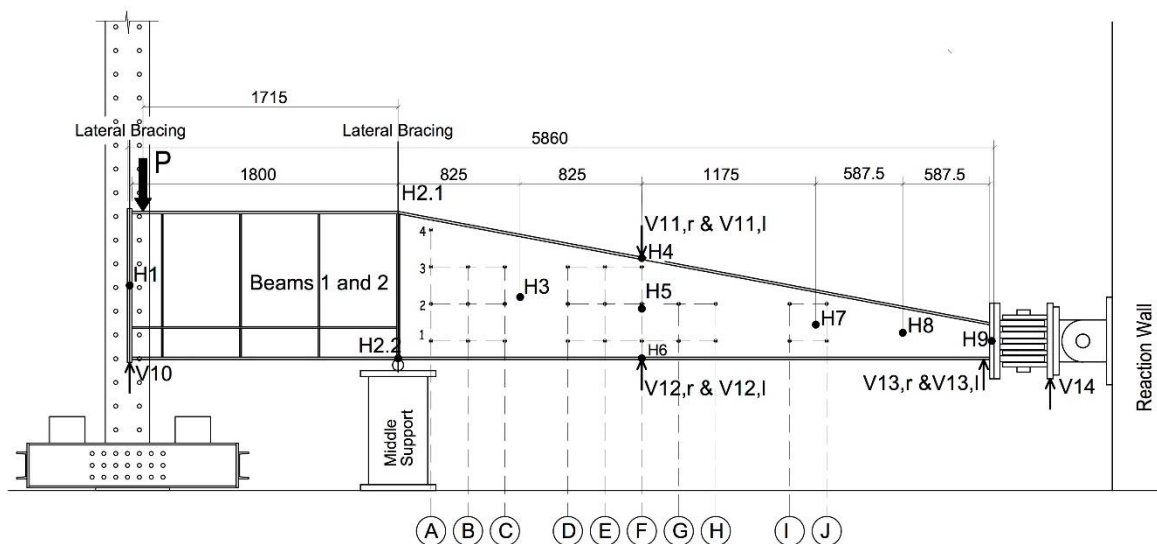
Figure 3.6 - Beams' test layout

It was intended to test the beams as simply supported, according to the test layout shown in *Figure 3.6*. At the shallow section, the beams were supported with bi-directional pinned connections, which allowed the free rotation in- and out-of-plane. At the intermediate support,

the vertical displacements were prevented as shown in *Figure 3.7a)*. The beams were laterally restrained at the point of load application and the intermediate support. The lateral braces used were coupled to roller-bearings, perpendicular to the free end (one roller-bearing on each side) (*Figure 3.7b*) and parallel to the intermediate support elements (two roller-bearings on each side), preventing twisting of the beam (*Figure 3.7c*).

Figure 3.7 - Support conditions beam tests: a) intermediate support; b) Lateral restraint at the free end; c)Lateral restraint at the intermediate support

The load was applied as a point load on the top flange of the beam 85 mm away from the end of the cantilever part.

Strains were measured using strain-gauges type FLA-6-11 glued to the web and the flanges. On the web, they were positioned in a quadratic mesh, and three strain gauges on each flange (top and bottom) at axes B, F and I, as shown in *Figure 3.6*.

For the measurement of vertical and lateral displacements during the experiment, LVDTs were installed at several locations along the beams. The horizontal (out-of-plane) displacements were recorded on the centroidal beam axis designated as *H3*, *H5*, *H7*, *H8* and H9 in *Figure 3.6*. In addition, on axis F, the out-of-plane displacements were measured at the top and bottom flanges. Additional measurements were obtained at the supports, in order to ensure the desired functionality of the implemented layout: at the intermediate support *H2.1* and *H2.2* measured the out-of-plane displacements for the top and bottom flanges, respectively and *H1* was measured at the point of load application.

The vertical displacements were also recorded at several locations. At the expected critical location (axis F) they were monitored on both flange tips for the top (in $V_{11,l}$ and $V_{11,r}$) and

bottom (in $V_{12,l}$ and $V_{12,r}$) flanges, at the shallow section $V_{13,l}$ and $V_{13,r}$. V_{10} measured the vertical displacement at the point of load application and V_{14} between the two pins.

3.3.4 Beam-column test

For the validation of the beam-column behaviour, the last test performed was on a member loaded in bending and compression. The specimen had the exact same dimensions as column C3. In this experiment, it was meant to validate the lateral-torsional buckling of a beam-column loaded with axial force and major axis bending moment. The load was applied with eccentricity (*Figure 3.8*), allowing for proportional increase of the bending moment and the axial force. The test layout is shown on *Figure 3.9*, where the member was restrained laterally at mid-span. At the shallow end, the specimen was connected to the reaction wall through a pinned connection, which allowed free rotation out-of-plane. At the deepest section where there was a welded cantilever section which served for the load application, it was vertically and laterally restrained.
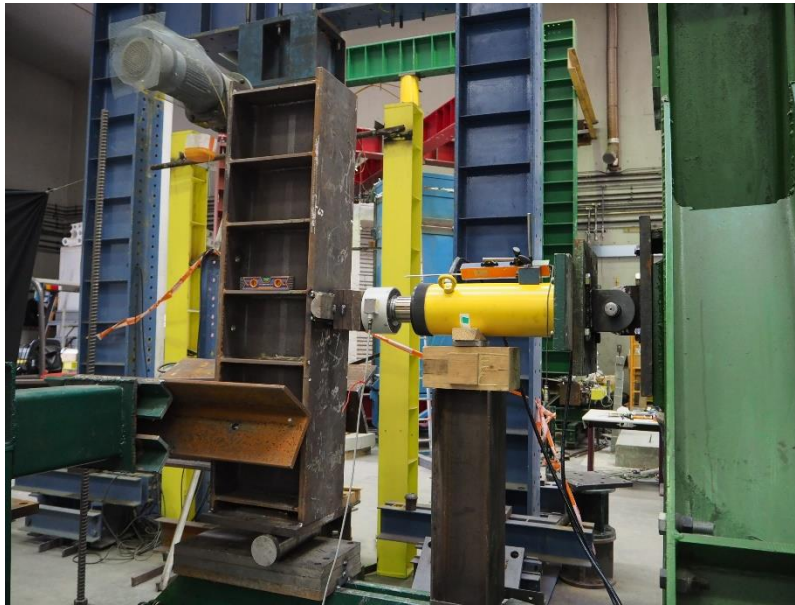
Figure 3.8 Point of load application

The vertical and horizontal displacements were measured at each meter of length of the member (*V1* to *V5* and *H2, H4, H7, H9*). Additional measurements were obtained at the expected critical locations at axis B and E, where the horizontal displacements were measured at the level of the flanges as well.
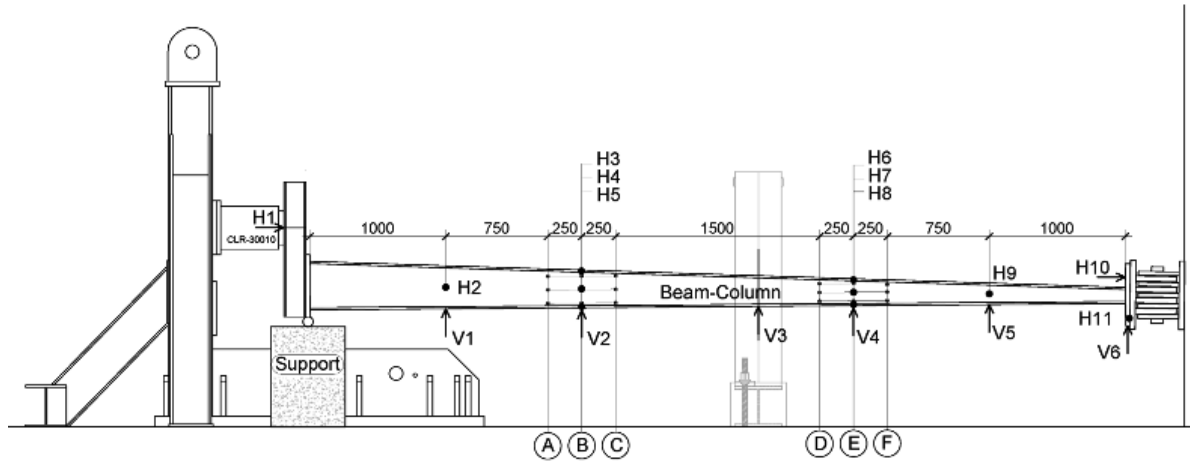
Figure 3.9 Test layout

3.3.5 Loading protocol

For each specimen, the loading was divided into two stages: firstly, a cycle of loading and unloading (in the elastic range) was applied and, in the second stage, the columns were loaded until failure.

Table 3.3 Loading protocol

Specimen	Load → Unload Cycles[kN]				1st phase	2nd phase
	1	2	3	4	kN/s	mm/s
C1	0 → 600 → 5				0.5	0.003
C2	0 → 400 → 5				0.5	0.003
B1	0→85→0	0→180→0	0→370→0	0→570→0	0.2	0.015
B2	0→65→0	0→130→0	0→260→0	0→400→0	0.2	0.015
C3	0 → 400 → 5				0.5	0.003
BC	0 → 50 → 5				0.25	0.0025

The first loading stage allowed for adjustments in the test layout (test specimen, hinges and reaction frame), and served for the elimination of initial gaps in the test layout. This initial stage also allowed to verify the functionality of the strain gauges, LVDT's and data logger.

In the first stage, the loading was applied in force control and in the second in displacement control. The speeds used in each test are given in *Table 3.3*.

For the beam tests four cycles of loading and unloading were performed. In the column tests, which were performed after the beam tests, it was considered sufficient to carry on only one cycle of loading and unloading.

The magnitude of each peak load was chosen as a percentage of the initially estimated beam/column resistance (maximum of 60%).

3.4 Experimental results

3.4.1 Complementary tests

3.4.1.1 Material properties

The complete characterization of the experiments requires the determination of the actual material properties. For that, standard coupons were extracted from each specimen and tested in tension. A total of six coupons were milled from each specimen: three from flanges and three from the webs, according to EN ISO 377 and ISO 6892-1. The value of the yield stress f_y is taken as the upper yield strength R_{eH} and the tensile strength R_m. is used for the ultimate strength f_u.

Table 3.4 - Mechanical properties of steel from of coupons tests for C1, C2, C3 and BC

Specimen	C1	C2		C3	
Location	-	flange	web	flange	web
f_y	376.7	371.3	362.1	385.5	450.8
f_u	570.3	571.0	507.4	535.4	595.3
E	208.1	213.1		206.0	

The yield and ultimate stresses are reported for each specimen according to the plate thickness, i.e. for specimens having different thicknesses in the web and in the flanges, the results are reported separately. The Young's modulus is calculated as an average from all tests performed per specimen. The results are summarized in *Table 3.4.*

Table 3.5 - Mechanical properties of steel from of coupons tests for B1 and B2

Specimen	B1		B2		BC	
Location	flange	web	flange	web	flange	web
f_y	421.4	422.7	405.3	388.4	391.9	443.1
f_u	552.9	543.7	551.1	526.7	540.4	588.8
E	208.4		203.9		210.2	

3.4.1.2 Measurement of geometrical imperfections

Geometrical imperfections are one of the most important features determining the global stability behaviour of beams and columns. They may be of different nature (*Figure 3.10*) and may have different impact on the buckling behaviour of steel members. For each member, the depths of the deep and shallow cross-sections were measured as well as the web and flange thicknesses at various locations along the member length.
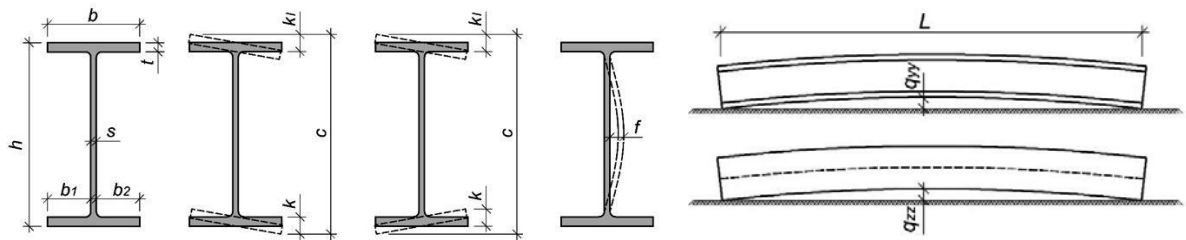
Figure 3.10 Geometrical imperfections

The imperfections were measured for both beams using the advanced measurement system *ROBOT Romer F-41800 Montoire,* as shown in *Figure 3.11*. The measurement procedure gives a map where the local deviations from the nominal geometry can be clearly seen.

The measurement on Beam 1 does not show any considerable local deformation in the web, besides the corner at the change of the cross-section with magnitudes of about 2.5 mm. However, this section falls in the zone of the support, and so it is not expected to influence the behaviour.

Figure 3.11 - Geometrical imperfections: a) Laser system used; b) 3D model

The maps for both beams are presented in *Figure 3.12*.
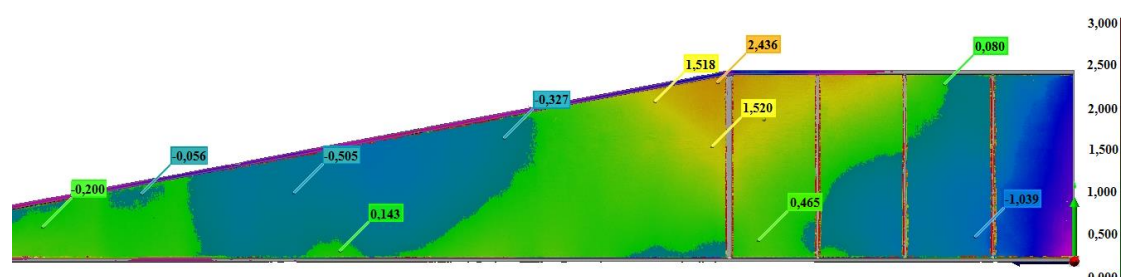
a)   Test B1
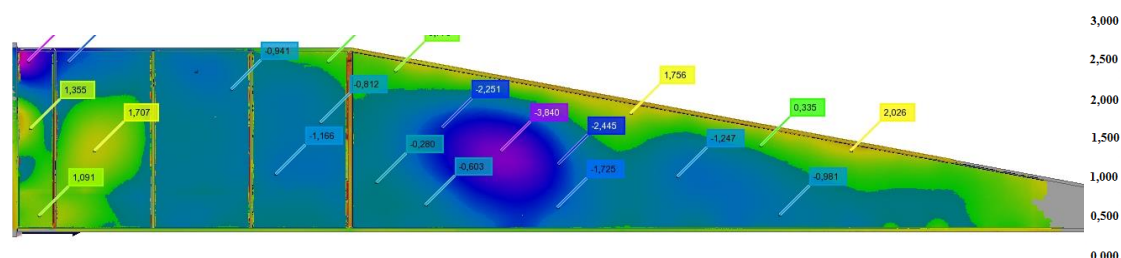
b)   Test B2

Figure 3.12 - Amplitudes of the geometric imperfections measured by the laser system

Regarding the initial out-of-plane deformation of Beam 1, the upper flange has a global deformation with a maximum amplitude of about 3.75 mm; the measurements of the deformation of the bottom flange are inconclusive. The initial out-of-plane deformation of Beam 2 revealed high local deformations of 3.85 mm between axes C and D. The maximum global out-of-plane imperfection of the tension flange is approximately 3 mm and in the bottom flange it is found to be of a smaller magnitude of about 1.5mm.

The columns measurement procedure involved a "low mass" nylon string which was tied to two nuts at the member's extremities and it was stretched to its maximum. The distance of the string to the member was then measured at each 0.50 m length. To obtain the magnitude of the imperfection the nuts height was subtracted. The measurement was performed for three lines

along the member web and one for each flange. The magnitude of the geometrical imperfection was considered as an average of the measurements.

Even though it is not an advanced measurement method, it allows for an initial idea of the magnitude the imperfections to be used in the numerical models.

The average results obtained for all members are shown on *Figure 3.13*.
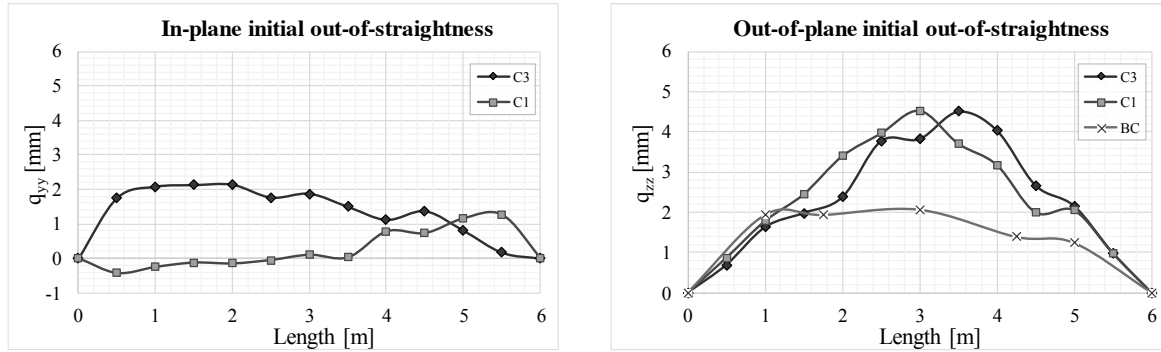
Figure 3.13 Initial out-of-straightness

3.4.1.1 Residual stresses

In order to completely characterize the behaviour of the tested specimens, residual stress measurements were also carried out for C1, C2, C3 and BC. The measurements were made on test pieces with dimensions representing different regions of the tapered columns and beam-columns corresponding to various taper ratios and depths (*Figure 3.14*). The approximate location of the column segments and the specimen dimensions are given in *Figure 3.15*. The length of the test pieces was chosen to be about 5 times the depth of the measurement cross-section in order to avoid any possible boundary effects in the measurement.
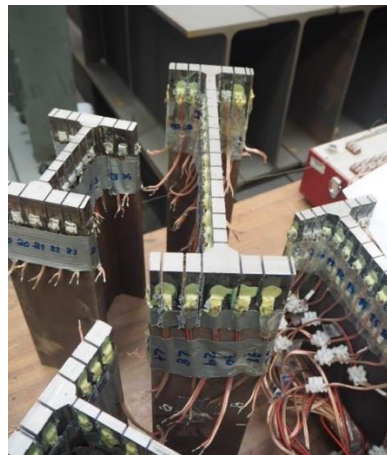
Figure 3.14 - Specimens after testing

Figure 3.16 shows the arrangement of strain gauges in each specimen. Electrical strain gauges (2x6 mm) manufactured by Tokyo Sokki Kenkyujo Co. Ltd. were used. Strain gauges were glued to both sides of the flanges and web of each specimen in order to calculate the average membrane stress afterwards. For specimens RS1 and RS5 strain gauges were glued also on the weld fillet. The test procedure followed the sectioning method *Tebedge et al.* (1973), which is a commonly adopted measurement procedure for structural engineering purposes *Spoorenberg et al.* (2010). The procedure involves longitudinal and transversal cuts which provoke the release of stresses locked in the test specimen, which in turn cause deformations. Then it is possible to record these deformations and transform them further into stresses using Hooke's law *Tebedge et al.* (1973).
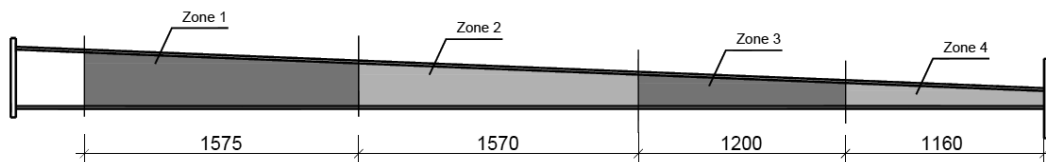
Figure 3.15 Location of specimens for the residual stress measurements
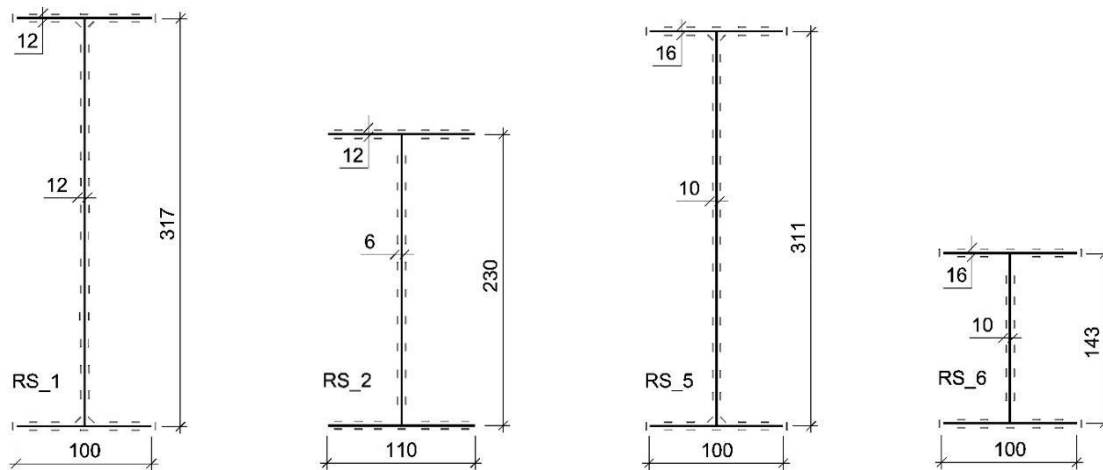
Figure 3.16 - Specimen dimensions and strain gauge arrangement

The cutting was performed using an electric band saw, which was continuously cooled by compressed air in order to avoid temperature disturbance of the measurement. The cutting sequence involved two transversal cuts as shown in *Figure 3.17* and then a series of longitudinal cuts, where the transverse cuts contributed to the largest part of the measured residual stresses. The data was continuously recorded during the experiment using data logger TML TDS 530

with extension box TML SSW-50D. The recording was terminated approximately 20 minutes after the last cut when no further fluctuations in the readings were noticed.

Figure 3.17 - Transversal and longitudinal cuts

The obtained measurements are given in *Figure 3.18* and *Figure 3.19*.
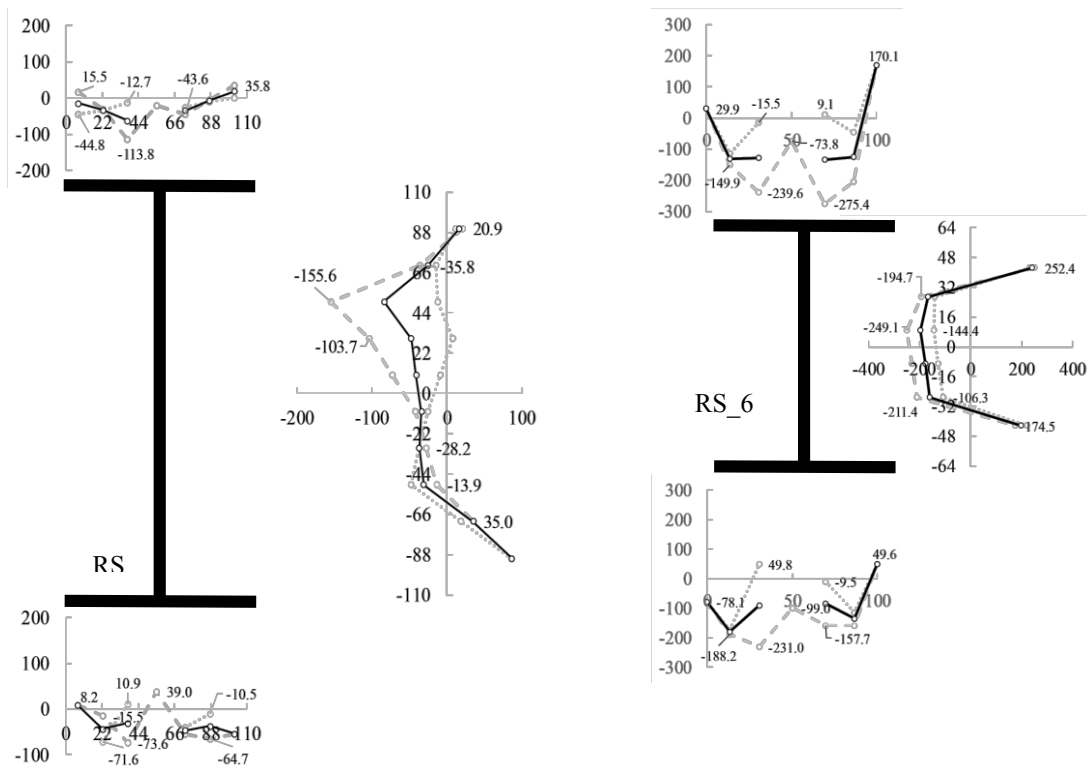
Figure 3.18 - Results for the welded specimens Column 2 and Beam-column in MPa

The measurements are further transformed in a non-dimensional form in *Figure 3.20*. The stress distribution for each section was normalized to the yield stress obtained from the tensile coupon tests. *Figure 3.20* shows that the peak tensile stress in the flanges varies from 0.3f_y up to the yield stress. The compression in the flange exhibits a maximum of 40 % of the yield stress,

although the majority of measurements it does not exceed 20 %. Furthermore, the variability of the residual stresses is assessed. For the tensile stresses, this assessment is based on the maximum values found in the flange-to-web junctions for both the flanges and the web. The residual compression is evaluated on the basis of an average compressive stress calculated by integration over the compression region for each outstand flange.
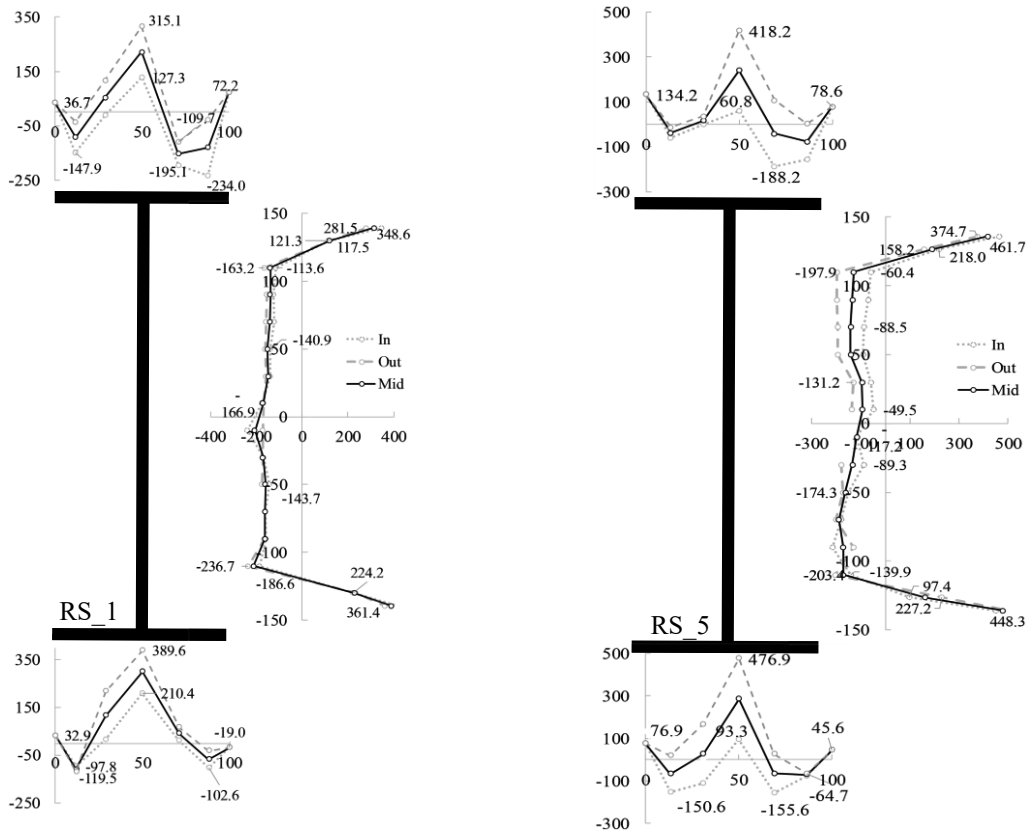
Figure 3.19 – Measured residual stresses for Column 1 and Column 3 in MPa

A histogram of the distribution of the compressive stress in the flanges is given in *Figure 3.21a* and the variation of the maximum tension is shown in *Figure 3.21b*. The statistical parameters are then summarized in *Table 3.6*.
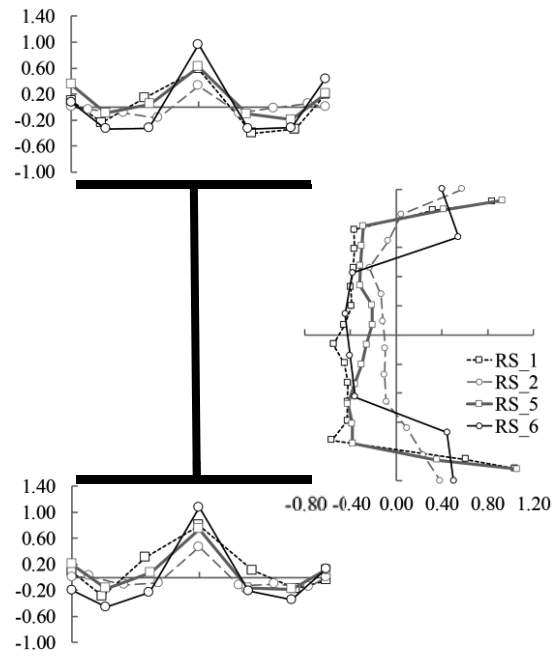
Figure 3.20 - Normalized residual stress distribution
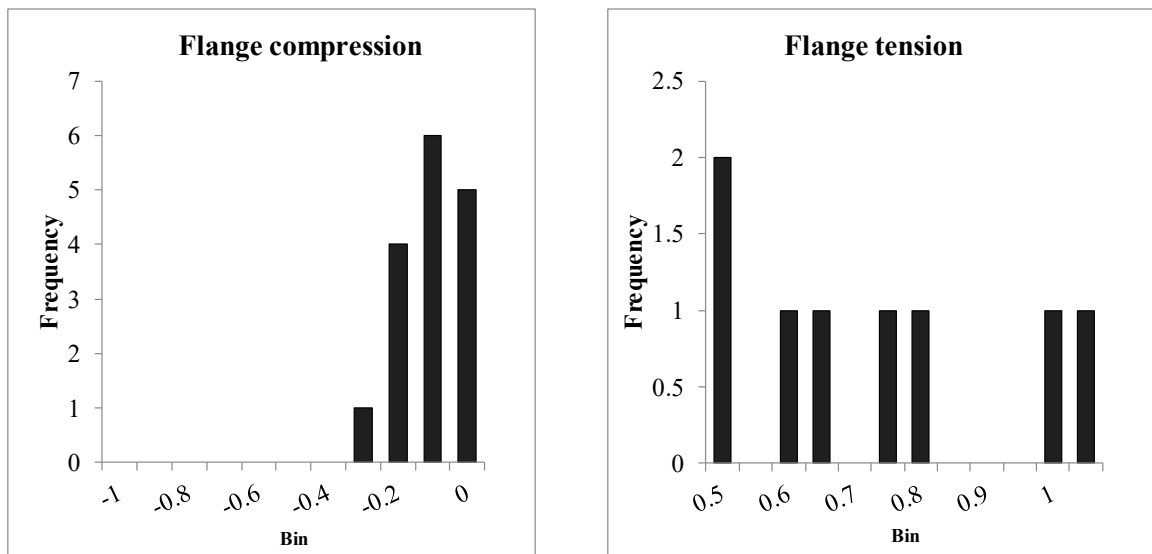
a)   *Average compression in the flanges*   b)   *Maximum tensile stress in the flanges*

Figure 3.21 - Histograms of the stress distributions in the flanges

Table 3.6 – Statistical parameters

-	Mean	St. dev.	C.o. V.	Min.	Max.
Flange compression	-0.15	0.09	0.62	-0.32	-0.01
Flange tension	0.70	0.25	0.36	0.32	1.07
Web compression	-0.29	0.125	0.43	-0.43	-0.13
Web tension	0.72	0.28	0.39	0.38	1.06

In the flanges, the average value of the compression is $-0.15f_y$ with a coefficient of variation of 62% and the average maximum tension is $0.7f_y$ with a coefficient of variation of 36%. For the web, the average compression is $-0.29f_y$ and the coefficient of variation is 43%, while the corresponding values for the maximum tension in the web-to-flange junction are $0.72f_y$ and 39%.

The mean value of the compression is about half of the ECCS pattern, even though there is a high variability. The residual tension in the flanges is also lower than the nominal value. In the web, the tension is slightly lower than the nominal and the compression is higher than the nominal. However, the residual stresses in the web are not as important for stability problems.

3.4.2 Column tests

3.4.2.1 Test C1

In this section, the results recorded during test C1 are summarized. The final deformation of the specimen is shown in *Figure 3.22*. Despite the large number of lateral restraints, C1 still buckled out-of-plane in between the lateral restraints almost simultaneously as it reached its in-plane resistance. Also, even though test C1 had a slender cross-section (cross-section class is 4 for 18% of its length), failure was driven by global rather than local instability phenomena.

The column's displacements and strains were monitored at several locations along the member length, aimed to facilitate the subsequent calibration of a numerical model and also to serve as control measurements in order to confirm the reliability of the results.

Figure 3.23 illustrates the load-displacement curve at the point of load application (H_1 and H_2). The maximum applied load during the experiment was 1397.6 kN. The loading was stopped when the applied force dropped to approximately P=1000kN.

Figure 3.22 Column 1 after the test
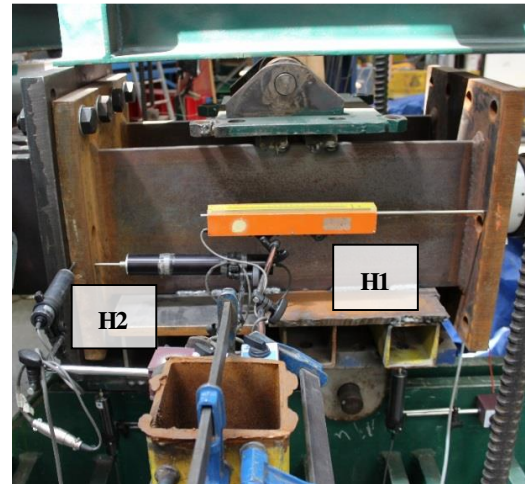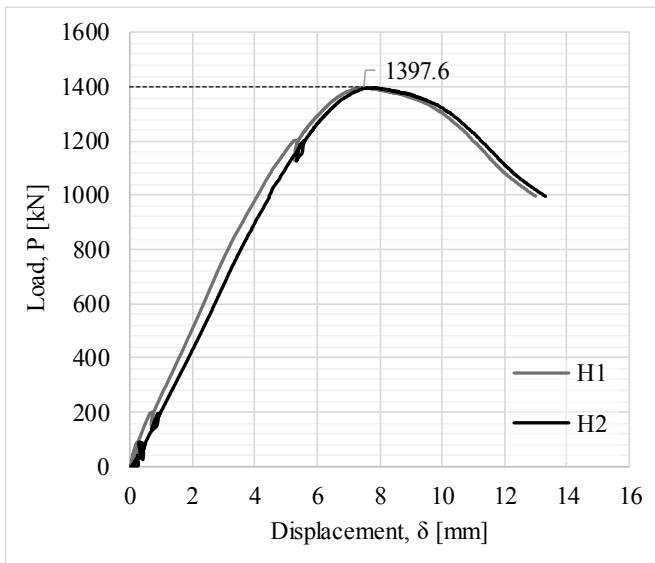
Figure 3.23 Load-displacement curves H_1 and H_2 for Column 1.

It is worth analyzing the vertical displacements along the column. *Figure 3.24* shows the evolution of the curvature at 200 kN intervals of loading at measurement points V_6 to V_{11}, V_{14} and V_{15}, until the maximum load $P_{ult,Exp}$ and after the maximum load was reached for two additional load steps. The amplification of the initially imperfect shape is clearly visible, which

is transformed at higher loads into the in-plane buckled shape. Yet, at the end of the experiment the out-of-plane deformations were more considerable than the in-plane ones.
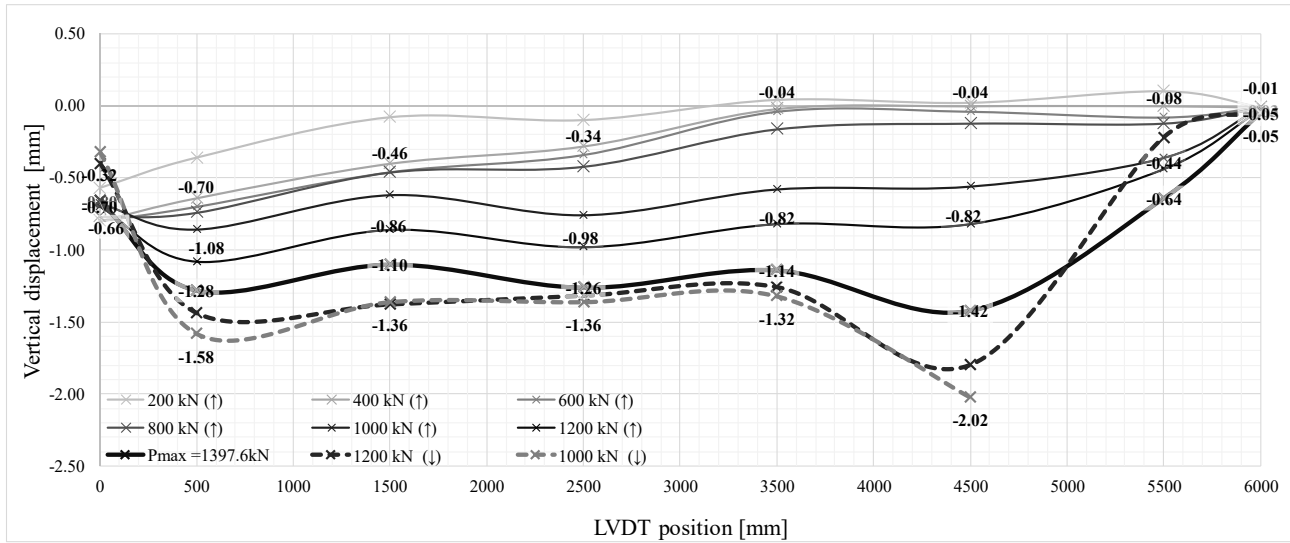
Figure 3.24 Variation of the vertical displacements along the length with increasing loading for test C1.
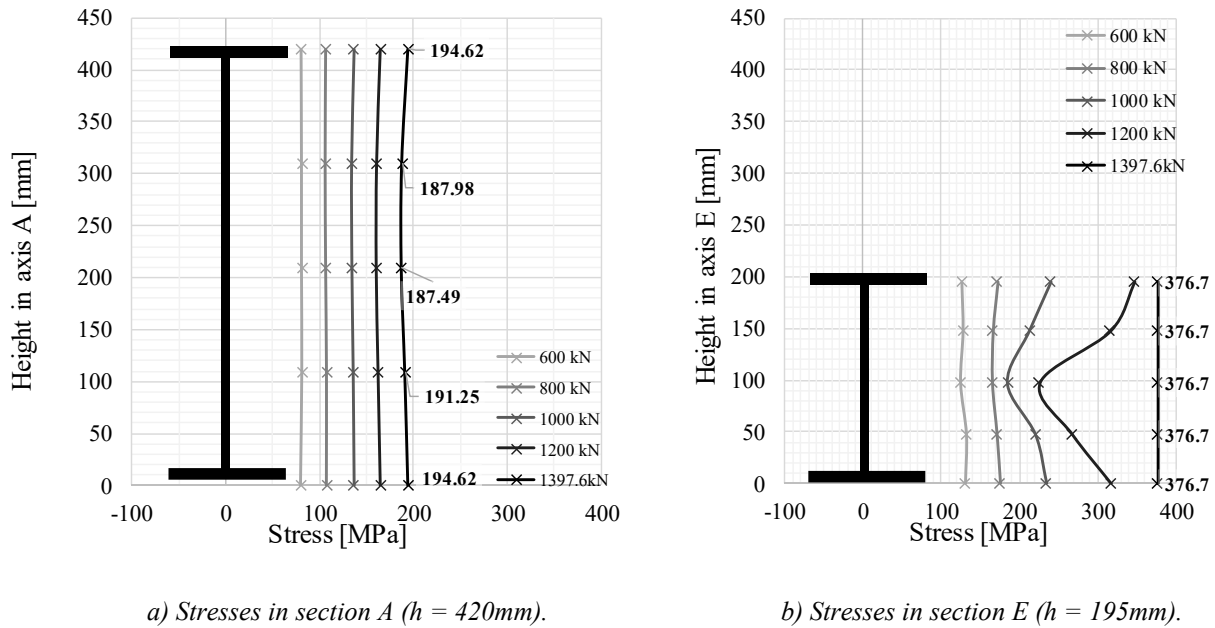
a) Stresses in section A (h = 420mm).   b) Stresses in section E (h = 195mm).

Figure 3.25 Stress distribution at sections A and E for various load levels

Furthermore, the stresses were also measured at several cross-sections along the member length. All strains were converted into stresses using the Young's modulus from *Table 3.4,* and since all stresses were in compression, a positive sign is used to represent them. Whenever the strains exceeded ε_y, the respective stresses were set equal to the measured yield stress.

The stress evolution for sections A and E are shown in *Figure 3.25*. Section A falls in the Class 3 region; nevertheless, the recorded stress distributions are purely elastic and far from the yield

limits given in *Table 3.4*. The other cross-section, at axis E, is in Class 1 and being smaller it was subject to higher stresses so that at the maximum load it was fully yielded.

3.4.2.2 Test C2

The second experiment, C2, was planned for an interaction between global and local buckling. In this case, similarly to C1, the column also buckled in between the lateral restraints. Since more than 85% of the member was in Class 4, it was also possible to observe local buckles on the web towards the deeper cross-section. *Figure 3.26* illustrates the failure of Column 2.

Figure 3.26 Collapse of C2

Figure 20 shows the load-displacement curve at the point of load application (*H₁* and *H₂*). The maximum applied load during the experiment was 1313.6 kN. The loading was stopped when the applied force dropped to approximately P=1000 kN.
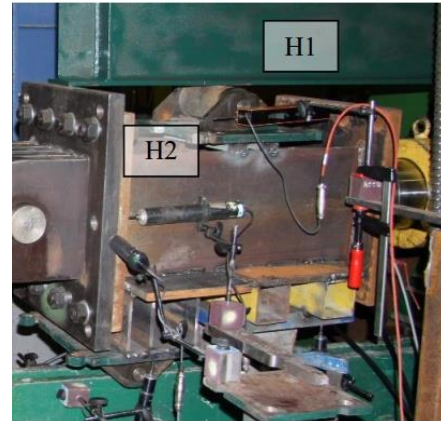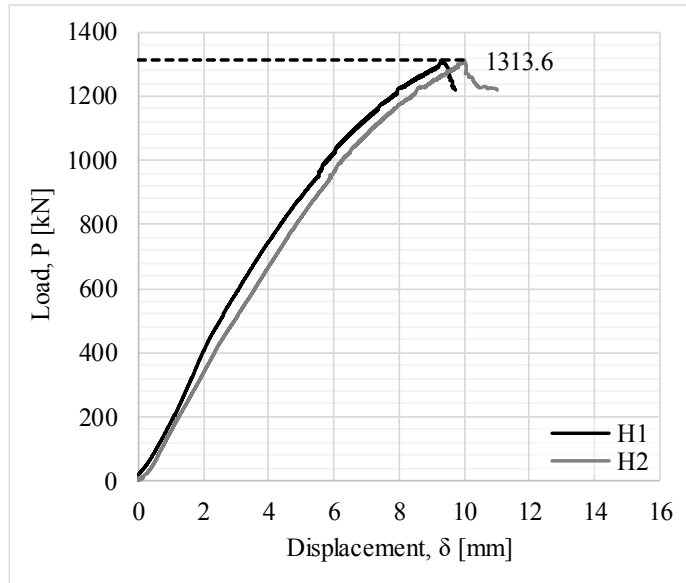
Figure 3.27 Load-displacement curves H_1 and H_2 for Column 2.
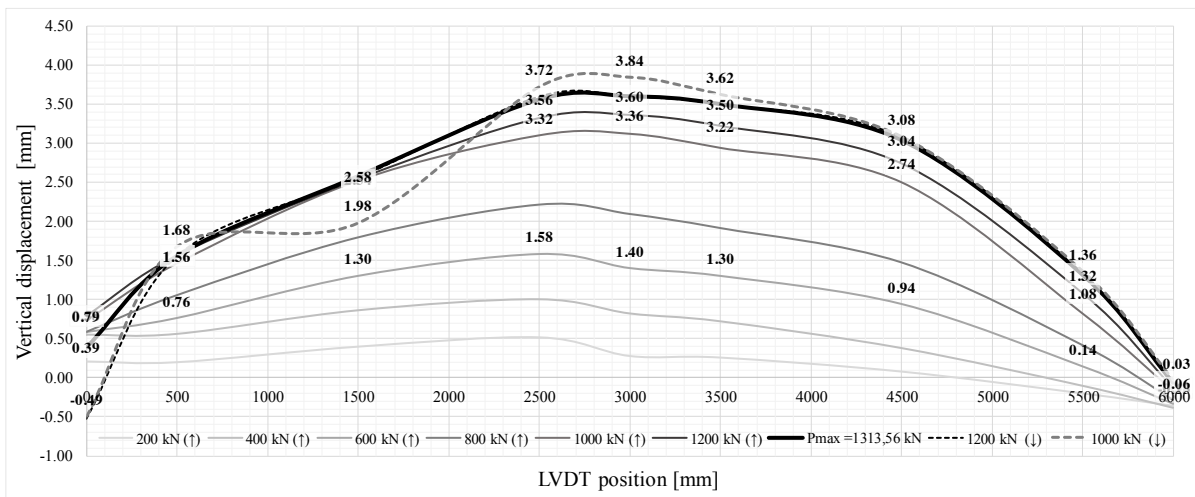
Figure 3.28 Variation of the vertical displacements along the length with increasing loading for test C2.

As in-plane buckling was the expected failure mode, the vertical deformations were measured at several locations for C2 as well. *Figure 3.28* shows the evolution of the curvature at 200 kN intervals of loading at measurement points V_4 to V_{10}, V_{13} and V_{14}, until the maximum load $P_{ult,Exp}$ and after the maximum load was reached for two additional load steps. In this case it is also possible to identify the amplification of the initially imperfect shape which is transformed at higher loads into the in-plane buckled shape. However, this increase at higher loads is found rather small, due to the fact that at the end of the buckled test the column buckled in between the lateral restraints.

a) Stresses in section B (h = 356mm).

b) Stresses in section F (h = 278mm).
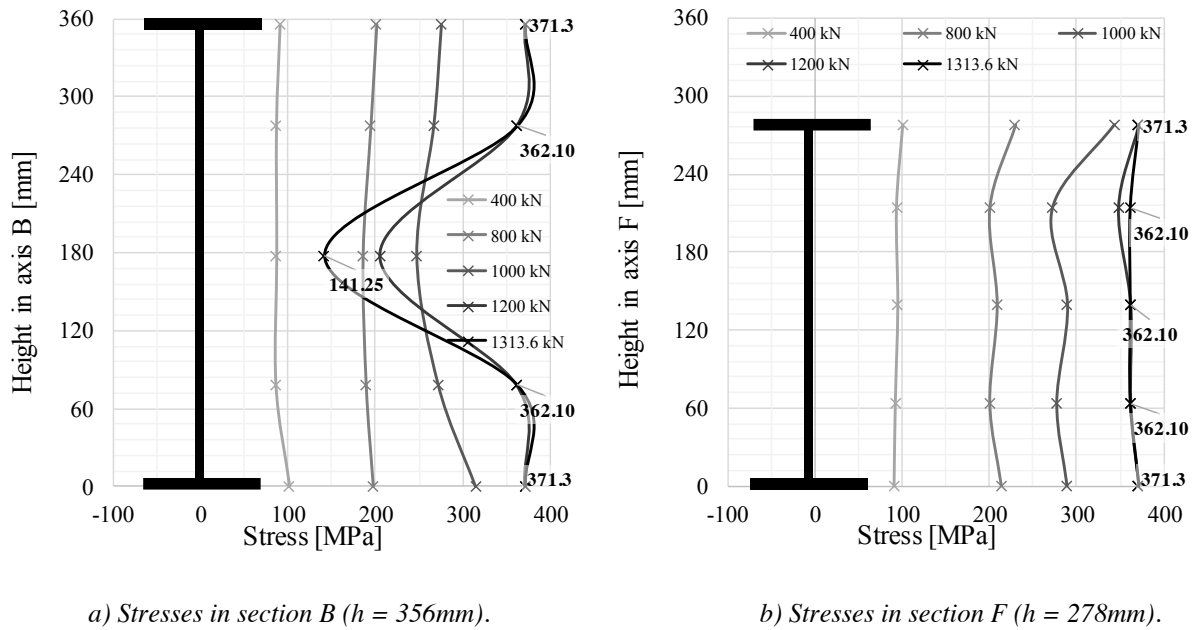
Figure 3.29 Stress distribution at sections B and F for various load levels

The stress evolution for sections B and F are shown in *Figure 3.29*. Section B falls in the Class 4 region, and the local buckling can be seen in the stress distribution for the load levels 1200 kN and the maximum 1313.6 kN. The other cross-section, at axis F, is also classified as Class 4, however closer to the limit with Class 3, and no local deformation were recorded.

3.4.2.3 Test C3

In this section, the results recorded during the test C3 are summarized. The final deformation of the specimen is shown in *Figure 3.30*. In this experiment, it was possible to observe distinct in-plane flexural buckling. The test C3 has a stocky cross-section (cross-section class is 4 for 5% of its length), failure was driven by global rather than local instability phenomena.

Figure 3.30 Column 3 after the experiment

Figure 3.31 illustrates the load-displacement curve at the point of load application (H_3 and H_2).
The maximum applied load during the experiment was 1460 kN. The loading was stopped after
the column buckled in-plane, which corresponded to a drop of the load to 800 kN.
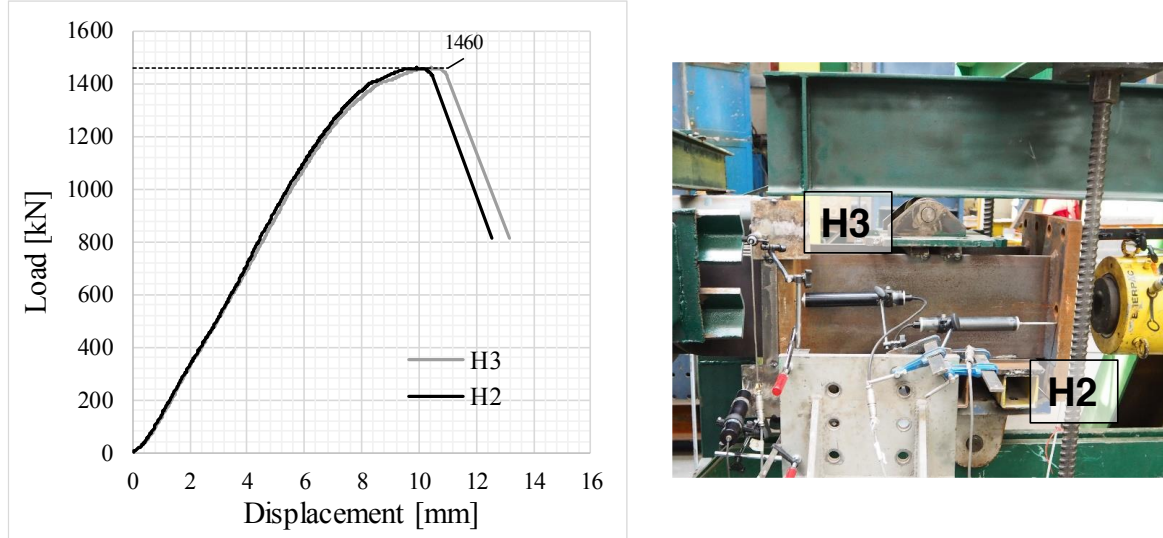
Figure 3.31 Load-displacement curves H₃ and H₂ for Column 3

Furthermore, *Figure 3.32* and *Figure 3.33* show the evolution of the curvature for various load
levels, where *Figure 3.33* illustrates the development of the in-plane displacements until the
maximum load was recorded. It is very similar to *Figure 3.24* and *Figure 3.28*, where for lower
load levels the shape amplifies the initially imperfect one. After the maximum load was
achieved, at a force of approximately 1460 kN, C3 buckled in-plane exhibiting an instantaneous
increase of the deformations, as shown in *Figure 3.33*.
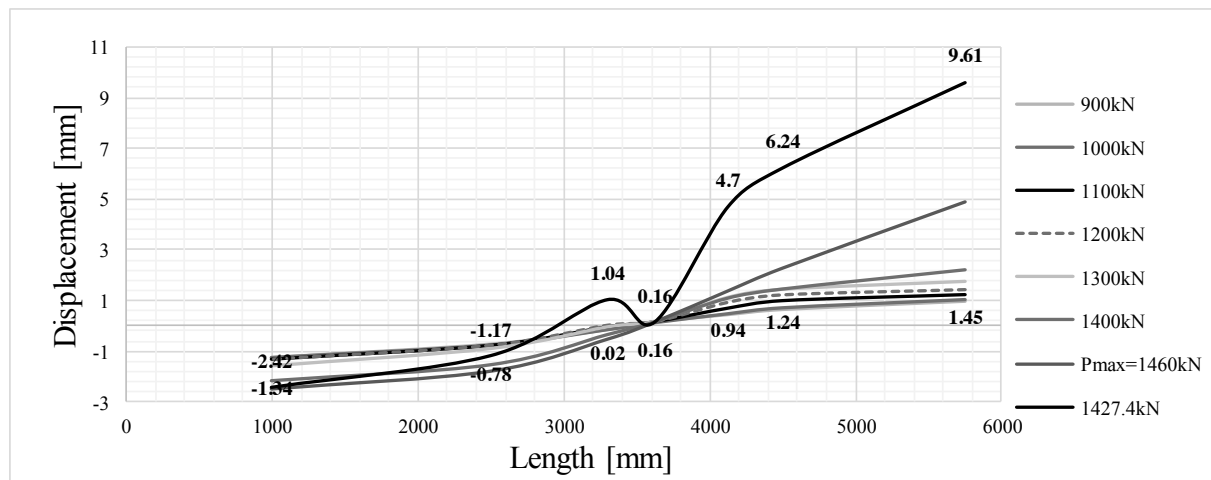
Figure 3.32 Variation of the vertical displacements along the length with increasing loading for test C1
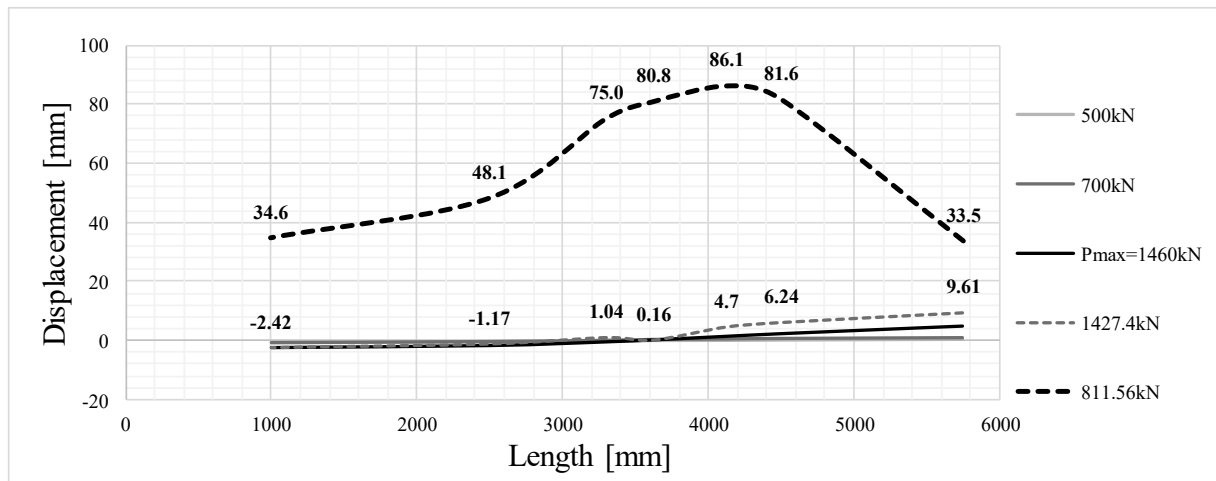
Figure 3.33 Variation of the vertical displacements along the length beyond the maximum load for test C3

The stress evolution for sections B and G are shown in *Figure 3.34*. Both cross-sections are in Class 1, no local buckling was registered neither observed during the experiment. However, in both cross-sections it is possible to observe the impact of the in-plane buckling behavior. For load levels up to the maximum load the member stresses are mostly in uniform compression; after the buckled position took place at 1427 kN the compressive stresses in the top flanges decrease and in Section G they even become tensile, due to the second order in-plane bending moment.

a) Stresses in section B (h=260 mm)

b) Stresses in section G (h=150 mm)
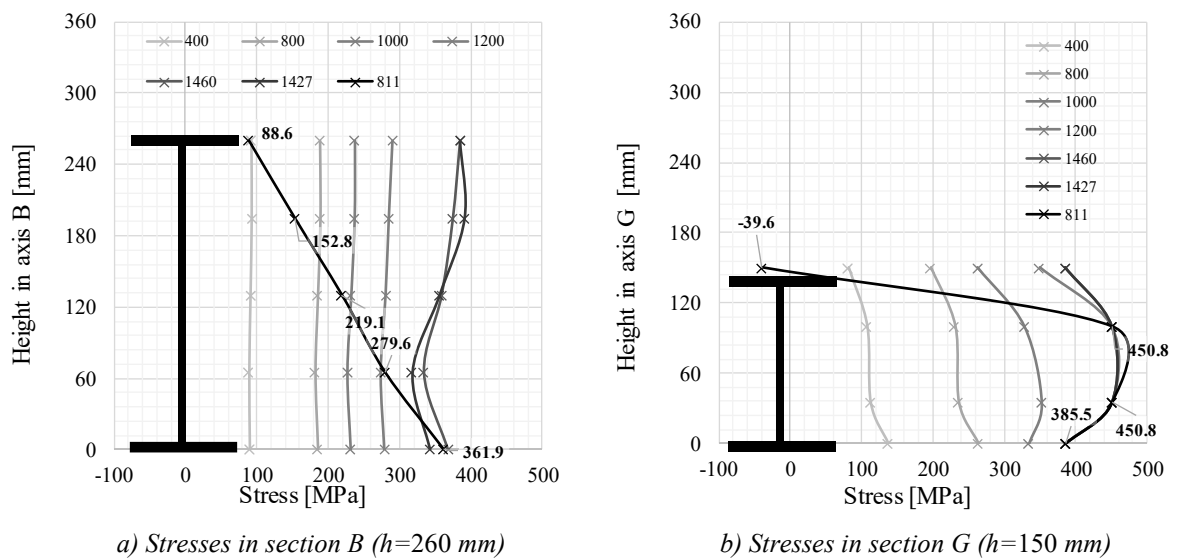
Figure 3.34 Stress distribution at sections B and G for various load levels

3.4.3 Beam tests

3.4.3.1 Test B1

In this section, the results recorded during test B1 are presented. The final deformation of the specimen is shown in *Figure 3.35*; as expected, it collapsed in lateral-torsional buckling. Also, as test B1 has a stocky cross-section (cross-section class is 1 for almost 90% of its length), failure was driven by global rather than local instability phenomena.

The beam's displacements and strains were monitored at several locations along the member length, aimed to facilitate the subsequent calibration of a numerical model and also to serve as control measurements in order to confirm the reliability of the results.

Figure 3.36 illustrates the load-displacement curve at the point of load application (V_{10}). The maximum applied load during the experiment was 1205 kN. The loading was stopped when a 20% drop in the applied force was approximately registered. After the maximum load was reached, for P=1113 kN, an abrupt load decrease caused by brittle failure of the weld at the top web-flange connection near to the intermediate support section was recorded. Hence, the experimental results are considered only until this load (see *Figure 3.36*).

Figure 3.35 - Collapse mode of test B1

The stresses at the cross-sections in axes A and F are plotted in *Figure 3.37* for the initial load cycles. The resulting stresses are clearly below the yield strength of the beam and thus confirm that the initial assumption for the load cycles that were performed in the elastic range. Furthermore, the development of stresses is illustrated in *Figure 3.38* for $0.7P_{u,exp}$, $0.8P_{u,exp}$ and $0.9P_{u,exp}$ (before collapse) and for $P_{u,exp}$. The deviation from a straight line is clear for both sections thus indicating the development of plastic strains at these sections.
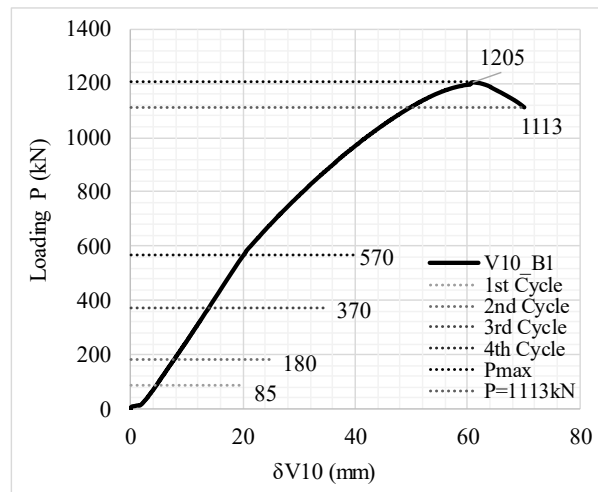
Figure 3.36 – Load-displacement curve at V10, Beam 1
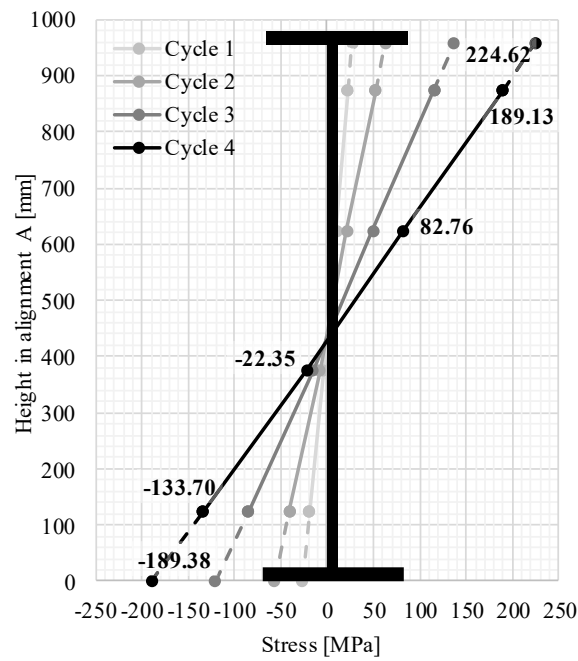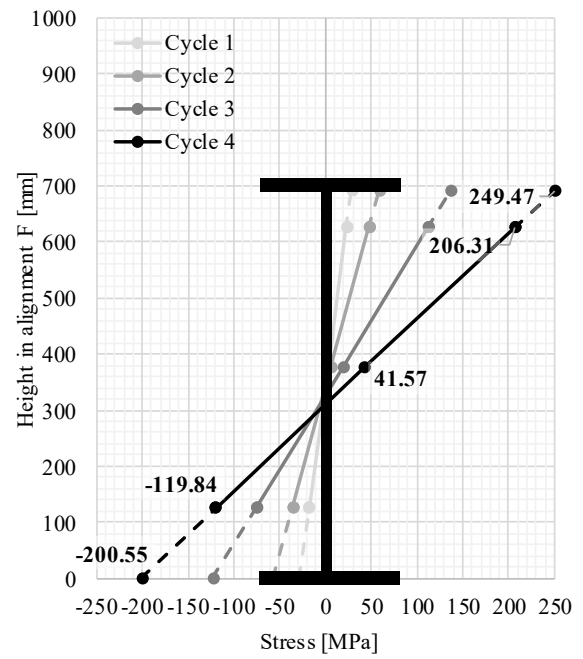
a) Section A (h = 958mm).   *b) Section F (h = 691mm).*

Figure 3.37 - Longitudinal stresses at section A and F for test B1 at 1st load stage

a) Section A (h = 958mm).   b) Section F (h = 691mm).

Figure 3.38 - Longitudinal stresses at section A and F for test B1 at 2nd load stage

The out-of-plane displacements at the centroid of the cross section are plotted in *Figure 3.39*. The rapidly increasing out-of-plane displacement at the maximum load is clearly identified, as well as the post-maximum displacements. The maximum displacement observed during the experiment was around axis F, between the measurements of LVDTs H5 and H7, about 1700 mm away from the deep end. This is also confirmed in *Figure 3.39.*

Figure 3.39 Lateral displacements at H3, H5, H7, H8 and H9 for various load levels for test B1

The cross-section at axis F was the one expected to be critical. Its vertical displacements were measured at both flange tips for the top and bottom flanges and the horizontal displacements

were measured at the middle of both flanges and the middle of the web. *Figure 3.40* illustrates the measured displacements for the maximum load.
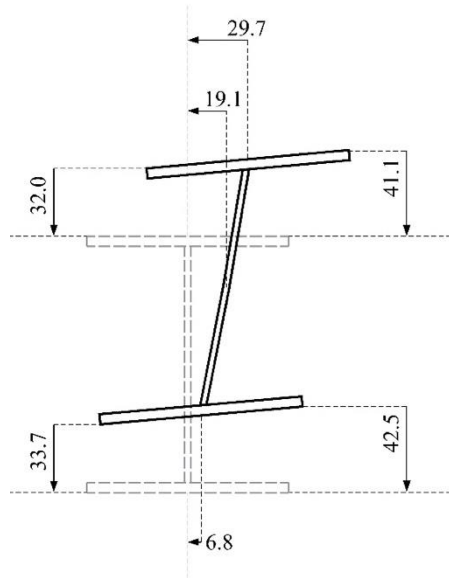
Figure 3.40 - Cross-section displacements at axis F (in mm)

3.4.3.2 Test B2

The failure mode of test B2 exhibited a buckled shape typical for a lateral torsional mode (*Figure 3.41*). Unlike test B1, local instability also occurred in the web between section C (cross-section class 4) and F (cross-section class 3), mostly visible in section E. It is highlighted that the local instability appears in a zone where the geometric imperfections present the highest values for the web, as shown in *Figure 3.12*.

Figure 3.41 - Collapse mode of test B2

The load-displacement curve at the point of load application is plotted in *Figure 3.42*. The magnitudes of the initial load cycles are also identified on that figure. The maximum applied load was 845.5 kN and the test was stopped for an applied load of 552.5 kN. Similarly to B1, the stress levels obtained for the initial cycles are plotted in *Figure 3.43*, that also indicate that the stress distributions remained elastic for the 4 cycles. Furthermore, the development of stresses is illustrated in *Figure 3.44* for $0.7P_{u,exp}$, $0.8P_{u,exp}$ and $0.9P_{u,exp}$ (before collapse) and for $P_{u,exp}$. The deviation from a straight line is clear for both sections thus indicating the development of plastic strains at these sections.
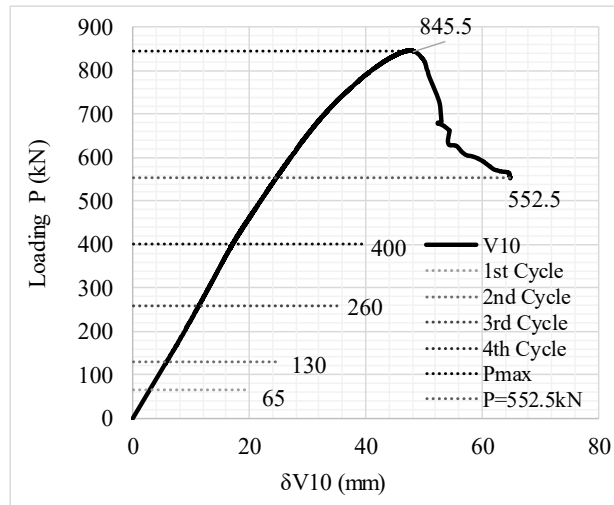
Figure 3.42 - Load-displacement curve at V_{10}, Beam 2
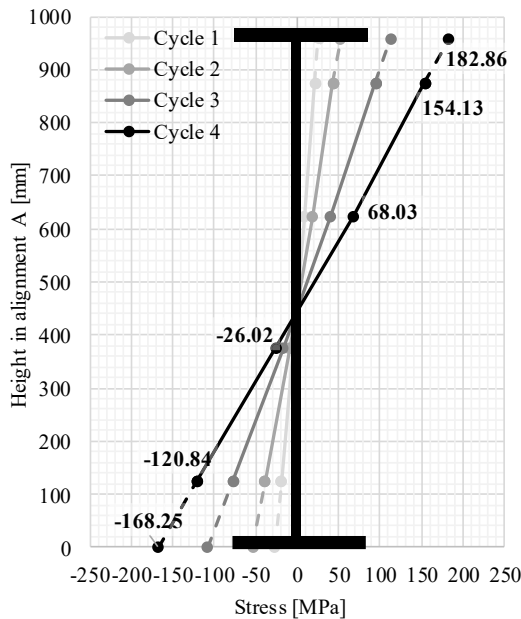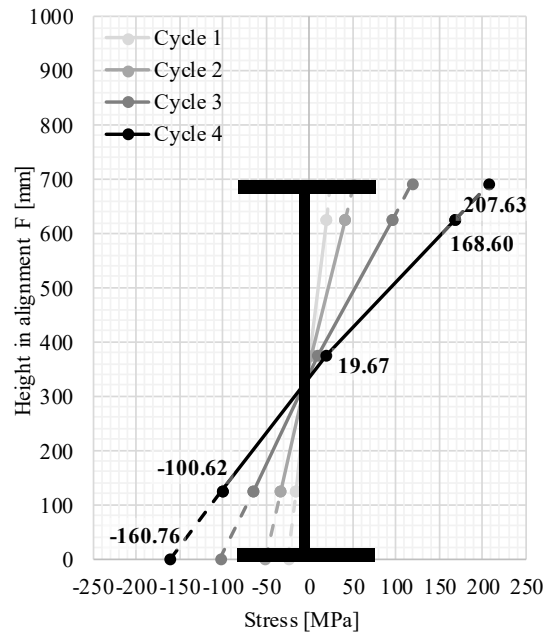
a) Section A (h = 958mm). b) Section F (h = 691mm).

Figure 3.43 - Longitudinal stresses at section A and F for test B2 at 1ˢᵗ load stage
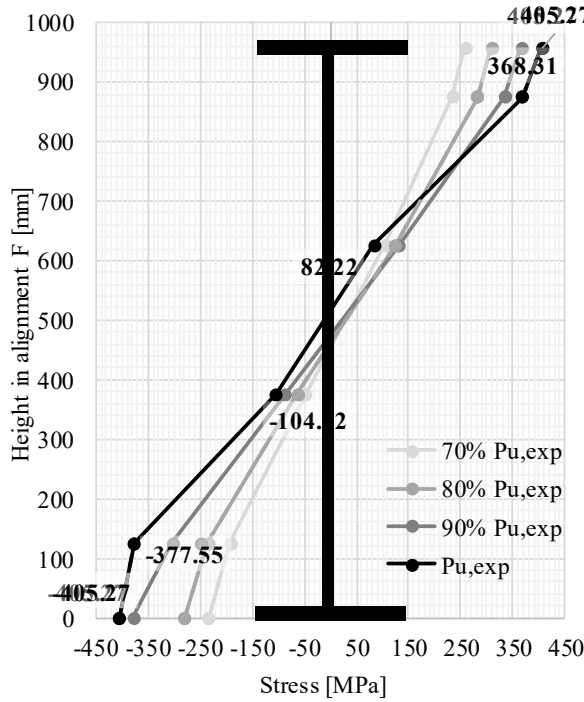
a) Section A (h = 958mm).
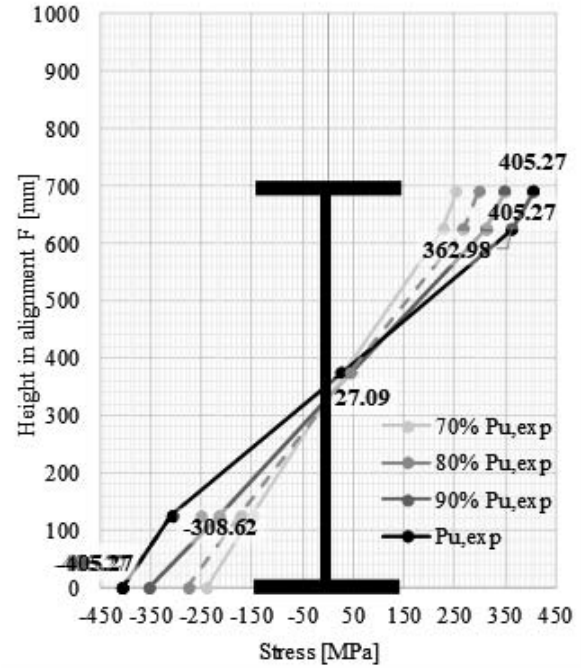
b) Section F (h = 691mm).

Figure 3.44 - Longitudinal stresses at section A and F for test B2 at 2nd load stage
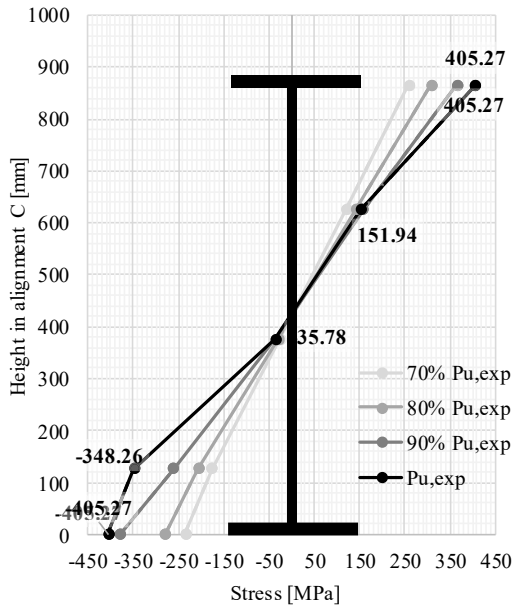
a) Section C (h = 865mm).
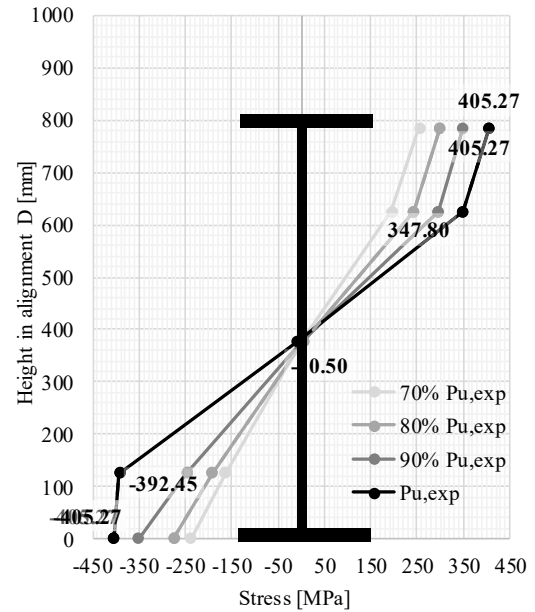
b) Section D (h = 785mm).

Figure 3.45 Longitudinal stresses at section C and D for test B2 at 2nd load stage

The out-of-plane displacements at measurement points H_3, H_5, H_7, H_8 and H_9 are plotted in *Figure 3.46* for different load levels.

| 87
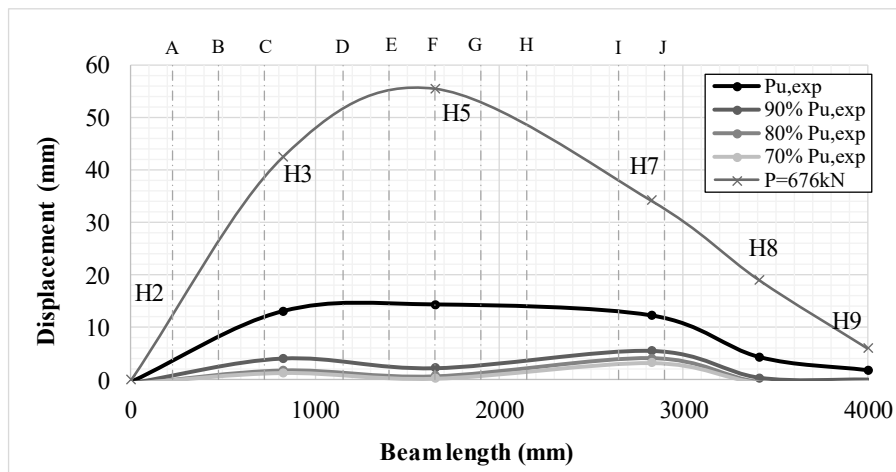
Figure 3.46 – Lateral displacements at H3, H5, H7, H8 and H9 for various load levels B2

The rapidly increasing out-of-plane displacement at the maximum load is clearly identified, which is even more pronounced at the end of the experiment. The maximum displacement observed during the experiment was between axes *D* and *F*, and between the measurements of LVDTs H_3 and H_5, about 1200 mm from the deep end. This is also shown in *Figure 3.46. Figure 3.47* illustrates the measured displacements at maximum load at cross-section F.
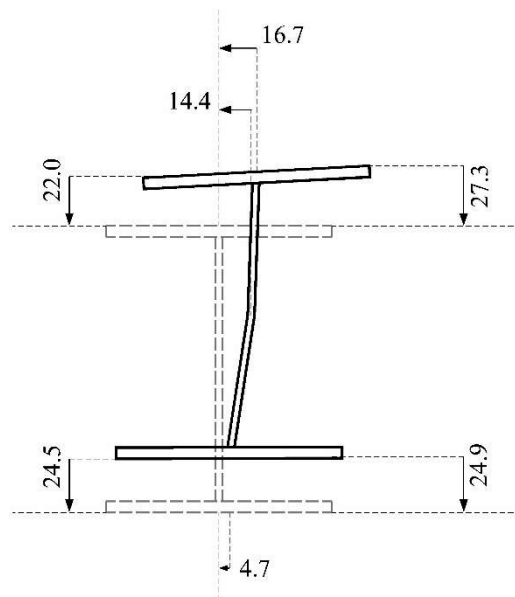
Figure 3.47 - Cross-section displacements at axis F

3.4.4   Beam-column test

Finally, in this section the results from the beam-column test are summarized. The member had identical geometry as C3, but the axial force was applied with an eccentricity at the deep end of the member.
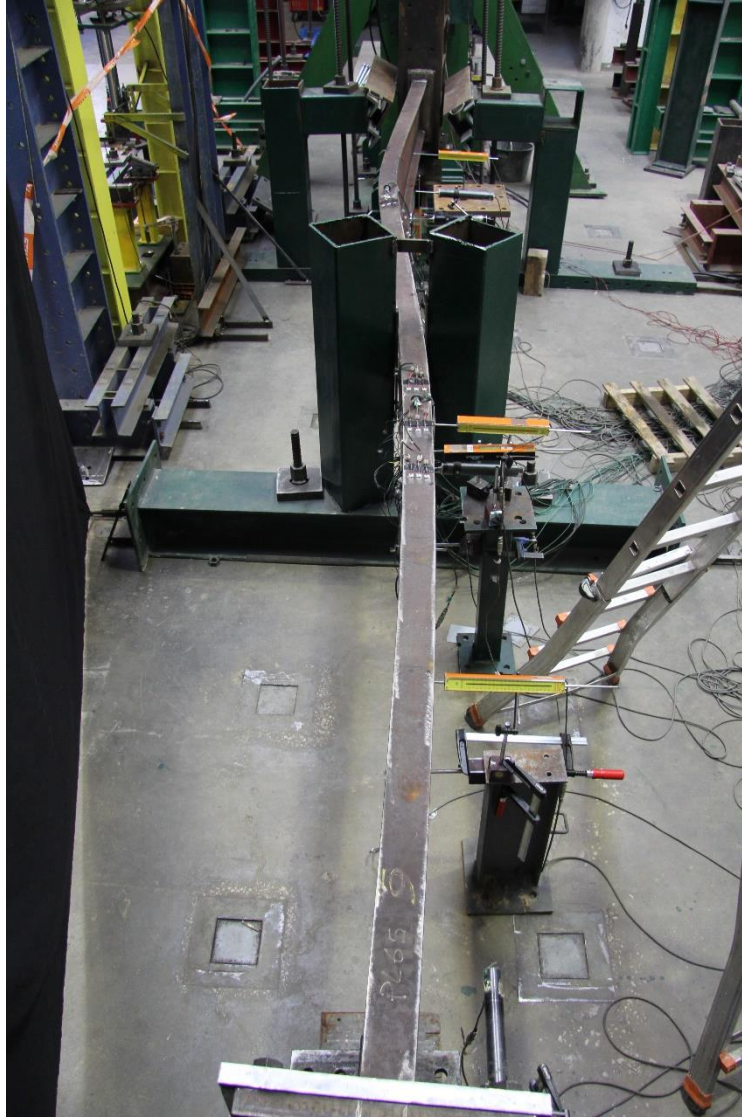
Figure 3.48 Deformation of the specimen after the test

The final deformation of the specimen is shown in *Figure 3.48*. As expected, the specimen collapsed in a lateral-torsional buckling mode. Also, since BC has a stocky section in almost all of its length, failure was driven by global rather than local instability phenomena.

Figure 3.49 illustrates the load-displacement curve at the point of load application (H_1). The maximum applied load registered during the experiment was 379 kN corresponding to a bending moment equal to 163 kNm. The loading was stopped when the applied force dropped to approximately P=270 kN.

Furthermore, *Figure 3.50 and Figure 3.51* show the evolution of the curvature for various load levels. *Figure 3.50* illustrates the development of the out-of-plane displacements and *Figure 3.51* the in-plane ones. The dotted line is added to illustrate the expected measurement of the

LVDT's at these points. Due to the large deformations the vertical and horizontal LVDT's at this point stopped recording data after the maximum load was reached.

The strains were also recorded at several locations. It is interesting to show the evolution of stresses for axis F (in the middle of the second span), *Figure 3.52* shows the stress distribution for a few load levels. The resulting distribution at maximum load and after the maximum is typical for lateral-torsional buckling.
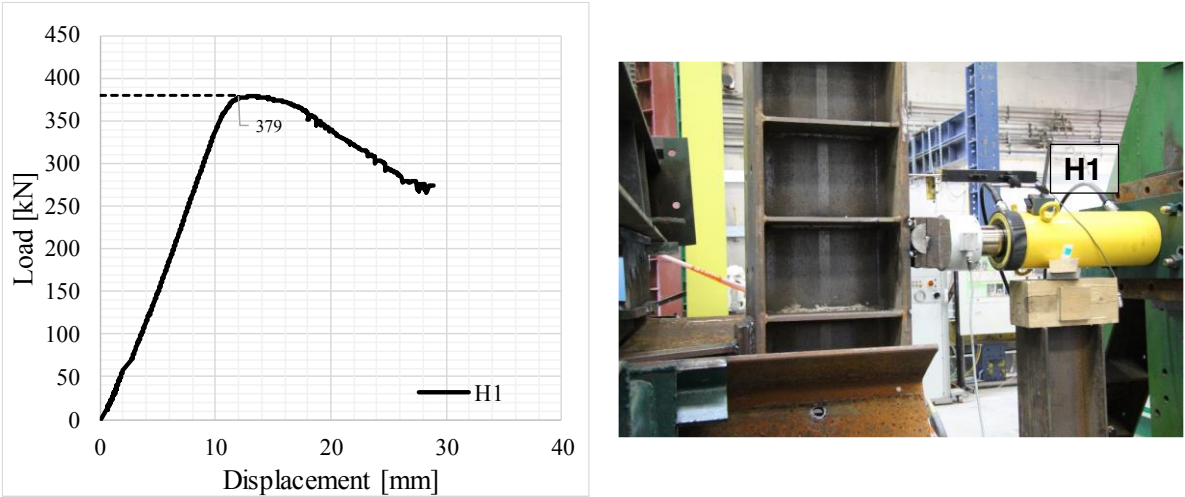
Figure 3.49 Load-displacement curves H1 for BC
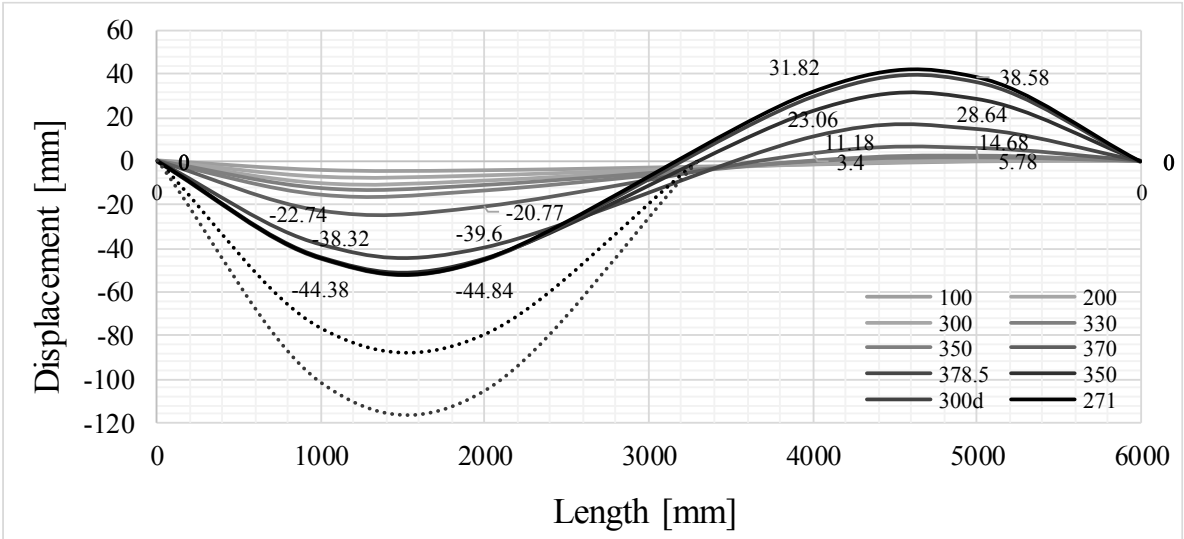
Figure 3.50 Out-of-plane displacement
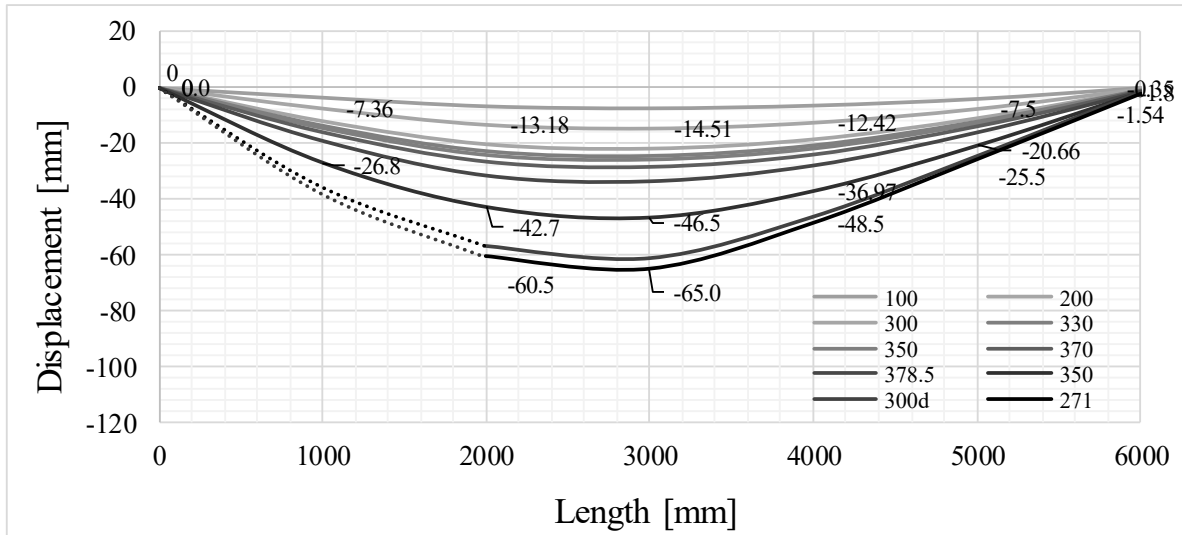
Figure 3.51 In-plane displacement
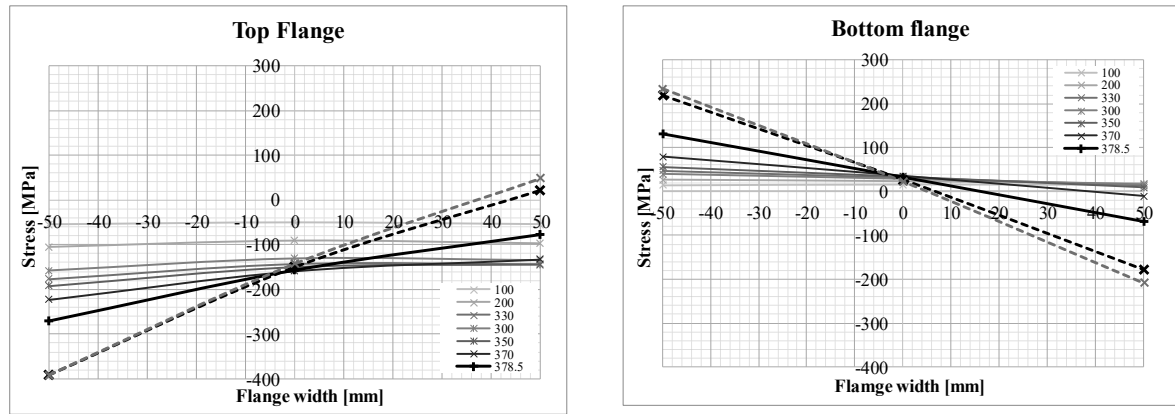
Figure 3.52 Stress distribution in the flanges at axis F

3.5 On the variation of the material and geometrical imperfections

3.5.1 Introduction

Finally, in this section, a discussion on the member imperfections for tapered columns, beams and beam-columns is presented. It is based on the measured imperfections from the experimental programme and on the collected data from the literature review in Section 3.2.

3.5.2 Residual stresses

The assessment of the residual stresses is based on stresses normalized to the yield stress obtained from coupon tests data points and their dispersion region along the section is normalized either to the flange width *b* or web depth *h*.

From all data sources, only the studies from *Prawel et al.* (1974) and *Shiomi & Kurata* (1980) report discrete results for the measured residual stresses on web-tapered members. The other sources are used for comparison and discussion.
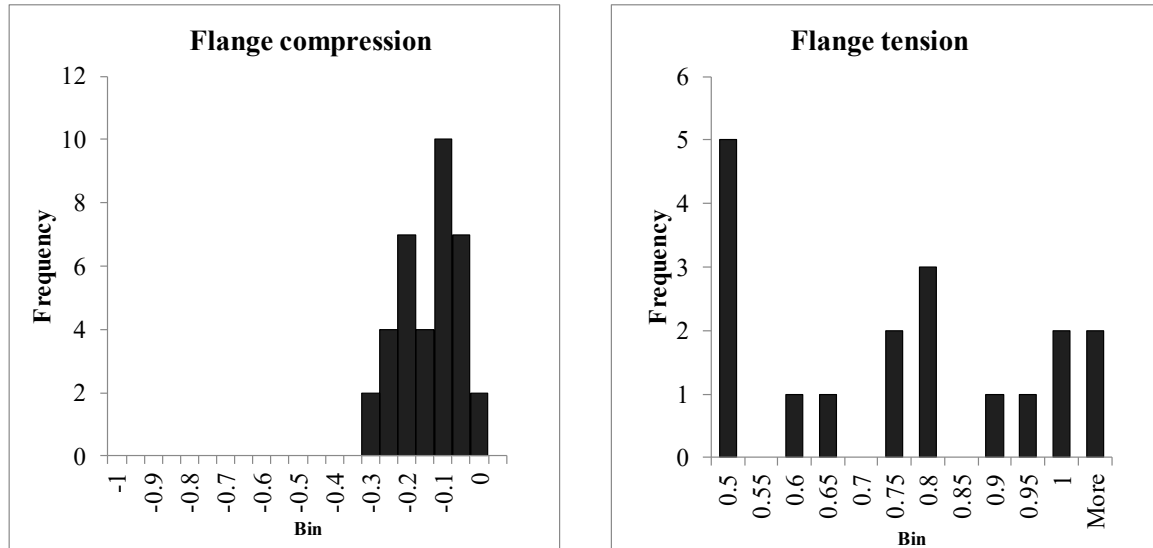
| a) Flange compression | b) Flange tension |

Figure 3.53 – Histograms: residual stresses

The compressive stresses in the flanges are assessed as an average compressive stress in each outstand flange. The mean value of the compression in the flanges is $-0.17f_y$ which is below the nominal profile currently used (according to the ECCS nominal pattern), yet with a large coefficient of variation. The statistics for the tensile stresses in the flanges are based only on the maximum value registered in each flange. The mean value is lower than the specified nominal f_y, with smaller variability in comparison to the flange compressive stress. The tension in the web is higher, in many cases approaching the yield stress. The web compression is found with high variability and a mean value higher than the recommended nominal.

Figure 3.53 and *Table 3.7* summarize the obtained statistics of the combination of results from the experimental programme and the measurements reported by *Prawel et al.* (1974) and *Shiomi & Kurata* (1980).

Chernenko & Kennedy (1991) provide a summary of residual stresses measurements collected from the literature with a mean value of average compressive stress in the flanges of $-0.25f_y$ and a standard deviation of about 32 %.

The mean value of the average compressive residual stress according to *Fukumoto & Itoh* (1981) is $-0.12f_y$ with a larger coefficient of variation of 46 %. These results compare well with

the experiments reported in the previous section, where the mean value was estimated to -0.15f_y with a slightly higher coefficient of variation of 62 %. When all data was combined, the mean value of the average compressive stress in the flanges was found slightly higher but with a smaller coefficient of variation. Besides the high coefficient of variation, the histogram of the distribution in *Figure 3.53* shows a trend towards smaller average compressive stress in the flanges. The residual tension in the flanges is represented by a more uniform-like distribution according to *Figure 3.53* and it varies from 0.5f_y up to the actual yield stress. The measurements performed by *Prawel et al.* (1974), *Salter et al.* (1980), *Avent & Wells* (1982), *Fukumoto & Itoh* (1981), *Shiomi & Kurata* (1980) report residual tension in the flanges approaching the yield stress.

Table 3.7 - Statistical parameters: residual stresses

-	Mean	St. dev.	C.o.V.	Min.	Max.
Flange compression	-0.17	0.08	0.50	-0.37	-0.01
Flange tension	0.70	0.27	0.38	0.15	1.07
Web compression	-0.38	0.25	0.66	-0.83	-0.11
Web tension	0.88	0.24	0.28	0.38	1.14

Most of these studies recommended residual stress patterns based on the measurements performed, where they suggest the yield stress as a maximum value for the tension in the flanges: *Prawel et al.* (1974) and *Avent & Wells* (1982) propose identical residual stress pattern, *Salter et al.* (1980) proposed similar to the ECCS pattern; for *Chernenko & Kennedy* (1991) the maximum tensile stress in the flange-to-web junction varies from 80% to 100% of the yield stress. These recommendations are safe-sided when compared to the test measurements.

Regarding the average compressive stress in the flanges, *Prawel et al.* and *Avent and Wells* propose a maximum of 0.5f_y which decreases to 0.3f_y. *Salter et al.* again is comparable with the ECCS pattern 0.23 f_y. and for *Chernenko and Kennedy* it is between 0.28f_y and 0.4f_y.

3.5.3   Geometrical imperfections

The initial out-of-straightness is usually assumed with the shape of the relevant buckling mode and amplitude of $L/1000$. In this assessment, particular attention is paid to the magnitude of the deviation from straight member and not the precise shape. Some of the experimental studies carried out measurements on the out-of-straightness (in and out-of-plane) and some studies report on the initial twist.

For some of the collected test results, the measurement was performed for the minor axis deformation, for other according to the major axis and for some tests the measurement direction was not even specified. In this grouping, all data was considered together, and split according to in and out of-plane. The statistical parameters are given in *Table 3.8* and the histogram is presented in *Figure 3.54*. It is highlighted that the majority of cases are web-tapered members (40 out of 48); *Shiomi & Kurata* (1980) report that the geometrical imperfection for tapered members tend to be higher due to the increased difficulty in fabrication.

The statistics obtained for the initial out-of-straightness are quite different from those presented by *Fukumoto & Itoh* (1981), nevertheless the statistics presented are based on a larger sample which covered uniform members of the same size. This can explain the difference in the mean values between both studies; on the other hand, the coefficients of variation reported by *Fukumoto & Itoh* (1981) are considerably higher. The results obtained for welded members were also compared to a similar study (*Fukumoto et al.,* 1980) on rolled beams that revealed a greater scatter for the welded beams and lower mean-to-nominal ratios.
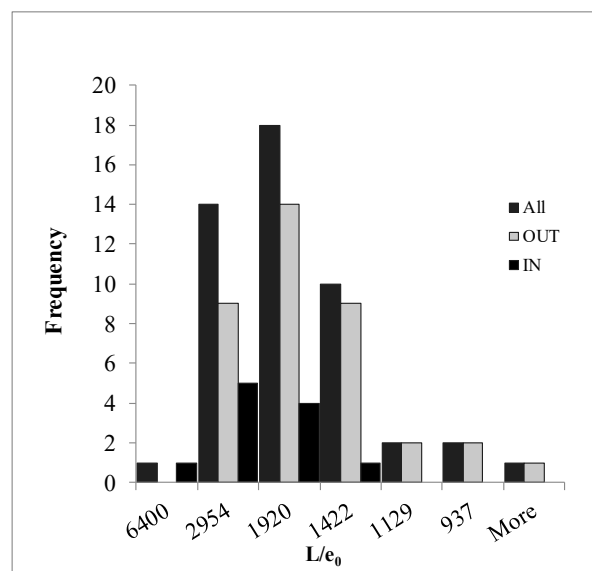
Figure 3.54 - Histogram of the distribution of the collected initial out-of-straightness

Further comparison with *Chernenko & Kennedy* (1991) shows closer fit for both indicators: mean and standard deviation, where the mean values lay between 1/2000 and 1/3500. Even though the coefficient of variation is about 40%, the mean values are at least twice less than the usually adopted imperfection of *L*/1000. The histogram in *Figure 3.54* shows the trend that the majority of the population is concentrated around the mean value, the large coefficient of variation is somehow inevitable, since there always be imperfections laying closer to the tolerance. The minimum value of the collected sample is lying above the current execution tolerance of *L*/750 in EN 1090-2:2011. *Chernenko & Kennedy* (1991) also mention that according to their study, members with geometrical imperfection which does not satisfy the tolerance occur in less than 2% of the specimens and in such cases the beams are subject to straightening.

Finally, if the results obtained are compared with the classical work on the development of the European buckling curves: the ECCS experimental programme by *Sfitensco* (1970); the theoretical basis by *Beer & Schluz* (1970) and the Monte Carlo simulation by *Strating & Vos* (1973). The out-of straightness used in by *Strating & Vos* (1973) based on the experiments *Sfitensco* (1970) has mean value of 0.00085L (*L*/1176.5) and c.o.v of 23.5%, which is the smaller than the one obtained in *Table 3.8* (46.7%). However the mean value calculated for the collected sample is about two times smaller (*L*/2160). Even though the development of the buckling curves was based on hot-rolled members, the results are illustrative of the improvement of the production quality nowadays.

Table 3.8 - Statistical parameters for the collected initial out-of-straightness

Subset	n	Mean	St. dev	C.o.V.	Min	Max
In	11	0.000342 (1/2924)	0.000123	0.36	0.00016 (1/6250)	0.000588 (1/1700)
Out	37	0.000499 (1/2004)	0.000231	0.46	0.00020 (1/5000)	0.00125 (1/800)
All	48	0.000463 (1/2160)	0.00022	0.476	0.00016 (1/6250)	0.00125 (1/800)

3.6 Summary

Chapter 3 was dedicated to the experimental background of the buckling behaviour of non-uniform members. Firstly, available experiments by other researchers were collected and presented in a comprehensive literature review. This collection covered non-uniform members in compression, bending and combination of bending and compression. Most of the studies carried out were based on I-section members fabricated by welding of plates. For that it was considered useful to extend the collection to experiments on member imperfections for welded sections.

This chapter also summarized six full-scale experimental tests on the stability behaviour of linearly web-tapered steel columns, beams and beam-column. The columns were tested under constant axial force aiming for the assessment of their in-plane flexural buckling resistance, the under linearly varying bending moment and one member was tested under bending and axial force. The material and geometrical properties of all members were characterized experimentally and detailed global results were reported. The test campaign also included residual stresses tests, where four specimens with different geometries were tested. The member geometrical properties were chosen to vary from stocky cross-sections to columns with slender (class 4) cross-sections, and therefore, they provide a good basis for their use as reference tests for the calibration and validation of numerical models.

Finally, the collected data for member imperfections was combined with the results from the experiments: out-of-straightness and residual stresses. It was shown that despite of the high variation, the mean values of the member imperfections were lower that the assumed in the calibration of the buckling curves and thus opening a future discussion on the magnitude of the imperfection factors.

4 NUMERICAL MODEL

4.1 Introduction

Numerical results are a powerful tool for the validation of design rules. They are often chosen instead of experiments because they are cheaper and significant amount of cases can be very rapidly achieved. However, the model should be carefully validated before applying it to a large parametric study in order to ensure correct results. The numerical model used later in this thesis is adapted from previous research in the field, namely, work by *Rebelo et al.* (2009), *Taras* (2010), *Marques* (2012) among others.

This chapter is dedicated to the numerical model used for the validation of design rules, related modelling assumptions and its validation with experimental results. Hence, in this chapter, firstly, the characteristics of the numerical model are described, providing details for the material modelling, boundary conditions and meshing; and then the assumptions for the member imperfections are presented. In a second step, the model validation with the experimental results presented in Chapter 3 is carried out.

4.2 Numerical model

4.2.1 General description

Members affected by stability problems are highly sensitive to second order effects which are introduced by various imperfections. In order to ensure the highest accuracy, advanced analyses were performed using geometrical and material non-linearities with imperfections. This type of analysis, also known as GMNIA, takes into account the second order effects in the members

due to their imperfect nature. Therefore, the results are assumed to represent closely the real behaviour.

In order to perform a GMNIA analysis, firstly a Linear Buckling Analysis (LBA) is performed to obtain the initial imperfection shape, which in this case is assumed to be the first buckling mode.

The numerical results used in this thesis were obtained using the FE software Abaqus and its versions 6.12, 6.14 and 6.17. Each structural element is modelled with four-node linear shell elements (S4) with six degrees of freedom.

The adopted mesh is 16 sub-divisions in the web and flanges and at least 100 divisions along the member's axis for every 10 m of length.

4.2.2 Material properties

The following constitutive assumptions are made:

- Linear isotropic elastic response, characterized by the Young's modulus E=210 GPa and Poisson ratio υ=0.3;

- von Mises yield criterion with uni-axial yield stress f_y specified according to the provisions of the product standard EN 10025;
- associated Levy-Saint-Venant flow rule;
- no hardening (i.e. perfect plasticity)
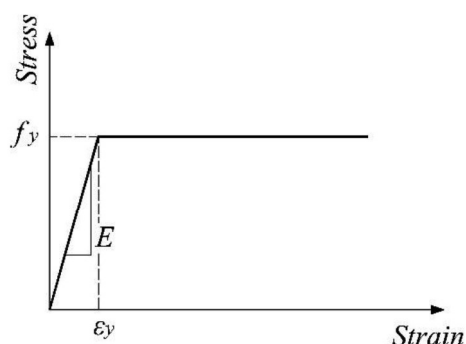
Figure 4.1 – Material constitutive law

4.2.3 Boundary conditions

If not mentioned otherwise, the boundary conditions are implemented as end fork conditions in the shell model. The following restraints are used – vertical (δ_y) and transverse (δ_z)

displacements and rotation about x-x axis (θ_x) are prevented at supports. In addition, the longitudinal displacement (δ_x) is prevented in node 1 according to *Figure 4.2* at one end of the element. End cross-sections are constrained to be plane, nevertheless allowing for the free warping of the end cross-sections, i.e. the flanges can move independently from the web.
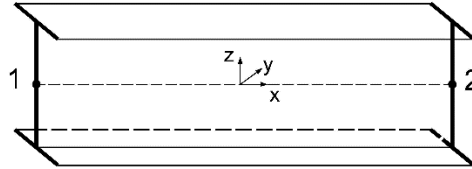
Figure 4.2 - Boundary conditions

The fixed boundary condition was implemented by restraining all DOFs at the end cross-section. The influence of slender webs was neglected by restraining them from local buckling and distortion.

Intermediate lateral restraints equally spaced may be applied at the extremes of the flanges according to *Figure 4.3*a and partial restraints according to *Figure 4.3*b.

Figure 4.3 - Location of the intermediate lateral restraints in the cross section

4.2.4 Loading

The load is applied using a load stepping routine, in which the increment size is chosen in order to meet the accuracy and convergence criteria. The equilibrium equations are solved for each increment using the Newton-Raphson iteration technique.

The load is always applied at the centre of the doubly-symmetric section, as shown in *Figure 4.4* and with reference to the plastic resistance of the shallow cross-section.
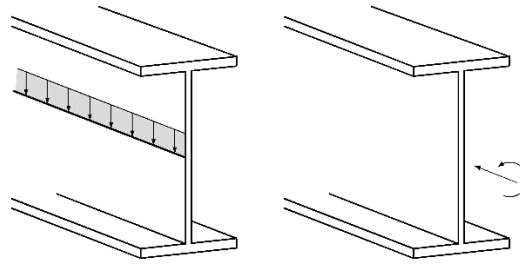
Figure 4.4 - Load application

4.2.5 Imperfections

Geometrical imperfections were incorporated in the shell model with the shape of the first or other buckling modes considered relevant for the studied case. The magnitude of the imperfection amplitude was chosen according to the recommendations of *ECCS pub. No.23*, (1976), $\delta_0=L/1000$, see *Figure 4.5*.

$$\delta_0(x) = \delta_{cr}(x)\bar{e}_0 = \delta_{cr}(x)\frac{L}{1000} \tag{4.1}$$
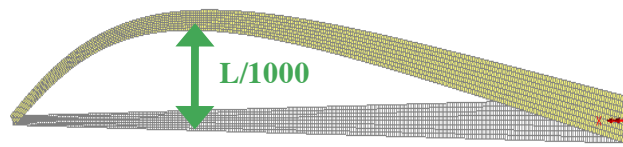
Figure 4.5 - Initial geometrical imperfection in the shape of the buckling mode

For members with partial restraints, L was adopted to be the length between the inflection points of the compressed flange.

Local imperfections are not considered provided that only global instability failure modes are analyzed. Therefore, the numerical models are prevented from developing local buckling deformations in the cross sections.

Material imperfection is introduced according to the recommendations of *ECCS publication No. 33*, (1984) shown on *Figure 4.6*. The residual stress patterns corresponding both to hot-rolled *(Figure 4.6)* and welded cross-section were considered.

(a) Hot-rolled, h/b<1.2   *(b) Hot-rolled, h/b>1.2*   *(c) Welded*
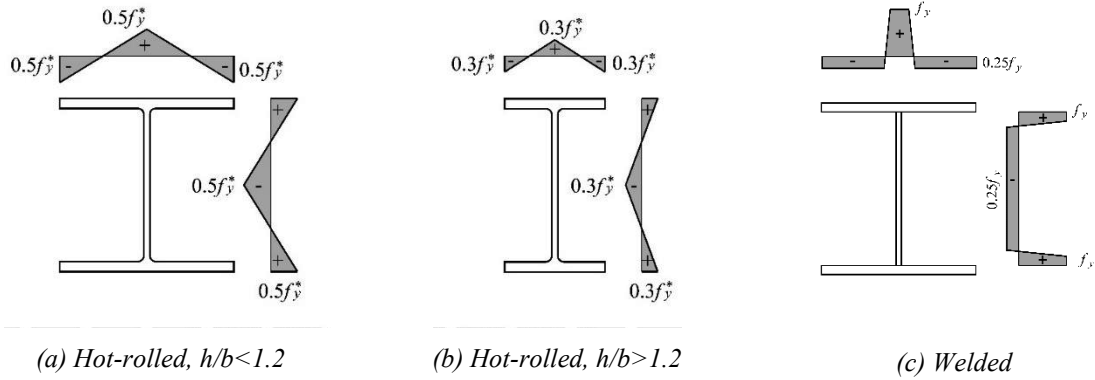
Figure 4.6– Residual stresses ("+" Tension and "−"Compression)

4.3 Comparison with experimental results

4.3.1 Introduction

The experiments presented in Chapter 3 had the objective of providing reliable data for the calibration of a numerical model, which is able to reproduce the real behaviour of web-tapered members. The numerical models were implemented using the same modelling assumptions and techniques as described in the previous section. However, in this case, since the objective is to accurately model the experiments, a few modifications in the ideal conditions were necessary since those are sometimes challenging to implement in the laboratory experiments.

In the following paragraphs the modelling of the beams and columns are presented separately, due to the difference of the buckling phenomena and test layout.

4.3.2 Columns

Even though a few modifications in the described model were necessary, it was aimed to maintain the model as simple as possible for validation purposes. Firstly, the material properties introduced were according to the results obtained for the coupon tests in section 3.4.1.1, i.e. including strain-hardening. About 20 points were chosen from the yield point to the ultimate tensile stress, in the numerical model. Those were transformed and introduced as true stresses and logarithmic strains, separately for the flanges and the webs.

The residual stresses were also introduced according to the measurements performed in section 3.4.1.1. The flanges were divided into 10 segments and the residual stresses were introduced as an average measured stress for each segment.

The initial geometrical imperfections were modelled as a combination of buckling modes, which resembled the measurement of the geometrical imperfections (see section 3.4.1.2). For *Column 1*, the adopted imperfection was the combination of a global buckling in-plane mode (1.6 mm) (*Figure 4.7a*) with an out-of-plane mode (4.7 mm) including local effects (*Figure 4.7b*).

For *Column 2*, the adopted imperfection was the combination of a global buckling in-plane mode (*Figure 4.8a*) with an out-of-plane mode including local effects (*Figure 4.8b*) with nominal amplitude of $L/1000$ for the in-plane mode and 2 mm for the local mode.
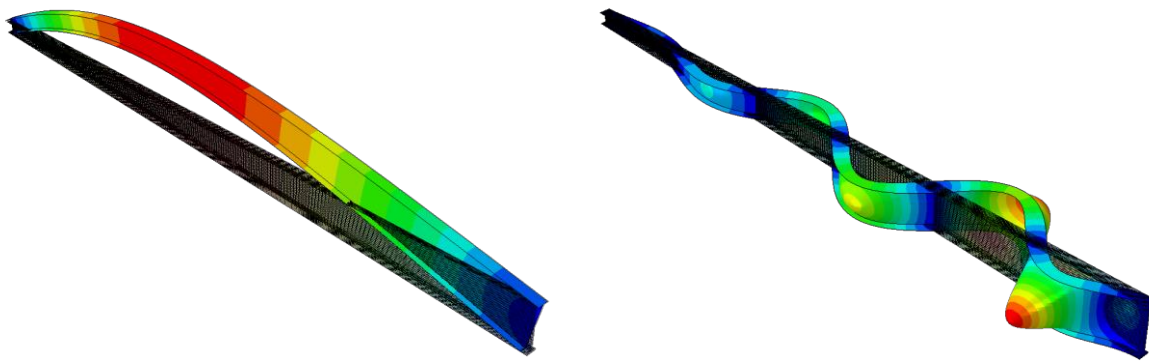
a) Column 1 in-plane mode   *b) Column 1 out-of-plane mode*

Figure 4.7 Buckling modes as initial imperfection C1
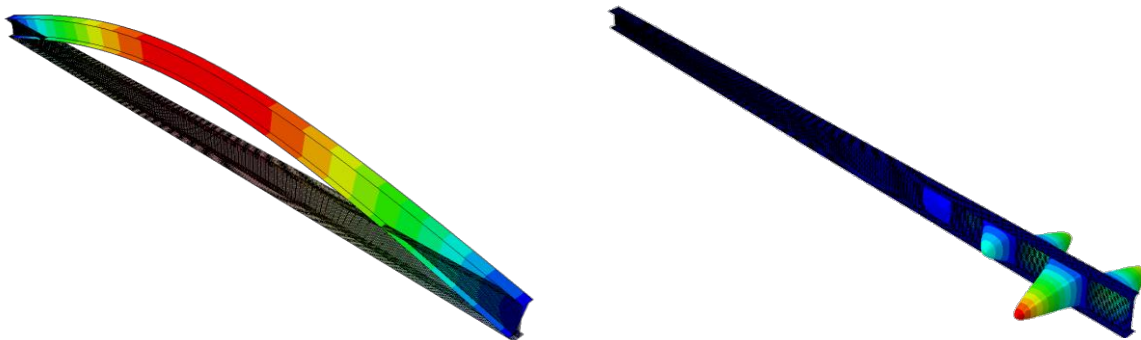
a) Column 2 in-plane mode   *b) Column 2 out-of-plane mode*

Figure 4.8 Buckling modes as initial imperfection C2

For *Column 3*, the adopted imperfection was the combination of a global buckling in-plane mode (2.4 mm) (*Figure 4.9a*) with an out-of-plane mode (4.5 mm) (*Figure 4.9b*).
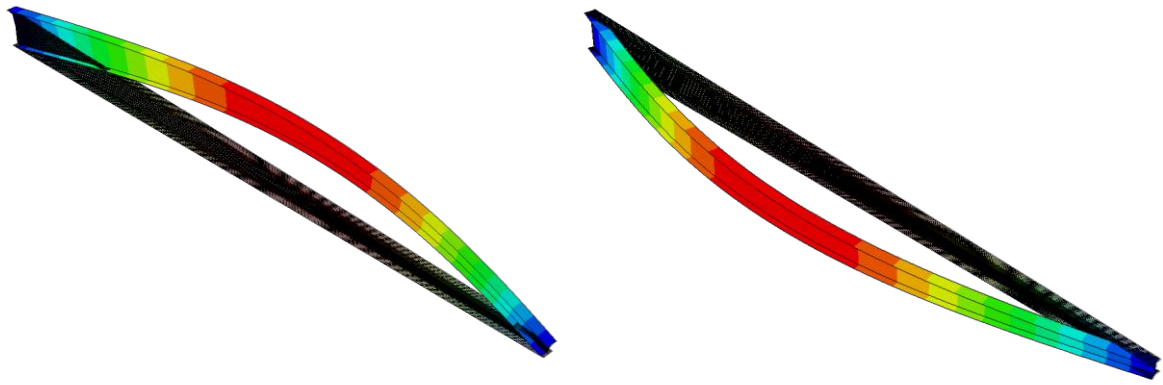
a) *Column 3 in-plane mode*   b) *Column 3 out-of-plane mode*

Figure 4.9 Buckling modes as initial imperfection C3

The boundary conditions were adopted in order to represent the experimental layout *Figure 4.10*. Firstly, the actual buckling length of the members was longer than the actual member length due to the physical dimensions of the supports. To account for this, the boundary conditions were modelled outside of the member at a distance which coincides with the actual axis of rotation of the hinge. The out-of-plane rotations were restrained. The presence of small eccentricities in the layout were included by adding small rotations at the point of load application.

Finally, the resulting load-displacement curves at the point of load application are shown in *Figure 4.11*. In each case, it was possible to achieve satisfactory agreement between the numerical and experimental results in both shape and magnitude. The obtained results and the respective difference between numerical and experimental results are given in *Table 4.1*. A comparison between the experimental and numerical deformations can be seen in *Figure 4.12*.

Another important parameter for the design of non-uniform members is the critical cross-section which governs the design. For that, these critical locations obtained from the numerical model and experimental tests are now compared. The experimental critical location was estimated approximately as the cross-section with maximum deformation after the test. The numerical critical location was chosen to correspond to the element with the highest strain at the maximum load. In *Table 4.1*, it is possible to compare the experimental and numerical results. Since this quantity is highly dependent on the member imperfections, an exact match can be hardly achieved. Nevertheless, the obtained results show very good agreement.
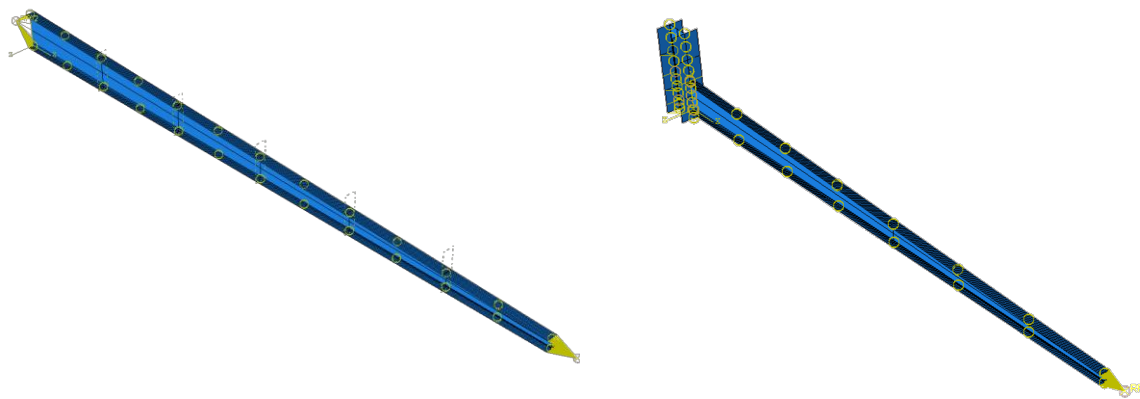
Figure 4.10 Column and beam-column models

a) Column 1

b) Column 2

c)   Column 3

d)   Beam-column
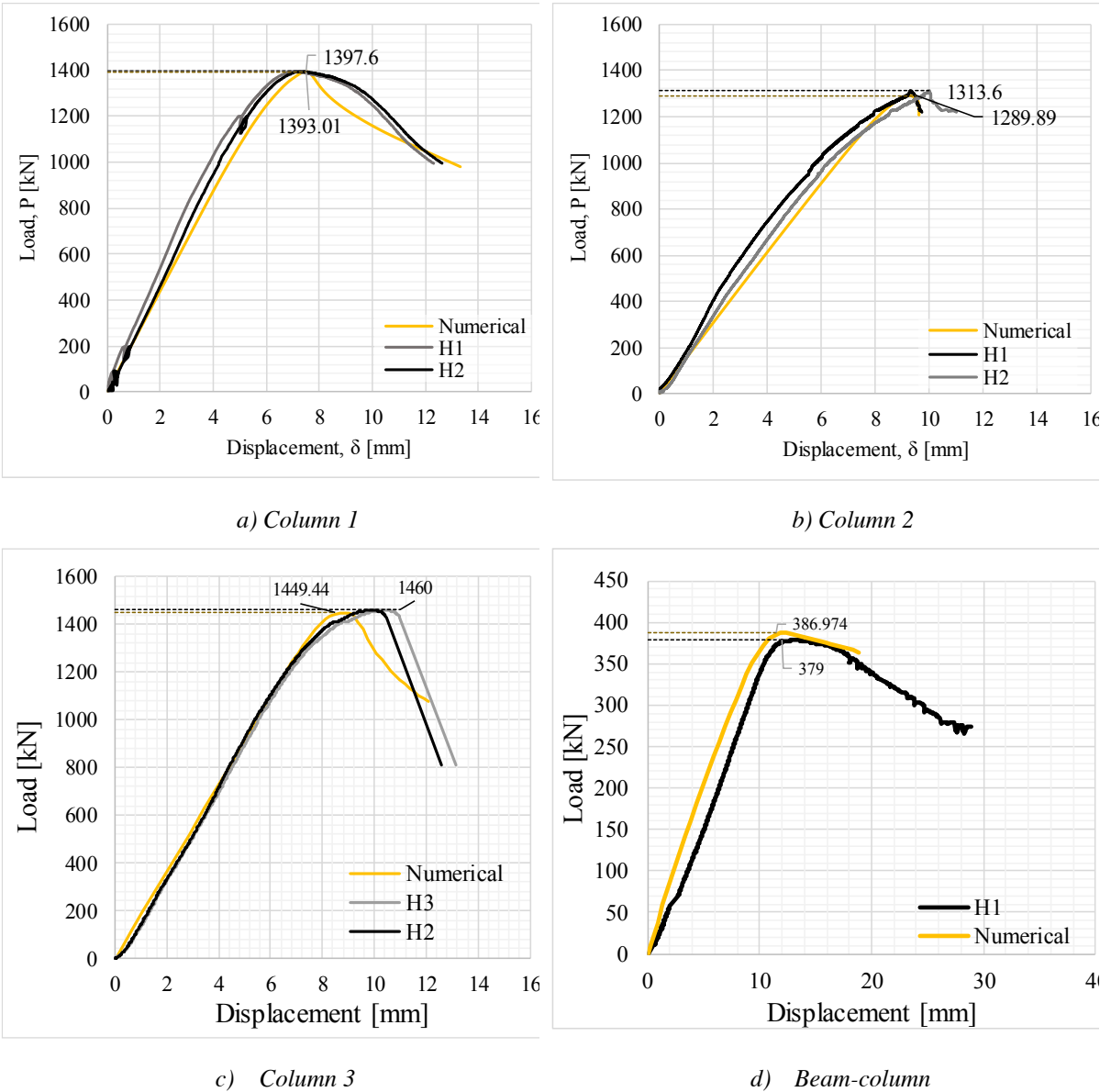
Figure 4.11 Numerical and experimental results for each experiment

Table 4.1 Numerical and experimental results

Test	Maximum load		Δ	Critical location x/L	
	Experimental	Numerical		Experimental	Numerical
-	kN	kN	-	-	-
C1	1397.6	**1393.0**	-0.3%	0.110	**0.082**
C2	1313.6	**1289.9**	-1.8%	-	**0.250**
C3	1460.0	**1449.4**	-0.7%	0.125	**0.153**
BC	379.0	**386.9**	+2%	0.708	**0.773**

Figure 4.12 Column 3: numerical and experimental deformed shape

4.3.3 Beams

Firstly, the model simulated the complete beam, including the segment with uniform cross-section. In fact, the option to include this segment for load application was specifically chosen to avoid uncertainties in the definition of the boundary conditions of the shell model at the deep end of the tapered beam in the numerical model.

Secondly, the two pinned connections at the shallow end of the beam do not act as perfect hinges. Each of these connections has physical dimensions, which in turn means that the test specimens have two different buckling lengths in and out of the beam plane, *Figure 4.14*. In addition, even though the pins were treated with lubricant before each experiment, the friction between the pin and the plates is not fully eliminated and thus introduces some degree of restraint.
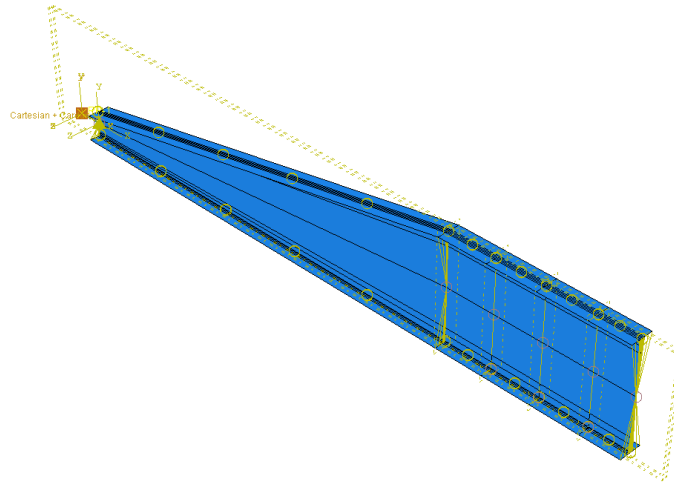
Figure 4.13 Numerical model

Hence, it was decided to tackle this deviation from the intended behaviour by introducing a spring at the beams' end, matching the behaviour directly obtained from the experiments. The spring was set to be fully rigid with respect to translation and rotation about the longitudinal beam axis (x-axis), it was free to rotate around the y and z axes, and the translations in y and z axes were calibrated to match the experimental results.
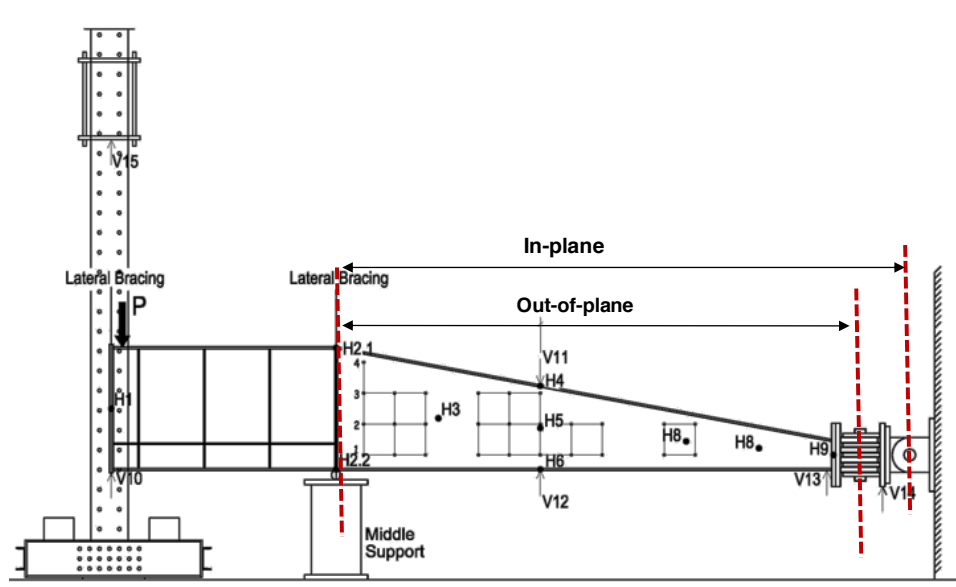
Figure 4.14 Buckling lengths

At the intermediate support, as the vertical and lateral displacements were restrained, the cross-section was modelled to remain straight (with warping restrained) corresponding to the configuration of the experiment. At the point of load application, the section was also modelled

to remain straight, its lateral displacement was restrained and the load was applied with displacement control.

The material properties were considered as an average from the coupon tests carried out in Chapter 3. The geometrical imperfections were modelled as a combination of buckling modes, which resembled the measurement of the geometrical imperfections (see section 3.4.1.2). Several shapes were checked in order to obtain the best fit. For *Beam 1*, the adopted imperfection was the combination of the modes in *Figure 4.15a* and *Figure 4.15b* corresponding to global buckling of the top or bottom flanges.

For Beam 2, it was chosen to have a similar configuration, a combination of the two global modes corresponding to buckling of the top or bottom flange Figure *4.16*a) and b), and additional local mode *Figure 4.16*c) to account for the large local imperfection from the measurements as shown in *Figure 3.11*.

In this experimental campaign, the residual stresses were not measured for the beams despite being a relevant parameter for the buckling resistance. For this reason, it was necessary to verify various options for their magnitude. Since all other relevant parameters were modelled as measured, the only "unknown" were the residual stresses.

| 107

a) Mode 1 Beam 1 (3.75 mm)   *b) Mode 2 Beam 1 (2.5 mm)*
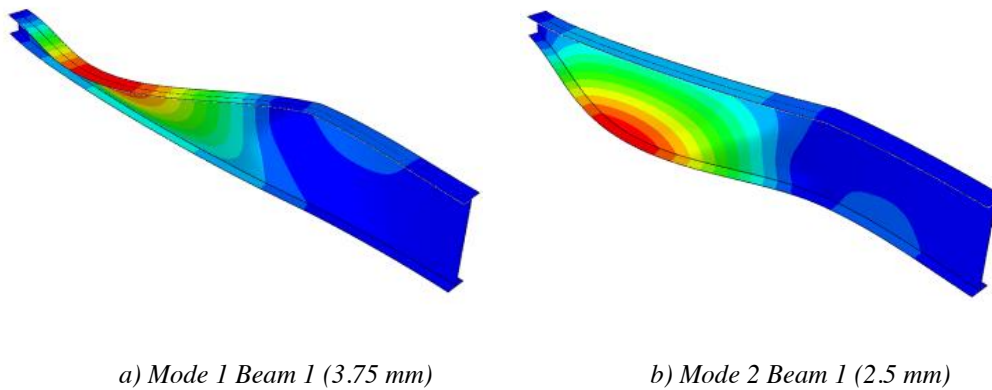
Figure 4.15Modes chosen as a shape of the initial geometrical imperfection: Beam 1

a) Mode 3 Beam 2 (3 mm)   b) Mode 5 Beam 2 (1.5 mm)   c) Mode 2 Beam 2 (3.85 mm)
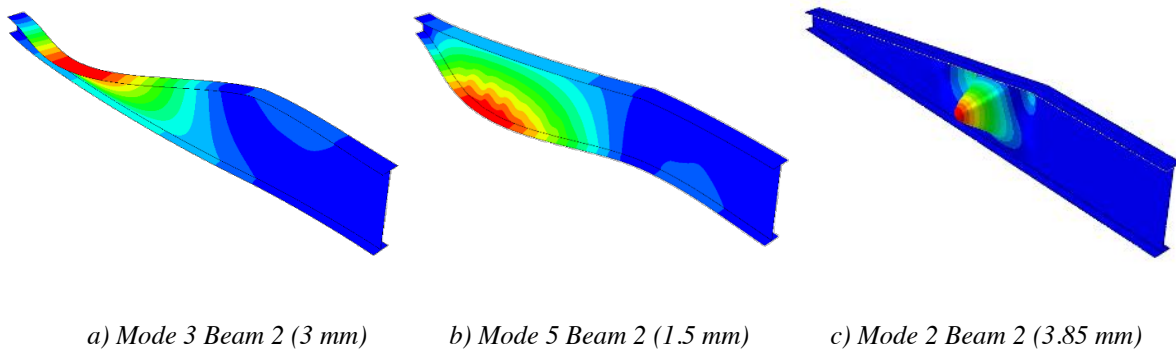
Figure 4.16 Modes chosen as a shape of the initial geometrical imperfection: Beam 2

The adopted residual stresses corresponded to the two following assumptions about the residual tensile stress: f_y=235 MPa or f_y=355 MPa, which are further referred to as *Pattern 235* and *Pattern 355*, respectively. In *Table 4.2*, it is possible to compare the results for the two different assumptions. It was found that *Pattern 235* gives better agreement with the experimental result for both beams: for *Beam 1*, an 8% difference instead of 17%, and for *Beam 2*, a 2% difference instead of -6%. The change in the residual stresses magnitude for both beams leads to a similar drop in the resistance of about 8%. This difference is found acceptable, keeping in mind the typical large scatter of the residual stresses in magnitude and shape.

The model behaviour was verified at various locations along the beam, to ensure a similar performance with respect to the experiments. The spring at the shallow beam end was calibrated exactly with the purpose of matching the readings during the experiments. Examples are given in *Figure 4.17* and *Figure 4.18*, where the first one compares the for horizontal displacement H6 of *Beam 1* and the second compares the vertical displacement at V_{12} of *Beam 2*.

Table 4.2 Results for the different assumptions on the residual stresses

Test	Experimental	Numerical Pattern 235	Δ	Numerical Pattern 355	Δ
-	kNm	kNm	-	kNm	-
B1	2066.6	**1921.2**	-8%	1768.5	-17%
B2	1452.6	**1488.1**	+2%	1375.1	-6%
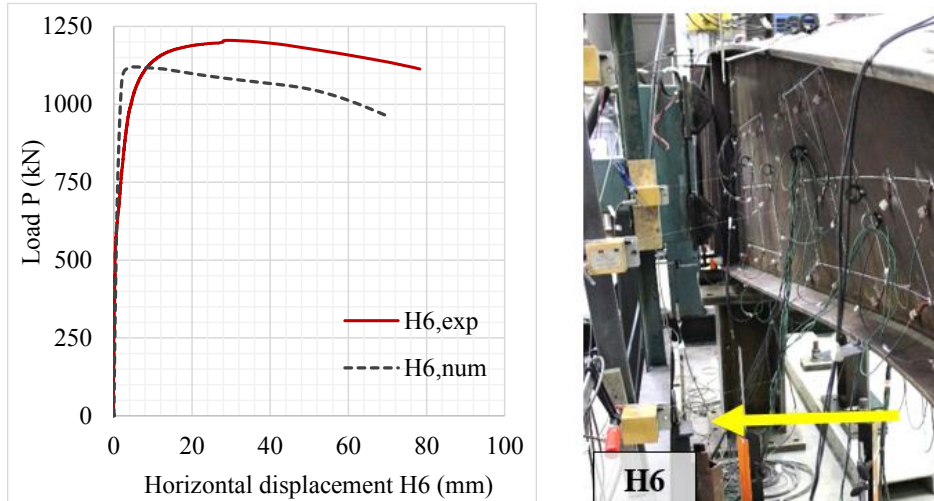
Figure 4.17 Horizontal displacement of Beam1 at H6 (axis F)
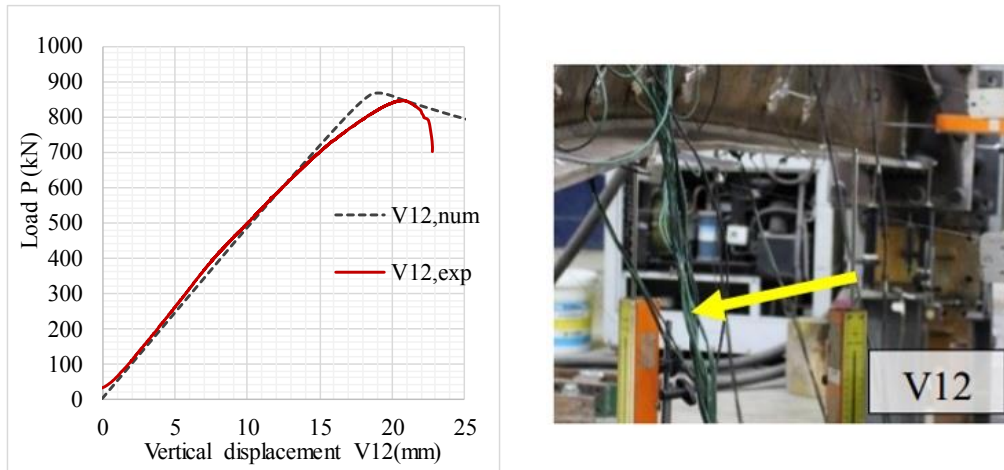
Figure 4.18 Vertical displacement of Beam 2 at V12 (axis F)

Finally, it can be concluded that if the numerical model adopted incorporates all relevant parameters, it accurately reproduces the behaviour of the tapered beams.

4.4 Final remarks

In this chapter the adopted numerical model was presented with all relevant modelling assumptions. It was also validated with experimental results on non-uniform columns, beams and beam-columns. It was seen that if the material and geometrical properties together with the correct measured imperfections are introduced in the model, a good agreement is achieved with the experimental results.

In the following chapters, if not mentioned otherwise, this numerical model is used for the parametric studies carried out and the validation of design rules.

5 SAFETY ASSESSMENT OF DESIGN RULES

5.1 Introduction

This chapter is dedicated to the assessment of the safety of Eurocode 3-1-1 stability design rules. As it was mentioned earlier, the main purpose of modern design codes is to provide design principles and application rules that lead to appropriate safety levels. However, because design codes combine a very large number of design rules that evolved over many decades of extensive research work, the safety level is not uniform across the various design rules and also within a single design rule. Eurocode 3 (2005) is no exception, despite the enormous work that was put in its development and the wide past proven experience that it incorporates. In addition, the development of new structural steels with largely improved mechanical and geometrical properties and dramatically improved quality control procedures, required a reassessment of the current safety levels of the stability design rules of EC3-1-1. For these reasons, a safety assessment of the available stability design rules in Eurocode 3 was carried out. Similar studies were done in the past and it is worth mentioning them. Project *Partial safety factors for resistance of steel elements to EC3 and EC4. Calibration for various steels products and failure criteria* (*Chabrolin et al.*, 2002) provided a justification for the adoption 1.0 instead of 1.1 for γ_{M0}. The assessment was carried out using the ENV1993 (1992) Annex Z, which is the predecessor of the current Annex D of EN 1990. The first project objective was achieved by performing a collection of available data at the time for the material properties of steel grades S235 to S460 and a large variety of cross-sections. The second objective was to provide sufficient evidence considering various limit states in order to avoid different values for the

partial factor regarding the stability design of members γ_{M1} in the national determined parameters. This objective was tackled by performing experimental tests and the collection of available data of experiments performed by others. Regarding γ_{M1}, it was concluded that 1.1 is quite satisfactory, besides the interaction between bending and axial force where lower factors were obtained.

A similar assessment was carried by *Muller* (2003), on the basis of the ECCS tests (*Figure 5.1*). *Taras* (2010) carried out a Monte Carlo simulation assuming similar variability for the basic variables as in the ECCS tests. The conclusions of both were that the ENV 1993 version for the partial factor γ_{M1} fits better the obtained results.
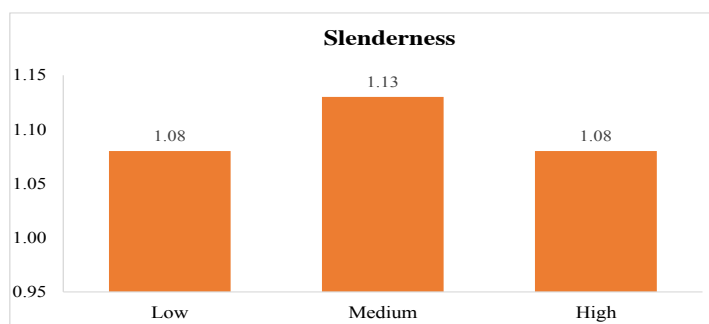
Figure 5.1 – Assessment by Muller (2003) for flexural buckling of columns

Later on, the research project PROQUA (2005), carried out a probabilistic assessment of the Eurocode design rules for steel and composite structures. The analysis included the load and the resistance sides. The results of the analyses revealed that the Eurocode rules have higher reliability than the requirements of EN 1990. The project gave recommendations for statistical data for the action and resistance sides including imperfections. The project conclusions state that the partial factors γ_{M0} and γ_{M1} would be equal to 1.0.

The European project *Optimizing the seismic performance of steel and steel-concrete structures by standardizing material quality control* OPUS (2013) collected large number of coupon tests reflecting the current production in Europe. The project was aiming at giving recommendations for the over-strength of the yield stress in the context of seismic design of structures. The data, however, is valuable for assessment of any other steel design rule because it is an updated version of what exists.

Finally, the SAFEBRICTILE project (Ref. Nº RFSR-CT-2013-00023) intended to contribute towards the harmonization of the reliability level of design rules for steel structures covering modes driven by ductility, stability and fracture. The project provided an objective and

consistent safety assessment procedure for the various failure modes that are relevant for steel structures. It also recommended statistical distributions of the relevant basic variables, which were collected continuously during the project in a database of steel properties. This chapter is a summary of the work carried out at the University of Coimbra covering the reliability assessment of the stability design rules.

It is organized as follows: i) firstly, the possible ways of safety assessment are summarized; ii) the statistical distributions of the relevant basic variables are discussed; iii) the stability design rules for I-shaped hot-rolled steel columns, beams and beam-columns is carried out.

5.2 Methods for safety assessment

5.2.1 Structural reliability

It is common to use the reliability index β as a measure of the structural safety. Its quantity is directly equivalent to the probability of failure.

$$\beta = -\Phi^{-1}(P_f) \tag{5.1}$$

In general, the probability of failure can be determined by exact analytical integration (whenever possible), numerical integration methods, approximate analytical methods such as first or second order reliability methods (FORM or SORM) and simulation methods.

According to Annex C of EN 1990 "*Design values should be based on the values of the basic variables at the FORM design point, which can be defined as the point on the failure surface (g() = 0) closest to the average point in the space of normalised variables.*"

The design is considered sufficient if the limit states are not reached when the design values are introduced into the analysis models, as given by:

$$E_d = E(a_{d1}, a_{d2}, \dots, F_{d1}, F_{d2}, \dots, \theta_{d1}, \theta_{d2}, \dots) \tag{5.2}$$

$$R_d = R(a_{d1}, a_{d2}, \dots, F_{d1}, F_{d2}, \dots, \theta_{d1}, \theta_{d2}, \dots) \tag{5.3}$$

E is load action; R is the resistance; F is an action; X is a material property; a is a geometrical property; θ is a model uncertainty.

The design shall be based on the limit state function $g(.)$, as the limiting condition is $g=0$ also referred as failure surface. FORM is used to find the failure surface, an increased accuracy can be achieved using SORM (Second Order Reliability Method), at the cost of higher computational effort.

Since EN 1990 allows to split in the resistances and actions, (see Section 2.6), it is possible to obtain the "failure surface" based only on the resistance side as in Eq.(2.78).

5.2.2 Design assisted by testing

One of the main objectives of the SAFEBRICTILE project consisted in the improvement of existing and the development of new procedures for the reliability assessment of design rules for steel structures. For this purpose, the existing procedures for the safety assessment of design rules verified by testing, given in EN 1990 Annex D, were reanalysed, adapted and expanded for the purposes and applications of the project and beyond. The main, semi-probabilistic reliability approach adopted in EN 1990 was kept as a reference framework for the developed safety assessment procedure. The procedure retains the semi-probabilistic approach of the Eurocodes, i.e. the assumption that the resistance component of the total reliability level (expressed by the reliability index β) has a fixed value. Recommendations on the reduction of the model variability were specified, namely, divisions into smaller groups, use of the tail approximation and weighting of different failure mores. The use of numerical experiments was also addressed and their compliance to physical tests in the laboratory, and requirements and limits for their application were developed.

The application of the procedure is summarized in *Figure 5.2.*
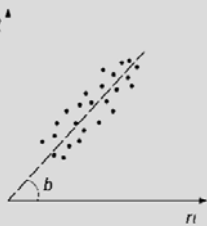
Step 1

Resistance function

$$r_{t,i} = g_{rt,i}(X_1, X_2 ... X_k)$$

The resistance function is a function of the selected relevant basic variables X_1, $X_2 ... X_k$

Experimental resistance

Experimental values $r_{e,i}$ for each test specimen (these results can be obtained from tests or numerical estimates from advanced simulations)

Basic variables

Pre-information is needed regarding the distributions of the basic variables X_j: *mean value* $\mathbf{X_{jm}}$ and *standard deviation* $\boldsymbol{\sigma_j}$

Step 2

Estimate mean vale of correction factor *b*

$$b = \sum_{i=1}^{n} r_{e,i} r_{t,i} \Bigg/ \sum_{i=1}^{n} r_{t,i}^2$$

The factor is a global value for the selected subset. The correction factor can be used as an indicator of the accuracy of the model, i.e. it should not strongly diverge from unity (0.85-1.15)

Estimate CoV of the error:

$$\delta_i = r_{e,i} / b r_{t,i} \qquad \Delta_i = \ln(\delta_i)$$

$$s_\Delta^2 = \frac{1}{n-1} \sum_{i=1}^{n} (\Delta_i - \overline{\Delta})^2$$

$$V_\delta = \sqrt{\exp(s_\Delta^2) - 1}$$

The CoV of the error is a global value for the selected subset and it represents the difference model estimate and the experimental estimate.

Step 3 (for each specimen i)

Determine the coefficient of variation V_{rt} – it relates to the basic input variables:

i) In case of simple product function, the following expression is used: $V_{rt} = \sum V_{Xj}^2$

ii) In case of more complicated resistance function, V_{rt} can be obtained for each specimen as:

$$V_{rt,i}^2 = \frac{1}{r_{t,i}(X_m)^2} \sum_{j=1}^{k} \left(\frac{\partial r_{t,i}(X_j)}{\partial X_j} \sigma_j \right)^2$$

Often, it is complicated to use the analytical expression of the partial derivatives and therefore, numerical estimate can be used. It can be determined from:

$$\frac{\partial r_{t,i}}{\partial X_j} \approx \frac{r_{t,i}(X_1,...,X_j + \Delta X_j,....X_k) - r_{t,i}(X_1,...,X_j,....X_k)}{\Delta X_j}$$

where ΔX_j is sufficiently small increment .

| 115

Step 4 (for each specimen i)

Determine design value of the resistance

$$Q_i = \sqrt{\ln(V_\delta^2 + V_{rt,i}^2 + 1)}$$

$$r_{d,i} = b r_{t,i}(X_m) \exp\left(-k_{d,\infty} Q_i - 0.5 Q_i^2\right)$$

Determine the partial safety factor, as a mean value from the safety factors for each specific case:

$$\gamma_{M,i}^* = r_{nom,i} \Big/ r_{d,i} \qquad \longrightarrow \qquad \gamma_M^* = 1/n \sum \gamma_{M,i}^*$$

Figure 5.2 Flow-chart for the test-based statistical evaluation procedure of EN 1990 Annex D

5.3 Statistical distributions of basic variables

5.3.1 Introduction

According to the procedure given in *Figure 5.2*, information about the scatter of the basic input parameters is required. Within the scope of the European project SAFEBRICTILE, data collection for material and geometrical properties was carried out. This collection aimed at providing reliable data for the application of the reliability assessment performed within the project. The data was collected in the European database provided by the project. It also collected data from previous collections in order to increase the data pool.

The collection of data aimed to attract contributions coming from different industries. In particular, focus was given to steel profiles and plates in different steel grades fabricated in 2013 and 2014. During the project, data was also collected from other sources such as, coupon tests performed at universities around Europe. These tests serve for independent comparison with the results which were supplied by the steel producers, as the steels tested at the university laboratories are supplied by random producers. Data was also collected from the literature: i) collection in *Simões da Silva et al* (2009) that comprised a large amount of tests (7454 coupon test results) tested between 1996 and 2007 for steel grades S235, S275, S355, S460 and S690; ii) data collected within the framework of the *European project OPUS* that comprises a large amount of data (25425 coupon test results) tested between 2007 and 2010 for steel grades S235, S275, S355, S460.

Regarding the geometrical properties, the tolerances on shape and dimensions (*Figure 5.3*) for H and I sections are standardized and the profiles are produced according to EN 10034:1993. This implies that the dimensions are continuously measured and their variation is bounded by the standard.
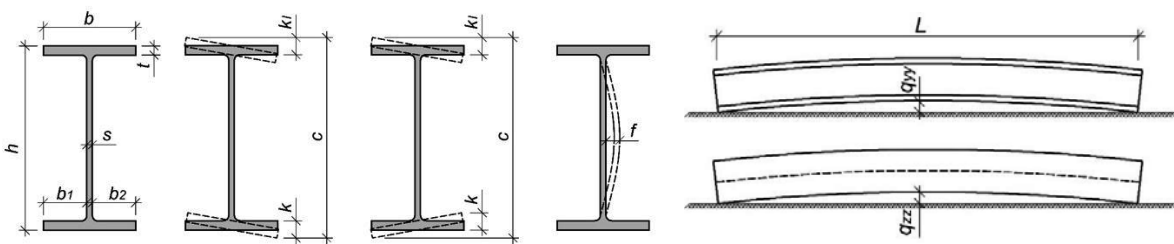
Figure 5.3 Measurements on H and I sections – cross - section

Data collection for geometrical properties of steel H and I profiles, according to the specifications of EN 10034:1993, was performed among several steel producers in Europe: *ArcelorMittal*, *Dillinger*, *Salzgitter*, *Stahlwerk-Thueringen*, *TataSteel*. The results were supplied only as statistical parameters.

The geometrical and material imperfections, however, are not standardized and there are not many sources of information. In Chapter 3, a collection of results various from literature sources was carried out. The conclusions, however, revealed high variability which is based on only several dozens of results unlike the material and geometrical properties where the collected data were several thousands. The out-of-straightness and the residual stresses, despite of being very relevant parameters do not appear explicitly in the Eurocode 3 stability design rules, for that reason they were not considered as random variables in the reliability assessment summarized by this chapter.

5.3.2   Material properties

Based on the collected data, recommendations for the distributions of the material properties were specified. These were adopted also in the present assessment. The SAFEBRICTILE recommendations are given in *Table 5.1*. They were specified in a normalized manner in order to be easily applicable to the variation of the yield stress with thickness according to EN 10025.

Table 5.1 Recommended distributions

Steel	$f_{y,nom}$	$f_{ym}/f_{y,nom}$	c.o.v.
S235	235	1.25	5.5%
S355	355	1.2	5%
S460	460	1.15	4.5%

Furthermore, the modulus of elasticity also being an important parameter for the stability behaviour is not a standardized property. The result of the measurement procedure is highly dependent on the party that performs it; hence for that reason, the available results are questionable. A recommendation for the distribution for the modulus of elasticity was adopted based on DNV (1995) that reports a mean value $E_m = E_{nom}$ and a c.o.v. of 5%. Since the statistical characterization of the modulus of elasticity is not so strongly supported by

experimental evidence and the testing procedures are not often as reliable with respect to this property, a sensitivity study is carried out with respect to this property by also considering a c.o.v. of 3%. Furthermore, from theoretical and methodological point of view the Young's modulus should not exhibit variability (*Feldman*, (2018))

5.3.3   Geometrical dimensions

Table 5.2 summarizes the recommended distributions for the geometrical properties of H and I hot-rolled sections.

Table 5.2 Recommended distributions

Dimension	b	h	t_w	t_f
mean/nom	1	1	1	0.975
c.o.v	0.9%	0.9%	2.5%	2.5%

They were based on more than 1000 collected data in the database and data supplied from steel producers in Europe. These statistics correlate well with that was reported in the past *Alpsten,* (1972) and results reported in *Taras* (2010), who reported statistics as given in *Table 5.3*.

Table 5.3 – Distributions on geometrical distributions Alpsten, G. (1972)

Dimension	b	h	t_w	t_f
mean/nom	1	1	1.025	0.975
c.o.v	0.9%	0.9%	4.0%	3.0%

Although the reports by *Alpsten.* (1972) and *Taras* (2010) are not recent, the statistical characterization of the cross-section dimensions is in line with the statistical indicators for area, moment of inertia and bending modulus as given in the report from the research project PROQUA, where the area, section modulus and moment of inertia are reported with a mean value of 0.99 the nominal and c.o.v varying from 1 to 4%.

Recently, as part of the Eurocode 3-1-1 revision, the final draft prEN 1993-1-1 (CEN/TC250, 2017) specifies recommended distributions for the basic variables for the calibration of the

partial factors in its Annex E. The recommended distributions are based on the recommendations of SAFEBRICTILE.

5.4 Safety level of the design rules

5.4.1 Scope and assumptions

The assessment encompasses the design rules for prismatic members in compression, bending and combination of bending and compression.

The comparison is carried out on the basis of partial safety factor γ_{M1}^{*} calculated using the procedure from Section 5.2.2 with the statistical data for basic variables from 5.3.

The buckling strength of the members is obtained using advanced numerical finite element simulations as described in Chapter 4.

For each case (flexural and lateral-torsional buckling), a wide range of I-shaped cross sections covering several buckling curves were analyzed across a wide ranges of slenderness. The parametric studies are organized by buckling mode and they are defined in Section 5.4.3 for members in compression, bending and combined bending and compression.

The safety assessment procedure was applied together with the following assumptions:

- The variability of the input variables in the design model is not considered for the calculation of V_δ; the value is obtained from nominal properties since the "experimental" results are considered with nominal properties;

- The coefficient of variation of the basic variables, V_{rt}, considers only the variability of cross section dimensions, yield stress and modulus of elasticity; for these parameters more information is known and documented with recent data;

For the flexural buckling of columns, the yield stress, f_y, is considered either according to the provisions of the product standard EN 10025, or from Table 3.1 of EC3-1-1. Since Table 3.1 of EC3-1-1 does not account for $t>80$ mm, for such cases, the same value of f_y as in EN 10025 was considered, see *Figure 5.4*.
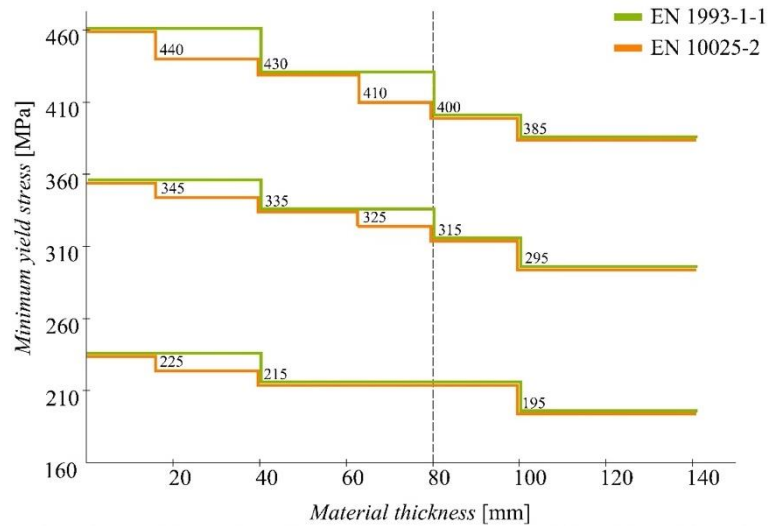
Figure 5.4 – Variation of the yield stress with thickness

For beams and beam-columns, the variation of the yield stress with thickness was assumed according to the product standard.

For columns, the geometrical imperfections were modelled using an initial sinusoidal imperfection introduced in the weak or strong axis of the cross-section, with an amplitude $e_0=L/1000$ at mid span. Residual stresses were considered according to *Figure 5.5*. The adopted value of $f_y{}^*$ indicated in *Figure 5.5* was $f_{y,235}=235$ MPa. Nevertheless, for comparison, equivalent cases were included using the nominal value of the yield stress f_y.
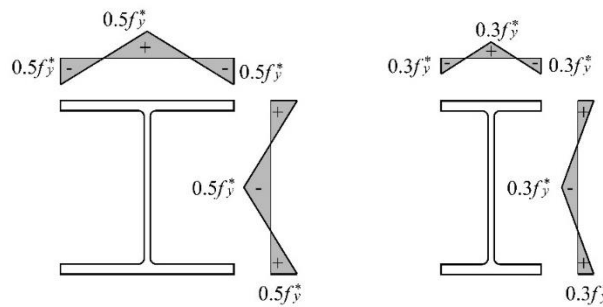
(a) Hot-rolled, h/b<1.2   (b) Hot-rolled, h/b>1.2
Figure 5.5 – Residual stresses ("+" Tension and "–"Compression)

As the main purpose of this study is the assessment of existing rules for prismatic members in compression, bending and a combination of bending and compression from EC3-1-1, in order to cover all types of hot-rolled sections according to *Table 6.2* of EC3-1-1, a wide range of I-shaped cross-sections was selected so that flange thickness and the ratio *h/b* would vary.

In this section, firstly, the scope of the parametric study is introduced; subsequently, the methodology for assessment of results is given and finally, the results are discussed.

5.4.2 Design resistance

5.4.2.1 Members in compression

For the evaluation of the flexural buckling resistance of steel columns, clause 6.3.1 in EC3-1-1 is considered to represent the theoretical result, r_{ti}, in the safety assessment procedure. The design procedure is summarized in Section 2.3.1 for simply supported members of length L, whereas the imperfection factors are summarized in *Table 2.2* for the cross section shapes covered by the parametric study. The imperfection factors are considered from *Table 2.2* and imperfection factors by *Snijder et al.* (2014) for hot-rolled heavy cross-sections with $t_f>100$ mm and $h/b>1.2$.

Table 5.4 - Imperfection factors and generalized imperfection limits for flexural buckling

Fabrication	Limits		Axis	EC3-1-1		(*Snijder et al.*, 2014)	
				S235 S355	S460	S235 S355	S460
Rolled	h/b>1.2	$t_f\leq40$ mm	y-y	0.21	0.13	-	-
			z-z	0.34	0.13		
		40 mm<$t_f\leq$ 100 mm	y-y	0.34	0.21	-	-
			z-z	0.49	0.21		
		$t_f>100$ mm	y-y	-	-	0.34	0.21
			z-z			0.49	0.34
	h/b≤1.2	$t_f\leq100$ mm	y-y	0.34	0.21	-	-
			z-z	0.49	0.21		
		$t_f>100$ mm	y-y	0.76	0.49	-	-
			z-z	0.76	0.49		

5.4.2.2 Members in bending

For the evaluation of the lateral-torsional buckling resistance, the methods described in Section 2.3.2 were used. A similar assessment performed in 2009 (*Rebelo et al.*, 2009) considered the General Case modified with the factor *f* from the Special Case. The method was included here for completeness.

5.4.2.3 Members in bending and compression

The design resistance of members in bending and compression was evaluated using the interaction formula with interaction coefficients for Method 2/Annex B (see Section 2.3.3) since it was foreseen that only this method would remain in a future version of Eurocode 3.

5.4.3 Parametric studies

5.4.3.1 Flexural buckling of columns

Table 5.6 summarizes the hot-rolled sections selected for the study, organized according to *Table 6.2* of Eurocode 3 (2005). The selection also includes 2 (two) American profiles.

The parametric study comprised 7332 numerical models, both for minor and major axis flexural buckling behaviour (3666 models for each mode). It includes several levels of slenderness, different steel grades, and two different levels of residual stresses (proportional to the yield stress or as a fraction of 235MPa), as given in *Table 5.5*.

Table 5.5: Parametric study for columns: additional parameters

Fabrication	$\bar{\lambda}$	Material and standard for f_y	Material imperfections
Rolled	0.5; 0.6; 0.7; 0.8 0.9; 1.0; 1.2; 1.4; 1.5 1.6; 1.8; 2.0; 2.5	**EN 10025:** S235 S355 S460	**h/b≤1.2:** $\frac{f_{y,235}}{f_y}$ **h/b>1.2:** $\frac{f_{y,235}}{f_y}$

Table 5.6: Sections of the parametric study for columns

Fabrication	Limits		Sections		
			h/b	t_f	Profiles
Rolled	h/b>1.2	$t_f \leq 40$ mm	1.22	40	HEM340
			1.3	19	HEA400
			1.7	40	HEM500
			1.92	6.9	IPE140
			2.19	40	HEM650
			1.74	5.2	IPE80
			1.82	5.7	IPE100
			1.33	24	HEB400
			1.67	28	HEB500
			1.95	7.4	IPE160
			1.41	40	HEM400
			1.50	24	HEB450
			1.28	40	HEM360
		40 mm<$t_f \leq 100$ mm	2.28	55.9	HL920x588
			2.29	62	HL920x656
			2.35	99.1	HL920x1077
			3.36	64	HE1000x584
			2.31	73.9	HL920x787
			2.30	68.1	HL920x725
			3.08	65	W920x310x576
			2.56	70	HL1000x748
			2.05	69.1	W610x325x551
			2.06	54	HE600x399
			2.36	46	HE700x352
			2.69	54	HE800x444
			3.01	54	HE900x466
		t_f>100 mm	1.231	130	HD400x1202
			2.4	109	HL920x1194
			1.201	106	HD400x900
			1.23	115	HD400x990
			2.37	115.1	HL920x1269
			2.31	115.1	HL920x1377
			1.25	125	HD400x1086
			1.26	140	HD400x1299
	h/b≤1.2	$t_f \leq 100$ mm	1.2	22.5	HEB360
			1.17	97	HD400x818
			0.96	8	HEA100
			1.0	19	HEB300
			1.1	39	HEM300
			1.0	10	HEB100
			1.0	15	HEB200
			1.17	17.5	HE360A
			1.09	67.6	HD400x551
			1.12	77.1	HD400x634
			1.04	52.6	HD400x421
			1.10	72.30	HD400x592
			1.00	17	HEB240
		t_f>100 mm	*No sections exist*		

5.4.3.2 Lateral-torsional buckling of beams
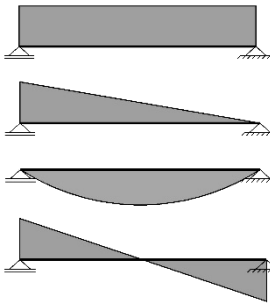
Table 5.7 summarizes the hot-rolled sections selected for the assessment of lateral-torsional buckling of prismatic beams.

Table 5.7 - Sections of the parametric study for beams.

Fabrication	Limits			Sections		
	EC3-1-1 Columns	t_f	EC3-1-1 Beams	h/b	t_f [mm]	Profiles
Rolled	h/b>1.2	$t_f \leq 40$ mm	h/b>2.0	2.22	13.5	IPE400
				2.50	16	IPE500
				2.73	19	IPE600
			h/b ≤2.0	1.82	5.7	IPE100
				2.00	8.5	IPE200
				2.00	9.8	IPE240
				2.00	10.7	IPE300
		40 mm<t_f≤100 mm	h/b>2.0	2.30	68.1	HL920x725
				2.56	70	HL1000x748
				2.31	73.9	HL920x787
				3.36	64	HE1000x584
				3.08	65	W920x310x576
				2.05	69.1	W610x325x551
			h/b ≤2.0	1.41	40	HE400M
				1.71	40	HE500M
				1.30	19	HE400A
				1.33	24	HE400B
				2.0	30	HE600B
				2.52	41.9	HL1000x443
				2.52	46	HL1000x483
				2.27	51.1	HL920x537
	h/b ≤1.2	t_f≤100 mm	-	1.00	19	HE300B
				1.00	15	HE200B
				1.00	10	HE100B
				1.13	20	HE100M
				1.10	21	HE300M
				0.95	8	HE120A
				1.09	67.6	HD400x551
				1.10	72.3	HD400x592
				1.12	77.1	HD400x634

The parametric study consists of 3523 numerical calculation runs. It includes several levels of slenderness and different steel grades (the ones currently included in EC3-1-1). The parameters are summarized in *Table 5.8*. Due to the diversity of the cross-sections and in order to avoid unrealistic lengths, only beams with ratios L/h < 40, where L is the beam length and h is the cross-section depth, were considered in the parametric study.

Table 5.8 - Parametric study for beams: additional parameters

Fabrication	$\bar{\lambda}_{LT}$	Material standard for f_y	Material imperfections	Load
Rolled	0.2; 0.4; 0.6; 0.8; 1.0; 1.1; 1.2; 1.3; 1.4; 1.5; 1.6; 1.7; 1.8; 2.0; 2.1	EN 10025: S235 S355 S460	h/b≤1.2: $f_{y,235}$ h/b>1.2: $f_{y,235}$	

5.4.3.3 Beam-columns
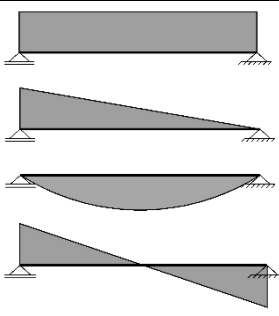
For the assessment of the members under bending and compression, numerical results by *Ofner* (1997) used in the calibration of the interaction formula, additional cases for lateral-torsional buckling under major axis bending moment and axial force performed in the scope of the Master's thesis by *Anwar* (2015) and additional cases carried out at UC were used. *Table 5.9* lists the selected hot-rolled sections and *Table 5.10* summarizes the parameters which give a total of 11 345 cases.

| 125

Table 5.9 - Sections of the parametric study for beam-columns.

Fabrication	Limits		h/b	t_f [mm]	Profiles	Source
Rolled	h/b >1.2	t_f≤40 mm	1.82	5.7	IPE100	Anwar (2015)
			1.95	7.4	IPE160	Anwar (2015)
			2.00	8.5	IPE200	Ofner (1997)
			2.5	16	IPE500	Ofner (1997)
			1.98	8	IPE180	Anwar (2015)
			2.12	12.7	IPE360	Anwar (2015)
			1.30	19	HE400A	Anwar (2015)
			1.67	28	HE500B	Anwar (2015)
			2.17	21	HE650B	Anwar (2015)
		40 mm<t_f≤100 mm	2.04	46	HE600x337	Anwar (2015)
			2.28	55.9	HL920x588	UC (2018)
			3.36	64	HE1000x584	UC (2018)
			2.36	46	HE700x352	UC (2018)
			2.69	54	HE800x444	UC (2018)
			2.20	46	HE650x342	Anwar (2015)
	h/b ≤1.2	t_f≤100 mm	1.0	19	HE300B	Ofner (1997)
			0.97	14	HE300A	Anwar (2015)
			1.01	43.7	HD400x347	Anwar (2015)
			1.05	29	HE300C	Anwar (2015)
			1.13	21.5	HE340B	Anwar (2015)

Table 5.10 - Parametric study for beam-columns: additional parameters

Fabrication	$\bar{\lambda}_z$	ϕ	Material standard for f_y	Material imperfections	Load
Rolled	0.4; 0.5, 0.6; 0.8; 1.0; 1.2; 1.4; 1.5, 1.6; 1.8;	5.67, 2.74, 1.73, 1.19 0.83, 0.57 0.36, 0.17 0	EN 10025: S235	h/b≤1.2: $f_{y,235}$ h/b>1.2: $f_{y,235}$	

5.5 Columns

5.5.1 Methodology

In the subsequent sections, the results for minor and major axis flexural bucking of columns are detailed. The following main topics are discussed:

– Influence of the specification of the minimum yield stress according to EN 10025 and Eurocode 3;

– Influence of the magnitude of residual stresses used in the numerical analyses;

– Influence of the imperfection factor α for steel grade S460;

– Validation of the buckling curves for heavy sections;

– Influence of the number of random variables;

Throughout the following paragraphs, charts and tables, the following methodology is adopted:

– The partial factors for different subsets are computed considering the procedure summarized in Figure 5.2.

– Whenever a subset according to slenderness is analyzed, the following division is adopted:

  ▪ *Low* slenderness – normalized slenderness $\bar{\lambda} \in [0.5; 0.8]$;

  ▪ *Medium* slenderness– normalized slenderness $\bar{\lambda} \in (0.8; 1.5]$;

- ▪ *High* slenderness – normalized slenderness $\bar{\lambda} \in (1.5; 2.5]$;

  – For the first 4 topics listed above, only the variability of the yield stress is considered, as a relative assessment is sufficient to establish the influence of each parameter;
  – In order to establish the influence of additional random variables, the following variables are considered: yield stress, geometrical dimensions of the cross-section and modulus of elasticity.

Hereby the results for minor axis and major axis flexural buckling are presented and discussed. Firstly, the reference cases for hot-rolled cross sections are analyzed: the value of the yield stress both in r_e and r_t is considered according to EN 10025 and the level of the residual stresses is proportional to <u>0.3(0.5) x 235 MPa</u> for *h/b>(≤1.2)*. Subsequently, the reference cases are analyzed considering the value of the yield stress and r_t according to *Table 3.1* of EC3-1-1, the experimental value r_e is computed according to the EN 10025, assuming it as the "reality". Finally, the reference cases are analyzed considering the level of the residual stresses proportional to <u>0.3(0.5) x f_y</u> for *h/b>(≤1.2)*;

5.5.2   Results and discussion – Minor axis flexural buckling

The parametric study was constructed aiming to cover all buckling curves for hot-rolled H and I sections and therefore, the sample includes members whose resistance is evaluated using different imperfection factors (*α* according to *Table 2.2*), different steel grades which are defined by different distributions, etc. Hence, further division into subsets is required, in order to avoid undesired bias of the results.

Since the reduction factor is mainly a function of slenderness, results should be assessed and organized by subsets of the slenderness ranges, as shown in *Figure 5.6*. The subsets are adopted according to Low [0.5; 0.8]; Medium (0.8; 1.5]; and High (1.5; 2.5]. A larger partial safety factor is observed for S460 in *Figure 5.6* when compared to the other steel grades for all slenderness ranges. A possible explanation for this value is that the imperfection factors currently adopted for steel grade S460 may not be appropriate. This was independently confirmed by *Lindner* (2015) and may thus require adjustment.
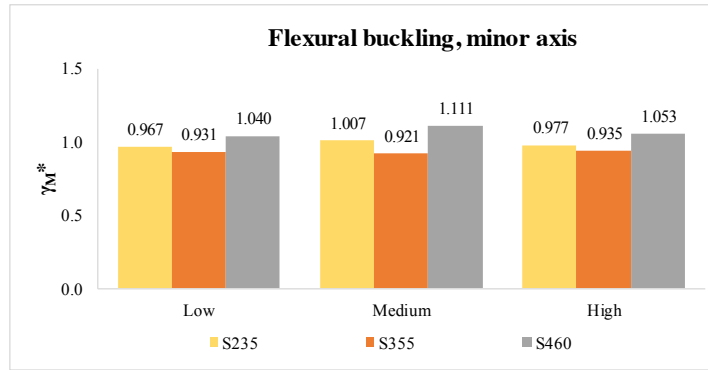
Figure 5.6 All results organized by slenderness for hot-rolled cross sections – f_y according to EN 10025

Figure 5.7 illustrates the results organized by the divisions given in *Table 2.2*, regardless of the slenderness range, thus allowing a direct comparison of the buckling curves in EC3-1-1. Firstly, it is clear that steel grade S355 leads to lower values of γ_{M1}. This is due to the relative amplitude of the residual stress with respect to the yield stress of the member when compared to S235 steel. *Figure 5.7* again confirms that the imperfection factors for S460 may not be adequate, except for $h/b>1.2$, $t_f>100$ mm because they were recently proposed and calibrated as this range was not available in the code (*Snijder et al.*, 2014). Finally, note that no cases with $h/b\leq1.2$ and $t_f>100$mm are included in the parametric study since no sections with these characteristics were found in catalogs.

Figure 5.7 All results organized by buckling curve division for hot-rolled cross sections – f_y according to EN 10025

5.5.2.1 *Influence of the variation of the yield stress with thickness*

The value of the yield stress in the theoretical value of the resistance r_t is now considered according to EC3-1-1, *Table 3.1* and the "experimental" resistance r_e is computed considering the sub-divisions according to EN 10025, and presented in relative terms with respect to the results of EN 10025 (*Figure 5.8*). Results of *Figure 5.8* are better interpreted together with *Figure 5.4*. The second group for S235 and third group give the same values since the specifications of the yield stress in EN 10025 and EC3-1-1 are equal for the cross sections

considered in the parametric study. On the other hand, for the first and fourth groups as well as second group for S355 and S460, differences are noted, for sections with thicknesses falling in the ranges (16; 40) and (63; 80), since the specifications in EC3-1-1 and EN 10025 are different in those ranges.
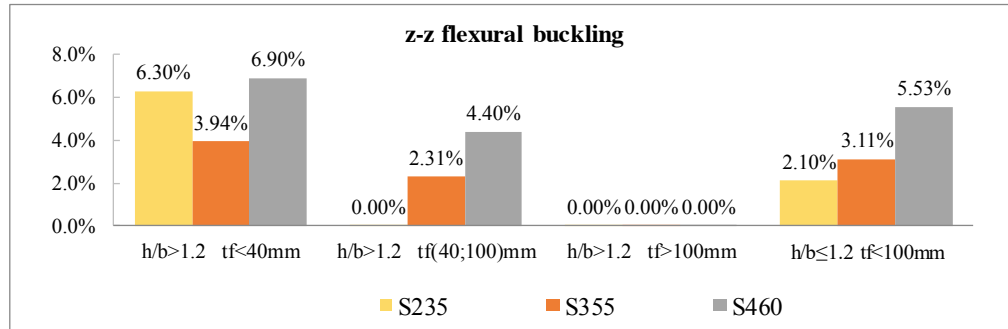
Figure 5.8 Percentage difference for normalized γ_{M1} between yield stress calculated according to EC3-1-1 and EN 10025

The results in *Figure 5.8* include thickness ranges that are different from the division according to EN 10025; hence, *Figure 5.9* compares results between EN 10025 and EC3-1-1 for the intervals defined in EN 10025, highlighting maximum differences of about 8%.
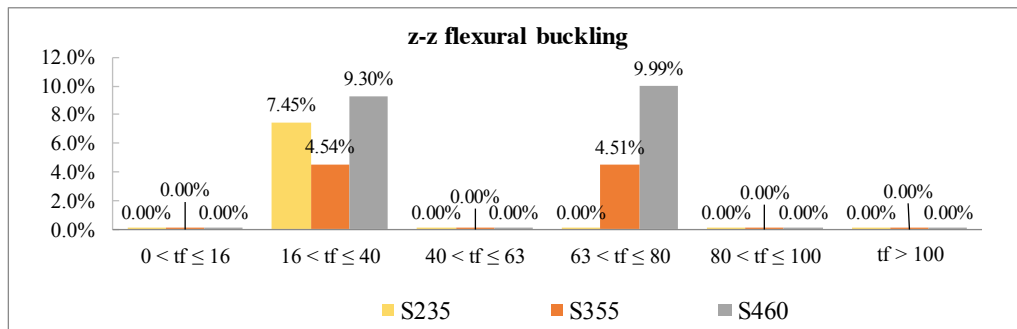
Figure 5.9 Percentage difference for normalized γ_{M1} between yield stress calculated according to EC3-1-1 and EN 10025

5.5.2.2 Influence of the assumptions for the residual stress

Figure 5.10 and *Figure 5.11* present relative results for the partial factor similarly to *Figure 5.7*, but assuming the conservative option that the level of the residual stresses is proportional to the yield stress 0.3(0.5) x f_y for h/b>($\leq$1.2). Since a higher level of the residual stresses is now considered (more conservative), the partial safety factor is expected to increase. This is observed both for steels S355 and S460, see *Figure 5.10* and *Figure 5.11* respectively. For steel grade S235, the analysis is not relevant.
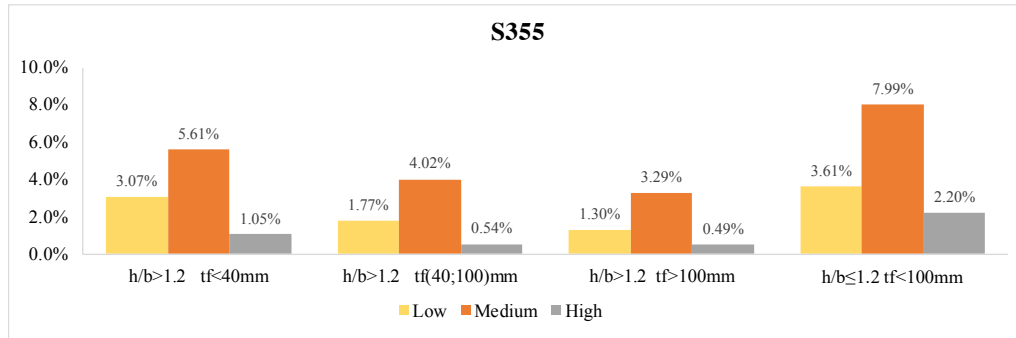
Figure 5.10 All results organized by buckling curve and slenderness division for hot-rolled cross sections and steel grade S355 – residual stress proportional to the actual value of f_y (f_y according to EN 10025)

Figure 5.10 and *Figure 5.11* represent the subsets by buckling curve, slenderness and steel grade. It is clearly seen that the influence of the residual stresses has higher impact in the medium slenderness range, as expected. Moreover, *Figure 5.11* further shows that the adoption of residual stresses proportional to the yield stress 0.3(0.5) x f_y is too conservative.
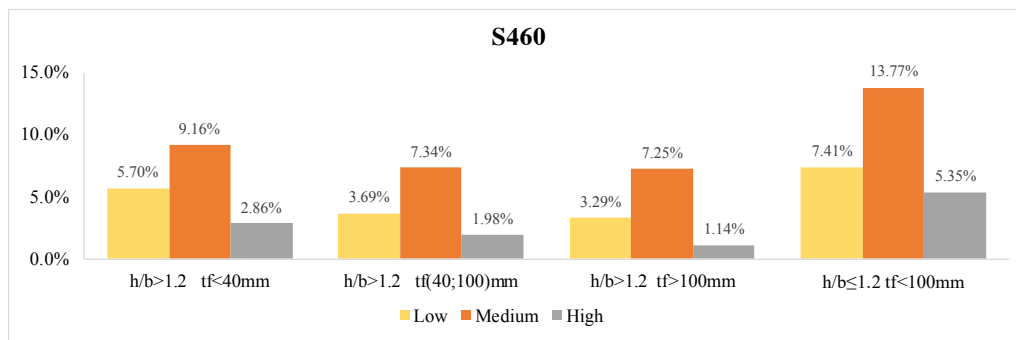
Figure 5.11 All results organized by buckling curve and slenderness division for hot-rolled cross sections and steel grade S460 – residual stress proportional to the actual value of f_y (f_y according to EN 10025)

5.5.2.3   *Evaluation of the partial safety factor considering new imperfection factors for S460*

It was already seen that the results for steel grade S460 are significantly higher than those for the other steel grades. A possible improvement can be introduced by considering higher imperfection factors for minor axis flexural buckling as shown in *Table 5.11* (values in bold).

Figure 5.12 and *Figure 5.13*, similarly to *Figure 5.6* and *Figure 5.7* show the results according to slenderness and buckling curve division, respectively. The improvement of using higher imperfection factors for steel grade S460 is clear.

Table 5.11 New imperfection factor for steel grade S460, minor axis

Fabrication	Limits		Axis	EC3-1-1		Snijder et al. (2014)	
				S235 S355	S460	S235 S355	S460
Rolled	h/b>1.2	t_f≤40 mm	y-y	0.21	0.13	-	-
			z-z	0.34	**0.21**		
		40 mm <t_f≤100 mm	y-y	0.34	0.21	-	-
			z-z	0.49	**0.34**		
		t_f>100 mm	y-y	-	-	0.34	0.21
			z-z			0.49	0.34
	h/b≤ 1.2	t_f≤100 mm	y-y	0.34	0.21	-	-
			z-z	0.49	**0.34**		

*h/b≤1.2 and t_f>100 mm is not included in the table, because no cross-sections were found
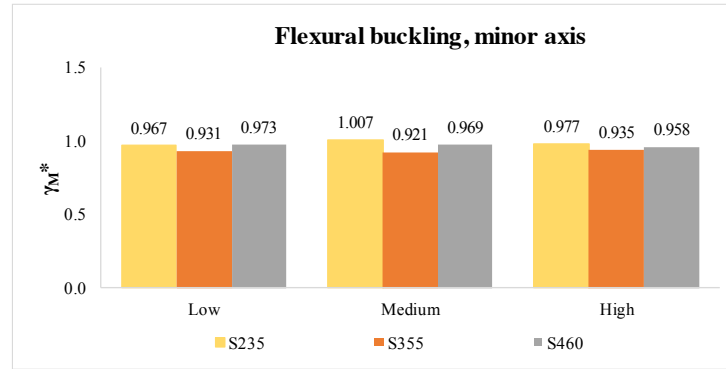
Figure 5.12 All results organized by slenderness for hot-rolled cross sections – f_y according to EN 10025

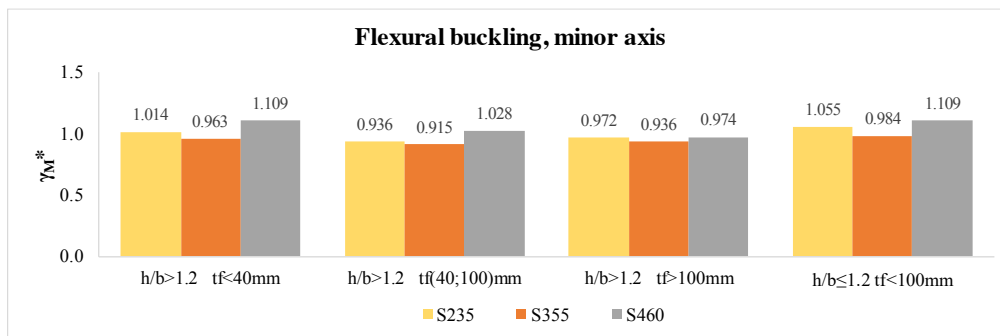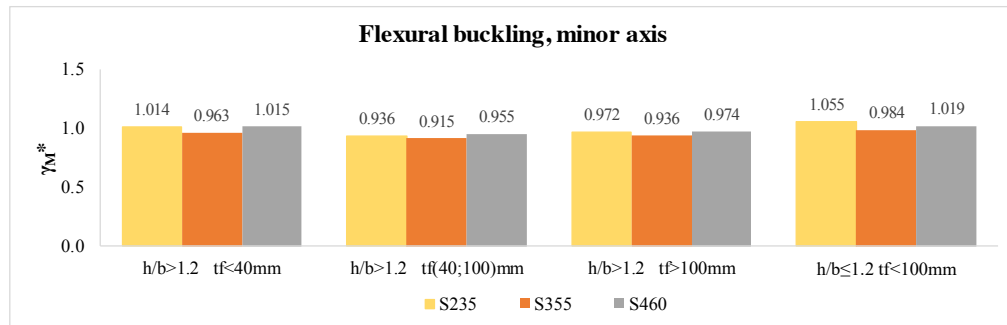*Figure 5.13 All results organized by buckling curve division for hot-rolled cross sections – f_y according to EN 10025*

5.5.3 Results and discussion – Major axis flexural buckling

Identically to minor axis flexural buckling, the safety assessment is computed considering the Annex D procedure and the variability of yield stress only. Firstly, the reference cases for hot-rolled cross sections are analyzed: the yield stress both in r_e and r_t is considered according to

EN 10025. Unlike minor axis flexural buckling, the relative values of the partial safety factor are more uniform for the different steel grades (*Figure 5.14*).
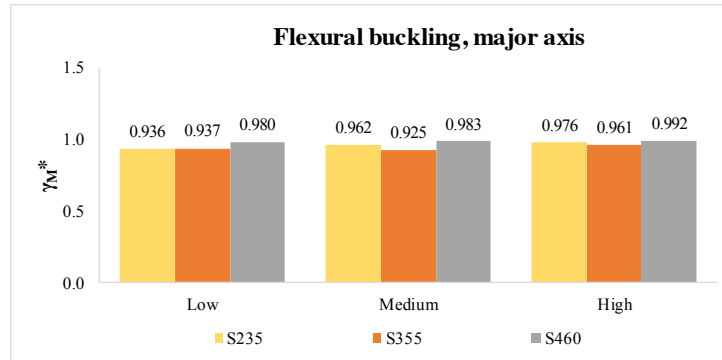
Figure 5.14 All results organized by slenderness for hot-rolled cross sections – f_y according to EN 10025

Similarly to *Figure 5.7* for minor axis flexural buckling, *Figure 5.15* illustrates the results organized according to the divisions presented in *Table 2.2*, regardless of the slenderness range, thus allowing a direct comparison of the buckling curves specified in EC3-1-1. All cases fall within an acceptable range of variation of the partial safety factor.
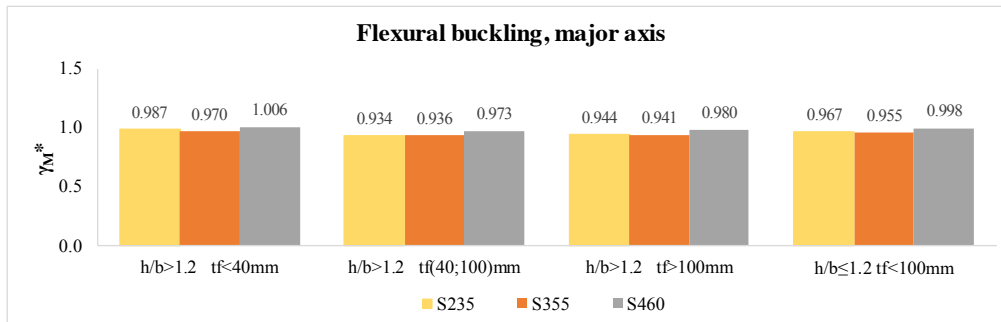
Figure 5.15 All results organized by buckling curve division for hot-rolled cross sections – f_y according to EN 10025

Furthermore, when the influence of the variation of the yield stress with increasing flange thickness was analysed, similar conclusions were drawn. Identical results were found when the residual stresses were assumed proportional to the yield stress as in Section 5.5.2.2.

5.5.4   Influence of the number of random variables

In the previous sub-sections, only f_y was considered as a random variable. In reality, in the case on flexural buckling of columns, other basic variables also affect the behaviour of a column, such as the cross-section dimensions and the Young's modulus. It is noted that geometrical and material imperfections such as initial curvature and residual stresses are not included as basic

random variables as they are included implicitly in the design model (*Simões da Silva et al. 2014*).

Hence, the following random variables are included in the analysis:

- Yield stress – f_y;
- Geometrical dimensions – b, h, t_w, t_f;
- Young's modulus – E;

The distributions of the basic variables are considered as given in Section 5.3. The influence of the number of basic variables is accounted as their number is gradually increased. The following cases are considered:

- **Annex D (fy)** – considers the yield stress as the only basic variable, the other parameters are assumed as deterministic quantities with no variability;
- **Annex D (fy+CS)** – considers the yield stress and the geometrical dimensions of the cross-section as random variables;
- **Annex D (fy+CS+E)** – considers the yield stress, the geometrical dimensions of the cross-section and the modulus of elasticity as random variables;

γ_{M1}^* is calculated for both major and minor axis flexural buckling for all three cases.

5.5.4.1 Minor axis flexural buckling

Subsets of steel grade and slenderness are analysed in *Figure 5.16* for Annex D (f_y + CS + E), partial factors obtained for minor axis and considering the assumptions previously made. As expected, higher values of γ_{M1}^* are obtained, the rate of increase of γ_{M1} rises with increasing slenderness as Young's modulus and geometrical dimensions (moment of inertia) become more relevant in the medium and high slenderness ranges.
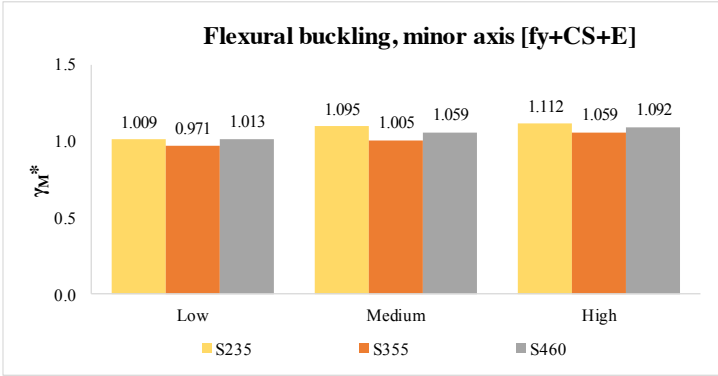
Figure 5.16 - All results organized by slenderness and steel grade – using fy, cross-section dimensions and modulus of elasticity as random variables

Similarly, results split according to buckling curve and steel grade are given in *Figure 5.17*.
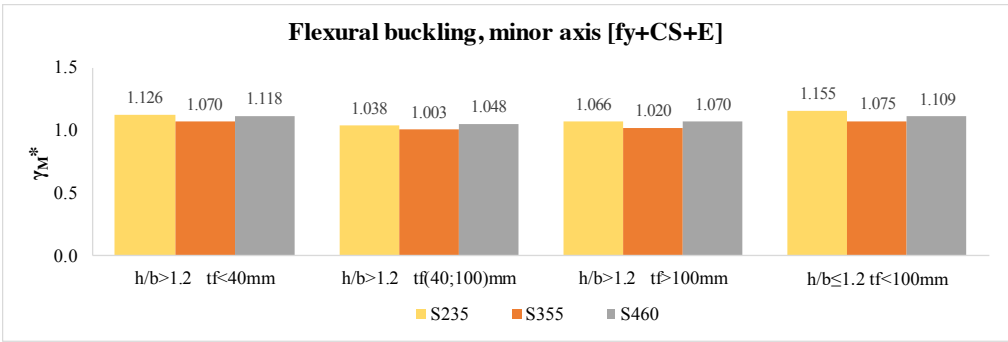
Figure 5.17 - All results organized by buckling curve for hot-rolled cross sections – using fy, cross-section dimensions and modulus of elasticity as random variables

Finally, a comparison of different assumptions of the coefficient of variation of the Young's modulus is illustrated in *Figure 5.18*, where the differences become more significant for high slenderness.
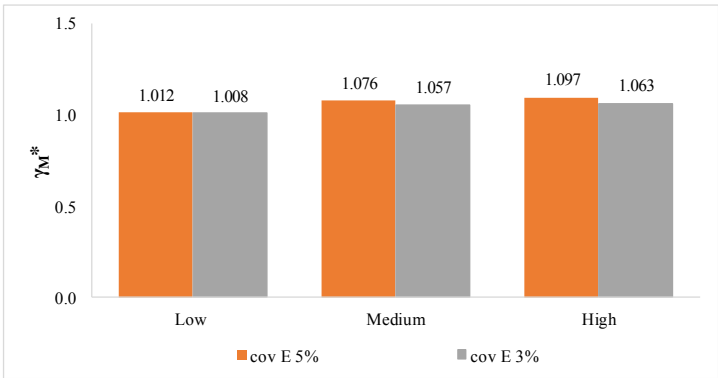
Figure 5.18 - Assessment of different assumptions of the coefficient of variation of the modulus of Elasticity

5.5.4.2 *Major axis flexural buckling*

The same evaluation was performed for major axis of flexural buckling. The results are similar to the conclusions in the previous section, i.e. the presence of the modulus of elasticity leads to higher values for γ_{M1} (*Figure 5.19* and *Figure 5.20*). However, in general, the values of the γ_{M1} for major axis flexural buckling are lower than those for minor axis as presented in section 5.5.4.1.
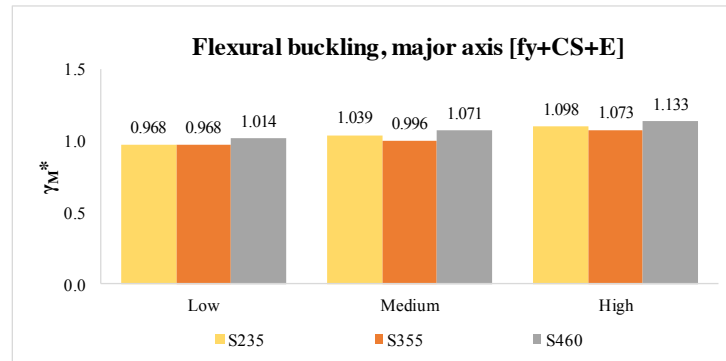
Figure 5.19 - All results organized by slenderness and steel grade – using fy, cross-section dimensions and modulus of elasticity as random variables
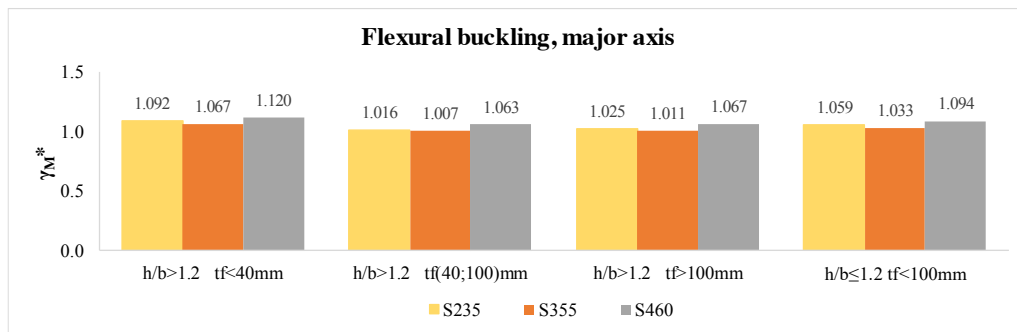
Figure 5.20 - All results organized by buckling curve for hot-rolled cross sections – using fy, cross-section dimensions and modulus of elasticity as random variables

5.5.5 **Assessment of the partial factor**

The previous section analysed the design rules for the flexural buckling of columns in terms of the required value of the partial factors γ_{M1}^* to match the target probability of failure specified in EN 1990. The analysis was carried out relatively because the value of γ_{M1}^* is highly dependent on the quality of the design rules and scatters for the various subsets that are considered. It was shown that the design rules provide consistent results across the various possible subsets, with small scatter on the value of γ_{M1}^*.

In this section it is proposed to discuss the adoption of a single global γ_{M1} for flexural buckling of columns that is in line with the failure probability in EN 1990 and incorporates all the viewpoints that support code drafting and the choice of safety factors.

Table 5.12 summarizes the partial factors obtained for minor and major axis, now given as absolute values instead of normalized values.

Table 5.12 - Values of γ_{M1} obtained using different random variables for major and minor axes flexural buckling

Limits		Axis	Annex D (fy)		Annex D (fy+CS)		Annex D (fy+CS+E)	
			S235 S355	S460	S235 S355	S460	S235 S355	S460
h/b>1.2	$t_f \leq 40$ mm	y-y	0.978	1.006	1.030	1.066	1.079	1.120
		z-z	0.989	1.015	1.055	1.077	1.098	1.118
	40 mm $<t_f \leq 100$ mm	y-y	0.935	0.973	0.973	1.018	1.011	1.063
		z-z	0.925	0.955	0.983	1.011	1.021	1.048
	$t_f > 100$ mm	y-y	0.943	0.980	0.978	1.021	1.018	1.067
		z-z	0.954	0.974	1.008	1.032	1.043	1.070
h/b≤ 1.2	$t_f \leq 100$ mm	y-y	0.961	0.998	1.004	1.047	1.046	1.094
		z-z	1.020	1.019	1.079	1.075	1.115	1.109

Table 5.13 - Average γ_{M1} for minor and major axis flexural buckling, according to buckling curves and slenderness

	Axis	Annex D(fy)	Annex D(fy+CS)	Annex D(fy+CS+E)
Mean value	y-y	0.937	0.988	1.035
	z-z	0.936	1.002	1.041
CoV	y-y	3.8%	4.5%	6.4%
	z-z	4.1%	4.4%	5.6%

Further division into subsets according to slenderness is performed in order to be able to compare the different slenderness ranges (*Simões da Silva et al.* (2016)). Even though finer

subsets into slenderness, steel grade and buckling curve are adopted, partial factors higher than unity are mostly only observed when the Young's modulus is included.

Table 5.13 summarizes the mean and standard deviation of γ_{M1} for the three different sets of random variables that were considered. It is concluded that depending on the random variables included in the analysis (just f_y; f_y and cross-section geometry; or f_y, cross-section geometry and modulus of elasticity E) the average value of γ_{M1} varies from 0.936 to 1.041 with the c.o.v varying from 3.8% to 6.4%. The mean value is lower than 1.05 for the more unfavourable case and the c.o.v. is low. Additionally, in general, the values of the γ_{M1} for major axis flexural buckling are similar to those for minor axis.

Recalling that the currently recommended value of γ_{M1} in Eurocode 3, part 1, is 1.0, and comparing with available data from the literature that led to the choice of $\gamma_{M1} = 1.0$, the results presented in this report for γ_{M1} are lower. In *Muller* (2003), a study on the flexural buckling resistance of hot-rolled sections was done and the corresponding partial safety factors were assessed, see *Figure 5.1*, corresponding to an average value of γ_{M1} for minor axis flexural buckling of 1.097 (cf. 0.937 as these results only considered the variability of f_y).

It is interesting to note that the observed trend (also in *Muller* (2003)) of an increasing value of γ_{M1} in the intermediate slenderness range disappears when variability in cross-section and Young's modulus is included: in this case the value of γ_{M1} increases monotonically with slenderness. It is noted that the higher value of γ_{M1} for high slenderness is not so relevant because of practical reasons (practical range of column slenderness), as the parametric study included normalised slenderness ($\bar{\lambda}$) up to 2.5. It is therefore recommended to keep $\gamma_{M1}=1.0$ for columns. This recommendation was taken in the final draft of prEN 1993-1-1 (CEN/TC250, 2017).

5.6 Beams

5.6.1 Methodology

In the following sections, the results for lateral-torsional buckling of beams are detailed. The main topics that are discussed are:

- Comparison of the various design methodologies for the determination of the lateral-torsional buckling resistance of hot-rolled I-beams with fork conditions;

–   Influence of the bending moment distribution;

–   Assessment of the imperfection factors for the New EC3 method;

–   Influence of the number of random variables

Throughout the following paragraphs, charts and tables, the following methodology is adopted:

–   The General Case is presented as the reference method for comparative purposes;

–   The partial factors for the different subsets are computed considering the *Annex D* procedure summarized in *Figure 5.2;*

–   A lower tail approximation is applied to all subsets;

–   Whenever a subset according to slenderness is analysed, the following division is adopted:

  ▪   *Low* slenderness – normalized slenderness $\bar{\lambda} \in (0.2; 0.8]$;

  ▪   *Medium* slenderness– normalized slenderness $\bar{\lambda} \in (0.8; 1.2]$;

  ▪   *High* slenderness – normalized slenderness $\bar{\lambda} \in (1.2; 2.1]$;

–   For the first three topics listed above, only the variability of the yield stress is considered, as a relative assessment is sufficient to establish the influence of each parameter;

–   In order to establish the influence of additional random variables, the following variables are considered: yield stress, geometrical dimensions of the cross-section and modulus of elasticity.

5.6.2   Overview

Before applying the Annex D procedure for statistical evaluation, it is useful to examine the design model accuracy. In *Figure 5.21* and *Figure 5.22* scatterplots for all the methods are given. In the abscissa, the estimation of the advanced numerical simulations is plotted, while the ordinates correspond to one of the design methods.

In order to give a quantitative measure of the model variations, the statistical parameters for the ratio experimental over theoretical values (r_e/r_t) are given in *Table 5.14*, where ratios higher than unity indicate a safe-sided estimation, and on the contrary, ratios lower than 1.0 indicate unsafe results. The General Case and GC/f show a high variability of the results, with coefficients of variation of 8.8% and 7.7% respectively. The ratios r_e/r_t vary from about 10% unsafe to about 40% safe.
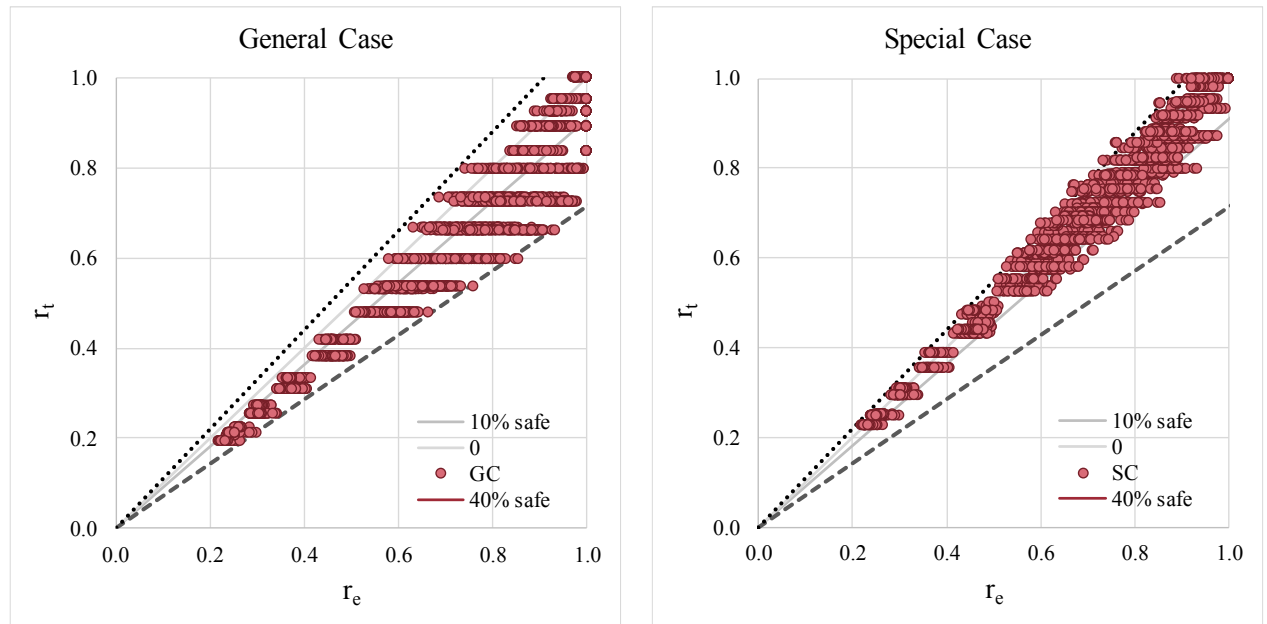
Figure 5.21 Scatterplots General and Special Case
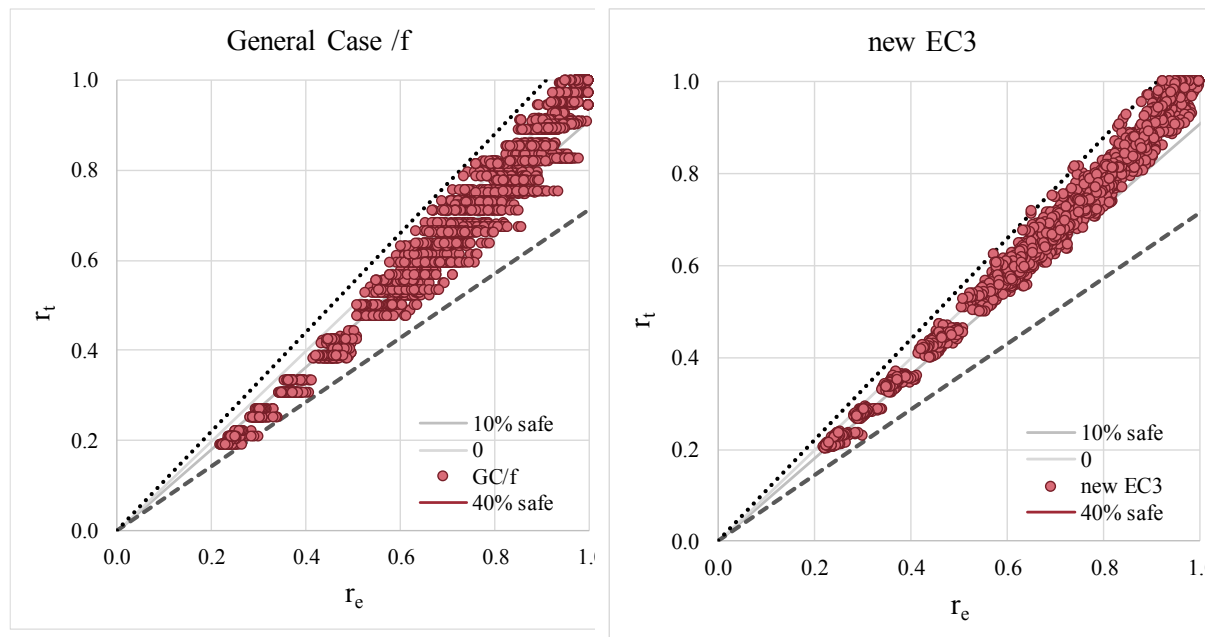
Figure 5.22 Scatterplots General Case/f and Taras

The other two methods, Special Case and New EC3 have lower coefficients of variation (4.9% and 4.5%, respectively) but the level of overestimation of the resistance by the Special Case is significantly higher than for the New EC3 method.

These results confirm earlier studies on the lateral torsional buckling of beams *Rebelo et al.* (2009), *Simões da Silva et al.* (2009) and *Taras* (2010) whereby a high scatter of the LTB

resistances across the slenderness was also observed, from unsafe to very safe for the three first methods.

Table 5.14 - Statistical parameters (>1.0 safe-sided)

	nEC3	GC	SC	GC/f
mean	1.03	1.13	1.01	1.08
cov	4.5%	8.8%	4.9%	7.7%
min	0.91	0.93	0.88	0.93
max	1.30	1.44	1.21	1.43
<0.97	144	20	625	73
<1	719	214	1230	431

5.6.3 Results and discussion: General Case

In this section the reference cases considering the General Case are presented. In *Figure 5.23* the γ_M* results are divided according to slenderness and steel grade. It is observed that there is not a significant difference between the considered steel grades. The higher results in the low slenderness range occur for all steel grades, reflecting the more decisive role that f_y plays for this slenderness range.
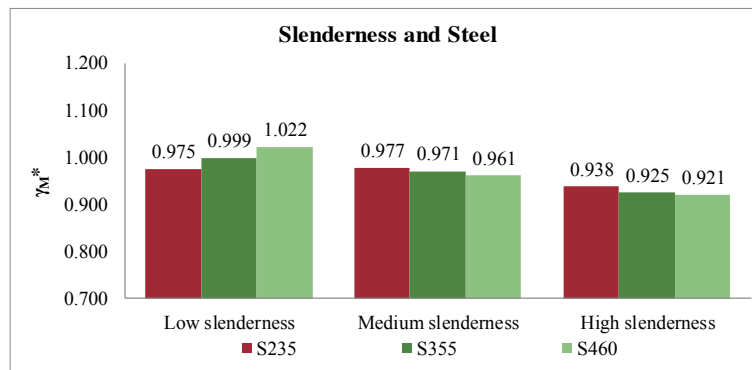
Figure 5.23 - γ_M organized by slenderness and steel*

Figure 5.24 and *Figure 5.25* organize the results by buckling curve division. The first compares different steel grades, while the latter compares different slenderness ranges. *Figure 5.24* shows that considering subsets organized by steel grade there is a trend of the γ_M* values to increase with the steel grade. This contrasts with the results of *Figure 5.25*, highlighting the importance of the consideration of subsets and the sensitivity of results to the choice of subsets *Taras et al.* (2017). *Figure 5.25* shows that the safety level of the two buckling curves is not homogeneous.
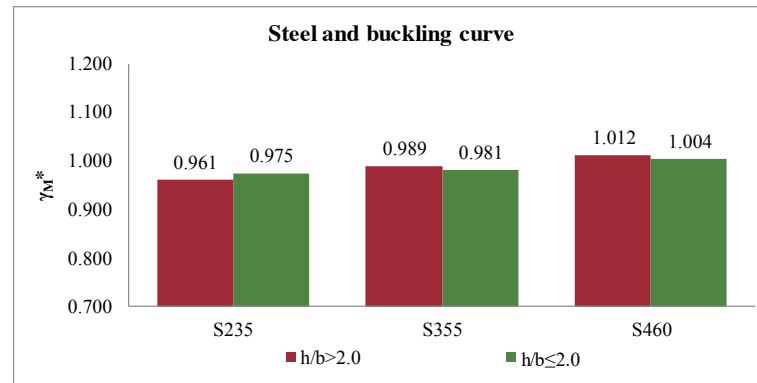
Figure 5.24 – γ_M*organized by buckling curve and steel grade for General Case
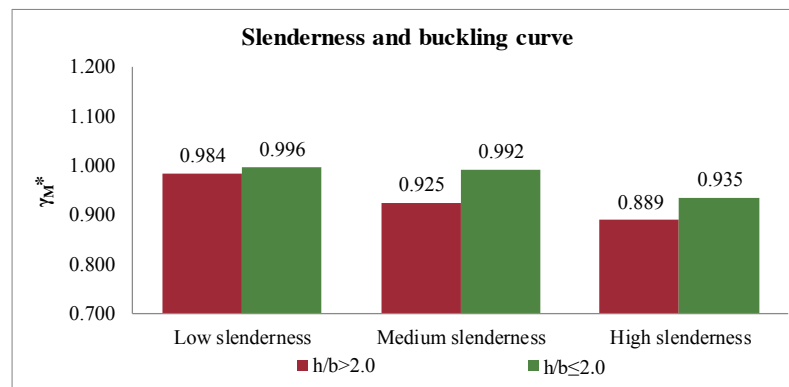
Figure 5.25 - γ_M*organized by buckling curve and slenderness for General Case

5.6.4 Comparison of the design methods

5.6.4.1 General results

This section compares the four methods. In particular, the influence of the buckling curves and the shape of the bending moment are examined in detail.
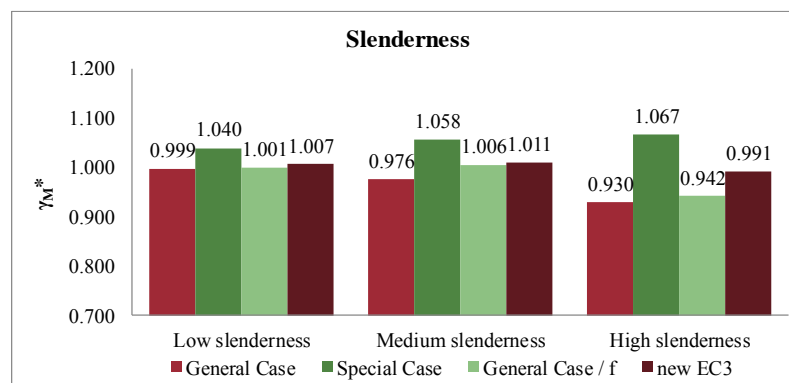
Figure 5.26 - γ_M*organized by slenderness

Figure 5.26 compares the General Case, the Special Case, General Case/f and the New EC3 method, according to the slenderness range based on all results available. The Special Case

exhibits lower safety, confirming the results of *Table 5.14*. The new EC3 method shows consistent safety across the various slenderness ranges, while the General case yields significantly higher safety for the Medium and High slenderness ranges.

5.6.4.2   *Influence of the buckling curve*

In order to verify the consistency according to the buckling curves, the respective subsets are considered. *Figure 5.27* and *Figure 5.28* compare the several methodologies organized by their respective buckling curve and slenderness divisions (General Case, Special Case and General Case/f are split for $h/b > \leq 2$, while for the New EC3 method the buckling curves are divided for $h/b > \leq 1.2$. This subdivision of the buckling curves presents the advantage of matching the subdivision of column buckling curves. The imperfection factors are adopted as given in *Table 2.4*.
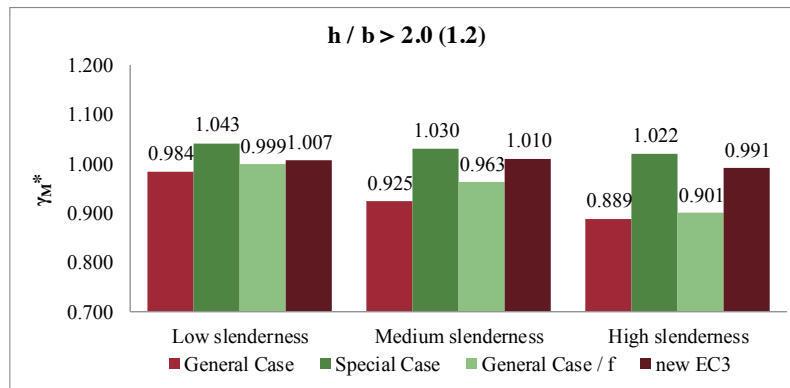
*Figure 5.27 γ_M*organized by buckling curve and slenderness*
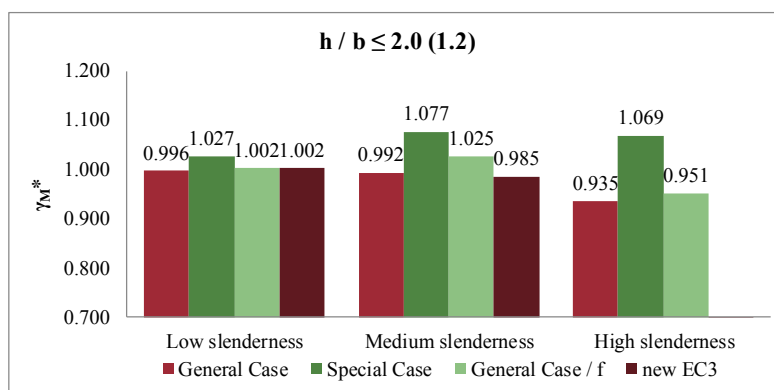
Figure 5.28 γ_M organized by buckling curve and slenderness*

It is seen that for all methods except the *newEC3* method, the results for $h/b \leq 2.0$ (1.2) are higher in the medium and high slenderness ranges.

Unlike the buckling curve divisions for columns, the imperfection factors for beams are independent of the flange thickness. In order to verify the influence of the flange thickness, further subsets according to the divisions for buckling curves for the columns are considered. *Figure 5.29, Figure 5.30* and *Figure 5.31* summarize the results according to slenderness for each interval of the column buckling curves. The results for General Case, Special Case and General Case /f given in *Figure 5.29* and *Figure 5.30* are not very different than the ones in *Figure 5.28*, the Special Case showing results with higher safety factors with significant differences in the medium and high slenderness. Finally, for $h/b \leq 1.2$ (*Figure 5.31*) all methods show similar results except the General Case in the intermediate slenderness range that is significantly more conservative. It is noted that, in this case, there are no cases in the high slenderness range because they would correspond to unrealistic long beams.
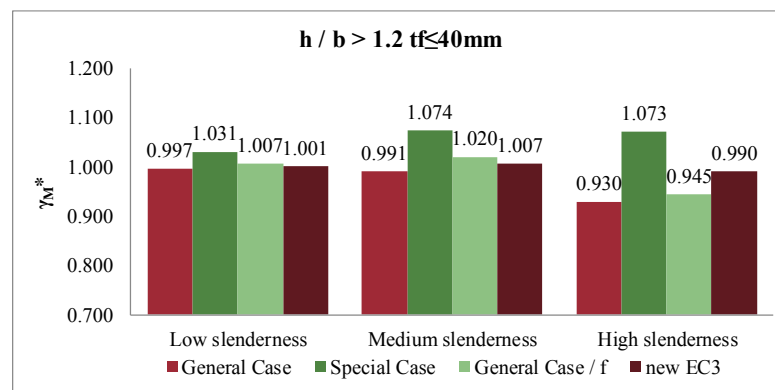
Figure 5.29- γ_M^* organized by buckling curve division for hot-rolled columns and slenderness
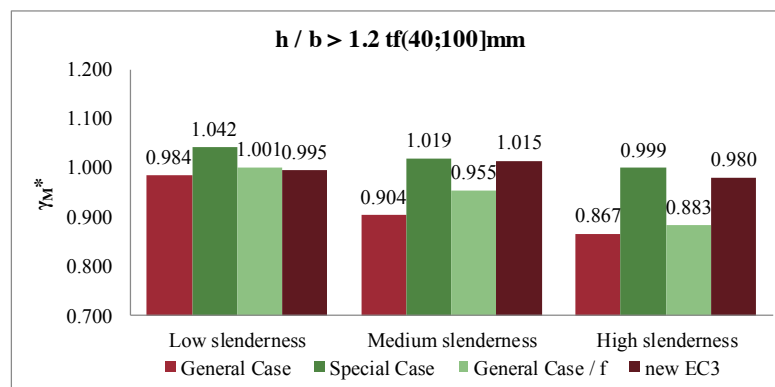
Figure 5.30 γ_M^*organized by buckling curve division for hot-rolled columns and slenderness
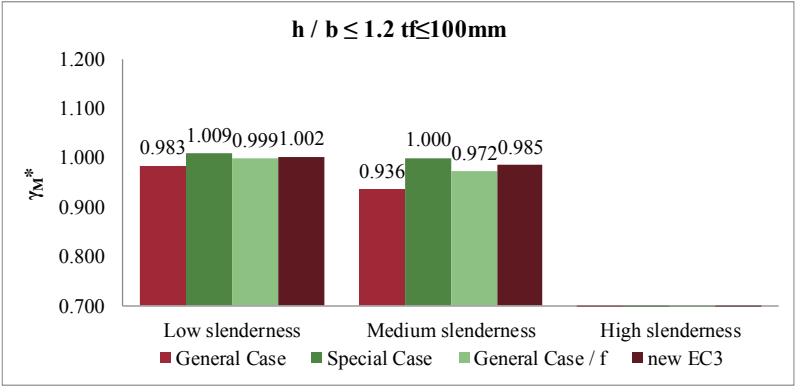
Figure 5.31 γ_M*organized by buckling curve division for hot-rolled columns and slenderness

5.6.4.3   Influence of the shape of the bending moment

The bending moment distribution is an important parameter, which influences the lateral-torsional buckling behaviour of beams. Hence, in this section divisions according to load case and slenderness are presented for the various methods (*Figure 5.32* to *Figure 5.36*).

Firstly, it is clearly seen that the General Case is unable to capture the beneficial effect of non-uniform bending moment distributions and thus severely underestimates the LTB resistance, (*Figure 5.32* to *Figure 5.36*). As discussed in *Rebelo et al.* (2009), the GC/f provides a good estimation of the resistance, despite the *f* factor being based on calibration to numerical results without any mechanical meaning *Taras* (2010). The New EC3 method provides relatively uniform partial factors for all load cases and across the various slenderness ranges. The Special Case exhibits considerably higher results mainly in the high slenderness range for all load cases.
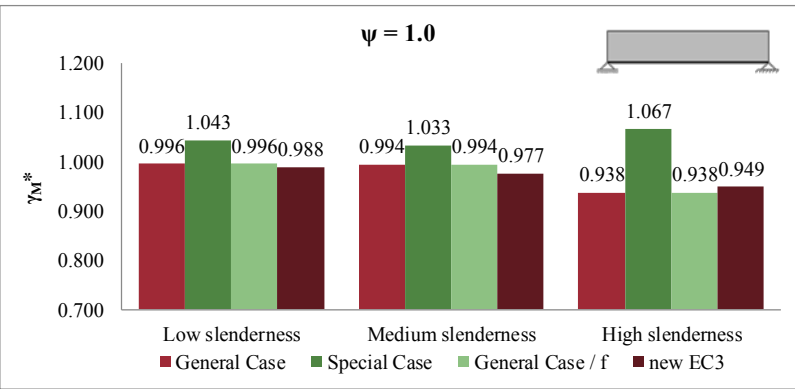
Figure 5.32 γ_M* organized by bending moment distribution – constant bending moment
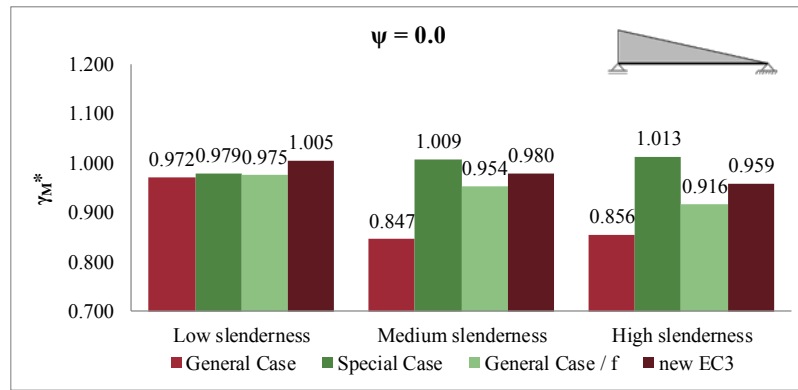
Figure 5.33 γ_M* organized by bending moment distribution – triangular bending moment
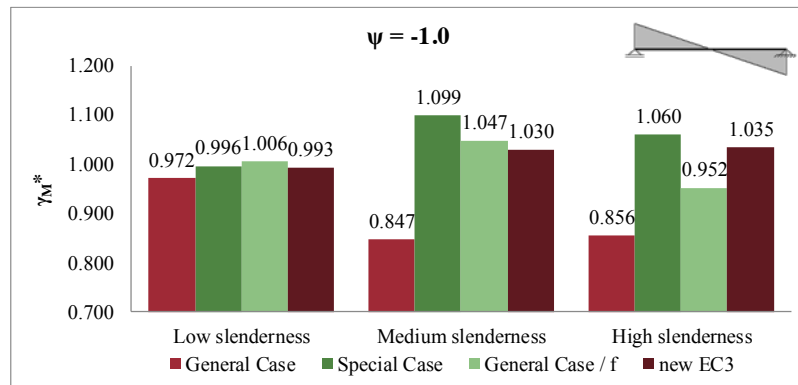
Figure 5.34 γ_M*organized by bending moment distribution – bi-triangular bending moment
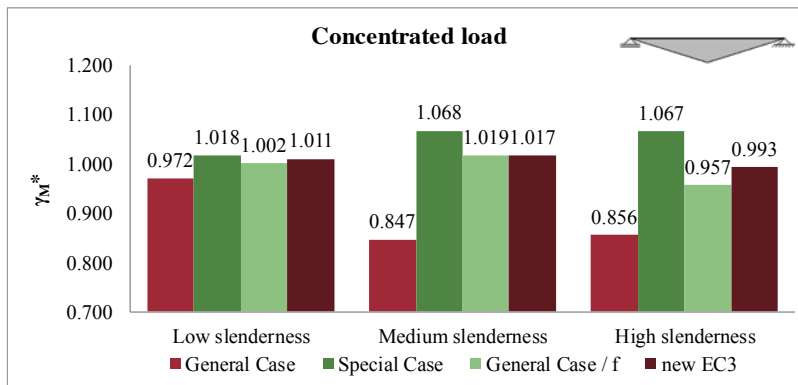
Figure 5.35 γ_M*organized by bending moment distribution – concentrated load
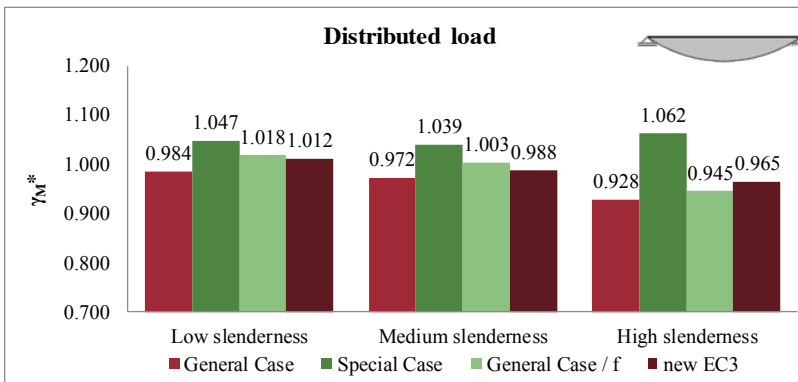
Figure 5.36 $\gamma M*$organized by bending moment distribution – distributed load

5.6.5 Buckling curves for the New EC3 method

Originally, the buckling curves for the New EC3 method were proposed as shown in *Table 5.15* that differs from *Table 2.4* for the range h/b>1.2, 40 mm<t_f≤100 mm.

Table 5.15 - Original imperfection factors for the New EC3 method

Fabrication		Limits			Source and Method		
		New EC3	EC3-1-1	EC3-1-1 GC; GC/f	EC3-1-1 SC	nEC3	
Rolled	h/b>1.2	t_f≤40 mm	h/b>2.0	0.34	0.49	$0.12\sqrt{\dfrac{W_{y,el}}{W_{z,el}}} \leq 0.34$	
			h/b≤2.0	0.21	0.34		
		40 mm<t_f≤100 mm	h/b>2.0	0.34	0.49	$0.12\sqrt{\dfrac{W_{y,el}}{W_{z,el}}} \leq 0.34$	
			h/b≤2.0	0.21	0.34		
	h/b≤1.2	t_f≤100mm	h/b>2.0	0.34	0.49	$0.16\sqrt{\dfrac{W_{y,el}}{W_{z,el}}} \leq 0.49$	
			h/b≤2.0	0.21	0.34		

Figure 5.37 compares the values of γ_M* for the thickness range 40 mm to 100 mm for all methods using the original imperfections from Table 11 for the newEC3 method. It shows that the Taras method presents worse results than the SC for this thickness range. This reflects the fact that the method was calibrated for sections with flange thicknesses lower than 40 mm (*Taras*, 2010).
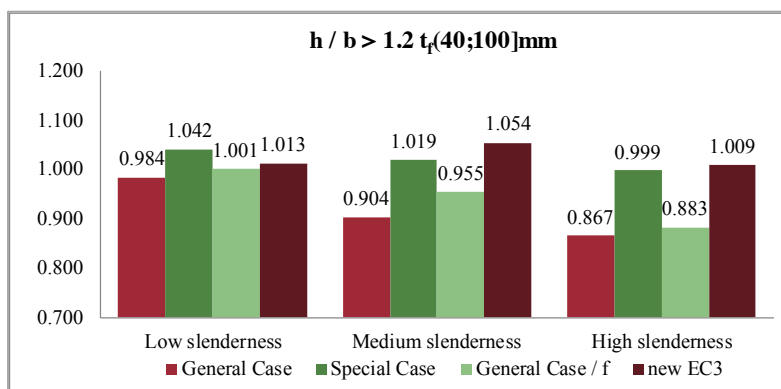
*Figure 5.37 γ_M*organized by buckling curve division for hot-rolled columns and slenderness(old imperfection factors)*

Hence, recalibration of the imperfections for the thickness range 40 mm to 100 mm led to the imperfection factor of *Table 2.4*. The corresponding comparison is illustrated in *Figure 5.38*,

showing a clear improvement by adopting the same buckling curve as for cross-sections with $h/b > 1.2$.
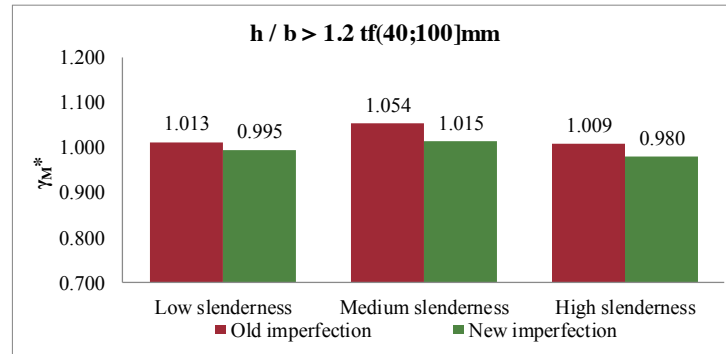
Figure 5.38 γ_M* evaluated using old and recommended imperfection factors for New EC3 method

5.6.6 Influence of the number of random variables

In all previous comparisons, only the yield stress f_y was considered as a random variable. In reality, in the case of lateral-torsional buckling of beams, other basic variables also affect the behavior of a beam, such as the cross-section dimensions and the Young's modulus. It is noted that geometrical and material imperfections such as initial curvature and residual stresses are not considered as basic random variables as they are included implicitly in the design model. Hence, in this section, the following basic variables are considered as random variables: yield stress – f_y; geometrical dimensions – b, h, t_w, t_f; and Young's modulus – E. Their statistical parameters were defined in Section 5.3. In order to highlight their influence, the following cases are considered:

- **Annex D (fy)** – considers the yield stress as the only basic variable, the other parameters are assumed as deterministic quantities with no variability;

- **Annex D (fy+CS)** – considers the yield stress and the geometrical dimensions of the cross-section as random variables;

- **Annex D (fy+CS+E)** – considers the yield stress, the geometrical dimensions of the cross-section and the modulus of elasticity as random variables;
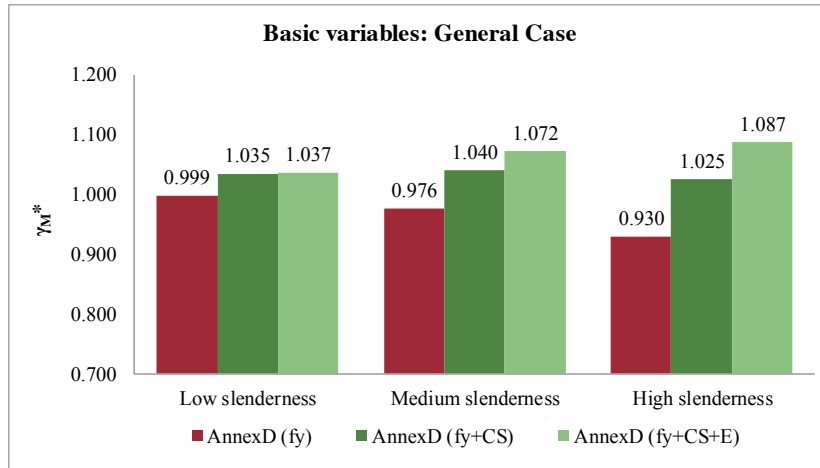
Figure 5.39 - γ_M* by slenderness and using different number of random variables: GC
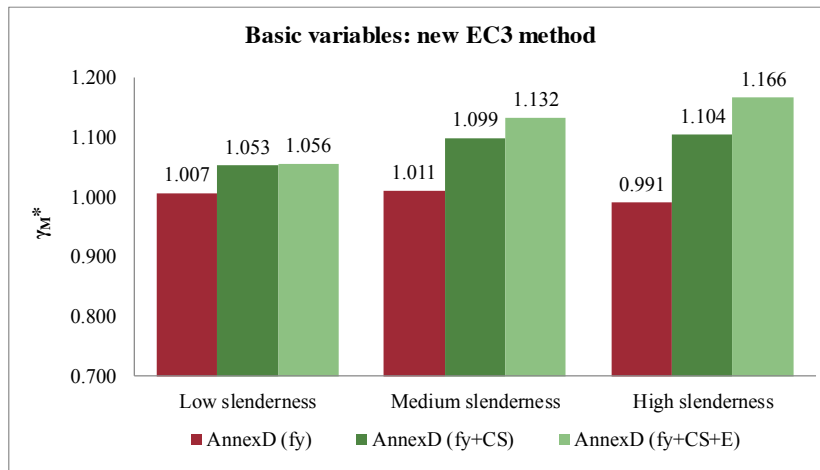
Figure 5.40 - γ_M* by slenderness and using different number of random variables: new EC3

The General Case is presented as the reference case for this assessment. *Figure 5.39* compares the results for the 3 cases defined above, according to slenderness range. Similarly, to the observations in *Simões da Silva et al*. (2016), the increased number of random variables leads to higher partial factors. This effect becomes more noticeable with increasing slenderness due to the increased influence of the geometrical properties and the modulus of elasticity. Similar results are obtained for the other methods. *Figure 5.40* illustrates the corresponding results for the New EC3 method.

5.6.7   Assessment of the value of the partial factor

Table 5.16 and *Table 5.17* summarizes the results for γ_M* for the three different sets of random variables that were considered and the four design methods, using a lower tail approximation due to the systematic deviation from a normal distribution. The conclusion from the previous section is confirmed for all methods - depending on the random variables included in the

analysis (just f_y; f_y and cross-section geometry; or f_y, cross-section geometry and modulus of elasticity E) the partial factor increases its magnitude.

Table 5.16 Values of γ_{M1}* obtained using different combinations of basic variables for General Case and Special Case

Limits		Annex D (fy)		Annex D (fy+CS)		Annex D (fy+CS+E)	
		GC	SC	GC	SC	GC	SC
h/b>1.2	$t_f{\leq}40$ mm	0.987	1.056	1.030	1.128	1.039	1.160
	40 mm<$t_f{\leq}100$ mm	0.983	1.032	1.017	1.082	1.020	1.094
	$t_f{>}100$ mm	-	-	-	-	-	-
h/b≤1.2	$t_f{\leq}100$ mm	0.983	1.010	1.018	1.050	1.018	1.052

Table 5.17 Values of γ_{M1}* obtained using different combinations of basic variables for New EC3 method and General Case/f

Limits		Annex D (fy)		Annex D (fy+CS)		Annex D (fy+CS+E)	
		nEC3	GC/f	nEC3	GC/f	nEC3	GC/f
h/b>1.2	$t_f{\leq}40$ mm	1.003	1.004	1.058	1.056	1.069	1.072
	40 mm<$t_f{\leq}100$ mm	0.978	0.978	1.027	1.018	1.034	1.023
	$t_f{>}100$ mm	-	-	-	-	-	-
h/b≤1.2	$t{\leq}100$ mm	1.006	0.999	1.051	1.038	1.054	1.039

| 149

Firstly, except for the Special Case, a good homogeneity of results is observed across the different buckling curves, with maximum variations of 0.05. Secondly, the Special Case systematically presents higher partial factors (0.05 higher on average) for most of the subsets (*Simões da Silva et al*. (2019)). The General Case presents the lowest partial factors. However, recalling *Table 5.14*, it is clearly over conservative, leading in many cases of practical relevance

to values of design resistance up to 40% lower than those obtained from advanced numerical simulations.

Table 5.18 Partial factors for beams and columns (fy+CS+E)

			Flexural Buckling		Lateral-torsional buckling		
Limits		Axis	S235 S355	S460	EC3	GC	nEC3
h/b>1.2	$t_f \leq 40$ mm	y-y	1.079	1.120	h/b>2.0	1.039	1.069
		z-z	1.098	1.118	h/b≤2.0		
	40mm<t_f≤100 mm	y-y	1.011	1.063	h/b>2.0	1.020	1.034
		z-z	1.021	1.048	h/b≤2.0		
	t_f>100 mm	y-y	1.018	1.067	-	-	-
		z-z	1.043	1.070			
h/b≤1.2	t_f≤100 mm	y-y	1.046	1.094	h/b≤2.0	1.018	1.054
		z-z	1.115	1.109			
	t_f>100 mm	y-y	-	-	-	-	-
		z-z					

Annex D (fy+CS+E)

Table 5.18 compares the γ_M* values for the General Case and the New EC3 method with the results obtained for the flexural buckling resistance of columns considering f_y, cross-section geometry and E as random variables, using the same statistical characterization of the random variables.

Furthermore, the γ_M* values for lateral-torsional buckling of beams were obtained using the lower-tail approximation, which takes into account only the worst results; for that reason further split as done for the columns Table 5.13 was not performed. Even though, the direct comparison between both buckling models reveals that the partial factors obtained for LTB of beams are generally lower than those obtained for flexural buckling of columns, giving a mean value of 1.053 and c.o.v of 1.7%. Hence, it is recommended to keep γ_{M1}=1.0 for beams. This recommendation was taken in the final draft of prEN 1993-1-1 (CEN/TC250, 2017).

5.7 Beam-columns

5.7.1 Methodology

In the following sections, the results for members under bending and compression are discussed. The main topics that are discussed are:

- Influence of the buckling mode: with and without lateral-torsional buckling;
- Influence of the bending moment distribution;
- Influence of the number of random variables

Throughout the following paragraphs, charts and tables, the following methodology is adopted:

- The partial factors for the different subsets are computed considering to the *Annex D* procedure summarized in *Figure 5.2;*
- Whenever a subset according to slenderness is analysed, the following division is adopted:
    - *Low* slenderness – normalized slenderness $\bar{\lambda} \in (0.4; 0.6]$;
    - *Medium* slenderness– normalized slenderness $\bar{\lambda} \in (0.6; 1.2]$;
    - *High* slenderness – normalized slenderness $\bar{\lambda} \in (1.2; 3.0]$;

Similarly to the other buckling modes, to establish the influence of additional random variables, the yield stress, geometrical dimensions of the cross-section and modulus of elasticity were considered.

In this case the theoretical resistance was obtained using the interaction factors for Method2/Annex B and corresponding to proportional increase of the applied forces. The limiting cases of a column and a beam were not considered in this assessment, since they were already covered by the assessments carried out for columns and beams. The method was applied with the imperfection factors for lateral-torsional buckling according to the New EC3 method.

In the assessment, all assumptions from *Boissonnade et al.* (2006) for the assessment of Method 2 were kept, namely i) cases where the cross-section resistance governs were not considered; ii) cases where the normalized axial force is less than 0.1 were also not considered.

5.7.2 Results without LTB

Figure 5.41 to *Figure 5.43* summarize the results obtained for beam-columns in bi-axial bending which do not fail in lateral-torsional buckling.

In case of beam-columns, similar conclusions to the columns and beams can be drawn: there is an increase of the partial factor with slenderness and the load cases with non-uniform bending distribution tend to be safe-sided.
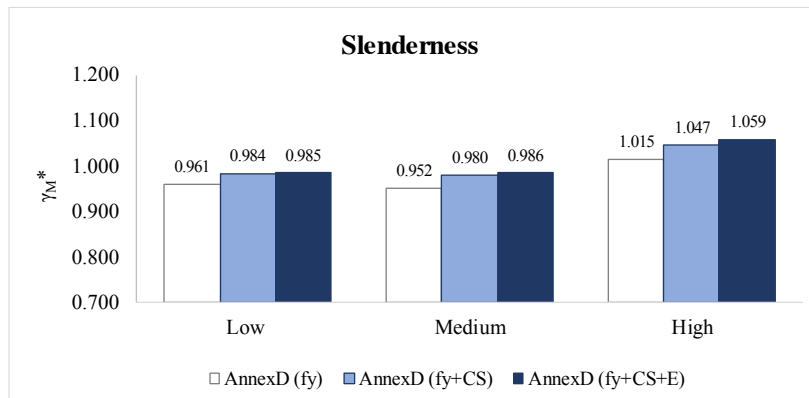
Figure 5.41 - γ_M* by slenderness and using different number of random variables: no LTB

Figure 5.41 to *Figure 5.43* show slight increase of the partial factor with slenderness, similar results within the different buckling curves. Regarding the different bending moment distributions, a small disturbance is found for bending moment distribution ψ=-1, which can be explained on the accuracy of the equivalent moment factors C_m for this load case.
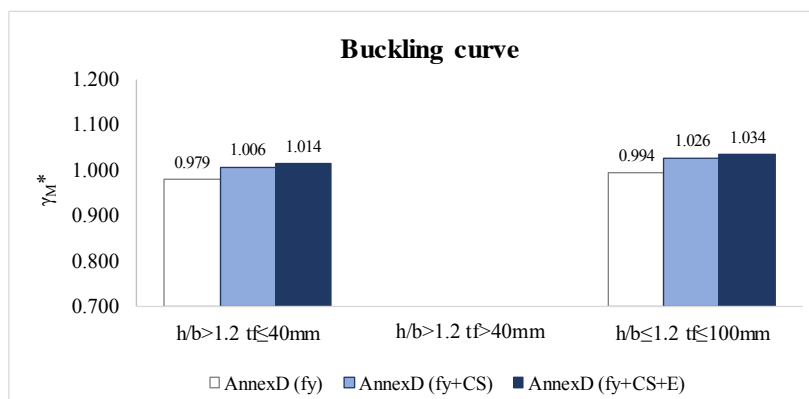
Figure 5.42 - γ_M* by buckling curve and using different number of random variables: no LTB
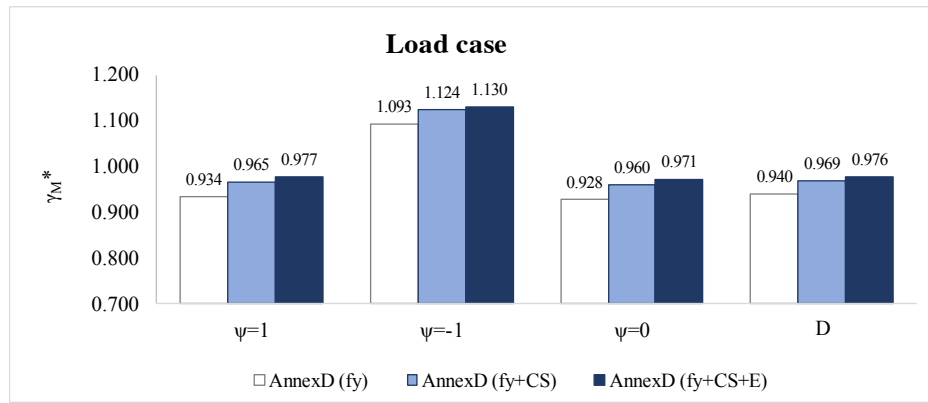
Figure 5.43 γ_M* for different bending moment distributions and using different number of random variables: no LTB

5.7.3 Results with LTB

In this section, the results regarding lateral-torsional buckling of prismatic hot-rolled beam-columns are discussed. *Figure 5.44* to *Figure 5.46* show the partial factors obtained for subsets according to slenderness, buckling curve division and load case, respectively.
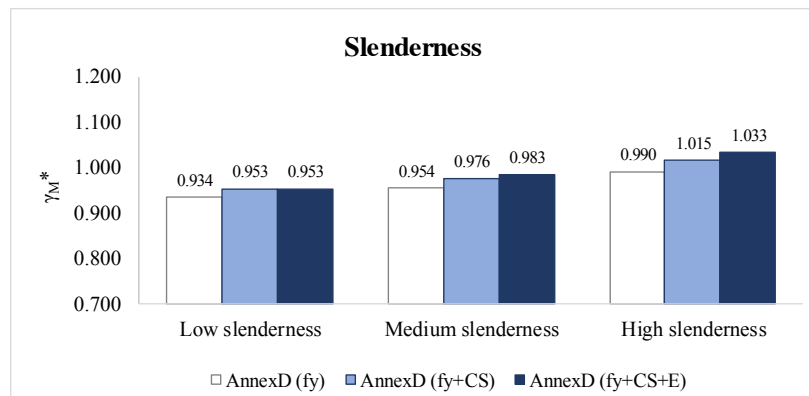
Figure 5.44 - γ_M* by slenderness and using different number of random variables: LTB
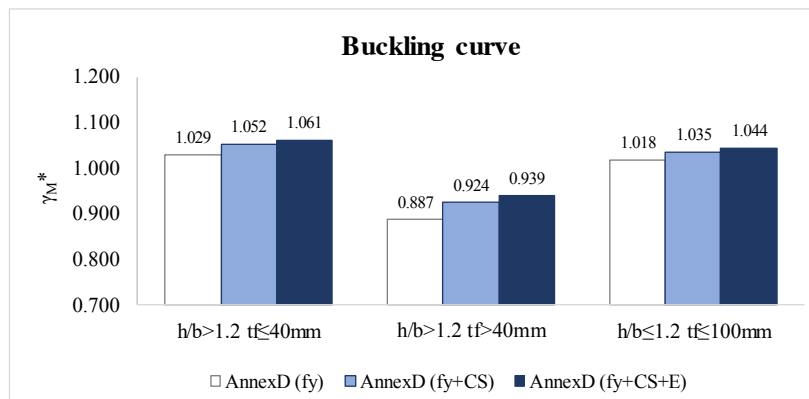
Figure 5.45 - γ_M* by buckling curve and using different number of random variables: LTB

The variation within the different buckling curves is not significant, despite the division of h/b>1.2 and flange thickness higher than 40 mm; however, in this subset, the number of data points is significantly lower than the other two.

The results for beam-columns without lateral-torsional buckling are found very similar to the ones without lateral-torsional buckling and thus indicating a homogeneous reliability within both failure modes.
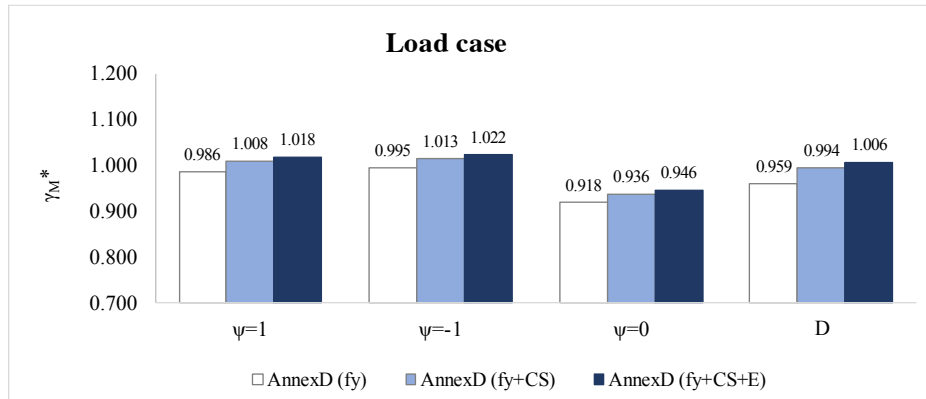
Figure 5.46 - γ_M* for different bending moment distributions and using different number of random variables: LTB

5.7.4 Influence of the number of basic variables

Figure 5.43 to *Figure 5.46* plot the results obtained for the different subsets considered, already including the variability of different number of basic variables. The same trend of increasing the partial factor with the increased number of variables considered is registered. However, in both cases with and without LTB, it is noted that the relative increase is not as big as it was found for columns and beams. This leads to the conclusion that the interaction factors are able to somehow "compensate" the variability of the random parameters.

5.7.5 Assessment on the value of the partial factors

The interaction formula from Eurocode 3 clause clause 6.3.3 for members in bending and compression with the interaction factors from Annex B was assessed. The assessment covered a large number of numerical simulations, covering various cross-section shapes, bending moment distributions, slenderness ranges. The obtained partial factors are summarized in Table 5.19 for the various types of basic variables.

Table 5.19 Values of γ_{M1}* obtained using the interaction formula

Limits		Annex D (fy)		Annex D (fy+CS)		Annex D (fy+CS+E)	
		No LTB	LTB	No LTB	LTB	No LTB	LTB
h/b>1.2	$t_f \leq 40$ mm	0.979	1.029	1.006	1.052	1.014	1.061
	40 mm<$t_f \leq 100$ mm	-	0.887	-	0.924	-	0.939
	t_f>100 mm	-	-	-	-	-	-
h/b≤1.2	$t_f \leq 100$ mm	0.994	1.018	1.026	1.035	1.034	1.044

It is seen that even when the modulus of elasticity is considered the partial factors do not diverge strongly from unity. Furthermore, the analysis in subsets of buckling curve and slenderness is carried out as in *Table 5.13* for columns. The results obtained show low mean value of the partial factor with coefficients of variation comparable to the results for columns (*Table 5.20*).

Table 5.20 - Average γ_{M1} per buckling modes (with and without LTB), according to buckling curves and slenderness

	Mode	Annex D(fy)	Annex D(fy+CS)	Annex D(fy+CS+E)
Mean value	No LTB	0.974	1.002	1.009
	LTB	0.964	0.989	0.999
Coefficient of variation	No LTB	3.5%	3.8%	4.2%
	LTB	7.9%	7.2%	7.2%

It is therefore recommended to keep γ_{M1}=1.0 for beam-columns. This recommendation was taken in the final draft of prEN 1993-1-1 (CEN/TC250, 2017).

5.8 Summary

In this chapter the safety assessment of the European stability design rules was summarized. It covered members in compression, bending and combination of bending and compression.

The safety assessment of EC3-1-1 rules for flexural buckling of columns with hot-rolled I-shaped cross sections led to the following conclusions:

– Influence of the adopted minimum yield stress using EN 10025 or Table 3.1 of Eurocode 3: the level of the minimum yield stress was assessed for both minor and major axis of flexural buckling of hot-rolled columns. It was shown that in both cases the values proposed in EC3 can reach up to 10% non-conservative in certain cases.

– Influence of the level of the residual stresses adopted in the numerical models: the buckling curves are currently calibrated for level of residual stresses proportional to the yield stress f_y, which was shown to be conservative. When the results were divided into slenderness – in the medium slenderness range, where the residual stresses are actually important, high differences were obtained. These variations are relevant for the group of buckling curves S235-S420, with increasing difference as the steel grade increases; about 8% were noticed for S355.

– Imperfection factor for flexural-buckling of columns about minor axis which are made of steel grade S460: it was shown that the imperfection factor currently prescribed for flexural buckling of steel columns made of S460 about the minor axis is not adequate. This change is already taken into consideration in the final draft of the new version Eurocode 3.

The safety assessment of EC3-1-1 rules for lateral-torsional buckling of prismatic beams with hot-rolled I-shaped cross sections led to the following conclusions:

– Similar conclusions as stated in for columns are also valid for beams concerning the influence of the adopted minimum yield stress using EN 10025 or Table 3.1 of Eurocode 3.

– The results highlight a strong sensitivity of γ_{M1}^* to the subsets that are considered in the calculation. This trend is also confirmed by comparing these results with the corresponding results from *Rebelo et al.* (2009) and *Simões da Silva et al.* (2009). This difference led to the consideration of a lower tail approximation that significantly improved the homogeneity of results.

– Regarding the different design methods considered, the conservative nature of the General Case was confirmed, the Special Case systematically led to higher values of γ_{M1}^* for the majority of subsets and the accuracy of the New EC3 method was confirmed. Regarding this method, an adjustment of the imperfection factors is proposed for cross-

sections with *h/b* >1.2 and flange thickness higher than 40 mm, because this geometric range was not considered in the original derivation of the imperfection factors.

The safety assessment of EC3-1-1 rules for prismatic members in bending and compression with hot-rolled I-shaped cross sections led to the following conclusions:

- Similar conclusions as stated in for columns and beams are also valid for beam-columns concerning the influence of the adopted minimum yield stress using EN 10025 or Table 3.1 of Eurocode 3;

- The results for the different buckling modes, with and without, lateral-torsional buckling were found very similar, showing that the interaction coefficients are calibrated with sufficient accuracy for both cases.

- The results highlight lower γ_{M1}^* - values than the ones calculated for columns and beams separately and thus indicating that the interaction factors are providing sufficient safety;

Table 5.21 Mean and c.o.v of γ_{M1}^*=1.0 for all modes

	Columns		Beams	Beam-columns		ALL
	y-y	z-z		No LTB	LTB	
Weight	20%	20%	20%	20%	20%	
γ_{M1}*Mean	1.035	1.041	1.053	1.009	0.999	**1.027**
γ_{M1}*c.o.v	6.4%	5.6%	1.7%	4.2%	7.2%	**5.0%**

Finally, the value of the partial safety factor was discussed and an assessment of the average γ_{M1}^* obtained from all subsets and for all buckling modes was carried out (*Table 5.21*). With the proposed modifications, it is recommended to keep γ_{M1}=1.0 for columns, beams and beam-columns. This recommendation was taken in the final draft of prEN 1993-1-1(2017).

6 A GENERAL FORMULATION FOR THE STABILITY DESIGN OF STEEL COLUMNS, BEAMS AND BEAM-COLUMNS

6.1 Introduction

In the previous chapters, several aspects regarding the stability design of members were discussed. The behaviour of non-uniform members was tested with full-scale experiments, it was shown that advanced numerical simulations with material and geometrical imperfections can accurately predict the buckling behaviour of non-uniform members. It was also shown how the safety and reliability of design rules can be assessed and adjusted if required. This chapter is dedicated to the extension of the stability design verification of columns, beams and beam-columns by developing a general formulation (GF), applicable to members with a generic non-uniform cross-section along their length, and arbitrary support and loading conditions.

Up to this point, the available possibilities for design of such non-standard cases are the General Method given in clause 6.3.4 of *Eurocode 3* (2005) or advanced numerical simulations. The applicability of the general method, however, is limited and in some aspects inconsistent (*Simões da Silva et al.*, 2010). In structures constructed using non-uniform members, the choice of imperfection factors is not straight-forward and their definition using standard procedures

may lead to either unsafe or over conservative solutions. As an alternative to the General Method, the stability of non-uniform members can be analysed using numerical GMNIA which, again, requires the definition of the correct imperfection shape and magnitude, but it is also a time-consuming procedure and the output is highly dependent on the experience of the user.

It was already discussed that the European buckling curves have the flexibility of adjusting imperfection factors according to their sections, yield stress, steel type and other relevant parameters. On the other hand, their major drawback is the need of adjusting imperfection factors and/or calibrating over-strength factors to account for the variation of the failure location, as done by *Taras* (2010) and *Marques* (2012).

In this chapter, a general formulation for the stability design of steel columns, beams and beam-columns with variable geometry, loads and supports is proposed. The aim is to follow, as much as possible, the specifications for uniform columns, beams and beam-columns. In particular, the need to verify separately the resistance of beam-columns for two buckling modes (in-plane and out-of-plane) is maintained. The approach uses the buckling mode as the shape of the initial imperfection and an amplitude previously calibrated for the standard prismatic simply-supported columns and beams in Eurocode 3. It avoids the calibration of additional factors because it is applied as an interaction equation and the first and second order contributions to the longitudinal stress utilization are added for each cross-section along the member length. Its organization follows the sequence: i) firstly, additional considerations from theoretical point of view are presented: torsion of non-uniform members and the Ayrton-Perry equation for beam-column; ii) secondly, the general formulation for the design of steel members is presented in a universal format covering any buckling mode; iii) thirdly, the various buckling modes are discussed separately in order to highlight specific aspects of the member behaviour; iv) finally, validation of the general formulation is carried out to show its consistency and accuracy.

6.2 Buckling of beam-columns: additional considerations

6.2.1 Ayrton-Perry equation for beam-columns

6.2.1.1 Scope

Chapter 2 summarized the analytical background regarding uniform members and their relevant theoretical developments. It was shown that having calibrated and reliable imperfection factors for the prismatic member, the Ayrton-Perry equation can be extended to other types of buckling

or non-uniform members. However, for lateral-torsional buckling of beam-columns, there is no imperfection factor since the Eurocode 3 uses interaction formula.

The following paragraphs summarize the derivation and calibration of an Ayrton-Perry equation for lateral-torsional buckling of beam-columns. It is performed assuming proportional loading, and it is applied with previously calibrated imperfection factors for the limit cases of columns and beams.

6.2.1.2 Derivation

The derivation is performed starting from the following assumptions:

- All members are prismatic and simply supported;
- The material is linear elastic until it reaches the yield stress f_y;
- The loads applied are: axial stress applied at the shear centre (N) and uniform bending moment (M_y);
- In the equations apply the approximations for small displacements and rotations and the Bernoulli hypothesis;
- The effect of pre-buckling deflections, namely i) the amplification due to the axial compressive force of the first order bending moments and deflections; ii) the effect of in-plane curvature on out-of-plane buckling, are neglected.

The amplification relationship for the lateral-torsional buckling of beam-columns was derived in Chapter 2. The relation given by Eq. (2.16) is essential for the derivation of the Ayrton-Perry equation for beam-columns. The next step for establishing the Ayrton-Perry equation is the linear yield criterion at mid-span:

$$\frac{N}{A} + \frac{M_y}{W_y} + \frac{M_z^{II}}{W_z} + \frac{M_w^{II}}{W_w} = f_y \tag{6.1}$$

in which the second order forces are

$$M_z^{II} = M_{y,Ed}\bar{\theta}_{tot} + N_{Ed}\bar{v}_{tot} = \left(M_{y,Ed}\bar{\theta}_0 + N_{Ed}\bar{v}_0\right)\frac{1}{1 - 1/\alpha_{cr}} \tag{6.2}$$

$$M_w^{II} = M_{y,Ed}\bar{v}_{tot} + r_0^2 N_{Ed}\bar{\theta}_{tot} - GI_t\bar{\theta} = \tag{6.3}$$

$$= \left(M_{y,Ed}\bar{v}_0 + r_0^2 N_{Ed}\bar{\theta}_0\right)\frac{1}{1 - 1/\alpha_{cr}} - GI_t\left(\bar{\theta}_0\frac{1}{1 - 1/\alpha_{cr}} - \bar{\theta}_0\right)$$

Then, Eq. (6.1) becomes:

$$\frac{N_{Ed}}{A} + \frac{M_{y,Ed}}{W_y} + \frac{M_{y,Ed}\bar{\theta}_0 + N_{Ed}\bar{v}_0}{W_z}\frac{1}{1 - 1/\alpha_{cr}} +$$

$$+ \frac{M_{y,Ed}\bar{v}_0 + r_0^2 N_{Ed}\bar{\theta}_0}{W_w}\frac{1}{1 - 1/\alpha_{cr}} - \frac{GI_t}{W_w}\left(\bar{\theta}_0\frac{1}{1 - 1/\alpha_{cr}} - \bar{\theta}_0\right) = f_y \qquad (6.4)$$

After a few straight-forward transformations, the equation is rearranged as:

$$\frac{N_{Ed}}{A} + \frac{M_{y,Ed}}{W_y} + \frac{\bar{\theta}_0}{W_z}\frac{1}{1 - 1/\alpha_{cr}}\left(\frac{N_{Ed}\bar{v}_0}{\bar{\theta}_0} + M_{y,Ed} + \frac{h}{2}\frac{N_{cr,z}}{\alpha_{cr}}\right) = f_y \qquad (6.5)$$

For doubly symmetrical sections, there is a geometric relationship between the lateral displacement and the section rotation, as defined by Eq. (6.6) and *Figure 6.1*. This relation allows to express the initial imperfection of Eurocode 3, $\bar{e}_0$, for columns and beams as a function of the lateral displacement and the rotation of the section:

$$\bar{e}_0 = \bar{v}_0 + \bar{\theta}_0\frac{h}{2} \qquad (6.6)$$
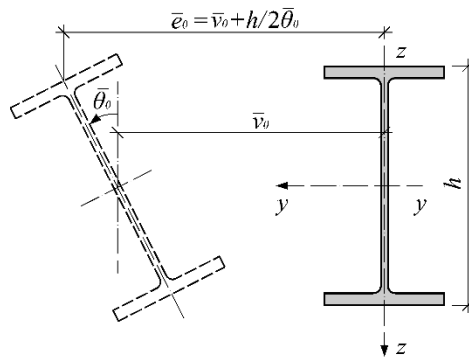
Figure 6.1 - Amplitude of the initial imperfection

Then Eq. (6.5) is transformed to

$$\frac{N_{Ed}}{A} + \frac{M_{y,Ed}}{W_y} + \frac{\bar{\theta}_0}{W_z}\frac{M_{y,Ed}}{1 - 1/\alpha_{cr}}\left(\frac{N_{Ed}\bar{v}_0}{M_{y,Ed}\bar{\theta}_0} + 1 + \frac{h}{2}\frac{N_{cr,z}}{\alpha_{cr}}\right) = f_y \tag{6.7}$$

The above equation can be solved for the bending moment or the axial force. Here it is shown how the reduction factor is applied to the axial force.

$$\chi_{BC}^N = \frac{N_{Ed}}{Af_y} = \frac{1}{\phi_{BC} + \sqrt{\phi_{BC}^2 - \beta_M\bar{\lambda}_{BC}^2}} \tag{6.8}$$

With

$$\phi_{BC} = 0.5\left(\beta_M + \eta_{tot} + \bar{\lambda}_{BC}^2\right) \tag{6.9}$$

where

$$\eta_{tot} = \alpha_{BC}\left(\bar{\lambda}_z - 0.2\right)\frac{\bar{\lambda}_{BC}^2}{\bar{\lambda}_z^2} \tag{6.10}$$

with a proposed interpolation between the imperfection factors for a column and a beam.

The interpolation of the imperfection factor is defined as a function of the ratio between the applied axial force and the bending moment (ϕ):

$$\phi = \frac{M_{pl}/M}{N_{pl}/N} \tag{6.11}$$

For high axial forces, it tends to the imperfection for flexural buckling of columns α_z and for high bending moments it becomes α_{LT}.

$$\alpha_{BC} = \begin{cases} \alpha_{LT}\left(1 - \frac{\phi}{2}\right) + \alpha_z\frac{\phi}{2} & \phi \le 1.0 \\ \alpha_{LT}\frac{1}{2\phi} + \alpha_z\left(1 - \frac{1}{2\phi}\right), & \phi \ge 1.0 \end{cases} \tag{6.12}$$

The normalized slenderness is given by:

$$\bar{\lambda}_{BC} = \sqrt{\frac{Af_y}{N_{cr,MN}}} \tag{6.13}$$

The result of the verification shows an axial load level that can be resisted for a given ratio between the bending moment and axial force. In particular, if the applied axial force is equal to the flexural strength of the element, it will not be able to withstand any additional bending moment; if the axial stress equals zero, the resistance of the member is equal to the lateral-torsional buckling one. The equation can be equivalently written for the bending moment, and even as a global out-of-plane reduction factor relevant to both moment and axial force:

$$\chi_{op} = \frac{R_b}{R_{pl}} = \chi_{BC}^N \left(1 + \frac{1}{\phi}\right) = \frac{1}{\phi_{op} + \sqrt{\phi_{op}^2 - \bar{\lambda}_{op}^2}} \tag{6.14}$$

with

$$\phi_{op} = 0.5\left(1 + \eta_{op} + \bar{\lambda}_{op}^2\right) \tag{6.15}$$

and

$$\eta_{op} = \frac{\eta_{tot}}{1 + \frac{1}{\phi}} \tag{6.16}$$

The normalized slenderness is given by:

$$\bar{\lambda}_{op} = \sqrt{\frac{R_{pl}}{R_{cr}}} = \bar{\lambda}_{BC} \frac{1}{\sqrt{1 + \frac{1}{\phi}}} \tag{6.17}$$

6.2.1.3   *Assessment of the accuracy of the Ayrton-Perry equation for beam-columns*

A validation of the Ayrton-Perry equation for beam-columns is carried out to demonstrate its consistency and accuracy. It is compared to advanced numerical simulations (GMNIA).

Numerical results are used from a parametric study carried out at the University of Coimbra in the scope of the Master's thesis by *Anwar* (2015). The main parameters included in the parametric study are given in *Table 6.1*. To cover the use of different buckling curves, several thicknesses t_f of the section flanges and h/b ratios within the two groups > or ≤1.2 were considered. In addition, several ratios of the bending moment in the principal axes $M_{y,Ed}$ and axial force N_{Ed} were also considered.

All sections considered are compact (Class 1 or 2), and their plastic resistance is used in the checks.

The difference between theoretical and experimental resistance is used as a measure of the accuracy of the new formulation. The "theoretical" result obtained using the new formulation is the reduction factor χ^N_{BC}, which is calculated at the same ratio ϕ as the numerical result. Likewise, the numerical results can be represented as a pair of N / N_{pl} and M / M_{pl}.

Table 6.1 – Parametric study for prismatic beam-columns

Steel	$\bar{\lambda}_z$	ϕ	Limit	h/b	t_f	Section
				1.82	5.7	IPE100
				1.95	7.4	IPE160
				1.98	8.0	IPE180
		∞ 5.67		2.12	12.7	IPE360
	0.4	2.74				
	0.6	1.73	h/b >1.2	1.30	19	HE400A
	0.8	1.19		1.67	28	HE500B
	1.0	0.83		2.04	46	HE600x337
S235	1.2	0.57		2.17	31	HE650B
	1.4	0.36		2.20	46	HE650x342
	1.6	0.17				
	1.8			0.97	14	HE300A
		0		1.00	19	HE300B
			h/b≤1.2	1.01	43.7	HD400x347
				1.05	29	HE300C
				1.13	21.5	HE340B

An illustration is given in *Figure 6.2*, where the plots are obtained using the new imperfection (Method), and the result of advanced numerical simulations (GMNIA). These are presented for two sections IPE360 and HE300A and for three levels of slenderness λ_z = 0.4; 1.0 and 1.6.

It is also noted that these figures show a larger difference between the analytical and numerical estimates at low slenderness, which is explained by the fact that this formulation, and the Ayrton-Perry equations in general, use an elastic yield criterion. The latter results in more conservative estimates for the lower slenderness, as illustrated in *Figure 6.2*.

In *Figure 6.3* they are demonstrated for various ratios of bending moment and axial force for the same profile and a reasonable range of normalized slenderness ratios. It shows the buckling reduction factors calculated using Eq. (6.8) and Eq.(6.14).
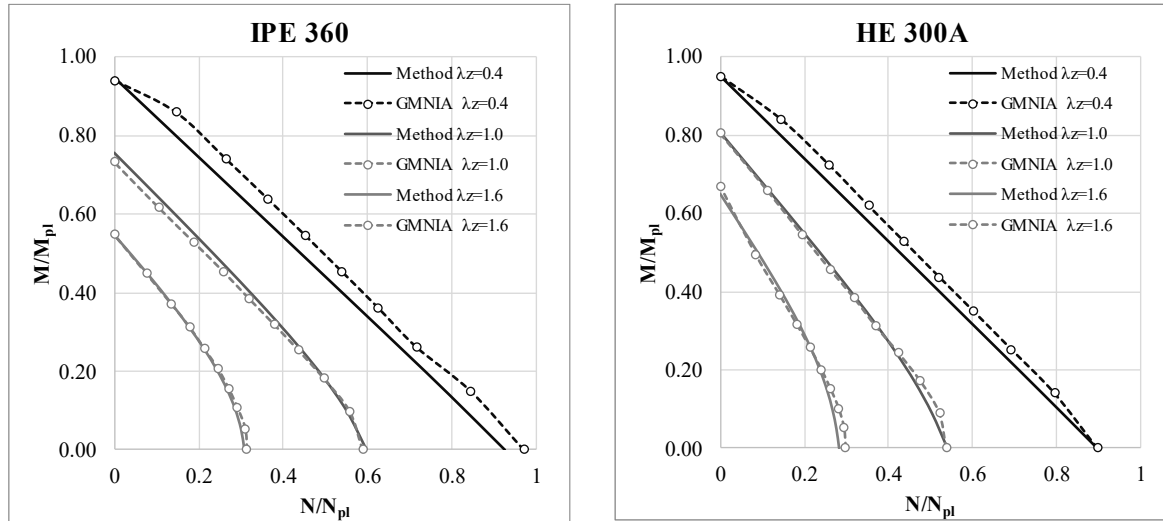
Figure 6.2 - Comparison between the proposed method and numerical results

The buckling curve representation helps for a better understanding of a global out-plane reduction factor; it develops in a normalized format which is somehow "independent" of the ratio of the bending moment to the axial force. Nevertheless, since the conversion is direct, both factors correspond to the same level of precision.

In *Table 6.2*, the statistical parameters (mean value, coefficient of variation, minimum and maximum values, total number of cases, number of cases smaller than 1 and less than 0.97) are compared for the beam-column Ayrton-Perry equation and the Eurocode 3-1-1 interaction formula.

Figure 6.4 shows the dispersion plots obtained for the Ayrton-Perry equation and the interaction formula, respectively. The mean value of r_e / r_t for the new equation is 1.03 and the coefficient of variation is approximately 4.9%, which are slightly lower than the Interaction formula. The minimum values for both methods are very similar, however, most "unsafe" results are found between 0.97 and 1.0 with the Ayrton-Perry equation having a larger amount of points falling below 1.0.
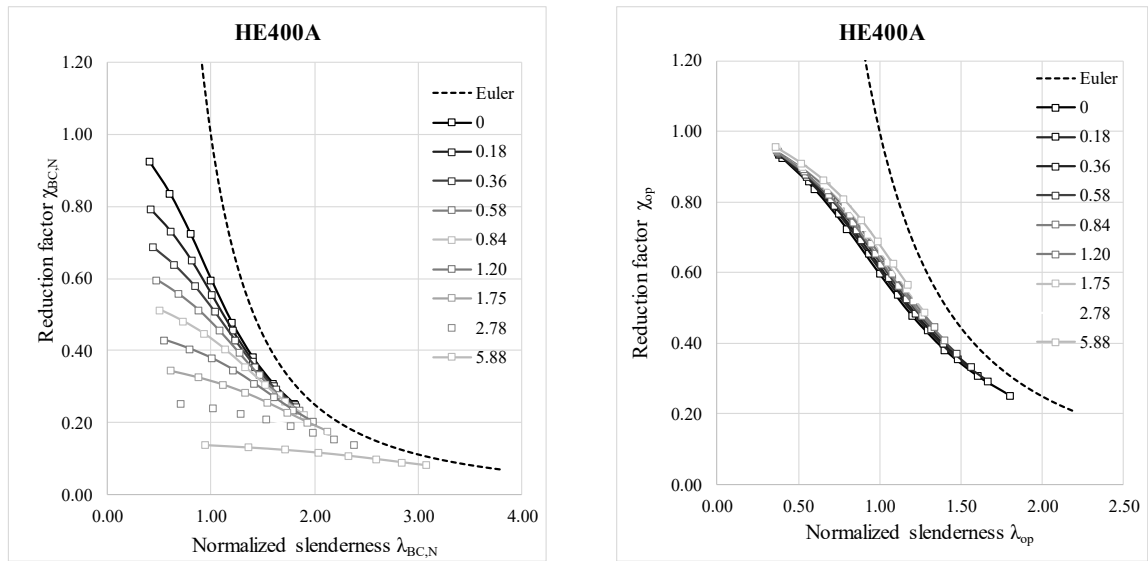
Figure 6.3 – Different representations of the reduction factors for lateral-torsional buckling of beam-columns

Table 6.2 - Statistical parameters

	Mean value	C.o.v	Min value	Max value	N	$N_{<1}$	$N_{<0.97}$
χ^N_{BC}	1.03	4.9%	0.88	1.17	1120	400	111
Interaction formula	1.08	5.5%	0.95	1.24	1120	124	5
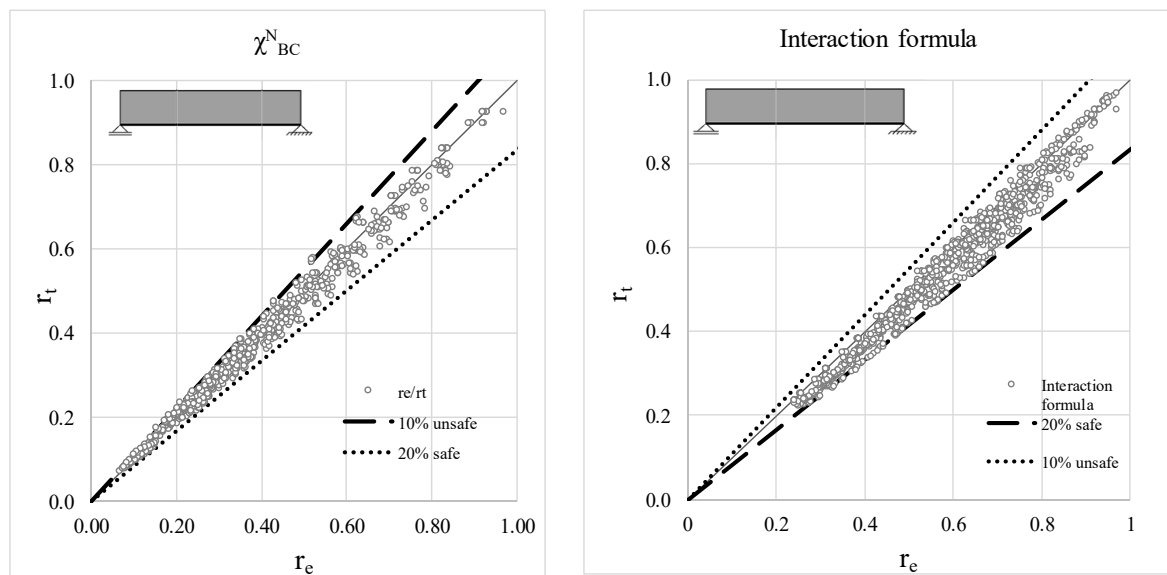
Figure 6.4 - Scatter plots

A similar derivation was performed in *Tankova et al.* (2017). However, it was based on fixed level of the axial force, which results in slightly different amplification relationship. The

method also included calibration for non-uniform bending moment distributions and corresponds to comparable safety levels. It is very suitable for hand calculation, but for the purposes of this chapter, the proportional increase of both bending moment and axial force is found more appropriate.

6.2.2 Torsion of non-uniform members

Due to their varying geometry and/or boundary and loading conditions, non-uniform members exhibit a different behaviour when compared to the uniform ones. As already stated in Chapter 3, the first studies on the torsional behaviour of non-uniform members were found by *Lee (1956)* and *Lee & Szabo* (1967). Their developments were later used by *Kitipornchai & Trahair (1972)*, where they provided the theoretical basis for the lateral-torsional buckling of tapered beams. In order to formulate the differential equations for the lateral-torsional buckling of tapered beams, it was necessary to establish the theoretical background for torsion of non-uniform beams where the divergence in the behaviour between prismatic and tapered beams is found.

Given the non-uniform beam subject to torsion shown in *Figure 6.5*, the uniform torsional moment component is given by:

$$T(x) = GI_t \frac{d\theta(x)}{dx} \tag{6.18}$$

(a) Deformations of the cross-section   (b) *Flange moment and shear*
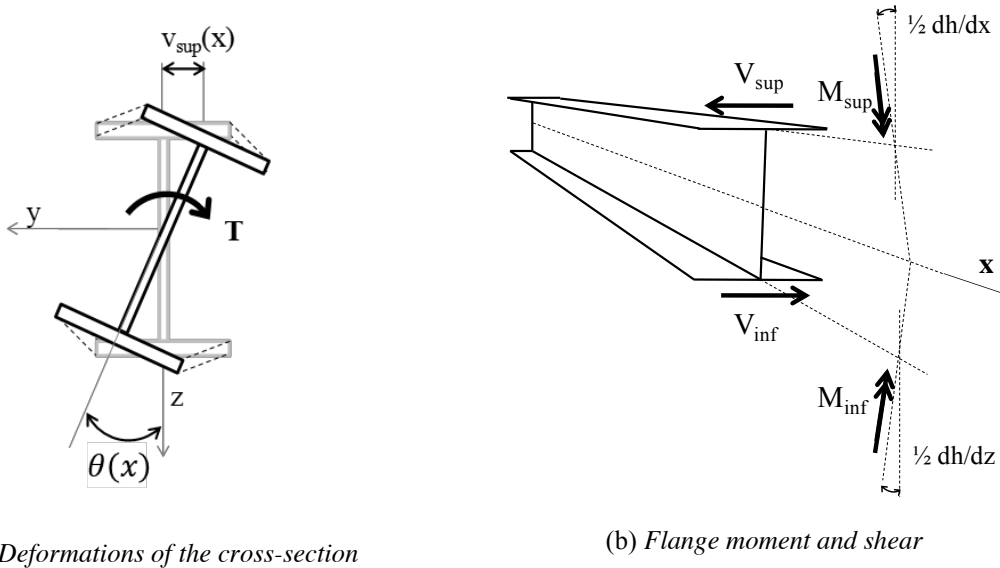
Figure 6.5 Tapered beam subject to torsion

This term remains unchanged for non-uniform beams. The non-uniform torsional moment is given by

$$T_W(x) = -EI_w \frac{d^3\theta(x)}{dx^3} - EI_\psi \frac{d\theta(x)}{dx} \qquad (6.19)$$

In Eq.(6.19) an additional warping component appears relatively to the prismatic beam case due to the inclination of the flanges given by $-2\left(\frac{1}{2}\frac{d\theta(x)}{dx}\right)M_{sup}$, see *Figure 6.5(b)*. Combining both components, the torsional moment for non-uniform beams was established:

$$T_W(x) = GI_t \frac{d\theta(x)}{dx} - EI_w \frac{d^3\theta(x)}{dx^3} - EI_\psi \frac{d\theta(x)}{dx} \qquad (6.20)$$

in which $I_\psi = \left(\frac{2}{h}\frac{dh}{dx}\right)^2 I_W$.

With the correct torsional expression for tapered beams, it was possible to derive the differential equation for the lateral-torsional buckling of simply-supported tapered beams.

6.3 General formulation for the stability verification of steel members

6.3.1 Overview

In Chapter 2 it was shown how the member design rules in Eurocode 3 were derived for uniform members. The uniform loads and geometry present the advantage of *a priori* known failure location of the member, which permits the definition of the maximum utilization due to longitudinal stresses in the flanges as a simple sum of the stress components from the first and the second order forces. The imperfection factors were then calibrated to experimental and/or numerical results. The beneficial effect of variable loads is considered by calibration of additional factors which account for the difference in the location where the maximum of the first and second order forces occur.

A similar approach was used for the extension of the Ayrton-Perry verification format to symmetrically web-tapered columns and beams (*Marques et al.*, 2012, *Marques et al.*, 2013).

The extension was achieved by calibration of the critical location, which does not occur at mid-span, as shown in *Figure 6.6,* whereby the stress utilization in the most compressed fibre of a flange of a web-tapered column buckling about its major axis is a combination of a non-linear distribution of the first and second order stress components. However, this approach presents the drawback that it is only valid for symmetrically web-tapered columns and beams. Extension to other geometries, load cases or support conditions requires new derivations.
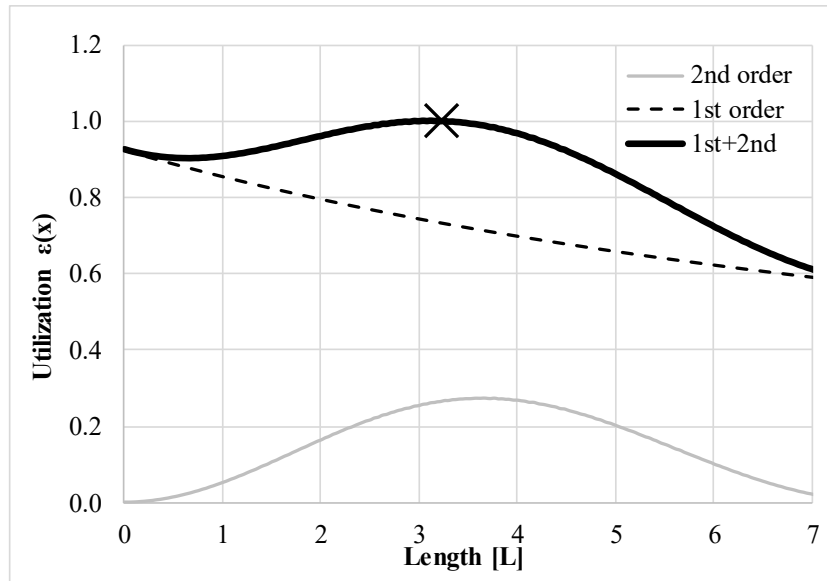
Figure 6.6- Stress utilization

The third objective of this research work, stated in Chapter 1, was to develop a procedure applicable to members with varying geometry, subject to arbitrary loading and boundary conditions.

The proposed procedure adopts the Ayrton-Perry design philosophy, however in a "raw" format of an interaction equation, and not as reduction factor χ calculation as the well-known design equations for columns and beams, derived in Section 2.4.2 and 2.4.3.2.

The interaction equation consists of linear stress utilization that includes: (i) normal stresses due to applied forces; (ii) normal stresses due to second order forces.

This interaction between first and second order stresses is consistent with the Eurocode 3 procedures where the reduction factors χ was also derived on the basis of a linear direct stress condition assuming that the shape of the initial imperfection follows the same shape as the buckling mode (Eq. (2.53)).

Hence, it is beneficial to assume that the relevant buckling mode and critical load factor can be obtained numerically by a Linear Buckling Analysis (LBA), which can be used to compute the direct stresses due to second order forces. The terms concerning the stress utilization due to second order forces are amplified by the imperfection according to the relevant buckling mode and thus, keeping consistency with the rules for prismatic members.

The developed interaction equation needs to be applied for all potential failure modes. Hence, as in clause 6.3.3 of EN 1993-1-1, it is necessary to apply it twice, for failure induced either by in-plane instability or failure induced by out-of-plane instability.

6.3.2   General formulation (GF)

Consider the generic member of *Figure 6.7*, which has variable geometry and loading along its length and non-standard boundary conditions.
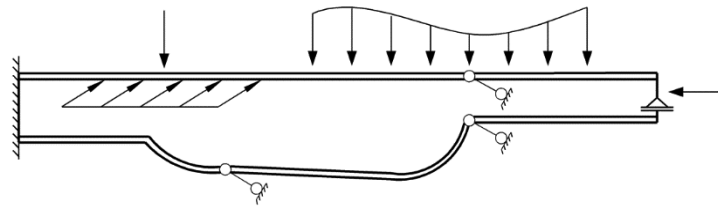
Figure 6.7 – Non-uniform member subject to non-uniform loading

with the following assumptions:

- eigenmode and eigenvalue obtained from LBA are used to calculate the 2nd order forces in the member;
- The effect of pre-buckling deflections, namely i) the amplification due to the axial compressive force of the first order bending moments and deflections; ii) the effect of in-plane curvature on out-of-plane buckling, are neglected for lateral-torsional buckling modes;
- The material is linear elastic until it reaches the yield stress f_y;
- In the equations apply the approximations for small displacements and rotations and the Bernoulli hypothesis;
- the imperfection factors are adopted for each second order component according to the corresponding buckling direction

The utilization ratio of this generic member may be expressed by equating the total longitudinal stress, σ, due to first and second order forces, to the yield stress, f_y, for each cross-section along its length:

$$\frac{\sigma(x)}{f_y} = \frac{N(x)}{A(x)f_y} + \frac{M_y(x)}{W_y(x)f_y} + \frac{M_z(x)}{W_z(x)f_y} + \frac{M_y^{II}(x)}{W_y(x)f_y} + \frac{M_z^{II}(x)}{W_z(x)f_y} + \frac{M_w^{II}(x)}{W_w(x)f_y} \qquad (6.21)$$

where $A(x)$ is the cross-section area, $W_y(x)$ and $W_z(x)$ are the section moduli relative to the y- and z axes, respectively, and $W_w(x) = I_w(x)/w_{max}(x)$ is the warping modulus at location x along the member, with $w_{max}(x) = hb/4$.

Then, as long as the second order contributions can be determined, the buckling resistance may be verified for an appropriate number of locations along the member and checking if the inequality is satisfied:

$$\frac{N(x)}{A(x)f_y} + \frac{M_y(x)}{W_y(x)f_y} + \frac{M_z(x)}{W_z(x)f_y} + \frac{M_y^{II}(x)}{W_y(x)f_y} + \frac{M_z^{II}(x)}{W_z(x)f_y} + \frac{M_w^{II}(x)}{W_w(x)f_y} \leq 1.0 \qquad (6.22)$$

The second order bending moments are obtained from the buckling mode shape and critical load factor according to:

$$M_y^{II}(x) = \frac{-EI_y(x)w''_{cr}(x)}{\alpha_{cr} - 1}\bar{\delta}_{0,y} + \frac{N(x)w_M(x)}{\alpha_{cr} - 1}$$

$$M_z^{II}(x) = \frac{-EI_z(x)v''_{cr}(x)}{\alpha_{cr} - 1}\bar{\delta}_{0,z} + \frac{N(x)v_M(x)}{\alpha_{cr} - 1} \qquad (6.23)$$

$$M_w^{II}(x) = \frac{-EI_w(x)\theta''_{cr}(x)}{\alpha_{cr} - 1}\bar{\delta}_{0,w}$$

where $\bar{\delta}_{0,y}$, $\bar{\delta}_{0,z}$, and $\bar{\delta}_{0,w}$ are the amplitudes of the initial in-plane, out-of-plane and torsional imperfections, respectively.

The verification for any single member with variable geometry, boundary conditions and that is subject to arbitrary loading, may be done by verifying Eq. (6.22) at a sufficient number of locations along the member. At each position, the respective value of the first order axial force, $N(x)$, bending moments $M_y(x)$, $M_z(x)$, second order contributions obtained from the relevant buckling mode and cross-section properties, $A(x)$, $I_z(x)$, etc. are to be used. A simple illustration is given in *Figure 6.8*, where the verification at cross-section i is performed with the cross-sectional properties, normal force and mode shape at the same section i. It is noted that this

verification shall be performed for the global buckling modes which concern the behaviour of the studied member, for instance in and out-of-plane buckling. This means that for beam-columns, eq. (6.22) must be applied, in turn, for in-plane buckling and out-of plane buckling. It is further noted that the requirement to check the cross section resistance at the extremities of the member is automatically included, as the member is checked for a sufficient number of cross-sections, including the end-sections, as explained above.

This approach avoids the need of additional calibration of parameters such as the critical location and non-uniform bending moment factors, since it relies on the Ayrton-Perry equation in its "raw" format, i.e., as an interaction equation without the use of a reduction factor χ and any resistance buckling force or bending moment.
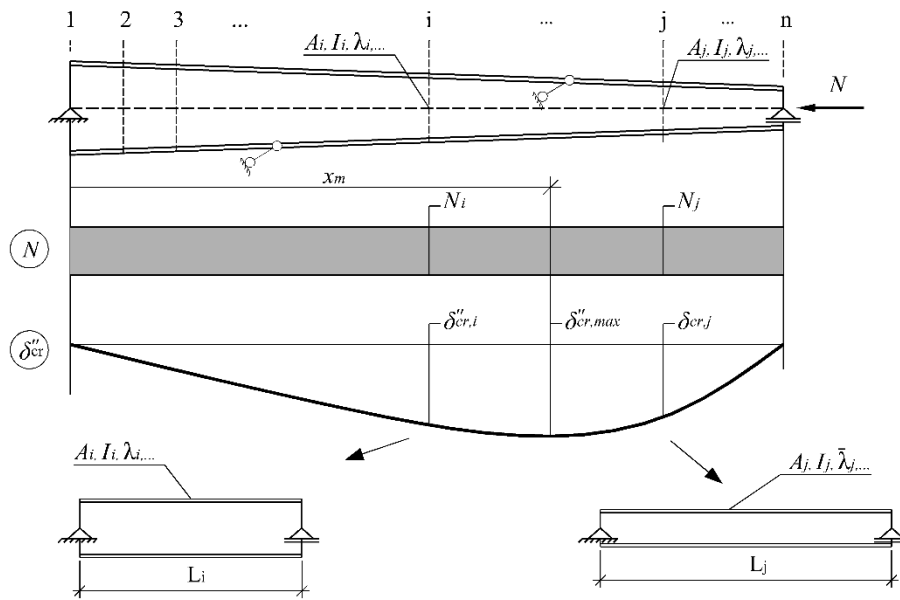
Figure 6.8 – Verification illustration

6.3.3 Buckling cases

The solution of the differential equations for a perfect member describes its elastic buckling behaviour, resulting in the critical load (moment and/or force). In a standard configuration, as shown in Chapter 2, the applied load which triggers the buckling of a member has a maximum, its critical load, i.e. for minor axis flexural buckling of a column loaded with axial force, it is the critical force $N_{cr,z}$. The applied load may consist of several components (forces and moments), and not all of them may be relevant to the buckling behaviour. For instance, for a

column loaded with axial force and minor axis bending moment, the bending moment does not contribute to the critical force $N_{cr,z}$, but it only affects the utilization ratio.

Hence, depending on the applied forces the resulting buckling modes may be active or passive. *Table 6.3* gives a summary of the possible buckling modes for doubly-symmetric sections, indicating the corresponding critical load and critical mode shape component (in or out-of-plane displacement and/or twist rotation). It is pointed out that the in-plane buckling modes are clearly distinguished from the lateral and lateral-torsional buckling ones and they cannot occur simultaneously.

Table 6.3 – Buckling cases

Buckling mode	Applied loads	Critical loads	Critical mode shape component
FB y-y	N	$N_{cr,y}$	$w_{cr}(\mathrm{x})$
	$N+M_y$		
	$N+M_y+M_z{}^*$		
FB z-z	N	$N_{cr,z}$	$v_{cr}(\mathrm{x})$
	$N+M_y$		
	$N+M_y+M_z{}^*$		
LTB	M_y	$M_{cr,N} + N_{cr,NM}$	$v_{cr}(\mathrm{x}) + \theta_{cr}(\mathrm{x})$
	$N+M_y$		
	$N+M_y+M_z{}^*$		
TB (FTB)	N	$N_{cr,x}$	$\theta_{cr}(\mathrm{x})(+ v_{cr}(\mathrm{x}))$

* The case of bi-axial bending is not treated here

In Chapter 2, it was shown for prismatic members that all these buckling cases are covered by the Eurocode 3 design rules by providing methodologies for the verification of the stability of isolated prismatic structural members and providing the necessary imperfection factors. The only condition is that the designer needs to choose the relevant buckling mode and the corresponding verification format.

The general formulation can be applied without the need of identifying explicitly the buckling mode beforehand. Each second order moment in Eq.(6.22) is obtained from the buckling mode in consideration using Eq. (6.23), amplified with the critical load multiplier α_{cr} and the amplitude of the initial imperfection, and since $w_{cr}(x)$, $v_{cr}(x)$ and $\theta_{cr}(x)$ cannot occur at the same time, the verification will fall in one of the buckling cases given in *Table 6.3*.

In the following sections, the general formulation is detailed for the buckling modes of *Table 6.3* separately in order to show how it works for each of them and discuss specific aspects relevant to the buckling mode. This does not restrict the generality of the procedure but rather helps for its better understanding.

6.4 Flexural buckling of columns

6.4.1 Verification format

In this section, focus is given to the simplest case of flexural buckling of a column subject to axial force. The general interaction equation Eq.(6.22) according to *Table 6.3* is reduced to Eq. (2.52). Eq. (2.52) holds true for both in-plane and out-of-plane flexural buckling; henceforth, in the following equations, the index *i* is used to represent both buckling modes.

$$\frac{\sigma(x)}{f_y} = \frac{N(x)}{A(x)f_y} + \frac{M_i^{II}(x)}{W_i(x)f_y} \leq 1.0 \qquad (6.24)$$

In Eq. (2.52), the second order bending moment is given by:

$$M_i^{II}(x) = EI_i(x)\delta''(x) \qquad (6.25)$$

where δ'' is the curvature for the respective buckling mode.

At each cross-section, the curvature can be calculated from the amplification relationship (*Marques et al.* (2012)):

$$\delta''(x) = \frac{N(x)\delta_0''(x)}{\alpha_{cr}N(x) - N(x)} \qquad (6.26)$$

as the initial imperfection, similarly to the derivation performed in Section 2.4.2, is assumed to have the same shape as the buckling mode:

$$\delta_0''(x) = \delta_{cr}''(x)\bar{\delta}_0 \tag{6.27}$$

i.e., the initial imperfection is proportional to the buckling mode shape δ_{cr}'', and the amplitude is given by δ_0. According to *Chladný & Stujberová* (2013), the amplitude of the imperfection of the equivalent member and the real member should be the same. This condition is expressed for the equivalent member by:

$$M_i^{II}(x_m) = N_{Ed,max}\delta_{tot} = N_{Ed,max}\delta_0\frac{1}{1 - 1/\alpha_{cr}} = \frac{\alpha_{cr}N_{Ed,max}\bar{e}_0}{\alpha_{cr} - 1} \tag{6.28}$$

while the second order bending moment for the real member at the maximum of the deformed shape is

$$M_i^{II}(x) = -EI_i(x)\delta_{cr}''(x_m)\bar{\delta}_0\frac{1}{\alpha_{cr} - 1} \tag{6.29}$$

that results in the amplitude of the imperfection to be used in the verification:

$$\bar{\delta}_0 = \frac{\alpha_{cr}N_{Ed,max}\bar{e}_0}{EI_i(x_m)|\delta_{cr}''(x_m)|} = f_\eta\bar{e}_0 \tag{6.30}$$

which is expressed in terms of the equivalent geometrical imperfection for the standard case of flexural buckling of uniform columns:

$$\bar{e}_0 = \alpha(\bar{\lambda}(x) - 0.2)\frac{W_i(x)}{A(x)} \tag{6.31}$$

However, additional terms from the mode shape and the geometrical properties calculated at the location x_m are also included. Ideally, x_m should be chosen as the correct critical location, which was shown earlier. In order to avoid an iterative procedure, the location x_m is adopted where the absolute value of δ_{cr}'' has maximum.

Let η be the amplitude of the generalized imperfection, which is finally given by:

$$\eta^*(x) = \alpha(\bar{\lambda}(x) - 0.2)f_\eta(x)|\delta_{cr}(x)|\frac{W_i(x)}{A(x)} \tag{6.32}$$

where $\bar{\lambda}$ is the normalized slenderness calculated from:

$$\bar{\lambda}(x) = \sqrt{\frac{A(x)f_y}{\alpha_{cr}N(x)}} \qquad (6.33)$$

The final verification equation is given by:

$$\varepsilon(x) = \frac{N_{Ed}(x)}{A(x)f_y} + \frac{-EI_i(x){\delta_{cr}}''(x)}{A(x)f_y\alpha_{cr} - 1}\alpha\big(\bar{\lambda}(x) - 0.2\big)f_\eta(x)|\delta_{cr}(x)| \leq 1.0 \qquad (6.34)$$

The verification can be seen as a verification of different "equivalent columns" with geometrical properties of the respective cross-section and critical load $\alpha_{cr}N(x)$ *(Figure 6.8)*

6.4.2 Design resistance

The resistance is expressed as a load multiplier, similarly to the critical load α_{cr}, but here it is called load multiplier leading to the member resistance, denoted as α_b. The resistance can be obtained using the following equation:

$$\frac{\alpha_b N_{Ed}(x)}{A(x)f_y} + \frac{-EI_i(x){\delta_{cr}}''(x)\alpha_b}{A(x)f_y\alpha_{cr} - \alpha_b}\alpha\big(\bar{\lambda}(x) - 0.2\big)f_\eta(x)|\delta_{cr}(x)| = 1.0 \qquad (6.35)$$

Eq. (6.35) is easily solved for α_b at each location along the member, being a quadratic equation. The resistance is given by the load factor which leads to a maximum utilization for the whole member equal to 1.0, i.e., to the lowest α_b for all locations. Alternatively, instead of solving Eq. (6.35) for α_b, the design resistance may be obtained using an incremental procedure for α_b.

6.4.3 Consistency with Eurocode 3

6.4.3.1 *Flexural buckling of prismatic column*

If the column is uniform loaded with an uniform axial force, the verification leads to:

$$\frac{N_{Ed}(x)}{A(x)f_y} + \frac{-EI_i(x){\delta_{cr}}''(x)}{A(x)f_y(\alpha_{cr} - 1)}\alpha\big(\bar{\lambda}(x) - 0.2\big)f_\eta N_{cr}(x)|\delta_{cr}(x)| = 1.0 \leftrightarrow$$

$$\frac{N_{Ed}}{Af_y} + \frac{EI_i\pi^2/L^2}{Af_y(\alpha_{cr} - 1)}\alpha\big(\bar{\lambda} - 0.2\big)\frac{N_{cr}}{EI_i\pi^2/L^2} = 1.0 \leftrightarrow \qquad (6.36)$$

$$\frac{N_{Ed}}{Af_y} + \frac{N_{Ed}}{Af_y(1 - N/N_{cr})}\alpha\big(\bar{\lambda} - 0.2\big) = 1.0 \leftrightarrow$$

$$\chi + \frac{\chi}{1 - \chi\bar{\lambda}^2} \alpha(\bar{\lambda} - 0.2) = 1.0$$

which is the Ayrton-Perry equation for the flexural buckling of prismatic columns as given in
Eq. (2.54).

6.4.3.2   Discussion

The general formulation relies on an interaction equation of linear stress utilization that
includes: (i) normal stresses due to applied forces; (ii) normal stresses due to second order
forces allowing the verification of members with varying geometry and loading conditions. It
was shown that the approach has the same basis as the column buckling curves and it leads to
the buckling curve equation for prismatic columns loaded with uniform axial force.
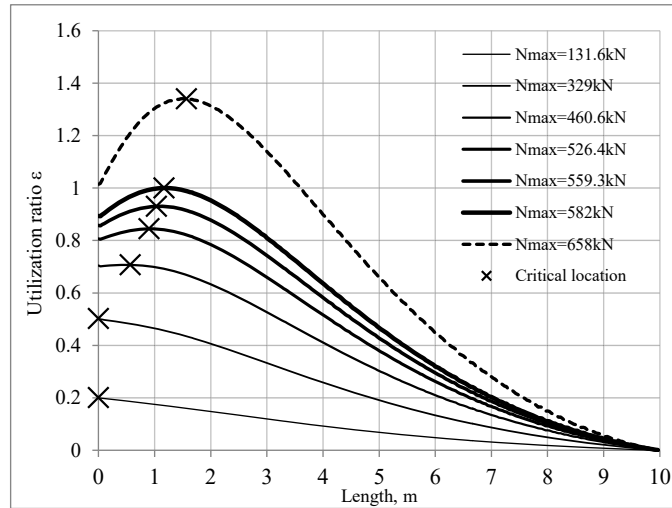
Figure 6.9 - Utilization ratio for various load levels

There is, however, an inevitable level of approximation in this generalization, since the equation
is nonlinear but the value of the imperfection for any level of loading is fixed, even if the
amplitude factor is still considered. In fact, this imperfection is valid when the equation is equal
to 1 and not <1: the location of the critical cross section varies with increasing of load along the
member since the relationship between first order and second order terms varies. For instance,
in *Figure 6.9,* the method is applied to a tapered column with taper ratio $\gamma_h = \gamma_b = 3$ (flange and
web tapered) loaded with a uniformly distributed axial force. The load level is changed and the
total utilization ratio is plotted along the column length. It can be seen that the critical position
changes with the level of applied force due to the change of the amplification of the second
order effects.

Furthermore, an example of application is presented to illustrate the benefit of using the GF. Consider a welded tapered column, which has restraints along the span with dimension 100x100x10x10 at the shallow section and web-taper ratio of 3. The usual approach would be to verify the member in three segments, using the procedure from *ECCS Publication No119*; however, instead of calculating various segments, using the proposed procedure it is possible to verify the whole member at once. Firstly, a LBA is performed for the member.
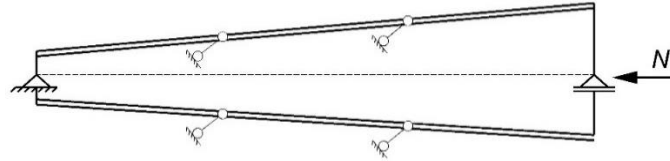
Figure 6.10 - Example 1: Tapered column with intermediate restraints

The buckling mode shape is given in *Figure 6.11*. The normalized shape for δ_{cr} and its derivatives are given in *Figure 6.12a*, which is used to verify the interaction equation at the various locations along the member, as shown in *Figure 6.12b*; that also illustrates the variation of the first and second order utilization ratios showing excellent agreement. The maximum resistance was compared with GMNIA and the results are given in *Table 6.4*.

Figure 6.11 Mode shape: column

a) Mode shape

b) Utilization ratio
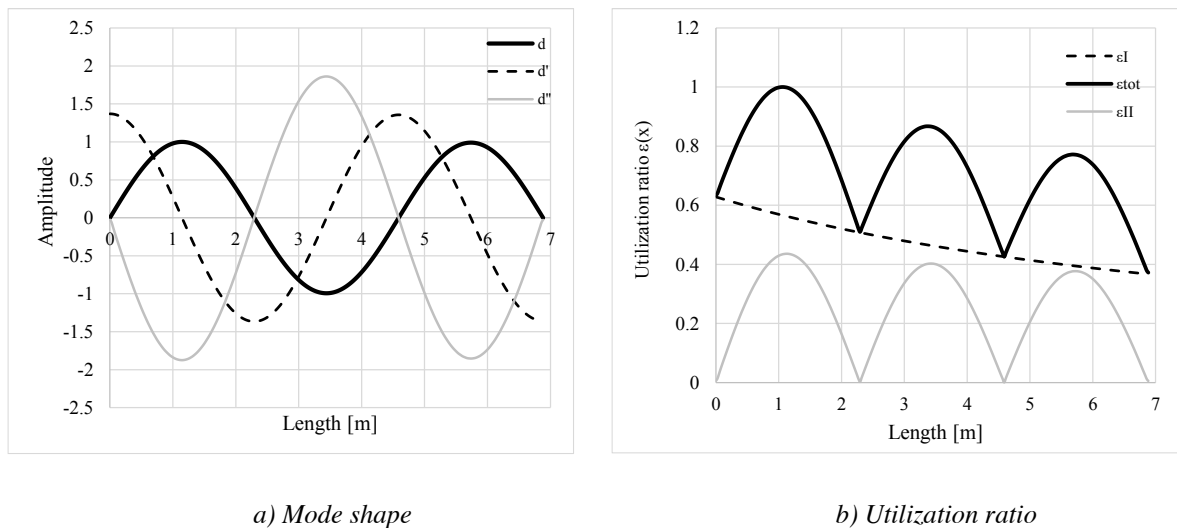
Figure 6.12 - Utilization ratio

Table 6.4 – Example tapered column

Example	Method	GMNIA	Difference
Tapered column	413kN	406kN	2%

6.5 Flexural buckling of beam-columns

6.5.1 Verification format

The case of flexural buckling of members loaded with bending moment and axial force is probably the most common in the engineering practice. The only difference with regard to members loaded with axial force only is the additional bending moment. In this case, it does not cause any additional buckling because it acts in the flexural buckling plane and the critical load factor will only depend on the applied axial force. However, the additional contribution from the bending moment should be added to the first and second order utilization. Then the stress, utilization becomes:

$$\frac{\sigma(x)}{f_y} = \frac{N(x)}{A(x)f_y} + \frac{M_i(x)}{W_i(x)f_y} + \frac{M_i^{II}(x)}{W_i(x)f_y} \leq 1.0 \tag{6.37}$$

with

$$M_i^{II}(x) = EI_i(x)\delta''(x) + M_{i,Ed}^{II}(x), \tag{6.38}$$

Leading to the following interaction equation:

$$\frac{N_{Ed}(x)}{A(x)f_y} + \frac{M_y(x)}{W_y(x)f_y} + \frac{EI_i(x)\delta_{cr}{}''(x)}{A(x)f_y(\alpha_{cr} - 1)}\alpha(\bar{\lambda}(x) - 0.2)f_\eta(x)|\delta_{cr}(x)| +$$

$$+ \frac{M_y(x)|\delta_{cr}(x)|}{(\alpha_{cr} - 1)W_y(x)f_y} \leq 1.0 \tag{6.39}$$

The second order contribution from the applied bending moment is separated from the second order contribution due to the initial imperfection. In addition, it is assumed that the second order moment due to the bending moment can be approximated by:

$$M_y^{II}(x) = \frac{N(x)w_M(x)}{\alpha_{cr} - 1} \approx \frac{M_y(x)|\delta_{cr}(x)|}{\alpha_{cr} - 1} \qquad (6.40)$$

6.5.2   On the beam-column behaviour

According to *Eurocode 3* (2005), the in-plane flexural buckling resistance of members loaded in bending and compression is performed using interaction formula. Its background was detailed in Chapter 2. The interaction factors were derived and calibrated in order to account for the various aspects that influence the beam-column behaviour. Regarding non-uniform bending moment distributions, both sets of interaction factors (Method 1 and Method 2) adopt the equivalent moment factor C_m in order to avoid the explicit consideration of the critical location. In contrast, the application of the general formulation does not require additional factors to account for the design location since the verification is performed at each cross-section and the influence of the location is implicitly included in the verification.

Furthermore, to take in the plasticity effects, the interaction factors for Method 1 include the plasticity factors C_{ii} and C_{ij} for cross-section Class 1 and 2. These factors account for the non-linear interaction between bending moment and axial force in the low/medium slenderness ranges but also for the fact that the full-plastic moment may not be reached with the increase of the slenderness. The factors reduce to the cross-section check for rectangular cross-section when the slenderness tends to zero. Similar factors were proposed by *Taras* (2010) for the Ayrton-Perry formulation for in-plane resistance of beam-columns in mono-axial bending.

The proposed general formulation, being applied a as linear interaction equation, is not able to capture the cross-section interaction at low slenderness. Therefore, there is a need of introducing a similar factor C_{ii} in order to account for this. A preliminary verification was carried out by using the C_{ii} factors taken from Method 1. The comparison was performed for three different profiles, three slenderness ratios and various ratios between the bending moment and axial force using numerical results from *Ofner* (1997).

Figure 6.13 illustrates the comparison between the interaction formula Method 1 (M1), Method 2 (M2), GMNIA and the general formulation for two sections at low slenderness. Furthermore, detailed results are given in *Table 6.5*. It is noted that the difference in applying C_{ii} or not is not considerable: the results get slightly safer at low slenderness, but for high slenderness the mean value gets lower because C_{ii} tends to the elastic moment and the general formulation is applied

with the plastic moment. However, this smaller difference is also due to the smaller shape factor for the sections considered ($W_{pl,y}/W_{el,y}$); if a minor axis flexural buckling is considered, the divergence would become higher.
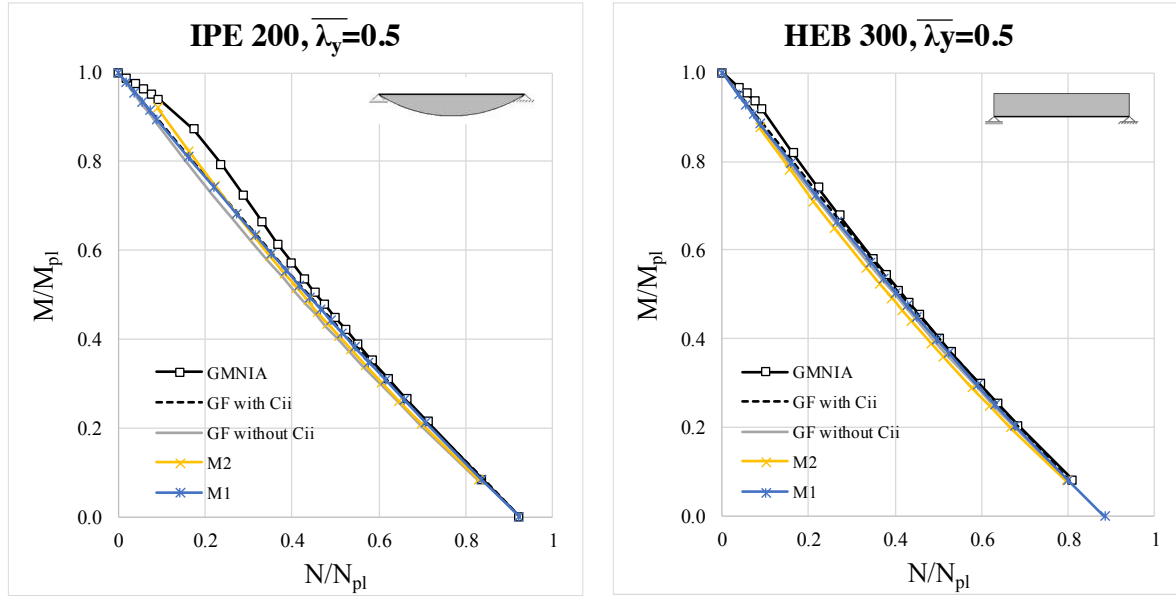
Figure 6.13 - Comparison between the different methods

Table 6.5 - Statistical parameters

	λ	**HEB 300**					**IPE 200**					**IPE 500**				
		n	m	Cov	Min	Max	n	m	Cov	Min	Max	n	m	Cov	Min	Max
GF with C$_{ii}$	0.5	100	1.022	2.3%	0.977	1.077	94	1.034	3.2%	0.979	1.111	94	1.039	3.6%	0.981	1.120
	1.0	97	1.043	2.9%	0.991	1.104	101	1.042	3.7%	0.983	1.123	96	1.047	3.7%	0.985	1.131
	1.5	99	1.053	4.9%	0.982	1.178	95	1.050	5.3%	0.970	1.179	98	1.055	5.4%	0.967	1.183
GF without C$_{ii}$	0.5	100	1.047	2.3%	1.005	1.103	94	1.066	3.9%	0.997	1.160	94	1.072	4.3%	0.999	1.177
	1.0	97	1.040	3.3%	0.989	1.103	101	1.041	4.8%	0.977	1.160	96	1.046	4.9%	0.980	1.172
	1.5	99	1.033	5.7%	0.958	1.194	95	1.027	6.6%	0.951	1.200	98	1.031	6.6%	0.953	1.205
IF-M1	0.5	110	1.010	1.8%	0.985	1.069	104	1.023	2.5%	0.988	1.107	104	1.026	2.6%	0.991	1.114
	1.0	106	1.030	2.6%	0.985	1.092	110	1.035	2.9%	0.979	1.097	105	1.038	2.9%	0.976	1.102
	1.5	109	1.024	2.7%	0.985	1.092	104	1.034	2.9%	0.977	1.103	108	1.037	2.9%	0.977	1.107
IF-M2	0.5	60	1.030	1.1%	0.991	1.051	63	1.034	2.0%	0.984	1.076	52	1.044	1.9%	1.011	1.083
	1.0	73	1.082	3.6%	1.014	1.231	80	1.046	3.7%	0.974	1.172	71	1.055	3.8%	1.000	1.179
	1.5	77	1.106	7.2%	1.011	1.348	77	1.079	7.2%	0.997	1.299	78	1.084	7.2%	1.004	1.306
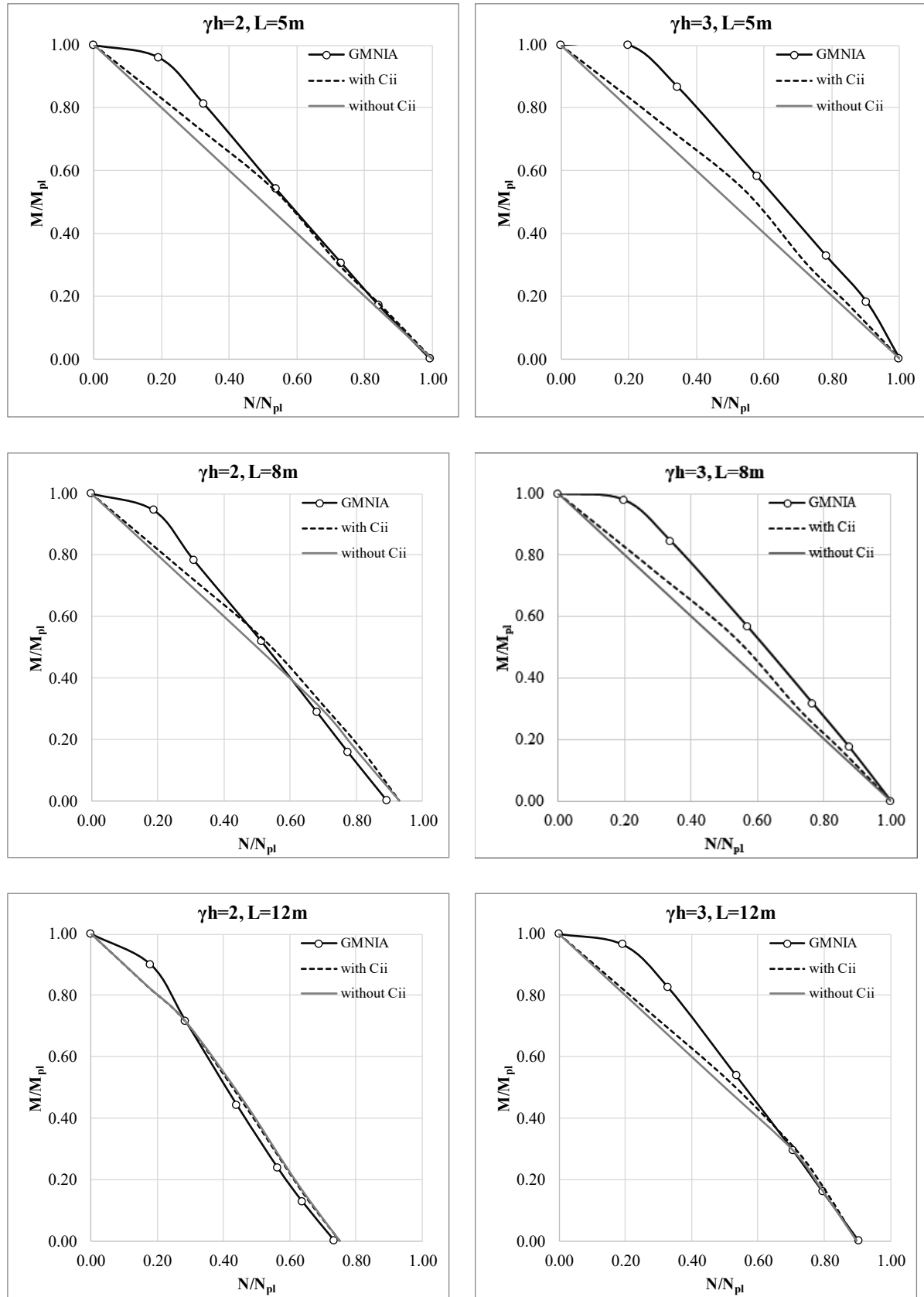
Figure 6.14 – Comparison for tapered member with shallow section 250x200x8x16 for different taper ratios and lengths

Furthermore, the factor C_{ii} was applied to tapered members. Its application to members with variable cross-section required the following adjustments: i) firstly, the C_m factors as recommended by the interaction formula were not considered since they are calibrated for uniform members; ii) secondly, the level of the axial force N_{Ed}/N_{pl} was considered constant as the ratio ϕ.

Figure 6.14 shows the results obtained for tapered members with γ_h=2 and for three different lengths.

At low slenderness, the members tend to their cross-section resistance, in such case, the use of C_{ii} helps to obtain resistances closer to GMNIA. However, for higher bending moments relative to the axial force, where the difference is larger, the improvements are minimal. At high slenderness, the results are closely approximated by GMNIA with and without the use of C_{ii} since the effect of plasticity vanishes.

The factor was calibrated for uniform members, and therefore, is not suitable for application with non-uniform members. Hence, this issue required further elaboration that is outside the scope of this thesis.

6.5.3   Design resistance

The design resistance is obtained as described for the flexural buckling of columns under axial force (Section 6.4.2) using the following equation:

$$\frac{\alpha_b N_{Ed}(x)}{A(x)f_y} + \frac{\alpha_b M_y(x)}{A(x)f_y} +$$

$$\frac{EI_i(x)\delta_{cr}{}''(x)\alpha_b}{A(x)f_y(\alpha_{cr} - \alpha_b)}\alpha\big(\bar{\lambda}(x) - 0.2\big)f_\eta(x)|\delta_{cr}(x)| + \frac{\alpha_b{}^2 M_y(x)|\delta_{cr}(x)|}{(\alpha_{cr} - \alpha_b)W_y(x)f_y} = 1.0 \tag{6.41}$$

6.5.4   Consistency with Eurocode 3

Even though the interaction formula of Eurocode 3 makes use of calibrated factors, it has its analytical background. It is shown in this section that the general formulation and the interaction formula are consistent for the case of flexural buckling of prismatic beam-columns. Considering Eq. (6.38) for a prismatic beam-column loaded with constant bending moment and axial force:

$$\frac{N_{Ed}(x)}{A(x)f_y} + \frac{M_y(x)}{W(x)f_y} + \frac{EI_i(x)\delta_{cr}''(x)}{A(x)f_y\alpha_{cr} - 1}\alpha\big(\bar{\lambda}(x) - 0.2\big)\frac{\alpha_{cr}N_{Ed}(x)|\delta_{cr}(x)|}{EI_i(x_m)|\delta_{cr}''(x_m)|}$$
$$+ \frac{M_y(x)|\delta_{cr}(x)|}{(\alpha_{cr} - 1)W_y(x)f_y} = 1.0$$

$$\leftrightarrow \frac{N_{Ed}}{N_{pl}} + \frac{\alpha_{cr}N_{Ed}}{Af_y(\alpha_{cr} - 1)}\frac{e_0 A}{W} + \frac{M_{Ed}(1 + \alpha_{cr} - 1)}{(\alpha_{cr} - 1)M_{Rd}} = 1.0$$

$$\leftrightarrow \frac{N_{Ed}}{N_{pl}} + \frac{1}{\left(1 - \dfrac{1}{\alpha_{cr}}\right)}\frac{N_{Ed}e_0 + M_{y,Ed}}{M_{Rd}} = 1.0$$

$$\leftrightarrow \frac{N_{Ed}}{N_{pl}} + \frac{1}{\left(1 - \dfrac{N_{Ed}}{N_{cr}}\right)}\frac{N_{Ed}e_0 + M_{y,Ed}}{M_{Rd}} = 1.0$$

(6.42)

It can be seen that Eq. (6.42) coincides with the interaction equations in their raw format, before the calibration of the interaction coefficients and is therefore valid for both methods – Method 1 and 2, as presented in the background document for its development, ECCS Pub. 119 (*Boissonnade et al.*, 2006).

6.6 Lateral-torsional buckling of beams

6.6.1 Verification format

For lateral-torsional buckling of beams the general interaction equation Eq.(6.22) and considering *Table 6.3,* becomes:

$$\frac{\sigma(x)}{f_y} = \frac{M_y(x)}{W_y(x)f_y} + \frac{M_z^{II}(x)}{W_z(x)f_y} + \frac{M_w^{II}(x)}{W_w(x)f_y}$$

(6.43)

where there are two second-order contributions, the out-of-plane bending moment depending on the lateral displacement:

$$M_z^{II}(x) = -EI_z(x)v''(x)$$

(6.44)

and the bi-moment depending on the twist rotation:

$$M_w^{II}(x) = -EI_w(x)\theta''(x).$$

(6.45)

| 185

For tapered beams, an additional warping component appears due to the inclination of the flanges (*Kitipornchai and Trahair*, 1972) leading to:

$$M_w^{II}(x) = -EI_w(x)\left(\theta''(x) + \frac{2}{h}\theta'(x)h'\right) \tag{6.46}$$

For simply supported beams it was possible to obtain the amplitude by the coupling of the lateral displacement and twist rotation (Eq. (2.9)). In a more general configuration (variation of the geometry along the member, different boundary and loading conditions, etc.), this relationship may not be held. For that reason, it was chosen to use both components of the mode shape in the definition of the initial imperfection, assuming that they are multiplied by the same amplitude:

$$v_0(x) = v_{cr}(x)\bar{\delta}_{0,LTB} \qquad \theta_0(x) = \theta_{cr}(x)\bar{\delta}_{0,LTB} \tag{6.47}$$

The resulting amplification relationship for the displacement and rotation is given by:

$$v(x) = \frac{1}{\alpha_{cr}-1}v_0(x) \tag{6.48}$$

$$\theta(x) = \frac{1}{\alpha_{cr}-1}\theta_0(x) \tag{6.49}$$

Similarly to a column, it is considered that the real beam should have the same resistance as an equivalent simply supported member. This equivalent beam has the same geometry as the real member at the critical cross-section and the same elastic critical moment. Hence, it is possible to obtain the required generalized imperfection by setting equal the second order utilization for the equivalent and real beam. The second order moments for a simply supported beam at mid-span are given by:

$$M_z^{II}(x_m) = M_{y,Ed}\theta_{tot} = M_{y,Ed}\theta_0\frac{1}{1-1/\alpha_{cr}} = \frac{\alpha_{cr}M_{y,Ed}\bar{e}_0\theta_{cr}(x_m)}{\alpha_{cr}-1} \tag{6.50}$$

$$M_w^{II}(x_m) = M_{y,Ed}v_{tot} - GI_t\theta = M_{y,Ed}v_0\frac{1}{1-1/\alpha_{cr}} - GI_t\left(\theta_0\frac{1}{1-1/\alpha_{cr}} - \theta_0\right) =$$

$$= \frac{\alpha_{cr}M_{y,Ed}\bar{e}_0\theta_{cr}(x_m)}{\alpha_{cr}-1}\left(\frac{v_0}{\theta_0} - \frac{GI_t}{M_{cr}}\right), \tag{6.51}$$

which when combined together form the second order utilization ratio for the equivalent member:

$$\varepsilon_M^{II}(x_m) = \frac{M_z^{II}(x_m)}{W_z(x_m)f_y} + \frac{M_w^{II}(x_m)}{W_w(x_m)f_y} =$$

$$= \frac{\alpha_{cr}M_{y,Ed}\bar{e}_0\theta_{cr}(x_m)}{W_z(x_m)f_y(\alpha_{cr}-1)}\left(1 + \frac{v_{cr}(x_m)}{\theta_{cr}(x_m)}\frac{W_z(x_m)}{W_w(x_m)} + \frac{GI_t(x_m)}{M_{cr}}\frac{W_z(x_m)}{W_w(x_m)}\right) = \tag{6.52}$$

$$= \frac{N_{cr,z}\bar{e}_0}{W_z(x_m)f_y(\alpha_{cr}-1)}$$

The second order utilization of the real beam at the location x_m is given by:

$$\varepsilon_M^{II}(x_m) = \frac{M_z^{II}(x_m)}{W_z(x_m)f_y} + \frac{M_w^{II}(x_m)}{W_w(x_m)f_y} =$$

$$= \frac{EI_z(x_m)\left(v''_{cr}(x_m) + \frac{h}{2}\theta''_{cr}(x_m) + \theta'_{cr}(x_m)h'\right)\bar{\delta}_0}{W_z(x_m)f_y(\alpha_{cr}-1)} \tag{6.53}$$

Equalling Eqs. (6.52) and (6.53) leads to the following expression for the amplitude of the imperfection:

$$\bar{\delta}_{0,LTB} = \frac{N_{cr,z}\bar{e}_0}{EI_z(x_m)\left(v''_{cr}(x_m) + \frac{h}{2}\theta''(x_m) + \theta'(x_m)h'\right)} = f_\eta \bar{e}_0 \tag{6.54}$$

This amplitude is used with the proposed generalization. It contains the equivalent geometrical imperfection $\bar{e}_0$ but also additional terms ensuring the consistency with the Eurocode 3 design rules. Ideally, the location x_m should be obtained in an iteration as the exact critical location of the beam; however, in order to avoid iterative process, x_m is assumed at the location where v''_{cr} reaches a maximum.

Finally, the generalized imperfection becomes:

$$\eta^*(x) = \alpha(\bar{\lambda}(x) - 0.2)f_\eta|\delta^{fl}(x)|\frac{W_z(x)}{A(x)} \tag{6.55}$$

$$\delta^{fl}(x) = v_{cr}(x) + \frac{h(x)}{2}\theta_{cr}(x) \tag{6.56}$$

$$f_\eta = \frac{N_{cr,z}}{EI_z(x_m)\left(v''_{cr}(x_m) + \frac{h}{2}\theta''(x_m) + \theta'(x_m)h'\right)} \tag{6.57}$$

and the utilization ratio is given by:

$$\varepsilon_M(x) = \frac{M_{y,Ed}(x)}{W_y(x)f_y} + \frac{EI_z(x)\left(v''_{cr}(x) + \frac{h}{2}\theta''_{cr}(x) + \theta'_{cr}(x)h'\right)}{A(x)f_y(\alpha_{cr}-1)}\eta(x) \leq 1.0 \tag{6.58}$$

with

$$\eta(x) = \alpha\big(\bar{\lambda}(x) - 0.2\big)f_\eta\big|\delta^{fl}(x)\big| \tag{6.59}$$

6.6.2   On the generalized imperfection factor

In section 6.4.1, it was shown that the application of the method is directly used with the column buckling curves for prismatic members. This is only possible because of the assumption of correspondence with the equivalent prismatic member. In the previous paragraph, it was shown that the generalized imperfection can be written in a way accounting for this assumption. Hence it is ready to be used with α-factors calibrated for prismatic beams. There are two possibilities for the adoption of the imperfection factor, the adoption of the *New EC3 method* or the *General Case*.

In Chapter 5, the safety assessment for prismatic beams showed that the *New EC3* method for lateral-torsional buckling of prismatic beams gave the best results in terms of partial factors. This is due to its mechanical consistency and calibration of the imperfections in a consistent way. For that, this is the preferred method to be used for the calculation of the imperfection factor.

The application of the *New EC3* imperfections for lateral-torsional buckling uses the normalized slenderness $\bar{\lambda}_z$. This brings a certain level of difficulty for the generalization to non-standard cases. For instance, let's consider the four cases given in *Figure 6.15* four beams with an IPE 200 cross-section, with the same length of 6.0 m and loaded with an uniform bending moment. Case 1 the reference case for which the imperfections are calibrated: a simply supported beam loaded with uniform bending moment. In *Case 2*, the beam has out-of-plane restraints on both

flanges, in *Case 3* it has a restraint on the compression flange and in *Case 4* it has a restraint on the tension flange.
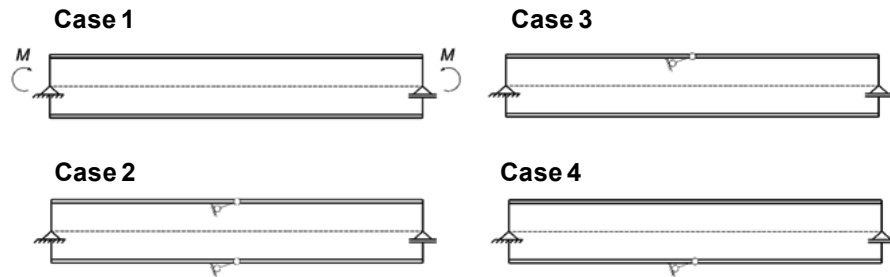
Figure 6.15 – Example: uniform member in bending with restraints

The critical moments and forces are given in *Table 6.6* and the buckled shapes in *Figure 6.16.* Under constant bending moment *Case 1*, the beam buckles in a half sine wave; for *Case 2* and *3,* the member buckles in two half-waves, since in both cases the compression flange which tends to buckle is the restrained one. In *Case 4* the beam buckles in a half-wave, however, the value of the critical moment is slightly higher due to the presence of the restraint, although it is not as effective as doubling the critical moment, but still the critical moment benefits from its presence.

| 189

The same member is considered loaded in compression, in order to obtain the corresponding minor axis critical force $N_{cr,z}$. Similarly to the beam case, in *Case 1* it buckles in a half sine wave, while in *Case 2* it buckles in two half-waves (*Figure 6.17*). *Cases 3* and *4* are identical for the member loaded in compression, as in for this particular geometry it buckles in 2 half-waves. For different geometrical arrangement, the member may even buckle in a torsional mode with a critical force between $N_{cr,z}$ and $4N_{cr,z}$.

Table 6.6 – Critical forces and moments for all cases

#	$M_{cr,abq}$ kNm	$M_{cr,theo}$ kNm	$N_{cr,z,abq}$ kN	$N_{cr,theo}$ kN
Case 1	23.2	23.0	81.9	81.9
Case 2	53.6	53.0	330.3	327.6
Case 3	53.6	53.0	330.3	327.6
Case 4	37.0	37.0	330.3	327.6

Case 1

Case 2

Case 3

Case 4
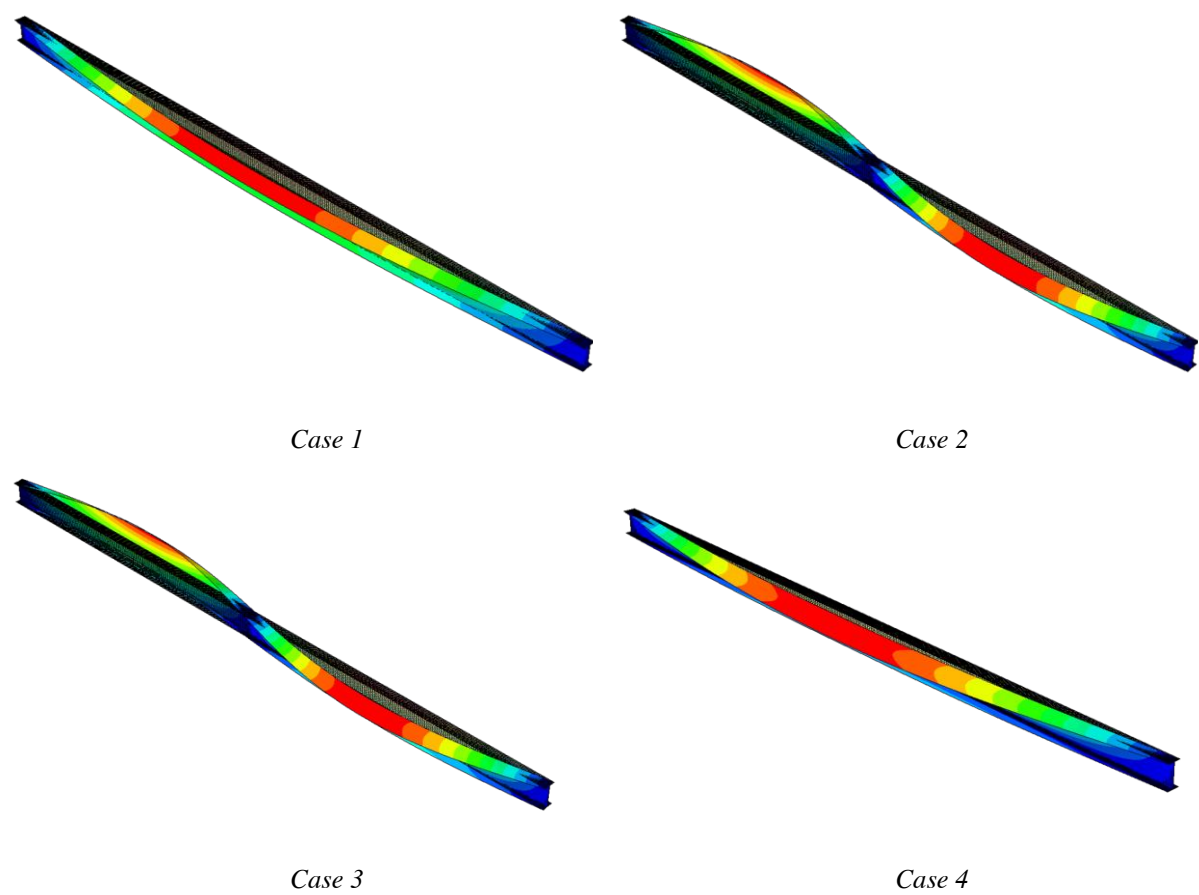
Figure 6.16 - Buckling modes: member loaded in bending

This feature introduces to a discontinuity since the relative increase of the critical force does not follow the relative increase of the critical moment as in cases 1 to 3.

Case 1

Case 2, 3 and 4
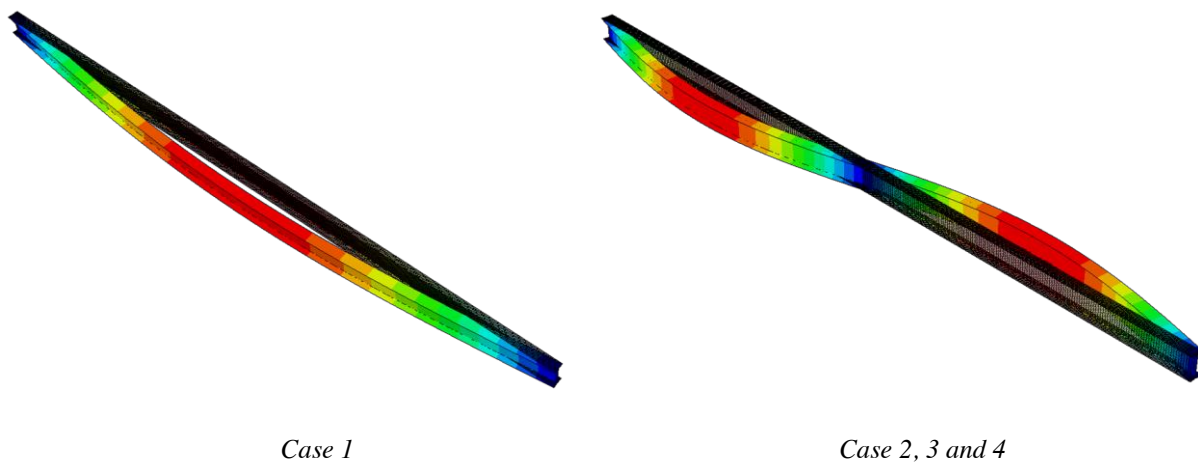
Figure 6.17 – Buckling modes: member loaded in compression

To overcome this discontinuity, it was assumed that the imperfection can be calculated for an equivalent elastic critical force $N_{cr,z,eq}$. This force is "retrieved" from the buckling mode using the differential equation for flexural buckling:

$$EI_z(x)v''_{cr}(x) + N_{cr,z}v_{cr}(x) = 0. \tag{6.60}$$

Then, the equivalent force becomes:

$$N_{cr,z,eq} = \frac{EI_z(x_m)|v''_{cr}(x_m)|}{|v_{cr}(x_m)|}. \tag{6.61}$$

It is this force that is used for the calculation of the normalized slenderness:

$$\bar{\lambda}(x) = \sqrt{\frac{A(x)f_y}{N_{cr,z,eq}}} \tag{6.62}$$

6.6.3 Design resistance

Similarly to flexural buckling, the design resistance is given by the load multiplier α_b, using Eq. (6.63):

$$\frac{\alpha_b M_{y,Ed}(x)}{W_y(x)f_y} + \frac{EI_z(x)\left(v''_{cr}(x) + \frac{h}{2}\theta''_{cr}(x) + \theta'_{cr}(x)h'\right)\alpha_b}{A(x)f_y(\alpha_{cr} - \alpha_b)}\eta(x) = 1.0 \tag{6.63}$$

6.6.4 Consistency with Eurocode 3

6.6.4.1 Lateral-torsional buckling of prismatic beam

The consistency of the GF with the existing rules for lateral-torsional buckling of prismatic beams is easily verified. For uniform members, the shape of the buckling mode is given by

$$v_{cr}(x) = \theta_{cr}(x) = \sin\frac{\pi x}{L}$$

and the utilization ratio is given by:

$$\frac{M_{y,Ed}(x_m)}{W_y(x_m)f_y} + \frac{EI_z(x)\left(v''_{cr}(x_m) + \frac{h}{2}\theta''_{cr}(x_m)\right)}{A(x_m)f_y(\alpha_{cr}-1)}\alpha(\bar{\lambda}(x_m)$$

$$-0.2)\frac{N_{cr,z}\left|v_{cr}(x_m) + \frac{h}{2}\theta(x_m)\right|}{EI_z(x_m)\left(v''_{cr}(x_m) + h/2\,\theta''(x_m)\right)} = 1.0 \leftrightarrow$$

$$\frac{M_{y,Ed}}{W_y f_y} + \frac{N_{cr,z}\left|v_{cr} + \frac{h}{2}\theta(x_m)\right|}{Af_y(\alpha_{cr}-1)}\frac{M_{y,Ed}}{M_{y,Ed}}\frac{W_y f_y}{W_y f_y}\alpha(\bar{\lambda}-0.2) = 1.0 \leftrightarrow \tag{6.64}$$

$$\frac{M_{y,Ed}}{W_y f_y} + \frac{M_{y,Ed}}{W_y f_y}\frac{\alpha(\bar{\lambda}-0.2)}{\left(1-\frac{M_{y,Ed}}{M_{cr}}\right)}\frac{\bar{\lambda}_{LT}^2}{\bar{\lambda}_z^2} = 1.0 \leftrightarrow$$

$$\chi_{LT} + \frac{\chi_{LT}}{1-\chi_{LT}\bar{\lambda}_{LT}^2}\frac{\bar{\lambda}_{LT}^2}{\bar{\lambda}_z^2}\alpha(\bar{\lambda}-0.2) = 1.0$$

which is exactly Eq. (2.58).

6.6.4.2 Discussion

The theoretical summary presented briefly in Section 6.6.1 is based on the assumption of constant bending moment distribution. However, a constant bending moment distribution is rare and therefore other bending moment distributions should be accounted for. Typically, the existing methods for LTB verification make use of calibrated factors which take into consideration the increase in the critical moment and the difference relative to the adopted buckling mode shape. The proposed method does not require any additional factors because it is applied as a direct interaction of the first and second order forces leading to the maximum load factor at the location of the beam where the utilization has a maximum and not at a pre-defined location such as mid-span.

An illustration is given in *Figure 6.18a*, where the utilization ratio for a web-tapered beam with $\gamma_h=3$ and a shallow end section of 100x100x10x10 loaded with a triangular bending moment is shown. The total utilization ratio as well as the first and the second order contributions are plotted *Figure 6.18a*. It shows that the failure location is found for a bending moment which is lower than the maximum applied moment. Furthermore, since both utilization ratios are non-linear, it is practically impossible to "guess" the critical location along the member. The

resistance obtained with the GF compares very well to GMNIA as shown in *Table 6.7*. This trend is confirmed for various slenderness ratios as plotted in *Figure 6.18b*.

Table 6.7 Comparison with GMNIA

Example	Method	GMNIA	Difference
Tapered beam with non-uniform bending moment	44.34	45.05kNm	1.6%
Tapered beam with restraint on the tension flange	24.3kNm	23.56kNm	3%
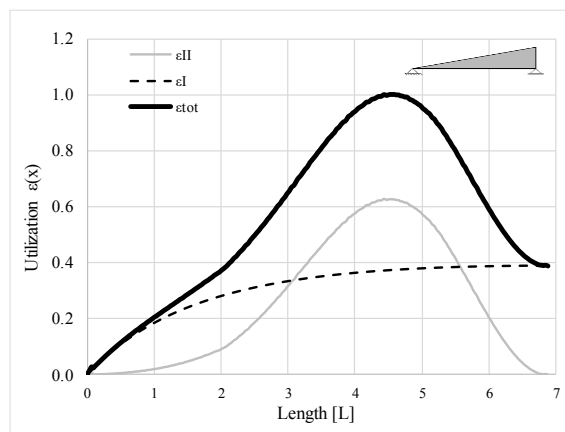
Example 2: web-tapered beam loaded with linearly varying bending moment	Comparison with GMNIA across various slenderness
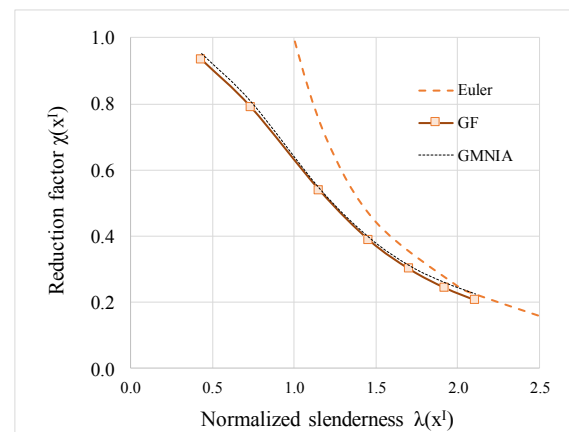
Figure 6.18 Web-tapered beam γh =3 with ψ=0

| 193

Another interesting application of the method is illustrated in *Figure 6.19*, a tapered beam with taper ratio of 2, loaded with a constant bending moment with a partial restraint on the tension flange. The tension flange restraints can contribute to higher lateral-torsional buckling resistance, but their efficiency depends on the geometry and loading of the beam. The buckling mode is shown in *Figure 6.20*. Critical shapes of the translation and twist rotation at the shear centre of the cross-section are shown in *Figure 6.21a*, which are used to compute the utilization ratio plotted in *Figure 6.21b*. At mid-span, it is observed that the second order utilization becomes close to zero due to the difference in the location of zero translation and twist rotation of the mode shape (*Figure 6.21a*). Table 6.7 shows the excellent agreement between the method and advanced numerical simulation.
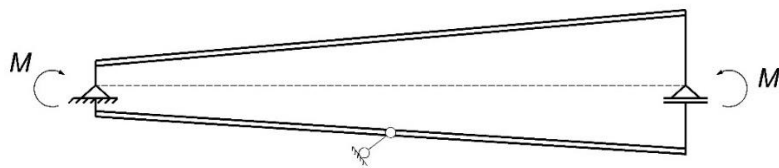
Figure 6.19 Example 3: Tapered beam with partial restraint on the tension flange
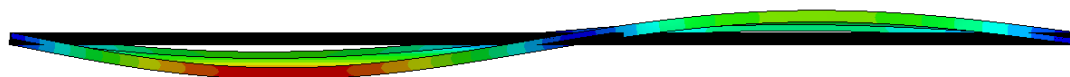
Figure 6.20 Mode shape
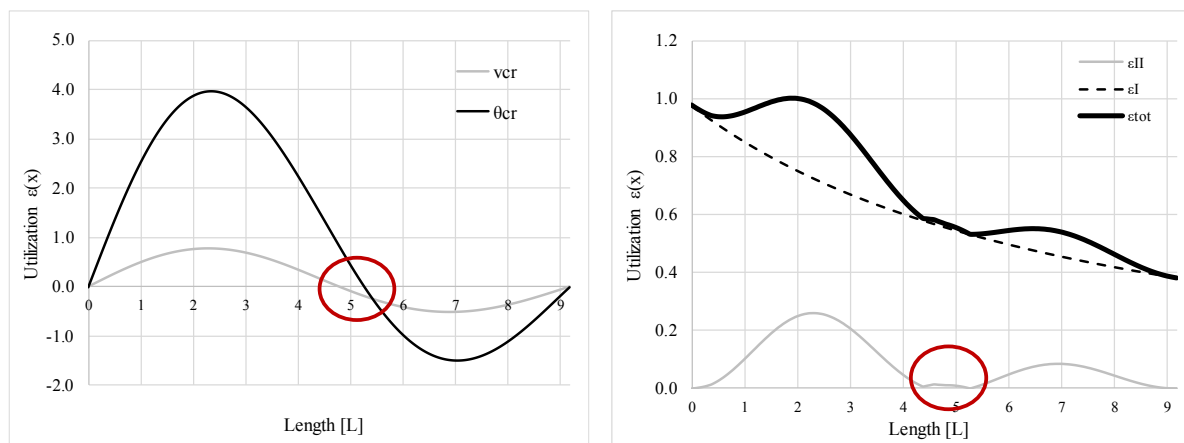
| a) | *Mode shape* | b) | *Utilization ratio* |

Figure 6.21 Beam with partial restraints on the compression flange

6.7 Lateral-torsional buckling of beam-columns

6.7.1 Introduction

The lateral torsional buckling of beam-columns is a joint case of the lateral-torsional buckling of beams and the flexural buckling of columns about their minor axis. It is also, the most complex buckling mode since its shape varies depending on the ratio between the applied bending moment and axial force. For high ratios of bending moment to axial force, the behaviour is more "beam-like" with a mixture of flexure and torsion, while for low ratios the behaviour is more "column-like" (*Figure 6.22*).
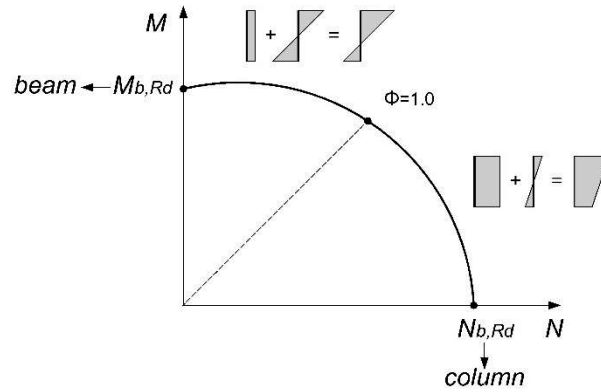
Figure 6.22 Beam-column behaviour for the variation between N and M

In the previous sections, it was shown how the proposed method works for columns and beams, where the application of the method was only possible together with previously calibrated imperfection factors for the uniform and simply-supported case. For beam-columns, however, Eurocode 3 provides interaction formula for members loaded in bending and compression. The interaction formula makes use of the expressions for beams and columns combining them through interaction factors which account for the joint action of the forces, which makes them not appropriate for the design formulation presented here. This led to the need of deriving an Ayrton-Perry equation for uniform beam-columns, presented in Section 6.2.

It is then used to derive the general verification format for lateral-torsional buckling of non-uniform beam-columns with various support, geometrical and loading conditions.

6.7.2 Verification format

For lateral-torsional buckling of members loaded in bending and compression, the interaction equation is given by:

$$\frac{\sigma(x)}{f_y} = \frac{N(x)}{A(x)f_y} + \frac{M_y(x)}{W_y(x)f_y} + \frac{M_z^{II}(x)}{W_z(x)f_y} + \frac{M_w^{II}(x)}{W_w(x)f_y}, \tag{6.65}$$

where there are two second-order contributions, the out-of-plane bending moment:

$$M_z^{II}(x) = -EI_z(x)v''(x) \tag{6.66}$$

and the bi-moment:

$$M_w^{II}(x) = -EI_w(x)\left(\theta''(x) + \theta'(x)h'\frac{2}{h}\right) \tag{6.67}$$

| 195

including the additional warping component appears due to the inclination of the flanges (*Kitipornchai & Trahair*, (1972)).

Following the same assumptions as for lateral-torsional buckling of beams, it is considered that the initial lateral displacement and twist rotation follow the buckling shape and have the same amplitude:

$$v_0(x) = v_{cr}(x)\bar{\delta}_0 \qquad \theta_0(x) = \theta_{cr}(x)\bar{\delta}_0 \tag{6.68}$$

with the same amplification relationship:

$$v(x) = \frac{1}{\alpha_{cr}-1}v_0(x) \tag{6.69}$$

$$\theta(x) = \frac{1}{\alpha_{cr}-1}\theta_0(x) \tag{6.70}$$

Then the interaction equation becomes:

$$\frac{N(x)}{A(x)f_y} + \frac{M_y(x)}{W_y(x)f_y} + \frac{EI_z(x)\bar{\delta}_0}{W_z(x)f_y}\left[\frac{v_{cr}(x) + \frac{h}{2}\theta_{cr}''(x) + \theta_{cr}'(x)h'}{\alpha_{cr}-1}\right] \le 1.0 \tag{6.71}$$

Adopting the same assumptions as for columns and beams, and using the second order contributions for the equivalent beam-column, which in this case are given by (6.2) and (6.3) for the weak axis bending moment and the bi-moment, respectively, it is possible to define the generalized imperfection as:

$$\eta^*(x) = \alpha(\bar{\lambda}(x) - 0.2)f_\eta\delta^{fl}(x)\frac{W_z(x)}{A(x)} \tag{6.72}$$

where f_η and $f_\eta\delta^{fl}(x)$ are given by Eqs. (6.56) and (6.57), leading to the utilization ratio

$$\varepsilon_{MN}(x) = \frac{N_{Ed}(x)}{A(x)f_y} + \frac{M_{y,Ed}(x)}{W_y(x)f_y} + \frac{EI_z(x)\left(v''_{cr}(x) + \frac{h}{2}\theta''_{cr}(x) + \theta'_{cr}(x)h'\right)}{A(x)f_y(\alpha_{cr}-1)}\eta(x) \le 1.0 \tag{6.73}$$

with

$$\eta(x) = \alpha(\bar{\lambda}(x) - 0.2)f_\eta\delta^{fl}(x) \tag{6.74}$$

The imperfection factor α is used as proposed in Section 6.2.1.2 and the normalized slenderness is used as in Section 6.6.2.

6.7.3 Beam-column buckling modes

It was already mentioned earlier that complexity of the beam-column behaviour arises from the variation in the relative ratio between the bending moment and the axial force, as well as across the various slenderness ranges. Since it is possible to have "beam-like" modes and "column-like"-modes, it was already ensured in the previous section that the imperfection magnitude varies from beam to column according to the applied loads. In this section, a discussion on the shape of the buckling mode is offered because it also varies according to the relative ratio of the bending moment and axial force, which is important for the application of the general formulation to ensure safe and economical design.

To illustrate the problem, the following example is proposed. Consider an uniform welded member with a cross-section 350x175x12x8 with a restraint on the compression flange and length L=5m, as shown in *Figure 6.23*, is loaded with five different ratios of uniform bending moment to the axial force.
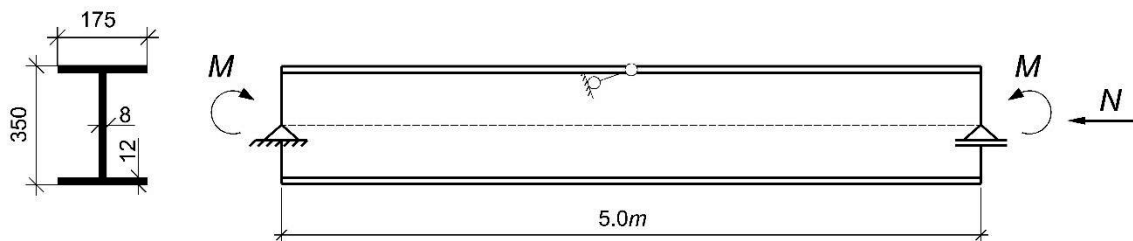
Figure 6.23 – Example member loaded in bending and compression with restraint on the compression flange

The buckling mode shapes are shown in *Figure 6.24*. For $\phi = 0.2$, 0.4 and 1.0, the behaviour is dominated by lateral-torsional buckling. In contrast, $\phi = 2.4$ and 5.0, the beam-column does not buckle in two half-waves but the bottom flange buckles in a single half-wave. This only shows that the compressive stress required to cause buckling of the bottom flange is lower than the compressive stress necessary to buckle the top flange in two half-waves.
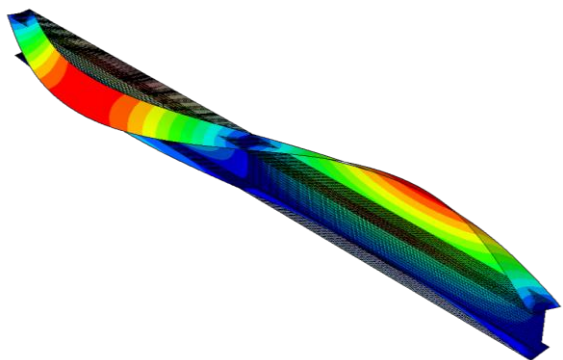
a) $\phi = 0.0$
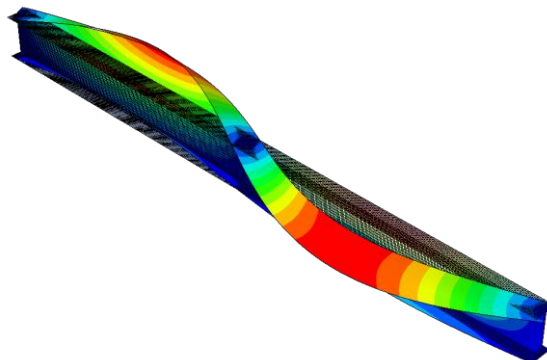
b) $\phi = 0.2$
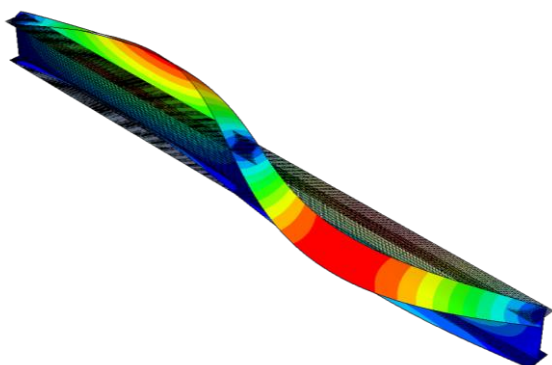
c) $\phi = 0.4$
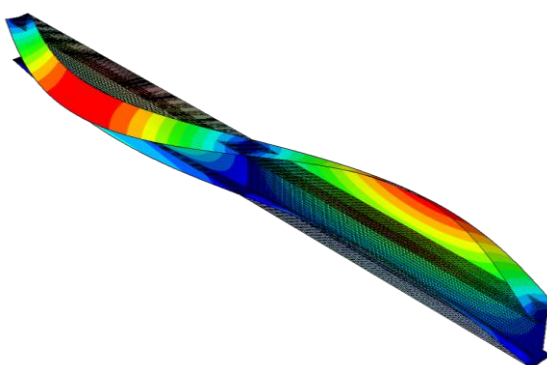
d) $\phi = 1.0$
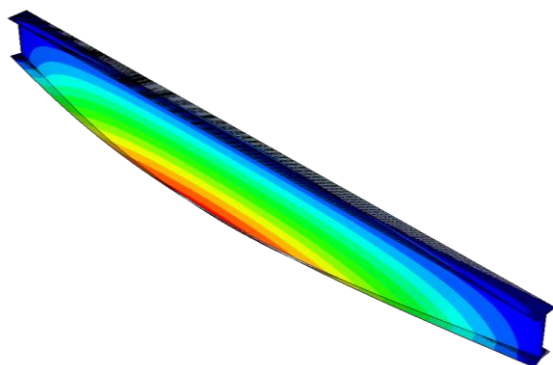
e) $\phi = 2.4$
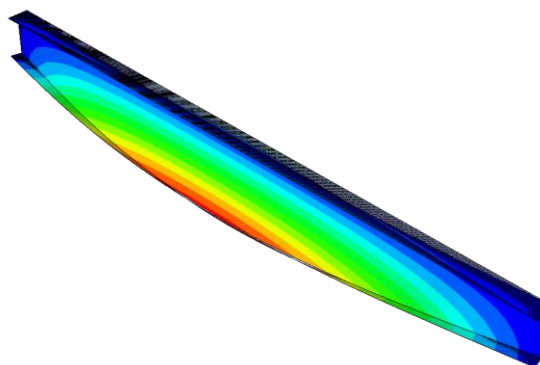
f) $\phi = 5.0$

Figure 6.24 – Buckling modes for different ratios of bending moment and axial force

The stresses that are present in the cross-section are shown in *Figure 6.25*. The buckling modes of *Figure 6.24* for $\phi = 0$, 0.2, 0.4 and 1.0 lead to a stress configuration for which the maximum compressive stress is equal to the sum of the absolute values of each stress component.
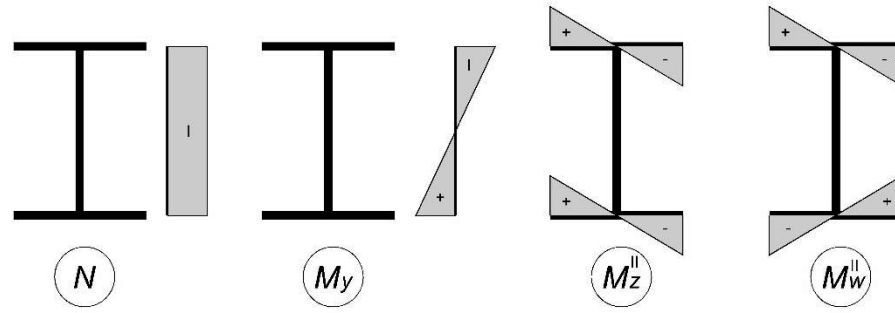
Figure 6.25 - Stresses in member under bending and compression

However, for the buckling modes of *Figure 6.24* for $\phi = 2.4$ and 5.0, the twist rotation exhibits opposite sign and results in the stress distributions as shown in *Figure 6.26*. For such pattern, it is not clear which is the flange governing the design, and therefore, it is required to verify both flanges according to Eq.(6.75).
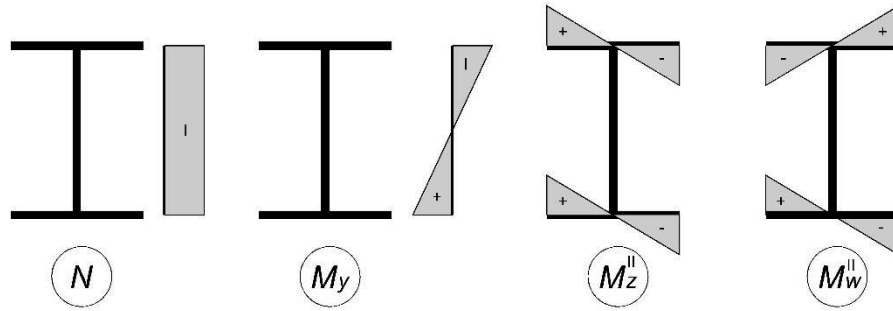
Figure 6.26 - Stresses in member under bending and compression

$$max \begin{cases} \dfrac{N}{A} + \dfrac{M_y}{W_y} - \dfrac{M_z^{II}}{W_z} + \dfrac{M_w^{II}}{W_w} \leq 1.0 \\[2mm] \dfrac{N}{A} - \dfrac{M_y}{W_y} + \dfrac{M_z^{II}}{W_z} + \dfrac{M_w^{II}}{W_w} \leq 1.0 \end{cases} \qquad (6.75)$$

6.7.4   Design resistance

Similarly to flexural buckling, the design resistance is given by the load multiplier α_b, according to Eq. (6.76):

$$\frac{\alpha_b N_{Ed}(x)}{A(x)f_y} + \frac{\alpha_b M_{y,Ed}(x)}{W_y(x)f_y} + \frac{EI_z(x)\left(v''_{cr}(x) + \frac{h}{2}\theta''_{cr}(x) + \theta'_{cr}(x)h'\right)\alpha_b}{A(x)f_y(\alpha_{cr} - \alpha_b)}\eta(x) = 1.0 \quad (6.76)$$

6.7.5   Consistency with the uniform member

Consistency with the existing rule for lateral-torsional buckling of prismatic beam is easily verified. In case of a prismatic steel beams with $N=0$, then Eq. (6.73) reduces to:

$$0 + \frac{M_{y,Ed}(x)}{W_y(x)f_y} + \frac{EI_z(x)\left(v''_{cr}(x) + \frac{h}{2}\theta''_{cr}(x) + \theta'_{cr}(x)h'\right)}{A(x)f_y(\alpha_{cr} - 1)}\eta(x) = 1.0$$

$$\frac{M_{y,Ed}(x_m)}{W_y(x_m)f_y} + \frac{EI_z(x)\left(v''_{cr}(x_m) + \frac{h}{2}\theta''_{cr}(x_m)\right)}{A(x_m)f_y(\alpha_{cr} - 1)}\alpha(\bar{\lambda}(x_m)$$

$$-0.2)\frac{N_{cr,z}\left|v_{cr}(x_m) + \frac{h}{2}\theta(x_m)\right|}{EI_z(x_m)\left(v''_{cr}(x_m) + h/2\,\theta''(x_m)\right)} = 1.0 \leftrightarrow \quad (6.77)$$

$$\frac{M_{y,Ed}}{W_y f_y} + \frac{N_{cr,z}\left|v_{cr} + \frac{h}{2}\theta(x_m)\right|}{Af_y(\alpha_{cr} - 1)}\frac{M_{y,Ed}}{M_{y,Ed}}\frac{W_y f_y}{W_y f_y}\alpha(\bar{\lambda} - 0.2) = 1.0 \leftrightarrow$$

$$\frac{M_{y,Ed}}{W_y f_y} + \frac{M_{y,Ed}}{W_y f_y}\frac{\alpha(\bar{\lambda} - 0.2)}{\left(1 - \frac{M_{y,Ed}}{M_{cr}}\right)}\frac{\bar{\lambda}_{LT}^2}{\bar{\lambda}_z^2} = 1.0 \leftrightarrow$$

$$\chi_{LT} + \frac{\chi_{LT}}{1 - \chi_{LT}\bar{\lambda}_{LT}^2}\frac{\bar{\lambda}_{LT}^2}{\bar{\lambda}_z^2}\alpha(\bar{\lambda} - 0.2) = 1.0$$

while $M_y=0$, then Eq. (6.73) reduces to:

$$\frac{N_{Ed}(x)}{A(x)f_y} + 0 + \frac{EI_z(x)\left(v''_{cr}(x) + \frac{h}{2}\times 0 + 0\times h'\right)}{A(x)f_y(\alpha_{cr} - 1)}\alpha(\bar{\lambda}(x)$$

$$-0.2)\frac{N_{cr,z}\left|v_{cr}(x) + \frac{h}{2}\times 0\right|}{EI_z(x_m)\left(v''_{cr}(x_m) + h/2\times 0 + 0\times h'\right)} = 1.0 \leftrightarrow \quad (6.78)$$

$$\frac{N_{Ed}(x)}{A(x)f_y} + \frac{-EI_i(x)v_{cr}''(x)}{A(x)f_y(\alpha_{cr}-1)}\alpha\big(\bar{\lambda}(x)-0.2\big)\frac{\alpha_{cr}N_{Ed}(x)|v_{cr}(x)|}{EI_i(x_m)|v_{cr}''(x_m)|} = 1.0 \leftrightarrow$$

$$\frac{N_{Ed}(x)}{Af_y} + \frac{EI_i\pi^2/L^2}{Af_y(\alpha_{cr}-1)}\alpha\big(\bar{\lambda}-0.2\big)\frac{N_{cr}}{EI_i\pi^2/L^2} = 1.0 \leftrightarrow$$

$$\frac{N_{Ed}(x)}{Af_y} + \frac{N_{Ed}(x)}{Af_y(1-N/N_{cr})}\alpha\big(\bar{\lambda}-0.2\big) = 1.0 \leftrightarrow$$

$$\chi + \frac{\chi}{1-\chi\bar{\lambda}^2}\alpha\big(\bar{\lambda}-0.2\big) = 1.0$$

6.8 Validation

6.8.1 Scope

In this section, the general formulation is validated against GMNIA resulta. The numerical models were carried out in accordance with the previously described procedure in Chapter 4. In this validation, special attention was paid to the applicability of the GF to non-uniform columns, beams and beam-columns as well as for members with varying loads along their length and load application (top/bottom flanges or shear centre, members with restraints only at one flange (compression or tension) and members which are not simply supported.

Firstly, the global parametric study is presented and its statistical assessment with respect to GMNIA results. Then the method is evaluated in comparison with existing methods for design of non-uniform members: the General method and the design methods for web-tapered columns and beams by *Marques* (2012).

6.8.2 Methodology

In order to have a common basis for comparison, the generalized reduction factors are considered at the first order failure location: $\chi^{GMNIA}(x_c^I)=\alpha_b^{GMNIA}/\alpha_{ult,k}^{CS}(x_c^I)$ and $\chi^{Method}(x_c^I)=\alpha_b^{Method}/\alpha_{ult,k}^{CS}(x_c^I)$, in which α_b^x is the resistance multiplier obtained numerically ($x=GMNIA$) or by the method ($x=Method$) and $\alpha_{ult,k}^{CS}$ is the cross section resistance multiplier. x_c^I is the location along the member where the utilization due to applied (first order forces) is maximum and becomes: $x_{c,N}^I$ for a column; $x_{c,M}^I$ for a beam.

The imperfection factors were considered according to Table 6.2 from Eurocode 3 for flexural buckling and for lateral-torsional buckling according to the new EC3 method. For beam-columns, the proposed interpolation in Section 6.2.1.2 was adopted.

6.8.3 Parametric study

The parametric study is summarized in *Table 6.8*. It covers several types of members, loading and support conditions, totalling 2213 cases.

Figure 6.27 shows the cases #1 from *Table 6.8,* Tap D type of member – web tapered with different inclinations of both flanges, including restraint to the tension flange and a built-in end at the deep section.
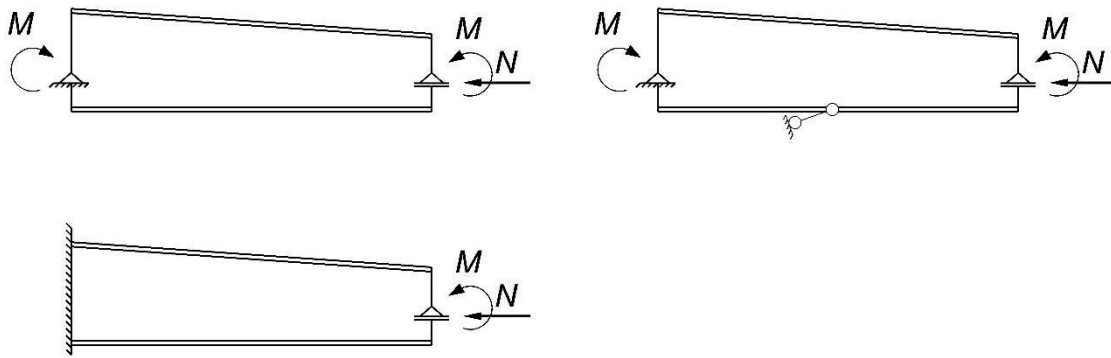
Figure 6.27 - Cases #1 Tap D member

Figure 6.28 illustrates prismatic members (Cases #2 and #8 in *Table 6.8*). They were considered with one restraint either to the compression or the tension flanges and two restraints to the tension flange.
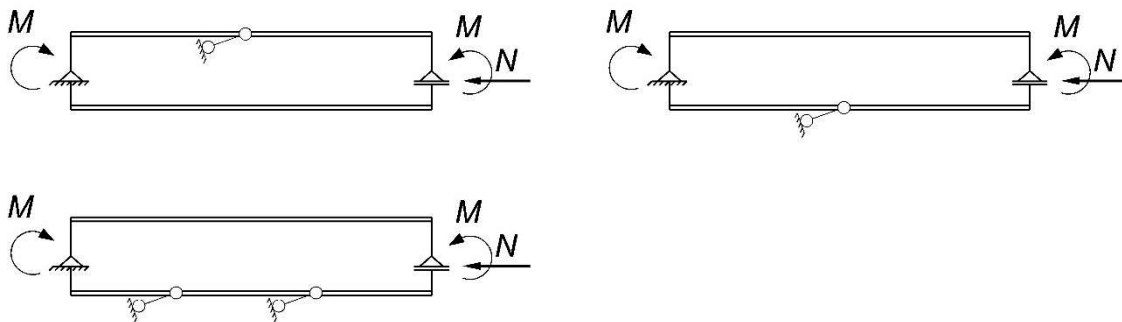
Figure 6.28 - Cases #3 Uniform member

Cases #3 are shown in *Figure 6.29*. They consist of members with a parabolic variation of cross-section whereby the deep section was takes as 1.5 times the shallow one. These members were also considered with no intermediate restraints, one restraint either to the compression or the tension flanges or two restraints to the tension flange.
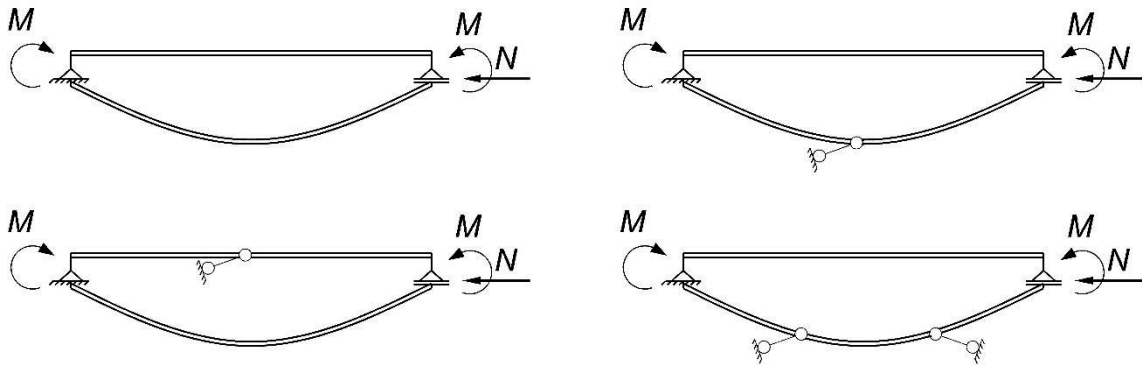
Figure 6.29 - Cases #3 Parabolic member

Figure 6.30 illustrates cases #4 to #7 from *Table 6.8*, Taper S type of member, web-tapered with symmetrical inclination of both flanges, without any restraint, with a tension flange restraint or fixed at the deep end. A part of them, cases #5, #6 and #7, were considered fictitiously as "rolled" by modelling the residual stress pattern for rolled sections. This aimed for the assessment of the consistency with the imperfection factors for rolled sections.
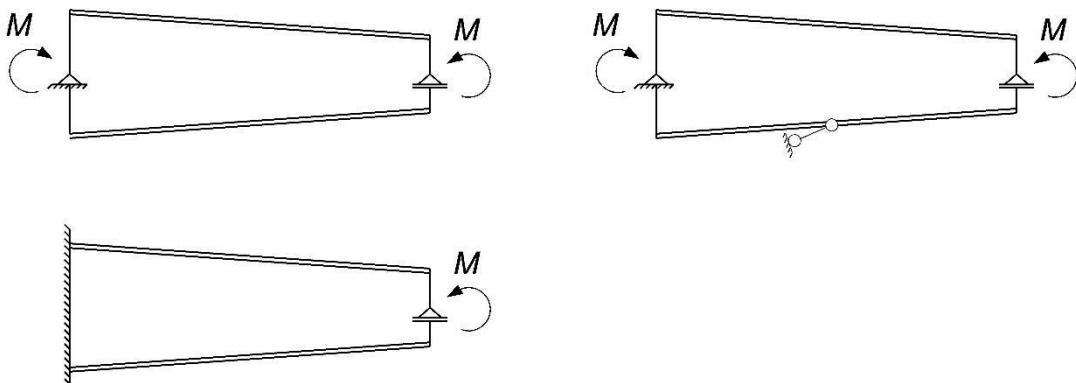
Figure 6.30 – Cases #4, #5, #6 Tap S member

Finally, cases #9 that correspond to numerical simulations carried out by *Ofner* (1997), that were also used to extend the parametric study with independent results by other author. They consist of prismatic section, restrained from out-of-plane buckling, for various ratios of bending moment to axial force and different bending moment distributions.

Table 6.8 - Parametric study

#	Member	Section hxbxt$_f$xt$_w$	L m	γh	γb	Supports	Restraints	Load	φ	ψ	N
1	Taper D	250x200x16x8	5-12	2,3,4	1	SS-SS	1x tension	My	0;0.2;0.4; 1;2.4,5	1	270
						SS-Fix	None	My+N			
2	Uniform	350x175x12x8	3-12	-	-	SS-SS	1x tension	My	0;0.2;0.4; 1;2.4,5	1	223
		250x200x16x8					2x tension	My+N			
		500x200x16x8					1x compression				
3	Parabolic	350x175x12x8	3-12	-	-	SS-SS	1x tension	My	0;0.2;0.4; 1;2.4,5	1	350
		250x200x16x8					2x tension	My+N			
		500x200x16x8					1x compression				
4	Taper S	IPE240eq	3-12	1,2,3, 4,5	2,3,4	SS-SS	Out	N	-	-	207
		HEA300eq									
5	Taper S	100x100x10x10		1,2,3, 4,5	1,2,3, 4,5	SS-SS	None	N	-	1,0	32
							Out				
6	Taper S	100x100x10x10	5-12	1, 1.2, 3, 4, 5, 6	1	SS-SS	None	My	-	1	60
7	Taper S	100x100x10x10	5-12	2, 3, 4, 5, 6	1	SS-SS	None	My	-	0, 0.5	120
						SS-Fix	1x tension			Distributed	
8	Uniform	HEB200	3-12	-	-	SS-SS	None	My	-	1, 0, -1	76
		IPE300					1x tension			Dist (top, bot, center)	
							1x compression				
9	Uniform (Ofner)	IPE200	3-18	-	-	SS-SS	Out	My+N	0.08-10	1, 0, -1	875
		HE300B								Dist., Conc.	
		IPE500									

2213

6.8.4 Statistical analysis

The statistical evaluation of the GF is carried out on the basis of the ratios r_e/r_t or $\chi^{GMNIA}/\chi^{Method}$. It covers all cases from *Table 6.8*, totalling 2213 members. The statistical parameters for all results and relevant subsets are presented in *Table 6.9* and *Figure 6.31* shows scatterplots for the different types of members considered in the parametric study.
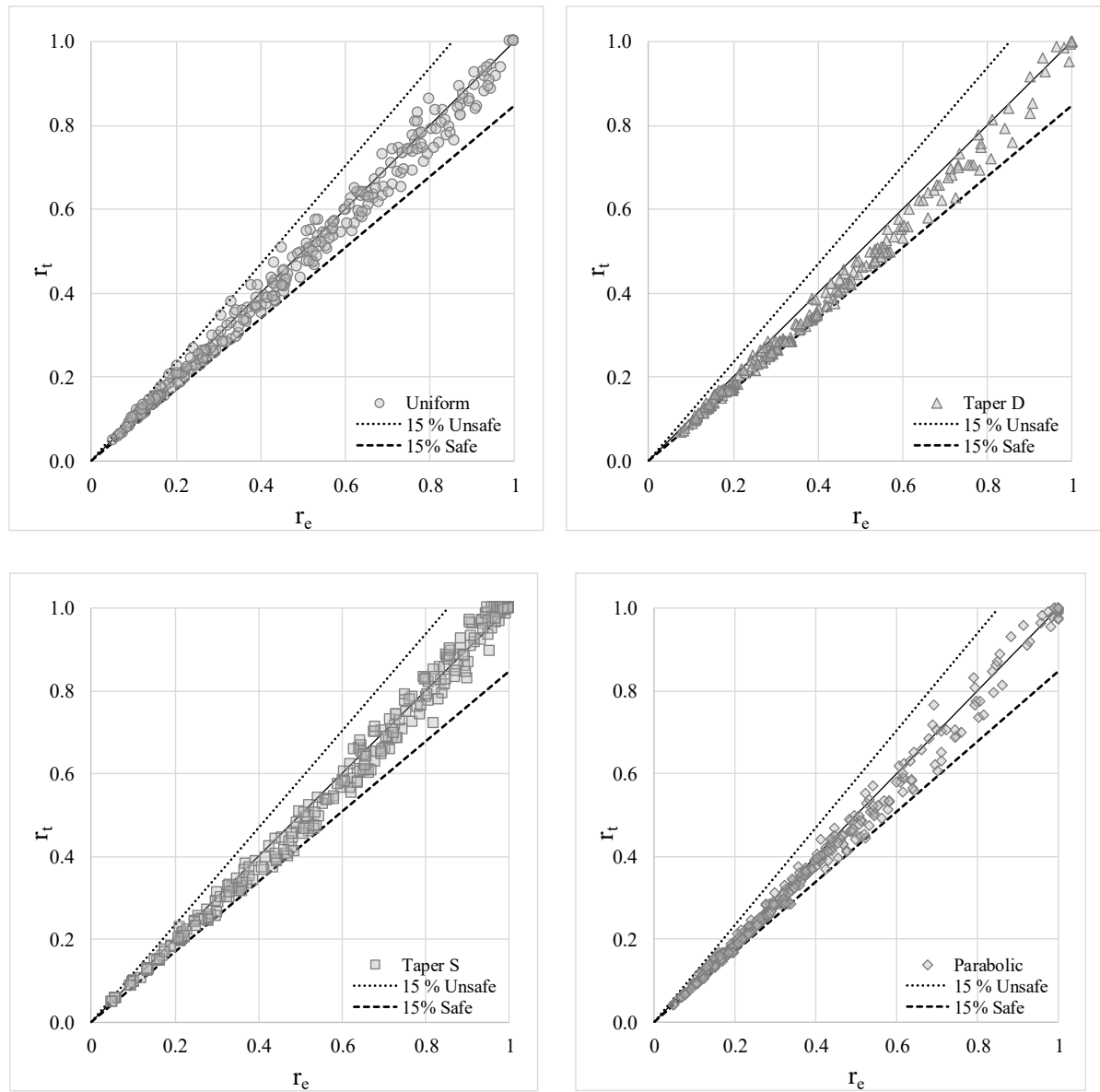
Figure 6.31: Scatter plot: All results

The comparison is performed based on statistical parameters, obtained for the ratios r_e/r_t, where r_e is the result from the numerical simulations and r_t is the result from the general formulation. The ratio r_e/r_t is higher (respectively lower) than unity when the "theoretical" result is a safe-sided (respectively non-conservative) estimate.

Table 6.9 and *Figure 6.31* show very good agreement between numerical and theoretical results, considering that the parametric study consists of "non-standard" members (with restraints, fixed supports, varying geometry along the member length, etc.). For uniform members, the results present similar accuracy when compared to Method 1 and better than Method 2 (see *Table 6.5*)

Table 6.9 - Statistical parameters

Subset	n	Average	Cov	Min	Max	N <0.95	N >1.1
All	**2213**	**1.05**	**5.2**	**0.878**	**1.205**	**34**	**398**
Uniform	1174	1.04	5.2	0.878	1.205	20	170
Taper D	270	1.08	4.98	0.966	1.188	-	118
Taper S	419	1.03	4.8	0.933	1.185	5	46
Parabolic	350	1.05	4.98	0.905	1.187	9	64
Columns	239	1.03	5.1	0.946	1.177	1	35
Beams	400	1.03	4.9	0.924	1.185	10	46
Beam-Columns	1574	1.05	5.2	0.878	1.205	23	317
Rolled	1163	1.04	4.95	0.929	1.205	6	138
Welded	1050	1.05	5.4	0.878	1.188	28	260

Table 6.9 and *Figure 6.31* show that the welded cases have more cases in percentage to the total which fall higher than 1.1 or lower than 0.95. This safety issue is directly linked to the imperfection factors used for welded sections. In *Marques* (2012), it was shown that the Eurocode 3 imperfection factors are unsafe in the intermediate slenderness range for welded cross-sections and they become over conservative for members with normalized slenderness ratio higher than 1.0.

6.8.5   Comparison with analytical methods from *Marques* (2012)

6.8.5.1   Scope

Furthermore, the method is compared with the theoretical method from *Marques* (2012) for flexural and lateral-torsional buckling of web-tapered columns and beams. The approach adopted by *Marques* (2012) relies on the exact critical location and the comparison is useful to evaluate the impact of the approximation for the critical location of the GF.

For the evaluation of results, the following methodologies are considered:

- GMNIA – Results given by the numerical models (geometrically and materially nonlinear analysis with imperfections);

- Application of proposed procedure for:

  – Flexural buckling of columns, (Eq. (6.34)) and the theoretical method from *Marques et al.* (2012) (LM) (Eq.(2.80))

  – Lateral-torsional buckling of beams (Eq.) and the theoretical method from *Marques et al.* (2013) (LM) (Eq.(2.86)):

6.8.5.2 Application of the method

Firstly, the shape of the utilization ratio was studied for the general formulation in comparison with the theoretical derivation given in *Marques* (2012). An example is illustrated in *Figure 6.32* for a tapered column with taper ratio $\gamma_h=\gamma_b=3$ loaded with uniformly distributed axial force. The utilization ratio is plotted for the load multiplier α_b along the column length. Both terms of the utilization ratio are separated, the utilization due to normal stresses due to applied forces (designated as ε_I) and normal stresses due to second order forces (designated as ε_{II}) and the sum of both – $\varepsilon_{tot.}$

| 207
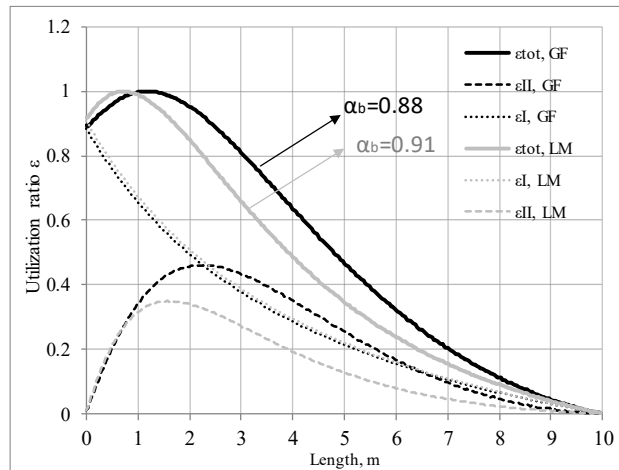
Figure 6.32: Utilization ratio

Since the amplification relationship is slightly different, the expected deviation in the critical position is inevitable as shown in *Figure 6.32*, the second order utilization for both methods are

different. However, in terms of maximum load multiplier α_b, both methods lead to similar predictions.

These comparisons are carried out for the same cases used to calibrate the theoretical model of *Marques et al.* (2012) and (2013) for flexural buckling of web-tapered columns and lateral-torsional buckling of web-tapered beams. These are the cases #5 and #6 from *Table 6.8*.

6.8.5.3 Tapered members – comparison with cases from Marques et al. (2012) and (2013).

The comparison is performed for the reduction factor χ (x_c^I), where in *Figure 6.33a*, *Figure 6.34a* and *Figure 6.35a*, the results for in plane, out-of-plane and lateral-torsional buckling are plotted.

The results are presented as a buckling curve representation (*Figure 6.33a, Figure 6.34a, Figure 6.35a*) where the abscissa is set to the normalized slenderness for the smallest cross-section so that, the predictions by the GF, GMNIA and the theoretical method from *Marques et al.* (2012) and (2013), are compared for the same normalized slenderness. The GF compares well providing similar resistances to GMNIA and the theoretical method proposed in *Marques et al.* (2012) and (2013).

(a) In plane buckling

(b) Scatter plot
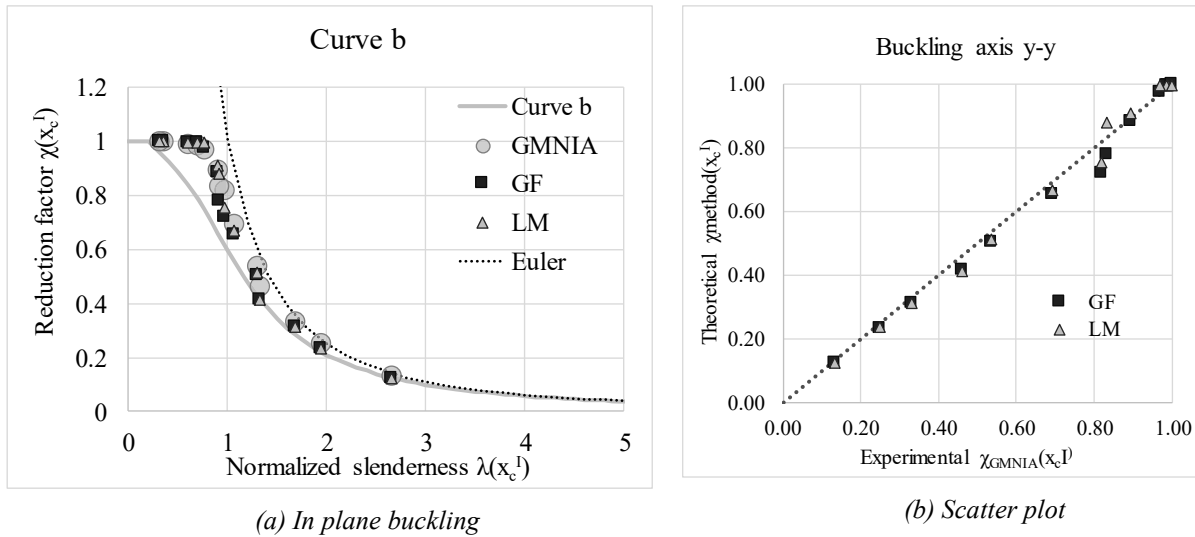
Figure 6.33: Theoretical vs experimental resistance – major axis flexural buckling

(a) Out-of-plane buckling　　　　　　　*(b) Scatter plot*
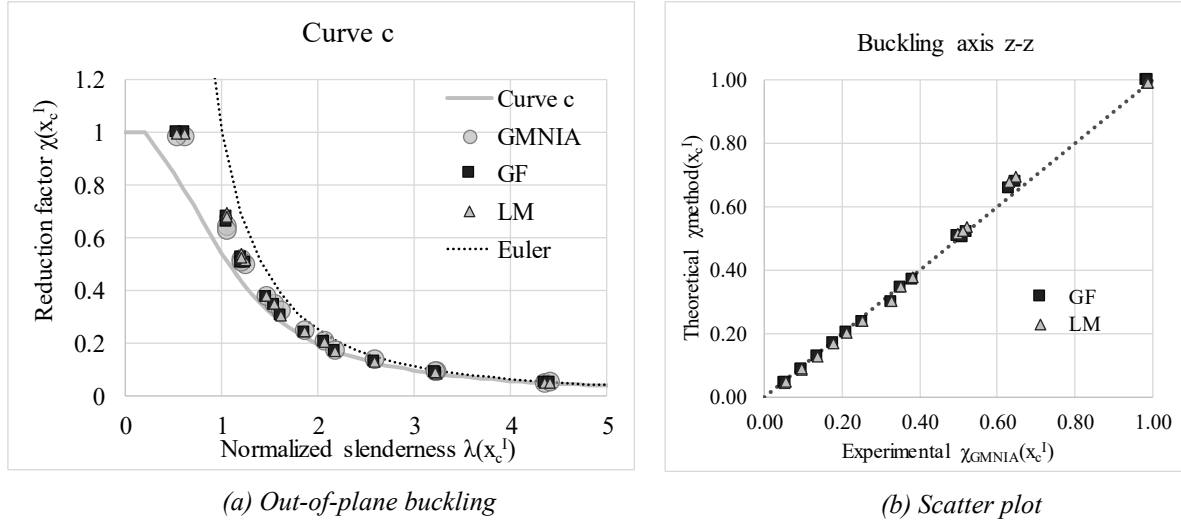
Figure 6.34: Theoretical vs experimental resistance – minor axis flexural buckling

Table 6.10 summarizes the statistical parameters for the two cases: flexural buckling and lateral-torsional buckling. Regarding tapered members, the mean value of the ratios $\chi^{GMNIA}(x_c^I)/\chi^{Method}(x_c^I)$ is slightly higher than unity with small coefficient of variation, thus indicating a good precision of both methods.

(a) Lateral-torsional buckling　　　　　　*(b) Scatter plot*
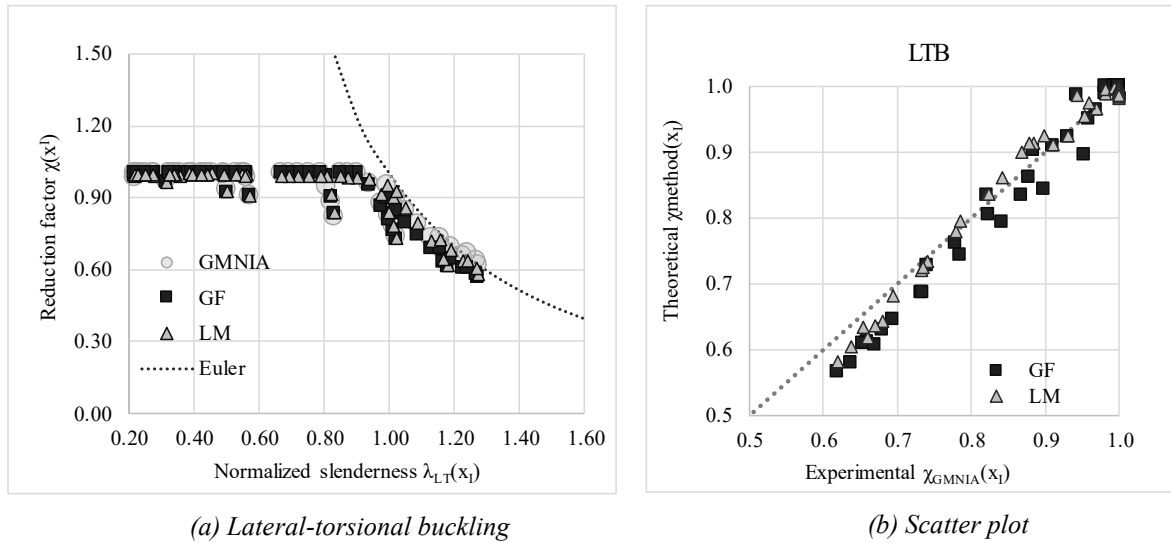
Figure 6.35: Theoretical vs experimental resistance – lateral torsional buckling

Figure 6.33b, *Figure 6.34b* and *Figure 6.35b* summarize the scatter plots for both methods and for the three buckling modes considered in this assessment, where the ordinate is the theoretical estimation $\alpha_{b,model}$ and the abscissa is the $\alpha_{b,GMNIA}$.

Table 6.10: Statistical parameters αb,GMNIA/ αb,model

Buckling mode	In plane (y-y)		Out-of-plane (z-z)		LTB	
	LM	GF	LM	GF	LM	GF
Mean	1.03	1.05	1.02	1.03	1.01	1.02
C.o.V	5%	5%	5%	4%	2.2%	3.4%
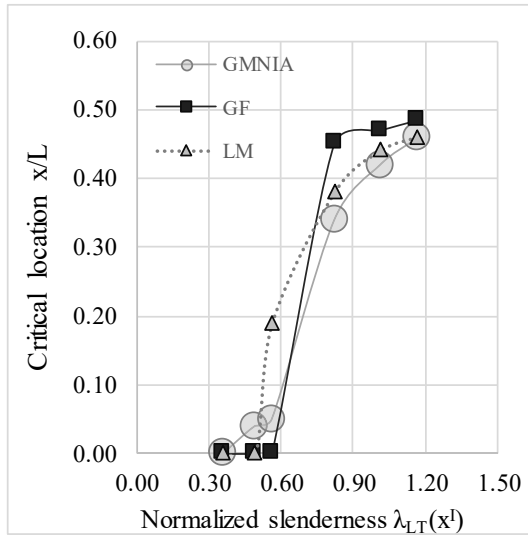
a) taper ratio γ_h=1.2
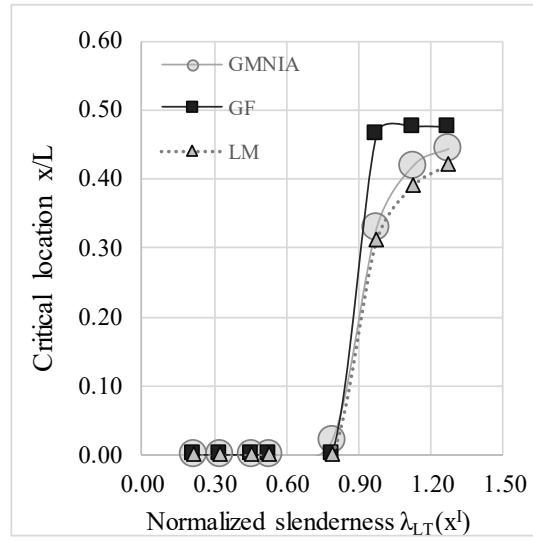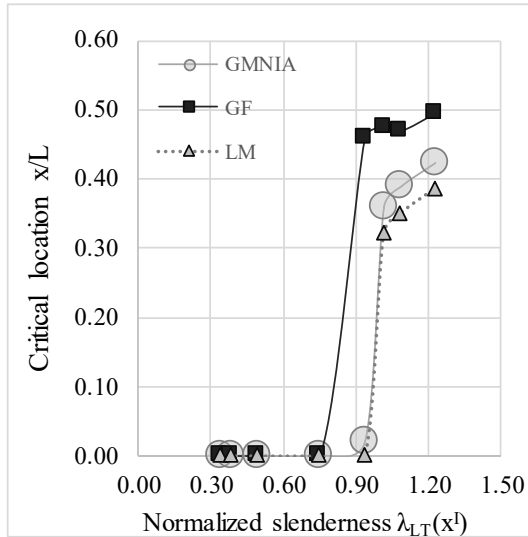
b) taper ratio γ_h=2
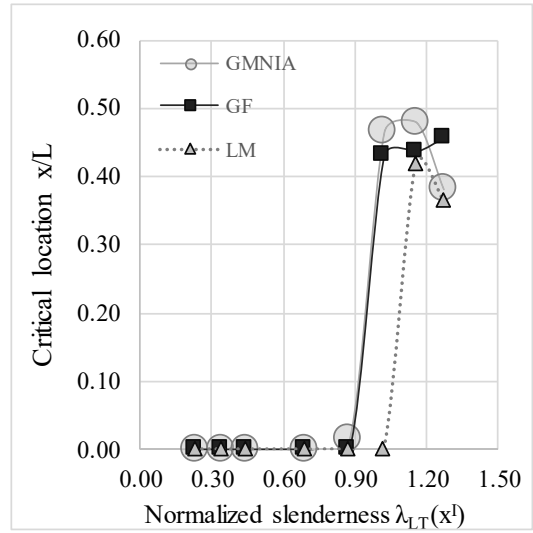
c) taper ratio γ_h=3

c) taper ratio γ_h=5

Figure 6.36 – Critical locations for lateral-torsional buckling of web-tapered beams

The critical location was also assessed the GF, GMNIA and the theoretical method from *Marques et al.* (2012) and (2013). *Figure 6.36* shows the variation of the critical location with increase of the member slenderness for web-tapered members with taper ratios 1.2, 2, 3 and 5 under constant bending moment. For the analysed cases, the critical location for the three methods was not found very different.

6.8.6 Comparison with the General Method

In this section comparison with the General Method given in clause 6.3.4 of Eurocode 3 (2005) is presented. The assessment was performed for a set of tapered members, Cases #1 from Table 6.8, which are simply supported, or with one end fixed, or with restraints to the tension flange.

The General Method was applied according to the recommendations of section 6.3.4, the in-plane resistance was obtained by using GMNIA in-plane with magnitude of the initial imperfection L/1000. The buckling curve used is curve c welded section in flexural buckling out-of-plane or lateral-torsional buckling General Case (for the smallest cross-section).
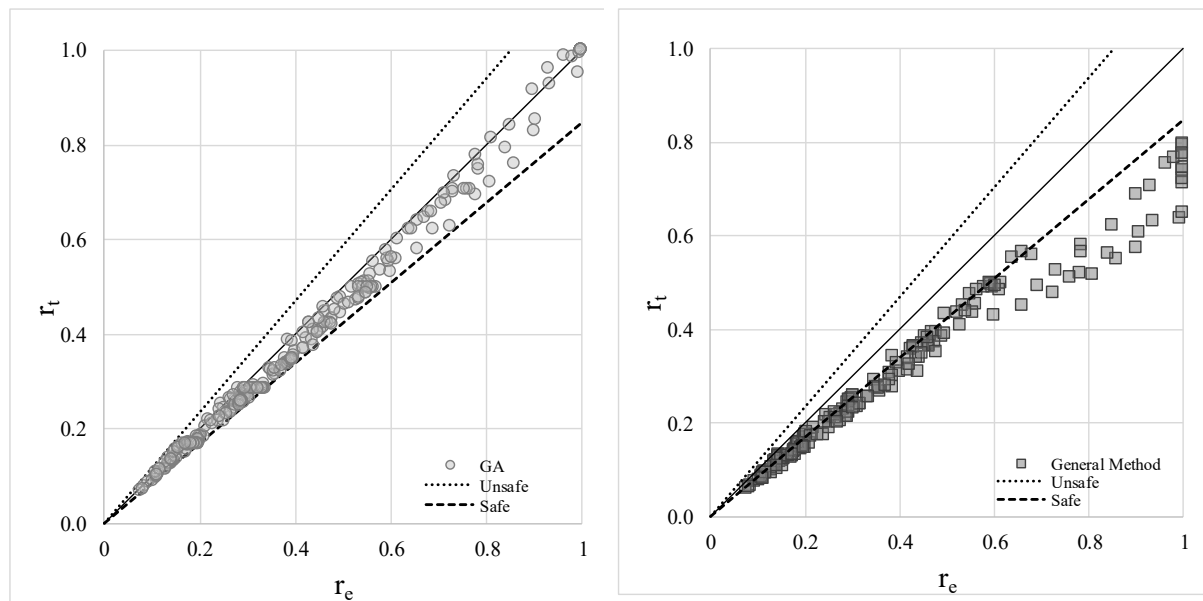
Figure 6.37 Scatterplot: Method vs General method

The scatterplots for both methods are given in *Figure 6.37*, the numerical results are plotted on the abscissa and the calculated estimations by both methods are on the ordinate. *Table 6.11* summarizes the statistical parameters for the General formulation and the General Method. The direct comparison of both methods on the basis of the statistical parameters favours the

proposed method: lower scatter and mean value of the ratio r_e/r_t much closer to unity than the General method.

Table 6.11 – Statistical parameters

	Subset	Mean	C.o.v	Min	Max	N	$N_{<1}$	$N_{<0.97}$
General formulation	All	1.08	4.98%	0.966	1.188	270	19	-
	SS-SS	1.08	4.2%	0.973	1.155	90	8	-
	Restraint	1.07	5.1%	0.966	1.169	90	5	1
	SS-Fix	1.09	5.5%	0.976	1.188	90	6	-
General method	All	1.28	7.7%	1.079	1.567	270	-	-
	SS-SS	1.25	8.1%	1.113	1.567	90	-	-
	Restraint	1.31	6.5%	1.162	1.566	90	-	-
	SS-Fix	1.27	7.9%	1.079	1.514	90	-	-

6.9 Example

Finally, an illustrative example is proposed to demonstrate the application of the General formulation. For this purpose, consider the beam-column shown in *Figure 6.38*. The first 5 meters of the member are with uniform cross-section 250x200x8x16, while the last 2.5 m web-tapered section which has a depth at the deepest cross-section equal to 500 mm.

The member is simply-supported at one end allowing for the longitudinal displacement and is fully-fixed at the other end. A discrete intermediate restraint at the bottom flange is added at the change of the cross-section. The applied loads are a concentrated axial force, a concentrated major axis bending moment at the left end and a uniformly distributed load along the member.

In this example, the verification of the in-plane buckling mode is omitted because it is not critical.

The general application of the method is summarized in the flowchart of *Figure 6.39*, where firstly the user shall determine the eigenmode and the corresponding critical load factor α_{cr} by linear buckling analysis. It is noted that the critical load multiplier should be higher than unity so that the verification would make sense.
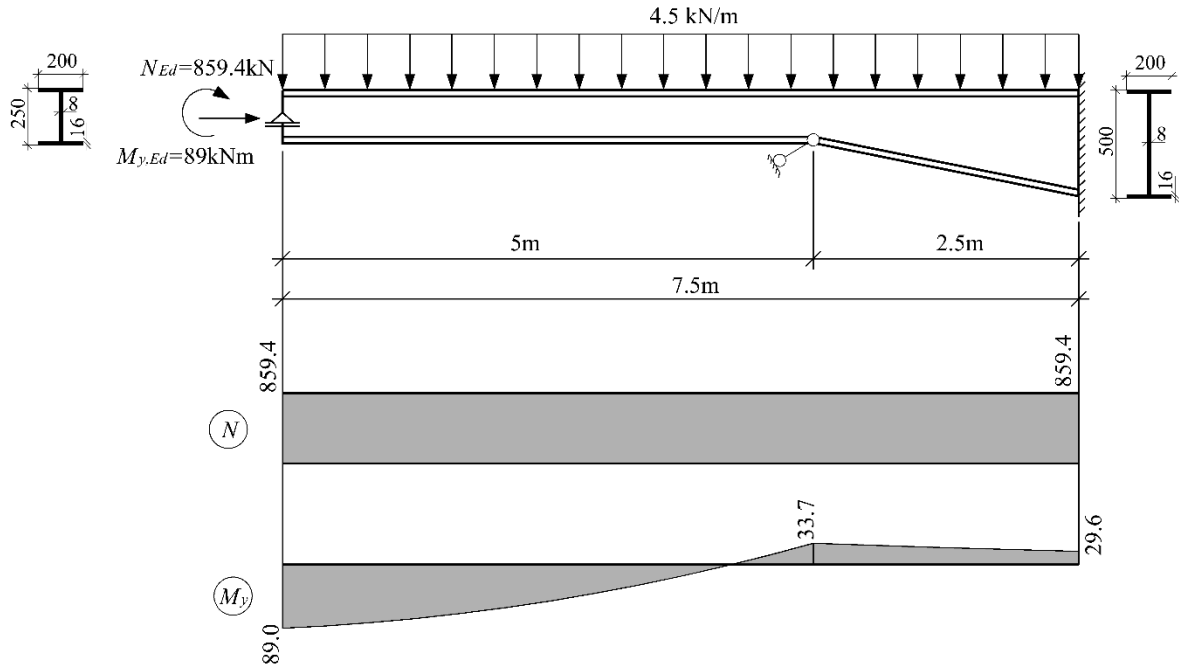
Figure 6.38 – Design example: geometry and first-order internal forces
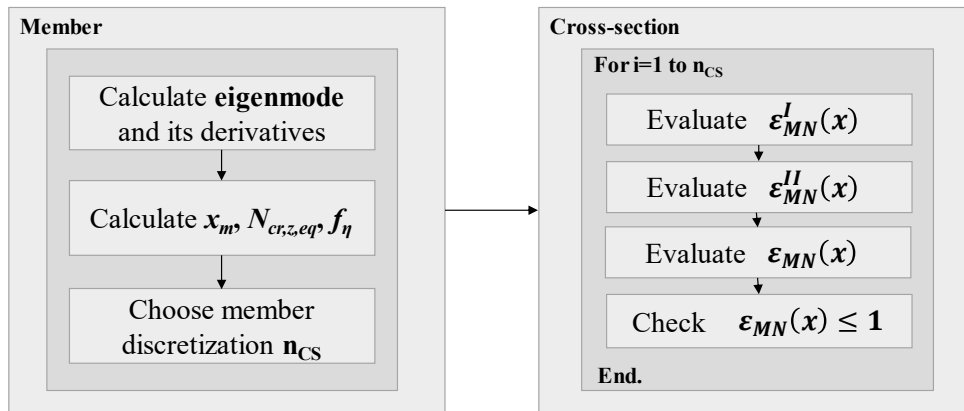
Figure 6.39 - Application of the method

In this case, the critical load factor corresponding to the applied forces is:

$$\alpha_{cr} = 2.24 \geq 1.0 \tag{6.79}$$

The mode shapes are shown in *Figure 6.40* for the lateral displacement $v_{cr}(x)$ and the twist rotation $\theta_{cr}(x)$. The discontinuity in the second derivative of the twist rotation is explained by the change of the cross-section and the torsional properties of the whole segment. The second derivatives, in this case, are obtained numerically using central finite differences, alternatively, they can be automatically supplied by the software.
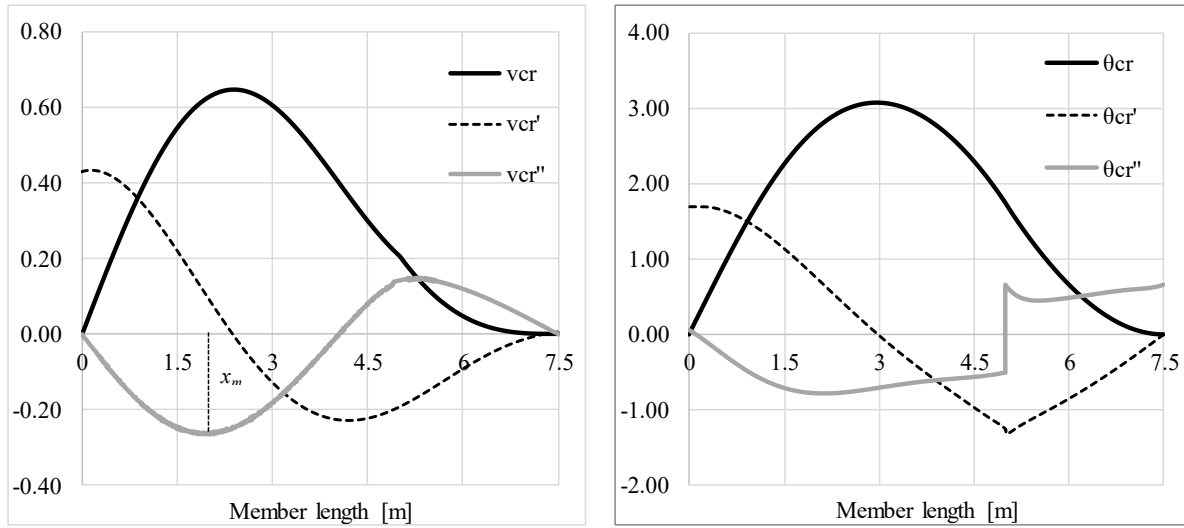
Figure 6.40 – Mode shapes

They are used to compute the location where maximum amplitude of the imperfection is taken and its magnitude from Eq. (6.72). The location x_m in this case is at 2.01m from the left beam end. Then the equivalent critical force $N_{cr,z,eq}$ is calculated from Eq.(6.61) :

$$N_{cr,z,eq} = \frac{EI_z(x_m)|v''_{cr}(x_m)|}{|v_{cr}(x_m)|} = \frac{210000 \times 10^3 \times 0.02134 \times 10^{-3} \times |-0.26|}{0.62} \tag{6.80}$$

$$N_{cr,z,eq} = 1876.6 kN$$

and the constant factor in Eq. (6.74) becomes:

$$f_\eta = \frac{N_{cr,z,eq}}{EI_z(x_m)(v''_{cr}(x_m) + h(x_m)/2\,\theta''(x_m) + \theta'(x_m)h'(x_m))} = \tag{6.81}$$

$$\frac{1876.6 kN}{210000 \times 10^3 \times 0.02134 \times 10^{-3}(0.26 + 0.125 \times 0.802 + 0.745 \times 0)} = 1.15$$

Finally, the utilization shall be verified at several locations along the member. For this, the member was divided into n_{CS}=15 parts 0.5 m each, as shown in *Figure 6.41*. The verification

of the utilization ratio is performed at each of the 16 cross-sections with the member geometry and loading corresponding to the respective location.
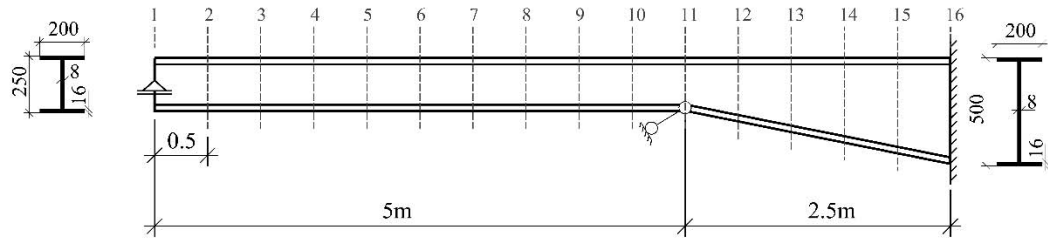
Figure 6.41 – Verification locations

The values corresponding to the eigenmode are given in *Table 6.12*.

Table 6.12 – Example: mode shape data

n_{CS}	x	h	h'	v_{cr}	v''	θcr	θ'cr	θ''cr	d(x)
-	m	mm	-	-	m^{-2}	m^{-1}	m^{-2}	m^{-3}	-
(1)	(2)	(3)	(4)	(5)	(6)	(7)	(8)	(9)	(10)
1	0.0	250	0.00	0.00	-0.001	0.00	1.68	0.00	0.00
2	0.5	250	0.00	0.22	-0.108	0.84	1.64	-0.26	0.32
3	1.0	250	0.00	0.41	-0.191	1.61	1.44	-0.55	0.61
4	1.5	250	0.00	0.55	-0.243	2.26	1.12	-0.73	0.83
5	**2.0**	**250**	**0.00**	**0.629**	**-0.263**	**2.73**	**0.75**	**-0.80**	**0.97**
6	2.5	250	0.00	0.65	-0.238	3.00	0.35	-0.80	1.02
7	3.0	250	0.00	0.60	-0.180	3.08	-0.02	-0.70	0.99
8	3.5	250	0.00	0.52	-0.100	2.98	-0.36	-0.68	0.89
9	4.0	250	0.00	0.41	-0.010	2.72	-0.68	-0.63	0.75
10	4.5	250	0.00	0.30	0.078	2.31	-0.97	-0.60	0.59
11	5.0	250	0.00	0.21	0.141	1.75	-1.26	0.00	0.42
12	5.5	300	0.10	0.11	0.140	1.15	-1.08	0.45	0.28
13	6.0	350	0.10	0.05	0.119	0.67	-0.85	0.48	0.16
14	6.5	400	0.10	0.01	0.084	0.31	-0.60	0.55	0.07
15	7.0	450	0.10	0.00	0.043	0.08	-0.31	0.60	0.02
16	7.5	500	0.00	0.00	-0.001	0.00	0.00	0.00	0.00

The required geometrical properties are given in *Table 6.13*.

The total utilization ration is calculated from Eq. (6.73), also given as:

$$\varepsilon_{MN}(x) = \varepsilon_{MN}^{I}(x) + \varepsilon_{MN}^{II}(x) \le 1.0 \tag{6.82}$$

In all expressions where there is a quantity (x) it means that it varies along the member.

| 215

The utilization due to first order forces $\varepsilon^I(x)$ is determined for each cross-section using the diagrams *Figure 6.38*:

$$\varepsilon^I_{MN}(x) = \frac{N_{Ed}(x)}{A(x)f_y} + \frac{M_{y,Ed}(x)}{W_y(x)f_y} \tag{6.83}$$

The obtained results are given by column (7) in *Table 6.14.*

The second order utilization is calculated in column (8) of *Table 6.14* by using the following expression:

$$\varepsilon^{II}(x) = \frac{EI_z(x)\left(v''_{cr}(x) + \frac{h(x)}{2}\theta''_{cr}(x) + \theta'_{cr}(x)h'(x)\right)}{A(x)f_y(\alpha_{cr}-1)}\eta(x) \tag{6.84}$$

The generalized imperfection calculated according to Eq. (6.72):

$$\eta(x) = \alpha(x)\left(\bar{\lambda}(x) - 0.2\right)\delta(x)f_\eta = 1.15\alpha(x)\left(\bar{\lambda}(x) - 0.2\right)\delta(x) \tag{6.85}$$

Table 6.13 – Example: cross-section properties

n_{CS}	x	A	$W_{y,pl}$	$W_{y,el}$	$W_{z,el}$	I_z	N_{Rd}	$M_{y,Rd}$
-	m	mm^2x10^2	mm^3x10^3	mm^3x10^3	mm^3x10^3	mm^4x10^4	kN	kNm
(1)	(2)	(3)	(4)	(5)	(6)	(7)	(8)	(9)
1	0.0	81.440	843.8	757.2	213.43	2134.3	1913.8	198.3
2	0.5	81.440	843.8	757.2	213.43	2134.3	1913.8	198.3
3	1.0	81.440	843.8	757.2	213.43	2134.3	1913.8	198.3
4	1.5	81.440	843.8	757.2	213.43	2134.3	1913.8	198.3
5	**2.0**	**81.440**	**843.8**	**757.2**	**213.43**	**2134.3**	**1913.8**	**198.3**
6	2.5	81.440	843.8	757.2	213.43	2134.3	1913.8	198.3
7	3.0	81.440	843.8	757.2	213.43	2134.3	1913.8	198.3
8	3.5	81.440	843.8	757.2	213.43	2134.3	1913.8	198.3
9	4.0	81.440	843.8	757.2	213.43	2134.3	1913.8	198.3
10	4.5	81.440	843.8	757.2	213.43	2134.3	1913.8	198.3
11	5.0	81.440	843.8	757.2	213.43	2134.3	1913.8	198.3
12	5.5	85.440	1052.4	946.8	213.45	2134.5	2007.8	247.3
13	6.0	89.440	1271.0	1143.2	213.47	2134.7	2101.8	298.7
14	6.5	93.440	1499.6	1346.5	213.49	2134.9	2195.8	352.4
15	7.0	97.440	1738.2	1556.4	213.51	2135.1	2289.8	408.5
16	7.5	101.440	1986.8	1773.1	213.53	2135.3	2383.8	466.9

with the mode shape at the compression flange (see column (10) of *Table 6.12*):

$$\delta^{fl}(x) = v_{cr}(x) + \frac{h(x)}{2}\theta_{cr}(x) \tag{6.86}$$

and the imperfection factor $\alpha(x)$ calculated as an interpolated value from Eq. (6.12):

$$\alpha(x) = \alpha_{LT}(x)\left(1 - \frac{\phi}{2}\right) + \alpha_z \frac{\phi}{2} \tag{6.87}$$

with imperfection factor $\alpha_z = 0.49$ according to *Table 2.2* for welded prismatic columns, and α_{LT} for welded prismatic beams from *Table 2.6*:

$$\alpha_{LT}(x) = 0.21\sqrt{\frac{W_{el,y}(x)}{W_{el,z}(x)}} \le 0.64 \tag{6.88}$$

The ratio of the applied loads ϕ is taken at the most loaded cross-section with first order forces (in this case section 1):

$$\phi = \frac{M_{y,pl}/M_{y,Ed}}{N_{pl}/N_{Ed}} = \frac{198.3/89}{1913.8/859.4} = \frac{2.228}{2.228} = 1.0 \tag{6.89}$$

Then Eq. (6.87) becomes:

$$\alpha(x) = 0.5\alpha_{LT}(x) + 0.49 \times 0.5 = 0.5\alpha_{LT}(x) + 0.245 \tag{6.90}$$

The variation of the imperfection factor is given in column (3) of *Table 6.14*.

Table 6.14 – Example: verification

n_{CS}	x	α	$\bar{\lambda}$	$M_{y,Ed}$	N_{Ed}	$\varepsilon^{I}{}_{MN}$	$\varepsilon^{II}{}_{MN}$	ε_{MN}
-	m	-	-	kNm	kN	-	-	-
(1)	(2)	(3)	(4)	(5)	(6)	(7)	(8)	(9)
1	0.0	0.443	1.01	89.0	859.4	0.90	0.00	0.90
2	0.5	0.443	1.01	81.7	859.4	0.86	0.03	0.89
3	1.0	0.443	1.01	73.3	859.4	0.82	0.12	0.93
4	1.5	0.443	1.01	63.8	859.4	0.77	0.20	0.975
5	**2.0**	**0.443**	**1.01**	**53.1**	**859.4**	**0.72**	**0.26**	**0.977**
6	2.5	0.443	1.01	41.3	859.4	0.66	0.25	0.91
7	3.0	0.443	1.01	28.4	859.4	0.59	0.20	0.79
8	3.5	0.443	1.01	14.3	859.4	0.52	0.12	0.64
9	4.0	0.443	1.01	0.8	859.4	0.45	0.05	0.50
10	4.5	0.443	1.01	17.1	859.4	0.54	0.07	0.60
11	5.0	0.443	1.01	34.5	859.4	0.62	0.04	0.67
12	5.5	0.466	1.03	33.7	859.4	0.56	0.04	0.60
13	6.0	0.488	1.06	32.9	859.4	0.52	0.01	0.53
14	6.5	0.509	1.08	32.0	859.4	0.48	0.01	0.49
15	7.0	0.528	1.10	31.2	859.4	0.45	0.00	0.45
16	7.5	0.548	1.13	30.4	859.4	0.43	0.00	0.43

The obtained utilization ratio along the member is plotted in *Figure 6.42*. It reaches a maximum at the 2 m and the maximum utilization is 0.977. The actual maximum utilization, where $\varepsilon_{MN}(x) = 1.0$, is found at 1.82 m.

In this example, the loading was chosen so that it corresponds to the member resistance; however, the verification is valid for lower loads as well.
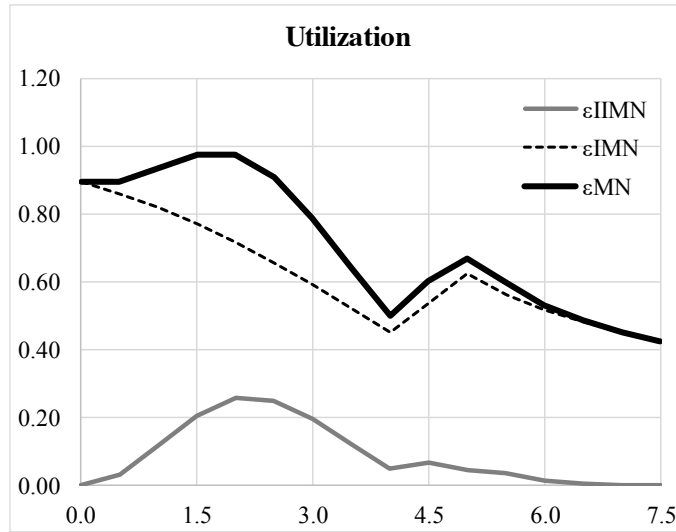
Figure 6.42 - Utilization ratio

Furthermore, this verification is compared to GMNIA result. The geometrical imperfection was considered with an equivalent length of 5 m corresponding to the inflexion point of the deformation of the compression flange (see *Figure 6.43*). This leads to 5.8% higher resistance than the one obtained with the general formulation.
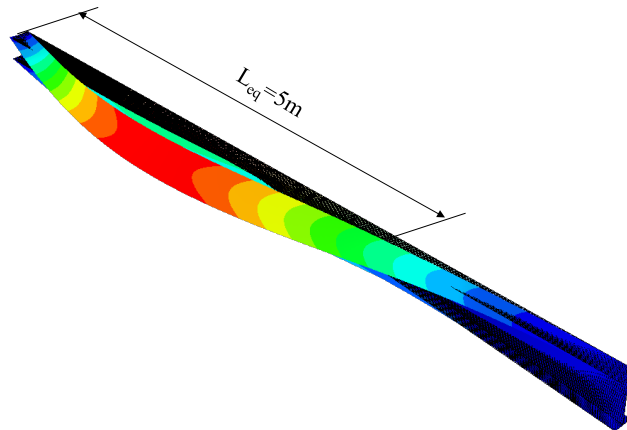
Figure 6.43 – Eigenmode for the applied loading

For comparison, the General Method is also applied. According to Eurocode 3, as summarized in Section 2.3.4. The critical load multiplier for the applied loads is given in Eq. (6.79). The ultimate load multiplier was obtained from in-plane GMNIA as:

$$\alpha_{ult,k} = 1.224 \tag{6.91}$$

Hence, the normalized slenderness becomes:

$$\bar{\lambda}_{op} = \sqrt{\frac{\alpha_{ult,k}}{\alpha_{cr,op}}} = \sqrt{\frac{1.224}{2.24}} = 0.739 \tag{6.92}$$

The buckling curve for minor axis flexural buckling of welded prismatic columns and lateral-torsional buckling of prismatic beams (General Case) of the prismatic part is curve c, which gives an imperfection factor α=0.49:

$$\phi_{op} = 0.5\left(1 + \alpha(\bar{\lambda}_{op} - 0.2) + \bar{\lambda}_{op}^2\right) = 0.5(1 + 0.49(0.739 - 0.2) + 0.739^2)$$
$$= 0.902 \tag{6.93}$$

The reduction factor is calculated from:

$$\chi_{op} = \frac{1}{\phi_{op} + \sqrt{\phi_{op}^2 - \bar{\lambda}_{op}^2}} = \frac{1}{0.902 + \sqrt{0.902^2 - 0.739^2}} = 0.702 \tag{6.94}$$

Finally, the verification is performed:

$$\frac{\chi_{op}\alpha_{ult,k}}{\gamma_{M1}} = \frac{0.702 \times 1.224}{1.0} = 0.86 \nleq 1.0 \tag{6.95}$$

The verification according to the General Method is not satisfied and therefore a larger cross-section should be used to resist the applied force.

6.10 Summary

In this chapter, a general formulation for the stability design of steel columns, beams and beam-columns with variable geometry, loads and supports was presented. The approach uses the buckling mode as shape of the initial imperfection and amplitude previously calibrated for the standard prismatic simply-supported columns and beams according to *Eurocode 3*.

The method was presented in its general form in a universal format covering any buckling mode. The various buckling modes are discussed separately, highlighting specific aspects of the member behaviour.

It was demonstrated that the general approach is more flexible in comparison to a procedure that relies on unavoidable calibration for each possible effect that might cause difference form the uniform member, as non-uniform members, non-standard loading cases, or irregular distribution of restraints, etc.

The method was thoroughly validated by comparison with a large number of advanced numerical simulations, yielding very good results with low scatter. Additionally, for standard prismatic members, its accuracy was similar to the results obtained with the code prescriptions of clauses 6.3.1, 6.3.2 and 6.3.3 of EC3-1-1.

7 CONCLUSIONS AND FUTURE RESEARCH

7.1 Conclusions

The goal of this thesis was to contribute towards safer yet economic stability design rules, which are general, but mechanically consistent. The goal was pursued by: i) data collection for basic variables relevant to the stability design in order to provide realistic estimations for their distributions; ii) safety assessment of the existing stability design rules to ensure that the existing imperfection factors correspond to the target reliability in the Eurocodes; and iii) the development of a general formulation for stability design of columns, beams and beam-columns.

Relatively to the first objective, the **data collection for basic variables relevant to stability design rules,** it was carried out in the scope of the European project SAFEBRICTILE. Data for material properties of steel were collected from: i) steel profiles and plates in different steel grades fabricated in 2013 and 2014; coupon tests performed at universities around Europe; iii) from the literature (collection in *Simões da Silva et al.,* 2009) and data collected within the framework of the *European project OPUS*). Concerning the geometrical properties, data collection for geometrical properties of steel H and I profiles, according to the specifications of EN 10034:1993, was performed among several steel producers in Europe: *ArcelorMittal, Dillinger, Salzgitter, Stahlwerk-Thueringen, TataSteel* and also among the partners of the SAFEBRICTILE project. This collection allowed for the recommendation of normalized distributions about the material and geometrical properties of rolled steel profiles. These

recommendations were considered in the final draft of prEN 1993-1-1 (CEN/TC250, 2017) for calibration of partial factors in its Annex E.

Furthermore, the data collection was extended to the member imperfections as a part of the experiments carried out on web-tapered members. The collection provided valuable information for the distributions of the imperfections for welded sections. The collected data for member imperfections was combined with the results from the experiments: out-of-straightness and residual stresses. It was shown that despite the high variation, the mean values of the member imperfections were lower than those assumed in the calibration of the buckling curves (*Strating & Vos*, 1973; *Beer & Schulz*, 1970), in line with the values assumed in the AISC standard, which allows for further studies in this field and improvement of the accuracy of the Eurocode 3-1-1 design rules.

Moreover, as a part of the second objective, **safety assessment of the European stability design rules on members in compression**, **bending and combination of bending and compression**. The results obtained led to the following main conclusions: the partial factor γ_{M1} for buckling resistance of columns, beams and beam-columns may be kept as $\gamma_{M1}=1.0$ for the current mix of steels that are sold in Europe (i.e., that match the standard characterization for the tensile properties of steel, cross-section geometry and Young's modulus that are included in Annex E of EN 1993-1-1 (2017) and result from the SAFEBRICTILE project), provided that the yield stress of steel is taken from product standards (EN 10025-2:2004) and into account the modified specification of buckling curves in prEN1993-1-1(2017). Additionally, the following conclusions are also highlighted:

- Influence of the adopted minimum yield stress using EN 10025 or Table 3.1 of Eurocode 3: the level of the minimum yield stress was assessed for both minor and major axis of flexural buckling of hot-rolled columns. It was shown that in both cases the values proposed in EC3 can reach up to 10% non-conservative in certain cases. These conclusions are considered applicable for beams and beam-columns.
- Imperfection factor for flexural-buckling of columns about minor axis which are made of steel grade S460: it was shown that the imperfection factor currently prescribed for flexural buckling of steel columns made of S460 about the minor axis is not adequate. This change is already taken into consideration in the final draft of the new version Eurocode 3.

- For beams, the results highlight a strong sensitivity of γ_{M1}^* to the subsets that are considered in the calculation. This trend is also confirmed by comparing these results with the corresponding results from *Rebelo et al.* (2009) and *Simões da Silva et al.* (2009). This difference led to the consideration of a lower tail approximation that significantly improved the homogeneity of results.

- Regarding the different design methods for LTB considered, the conservative nature of the General Case was confirmed, the Special Case systematically led to higher values of γ_{M1}^* for the majority of subsets and the accuracy of the New EC3 method was confirmed. Concerning this method, an adjustment of the imperfection factors is proposed for cross-sections with h/b >1.2 and flange thickness higher than 40 mm, because this geometric range was not considered in the original derivation of the imperfection factors. This change is already implemented in the final draft of prEN 1993-1-1;

- Regarding beam-columns, the results for the different buckling modes, with and without, lateral-torsional buckling were found very similar, showing that the interaction coefficients are calibrated with sufficient accuracy for both cases.

- The results highlight lower γ_{M1}^* - values than the ones calculated for columns and beams separately and thus indicating that the interaction factors are provide enhanced safety;

Finally, **a general formulation for the buckling resistance of single members built-up or not, uniform or not, with complex support conditions or not was developed** in line with the third objective. It relies on the consistent identification of the second order contributions in accordance with the applied loading, amplified by the imperfection according to the critical buckling mode. The verification is implemented as a sequence of cross-section verifications along the member length.

This general formulation is easily implemented as an additional cross-sectional verification or has a hand calculation procedure, provided the user can obtain the shape of the buckling mode and its derivatives. This is of enormous practical interest for the design of steel structures as it eliminates one of the major barriers in the stability verification of steel structures, as it greatly simplifies the implementation in structural design software.

The method was thoroughly validated by comparison with a large number of advanced numerical simulations, yielding very good results with low scatter. Additionally, for standard

prismatic members, its accuracy was similar to the results obtained with the code prescriptions of clauses 6.3.1, 6.3.2 and 6.3.3 of EC3-1-1.

7.2 Future research

The work carried out in the scope of this thesis has its limitations. In the following paragraph, the aspects which are considered worth exploring in the future are summarized:

- **Reliability assessment of the stability design rules for welded sections.** The reliability assessment of the stability design rules in Chapter 5 was carried out for hot-rolled sections; it is important extending it to welded sections since these are frequently used in steel design practice and it is important to ensure that they retain the same level of safety.

- **The data collection** on material and geometrical properties and imperfections shall be continued in order to provide a solid base for future assessments and calibration of new design rules. This can be easily achieved by maintaining the European database of steel properties developed in the scope of SAFEBRICTILE.

- **Imperfection factors for members in HSS.** Nowadays, the use of high strength steels is continuously increasing. This requires the adjustment the stability design rules in order to incorporate the specific aspects related to the use of HSS, such as for example, more favourable residual stress distributions, enhanced material properties, different plastic behaviour, etc.

- **Plasticity effects at low slenderness.** In the development of the general formulation it was noted that it requires an adjustment to account for plasticity effects in the low slenderness. Their incorporation shall be achieved in a transparent way so that it can be applied to various types of members, loading and support conditions.

- **Extend the scope of the validation**. The general formulation was validated for I-sections and various types of members, loading and supports. This validation should be extended to different types of cross-sections, slender cross-sections and bi-axial bending.

7.3 Publications

The research carried out in the scope of this thesis has resulted in the following publications by the time of its submission.

7.3.1 Publications in international journals (ISI)

− Tankova T., Simões da Silva L., Marques L., Rebelo C., Taras A., (2014). *Towards a standardized procedure for the safety assessment of stability design rules*, In: Journal of Constructional Steel Research, 103, pp. 290-302.
http://dx.doi.org/10.1016/j.jcsr.2014.09.010

− Simões da Silva L., Tankova T., Marques L, Rebelo C., (2016). *Safety assessment of Eurocode 3 stability design rules for the flexural buckling of columns*, In: Advanced Steel Construction – an International Journal, 12(3), pp. 328-358.
http://dx.doi.org/10.18057/IJASC.2016.12.3.7

− Tankova T., Marques L., Simões da Silva L., Andrade A., (2017). *A consistent methodology for the out-of-plane buckling resistance of prismatic beam-columns*, In: Journal of Constructional Steel Research, 128, pp. 839-852.
http://dx.doi.org/10.1016/j.jcsr.2016.10.009

− Tankova T., Martins J. P., Simões da Silva L., Simões R., Craveiro H., (2018). *Experimental Buckling Behaviour of Web Tapered I-Section Steel Columns*. In: Journal of Constructional Steel Research, 147, pp. 293-312.
https://doi.org/10.1016/j.jcsr.2018.04.015

− Tankova T., Martins J. P., Simões da Silva L., Marques L., Craveiro H., Santiago A. *Experimental Lateral-Torsional Buckling Behaviour of Web Tapered I-Section Steel Beams*, In: Engineering Structures, 168, pp. 355-370
https://doi.org/10.1016/j.engstruct.2018.04.084

- Simões da Silva L., Tankova T., Marques L., Rebelo C., Taras A. (2019). *Safety assessment of Eurocode 3 stability design rules for the lateral-torsional buckling of beams,* In: Advanced Steel Construction – an International Journal, 15(1).

- Tankova T., Simões da Silva L., Marques L. Stability verification of non-uniform steel members based on stress utilization: a general approach, Submitted to Journal of Constructional Steel Research 19 April 2018.

7.3.2 Other journals

- Simões da Silva L., Tankova T., Marques L., (2016). *On the safety of European stability design rules for steel members*, In: Structures, Invited paper for Special Edition dedicated to ICASS 2015, 8, 157-169.
http://dx.doi.org/10.1016/j.istruc.2016.07.004

- Tankova T., Marques L., Simões da Silva L., (2016). *Método geral para a verificação da estabilidade de elementos estruturais metálicos*, In: Revista da Estrutura de Aço, Centro Brasileiro da Construção em Aço, 5(3), pp 162-179.

7.3.3 Publications in international conference proceedings

- Tankova T., Marques L., Taras A., Simões da Silva L., Rebelo C., (2014). *Development of a simplified probabilistic methodology for safety assessment of stability of steel structures*, Eurosteel 2014, 7th European Conference on Steel and Composite Structures, Naples, Italy, September, 10-12.

- Tankova T., Simões da Silva L., Marques L., Andrade A. (2015), *Proposal of an Ayrton-Perry design methodology for the verification of flexural and lateral-torsional buckling of prismatic beam-columns,* In: Proc. Eight International Conference on Advances in Steel Structures, Lisbon, Portugal, July 22-24.

- Simões da Silva L., Marques L., Tankova T. (2015), *On the safety of stability design rules for steel members*, In: Proc. Eight International Conference on Advances in Steel Structures, Lisbon, Portugal, July 22-24 (2015) (keynote paper)

– Rodrigues J., Tankova, T., Marques, L., Martins, J., P., Simões da Silva, L, (2015). *Avaliação experimental do comportamento de elementos metálicos de secção variável*., X Congresso de Construção Metálica e Mista, Coimbra, Portugal, Novembro 2015

– Tankova T., Marques L., Simões da Silva, *Development of a new methodology for the stability design of steel members*, X Congresso de Construção Metálica e Mista, Coimbra, Portugal, November 2015

– Tankova, T., Rodrigues, J., Marques, L., Martins, J., P., Simões da Silva, L.(2016*), Experimental study on the buckling behaviour of tapered structural members*, Proc. The International Colloquium on Stability and Ductility of Steel Structures, Timisoara, Romania, May 30 – June 1 (2016), pp. 565-572

– Tankova, T., Marques, L., Simões da Silva, (2016). *Towards a general methodology for the stability design of steel members*, Proc. International Conference on Steel and Aluminium Structures, Hong Kong, China, 7-9 December (2016)

– Tankova, T., Martins, J.P, Simões da Silva L., Marques L., *"Numerical model for the buckling behavior of tapered steel members based on experimental tests",* In: Special Issue: Proceedings of Eurosteel 2017, 1, Issue 2-3, September 2017, pp. 1106-1115 http://dx.doi.org/10.1002/cepa.151

– Luís Simões da Silva, Trayana Tankova, Liliana Marques, Ulrike Kuhlmann, Andreas Kleiner, Jennifer Spiegler, H.H. Snijder, Rianne Dekker, Andreas Taras, Nicoleta Popa. (2017). *"Safety Assessment across Modes Driven by Plasticity, Stability and Fracture*", In: Special Issue: Proceedings of Eurosteel 2017, 1, Issue 2-3, September 2017, pp.3689-3698 http://dx.doi.org/10.1002/cepa.425

– Tankova, T., Simões da Silva, Marques, L., *Ayrton-Perry formulation for the buckling resistance of prismatic beam-columns*, In: Special Issue: XI Conference on Steel and Composite Construction, 1, Issue 4, December 2017, pp. 415-425 https://doi.org/10.1002/cepa.541

228 |

REFERENCES

Abambres M., Quach W.M. (2016). *Residual stresses in steel members: A review of available analytical expressions,* In: International Journal of Structural Integrity, 7, pp.70-94.

Abaqus (2012). v.6.12, Dassault Systems/Simulia, Providence, RI, USA.

Aguero A., Pallarés F.J., Pallarés L. (2015a). *Equivalent geometric imperfection definition in steel structures sensitive to flexural and/or torsional buckling due to compression*, In: Engineering Structures, 96, pp. 160-177.

Aguero A., Pallarés F.J., Pallarés L. (2015b). *Equivalent geometric imperfection definition in steel structures sensitive to lateral-torsional buckling due to bending moment*", In: Engineering Structures, 96, pp. 41-55.

AISC (2010), American Institute of Steel Construction, *Specification for Structural Steel Buildings, Chicago*, Illinois, USA.

Andrade A., Camotim D., Dinis P.B. (2007). *Lateral Torsional-Buckling of Singly Symmetric Web-Tapered Thin-Walled I-Beams*. In: Computers & Structures, 85, n. 17-18, pp. 1343-1359.

Andrade A., Providência P. and Camotim D. (2006). *Buckling formulae for doubly symmetric web-tapered I-section cantilevers acted by a tip load*, In: Proceedings of International Colloquium on Stability and Ductility of Steel Structures (SDSS 06 − Lisboa, 6-8/9), D. Camotim, N. Silvestre e P.B. Dinis (eds.), IST Press, pp. 323-330 (1).

Andrade A. (2012). *One Dimensional Models for the Spatial Behaviour of Tapered Thin-Walled Bars with Open Cross-Sections: Static, Dynamic and Buckling Analyses*. PhD thesis, University of Coimbra.

Anwar G. (2015). *Assessment and validation of an Ayrton-Perry design methodology for the verication of flexural and lateral-torsional buckling of prismatic beam-columns*. MSc thesis. University of Coimbra, 2015.

Avent R.R., Wells S. (1982). *Experimental study of thin-web welded H columns,* In: Journal of the structural division, 108, ST7, pp. 1464-1480.

Australian: Standards (1998). *AS4100-1998, Steel Structures*.

Ayrton W.E., Perry J. (1886). *On Struts.* The Engineer.

Badari B., Papp F. (2015) "*On design method of lateral-torsional buckling of beams: State of the art and a new proposal for a general type of design method*" In: Periodica Polytechnica Civil Engineering, 59, pp. 179-192.

Ban H., Shi G., Bai Y., Shi Y., Wang Y. (2013). *Residual stress of 460MPa High Strength Steel Welded I section Experimental Investigation and Modelling,* In: International Journal of Steel Structures, 13, pp. 691-705.

Baptista A.M., Muzeau J.P. (1998). *Design of Tapered Compression Members according to Eurocode 3*, In: Journal of Constructional Steel Research, 46, pp. 146-148.

Beg D., Hladnik L. (1994). *Eigenspannungen bei geschweisseten I-Profilen aus hochfesten Stählen*, In: Stahlbau, 63 (5).

Beg D., Hladnik L. (1996). *Slenderness Limit of Class 3 I Cross-section Mede of High Strength Steel*, In: Journal of Constructional Steel Research, 38, pp. 201-217.

Beer H., Schulz G. (1970). *Bases Théoriques des Courbes Européennes de Flambement*, In: Construction Métallique, no.3, pp. 37-57.

Bresler B., Lin T.Y., Scalzi J.B. (1968). *Design of Steel Structures*. 2nd ed. John Wiley and Sons, New York.

Boissonnade N., Greiner R., Jaspart J.P., Lindner J. (2006). *Rules for member stability in EN 1993-1-1, Background documentation and design guidelines*. In: ECCS (European Convention for Constructional Steelwork) Publication no. 119, Brussels, 2006.

Bradford M.A., Cuk P. (1988). *Elastic Buckling of Tapered Monosymmetric I-Beams*. In: Journal of Structural Engineering, 114, No. 5, pp. 977-996.

Bradford M.A. (1988a). *Lateral stability of tapered beam-column with elastic restraints*. In: The Structural Engineer, 66, No. 22, pp. 376-382.

Bradford M.A. (1988b). *Stability of Tapered I-Beams*. In: Journal of Constructional Steel Research, 9, pp. 195-216.

Braham M., Hanikenne D. (1993). *Lateral Buckling of Web Tapered Beams: an Original Design Method Confronted with a Computer Simulation*. In: Journal of Constructional Steel Research, 27, pp. 23-36.

British: British Standard Institution (1985). *Structural Use of Steelwork in Building. BS 5950 – Part I*, London, BSI.

Brown T. (1981)., *Lateral-Torsional Buckling of Tapered I-Beams*, In: Journal of Structural Division, ASCE, 107, Issue 4, pp. 689-697.

Butler D., Anderson G., (1963). *The Elastic Buckling of Tapered beam-columns*. In: Welding Research Supplement, pp. 29-36.

Butler D. (1966). *The Elastic Buckling Tests on Laterally and Torsionally Braced Tapered I – beams*. In: Welding Research Supplement, pp. 41-48.

Cajot L.G.; Haller M., Conan Y., Sedlacek G., Kraus O., Rondla J., Cerfontaine F., Johansson B., Lagerqvist O. (2005). *PROQUA – Probablistic quantification of safety of a steel structure highlighting the potential of steel versus other materials*, Final report. Technical Steel Research, contract No. 7210-PR/249.

CEN (1993). ENV 1993-1-1:1992, *Eurocode 3: Design of steel structures. General rules and rules for buildings* CEN, Brussels.

CEN (2002). EN 1990, *Eurocode – Basis of structural design*, CEN, Brussels

CEN (2004). European Committee for Standardization, EN 10025: 2004 – *Hot rolled products of structural steels*.

CEN (2004). EN 10025-2:2004. *Hot rolled products of structural steels - Part 2: Technical delivery conditions for non-alloy structural steels*. Brussels, European Committee for Standardisation.

CEN (2005). EN 1993-1-1, *Eurocode 3: Design of steel structures - Part 1-1: General rules and rules for buildings* CEN, Brussels.

CEN (2007). EN 15048-1:2007. *Non-preloaded structural bolting assemblies – Part1: General requirements*. Brussels, European Committee for Standardisation.

CEN (2009). EN1090:2009. *Execution of steel structures and aluminium structures - Part 1: Requirements for conformity assessment of structural components*, CEN, Brussels.

CEN (2011). EN 1090-2:2007+A1:2011. *Execution of steel structures and aluminium structures - Part 2: Technical requirements for steel structures*. Brussels, European Committee for Standardisation.

CEN/TC250 (2016). *Eurocode 3: Design of steel structures — Part 1-101: Design method for the stability of steel members under compression and bi-axial bending* – prCEN/TC 1993-1-101:2016.

CEN/TC250 (2017). *Eurocode 3: Design of steel structures - Part 1-1: General rules and rules for buildings*, CEN/TC 250/SC 3 N 2532 - prEN 1993-1-1 - Final draft.

Chabrolin B. CTICM, Labein, ProfilARBED, RWTH, SCI, TNO, SAES. (2002) ECSC Steel RTD Programme, *Partial safety factors for resistance of steel elements to EC3 and EC4 - Calibration for various steels products and failure criteria*. Final report. European Communities, EUR 20344 EN. 2002.

Chen W.F., Atsuta T. (1977). *Theory of Beam-Columns. Vol. 1: In-plane behaviour and design*. ISBN:0-07-010759-9. McGraw-Hill, Inc.

Chen,W.F., Atsuta, T. (1977). *Theory of Beam-Columns. Vol. 2: Space behaviour and design*. McGraw-Hill, Inc.

Chen W.F., Lui E.M. (1987). Structural Stability: Theory and implementation. Elsevier.

Chernenko D.E., Kennedy L.D.J. (1991). *An analysis of the performance of welded wide flange columns*, In: Canadian Journal of Civil Engineering, 18(4), pp. 537-555.

Chladny´ E, Stujberová M. (2013)," *Frames with unique global and local imperfection in the shape of the elastic buckling mode (part1)*", In: Stahlbau, 82.8, pp. 609–617.

Chladny´ E, Stujberová M. (2013)," *Frames with unique global and local imperfection in the shape of the elastic buckling mode (part2)*", In: Stahlbau, 82.9, pp. 684–694.

Clark J.W., Hill H.N. (1960). Lateral Buckling of Beams, In: Proceedings ASCE, Journal of the Structural Division, 68, ST7.

CSA (2009), Design of Steel Structures, CSA-S16-09, Canadian Standards Association (CSA), Toronto, Ontario, Canada.

CTCIM. LTBeamN. "*Lateral torsional buckling of beams software*". https://www.cticm.com/content/ltbeam-logiciel-calcul-moment-critique-deversement.

DNV (1995). *Guideline for Offshore Structural Reliability Analysis – Chapter 7*, DNV Report No. 95-2018, Det Norske Veritas, Hovik, Norway.

Dux P.F., Kitipornchai S. (1984). B*uckling approximations for inelastic beams*. In: Journal of Structural Engineering, ASCE, 110, pp. 559-74.

ECCS (1984). *Ultimate Limit State Calculation of Sway Frames with Rigid Joints*, Publication No.33 Brussels.

ECCS, Brussels. *Manual on Stability of Steel Structures*. 1976.

Engesser F. (1889). *Zeitschirift fur Architektur und Ingeniurwesen*.

Engesser F. (1895). *Ueber Knickfragen Schweizerische Bauzeitung,* XXVI, No.4 p. 24

Ermopoulos J.C. (1986), *Buckling of Tapered Bars under Stepped Axial Loads*, In: Journal of Structural Engineering, ASCE, 112(6), pp. 1346-1354

Ermopoulos J.C. (1997), *Equivalent Buckling Length of Non-Uniform Members*, In: Journal of Constructional Steel Research, 42(2), pp. 141-158

ESCS Steel RDT Programme, Research Project: Lateral-torsional buckling in Steel and Composite Beams, No. 7210-PR-183, testing of 4 Tapered Steel Beams. (2002)

Euler, L. (1744), "Methodus Inveniendi Lineas Curvas maximi minimive proprietate gaudentes", Lausanne and Geneva 1744.

Feldman M. (2018). *Private communication*. WG1 meeting. March 2018, Berlin.

Fukumoto Y., Itoh Y. (1981). *Statistical study of experiments on welded beams,* In: Journal of the structural division, 107, ST1, pp. 89-103.

Fukumoto Y., Itoh Y., Kubo M. (1980), *Strength Variation of Laterally Unsupported Beams*, In: Journal of the Structural Division, 106, pp. 165-181.

Galambos, T.V. (1968), *Structural Members and Frames*, Prentice-Hall, Upper Saddle River, N.J.

Galambos, T.V. (1998). *Guide to Stability Design Criteria for Metal Structures, Fifth Edition*". John Wiley & Sons Inc.

Galéa, Y. (1986). "Déversement des barres à section en I bissymétriques et hauteur d'âme bilinéairement variable". Construction Métallique.

Greiner R., Kaim P. (2003a). *Comparison of LT-buckling curves with test results*, Supplementary Report, ECCS TC8, No. 2003-10, May 2003

Greiner R., Kaim P. (2003b). *Comparison of LT-buckling curves with test results*, Supplementary Report, ECCS TC8, No. 2001-004, April 2001.

Greiner R., Kettler M., Lechner A., Jaspart J.P. Weynand K. Ziller, C., Örder, R. (2011). "SEMI-COMP+: *Valorisation Action of Plastic Member Capacity of Semi-Compact Steel Sections – a more Economic Design*", RFS2-CT-2010-00023, Background Documentation, Research Programme of the Research Fund for Coal and Steel – RTD.

Gulvanessian H., Calgaro J.A., Holicky M. (2002). *Designers' Guide to EN 1990. Eurocode: Basis of Design.* Thomas Telford Limited.

Gupta P., Wang S.T., Blandford G.E. (1996). *Lateral-Torsional Buckling of Non-prismatic I-Beams*. In: Journal of Structural Engineering, 122(7), pp. 748-755.

Hancock G.J., Trahair N.S. (1979). *Lateral buckling of roof purlins with diaphragm restraints*. Civil Engineering Transactions, Institution of Engineers, Australia, CE21, pp.10-5.

Hirt M.A., Crisinel. M. (2001). *Charpentes Métaliques – Conception et Dimensionnement des Halles et Bâtiments*, Traité de Génie Civil, 11, Press Polytechniques et Universitaires Romandes, Lausanne.

Hoglund T. (2014). *A unified method for the design of steel beam-columns*. In: Steel Construction, 7(4), pp. 230-245.

Horne M.R. (1954), *The Flexural–Torsional Buckling of Members of Symmetric I-Section Under Combined Thrust and Unequal Terminal Moments*, In: Q. J. Mech. Appl. Math., 7(4), pp. 410–426.

Horne M., Shakir-Khalil H., Akhtar S. (1979). "The Stability of Tapered and Haunched Beams". Proceedings of the Institution of Civil Engineers, 67(2), pp. 677-694.

ISO (2000). EN ISO 4017:2000. *Hexagon head screws. Product grades A and B*. International Organization for Standardization.

ISO (2000). EN ISO 4032:2000. *Hexagon nuts, style 1. Product grades A and B*. International Organization for Standardization.

ISO (2000). EN ISO 7089:2000. *Plain washers – Normal series – Product grade A*. International Organization for Standardization.

ISO (2009). ISO 6892-1:2009. *Metallic materials – Tensile testing – Part 1: Method of test at room temperature*. International Organization for Standardization.

ISO (2013). EN ISO 377:2013. *Steel and steel products - Location and preparation of samples and test pieces for mechanical testing*. International Organization for Standardization.

Janss J., Maquoi R., *Evaluation of test results on lateral torsional buckling in order to obtain strength function and suitable model factor*, Background report to Eurocode 3.

Kim Y.D. (2010). *Behaviour and Design of Metal Building Frames Using General Prismatix and Web-tapered Steel I section Members*., PhD thesis, Georgia Institute of Technology.

Kirby P.A., Nethercot D.A. (1979). *Design for Structural Stability*, Wiley, New York.

Kitipornchai S., Trahair N. (1972). "*Elastic Behaviour of Tapered Monosymmetric I-Beams*". Journal of Structural Division, ASCE, 101(8), pp. 1661-1678.

Kitipornchai S., Richter, N.J. (1978). *Elastic lateral-torsional buckling of beams with discrete restraints*, Civil Engineering Transactions, Institution of Civil Engineers, Australia, CE20, pp. 105-11.

Kitipornchai S., Trahair N.S. (1980). *Buckling Properties of Monosymmetric I-Beams*, *ASCE J. Struct. Div.*, 106(ST5), pp. 941–958.

Krefeld W., Butler D., Anderson, G. (1959). *Welded Cantilever Wedge Beams*. Welding Journal, 38 (3), pp. 97.

Kuhlmann U., Rasche C.S. (2017). *Next Generation of EUROCODE 3 – Evolution by Improvements and Harmonization*, In: Proc, XI Congresso de Construção Metálica e Mista, 23-24 November 2017, Coimbra Portugal.

Lee L.H.N. (1956). *Non-uniform Torsion of Tapered I-Beams*, In: Journal of the Franklin Institute, 262, p. 37.

Lee G.C., Szabo, B.A. (1967). *Torsional response of Tapered I-girders*, In: Journal of the Structural Division, ASCE, 93(ST5), pp. 233-252.

Lee G.C., Morrell M.L., Ketter R.L. (1972). *Design of Tapered Members*, In: Weld Res. Counc. Bull., 173, pp. 1-32.

Lei Z., Shu T.G. (2008). *Lateral buckling of web-tapered I-beams: A new theory*. In: Journal of Constructional Steel Research, 64 pp. 1379-1393.

Maquoi R., Rondal, J. (1978), *Mise en Équation des Nouvelles Courbes Européennes de Flambement*, Construction Métallique,.1, pp. 17-30.

Marques L. (2012a). *Tapered Steel Members: Flexural and Lateral-Torsional Buckling*, PhD Thesis, University of Coimbra.

Marques L., Taras A., Simões da Silva L. Greiner R., Rebelo, C. (2012b), *Development of a consistent design procedure for tapered columns*, In: Journal of Constructional Steel Research, 72, pp. 61-74.

Marques L., Simões da Silva L., Greiner R., Rebelo C., Taras, A. (2013). *Development of a consistent design procedure for lateral-torsional buckling of tapered beams*, In: Journal of Constructional Steel Research, 89, pp. 213–235.

Marques L., Simões da Silva L., Rebelo C., Santiago, A. (2014), *Extension of EC3-1-1 interaction formulae for the stability verification of tapered beam-columns*, In: Journal of Constructional Steel Research, 100, 122–135.

Massonnet C. (1947), *Buckling of Thin-Walled Bars with Open Cross Section*, Hommage Fac. Sci. Appl. Univ. Liege (Ed. G. Thone) (in French).

Michell A.G.M. (1899). *Elastic stability of long beams under transverse forces.* In: Philosophical magazine, 48, pp. 289-309.

Nethercot D.A, Trahair, N.S. (1976). *Lateral Buckling Approximations for Elastic Beams*, In: Struct. Eng., 54(6), pp. 197–204.

Naumes J. (2009). *Biegeknicken und Biegedrillknicken von Stäben und Stabsystemen auf einheitlicher Grundlage*, PhD thesis, RWTH Aachen, Germany.

Papp F. (2016). Buckling assessment of steel members through overall imperfection method. In: Engineering Structures, 106, pp.124-136.

Prandtl L. (1899). *Kipperscheinnungen*. Thesis. Munich.

Prawel S.P., Lee G.C. (1974). *Bending and Buckling Strength of Tapered Structural Members,* In: Welding Research Supplement. 1. 1974, pp. 75-84.

Raftoyiannis I.G., Ermopoulos J.C. (2005). *Stability of Tapered and Stepped Steel Columns with Initial Imperfections*, In: Engineering Structures, 27, pp. 1248-1257.

Rajasekaran S., (1993). *Instability of Tapered Thin-Walled Beams of Generic Section Part I: Theory*. In: Journal of Engineering Mechanics, 120(8), pp.1630-1640.

Rajasekaran S. (1993). *Equations for Tapered Thin-Walled Beams of Generic Open Section.Part II: Application*. In: Journal of Engineering Mechanics, 120, No.8, pp.1607-1629.

Rebelo C., Lopes N., Simões da Silva L., Nethercot D., Vila Real P.M.M. (2009). *Statistical Evaluation of the Lateral-Torsional Buckling Resistance of Steel I-beams, Part 1: Variability of the Eurocode 3 resistance model*, In: Journal of Constructional Steel Research., Elsevier, 2009, 65, pp. 818-831.

Robertson A. (1925). *The strength of struts*. In: ICE Selected Engineering Papers, ICE, London, Paper 28.

Rodgrigues J.R. (2016). *Caracterização Experimental de Elementos em Aço com Secção Variável*, MSc thesis. University of Coimbra, 2016

Ronagh H.R., Bradford M.A., Attard M.M. (2000). *Nonlinear analysis of thin-walled members with variable cross-section. Part I: Theory.*, In: Computers and Structures, 77, pp. 285-299.

Ronagh H.R., Bradford M.A., Attard M.M. (2000). *Nonlinear analysis of thin-walled members with variable cross-section. Part II: Application*, In: Computers and Structures, 77, pp. 301-313.

Saint-Venant B. (1855). *Memoite sur la torsion des prismes.* In: Memoires des Savants Etrangers, XIV, pp. 233-560.

Salter J.B., Anderson D., May I.M. (1980). *Tests on tapered steel columns*, In: The Structural Engineer, 58A, pp. 189-193.

Salvadori M.G. (1955). *Lateral Buckling of I-Beams*, In: Trans. ASCE, 120, p. 1165.

Salvadori M.G. (1956). *Lateral Buckling of Eccentrically Loaded I-Columns*, In: Trans. ASCE, 121, p. 1163.

Salzgeber G. (2000). *LT-buckling curves*, ECCS TC8, Report No. 2000-001, 20 March 2000.

Sfintesco D. (1970). *Fondement Expérimental des Coubres Européennes de Flambement*, Construction Métallique, no.3, pp. 5-12.

Shanley F.R. (1947). *Inelastic Column Theory*, In: J. Aeronaut. Sci., 14(5), p. 261.

Shiomi H., Kurata M. (1984). *Strength Formula for Tapered Beam-Columns.* In: J. Struct. Eng., 110, pp. 1630-1643.

Simões da Silva L., Rebelo C., Nethercot D., Marques L., Simões R., Vila Real P.M.M. (2009). *Statistical Evaluation of the Lateral-Torsional Buckling Resistance of Steel I-beams, Part 2: Variability of steel properties*, In: Journal of Constructional Steel Research, 65(4), pp. 832-849.

Simões da Silva L., Marques L., Rebelo C. (2010). *Numerical validation of the General Method in EC3-1-1 for prismatic members*, In: Journal of Constructional Steel Research, 66 (4), pp. 575-590.

Simões da Silva L., Simões R., Gervásio H., Couchman G. (2014). *Design of steel structures. Eurocode3: Design of steel structures. Part-1-1 - General rules and rules for buildings*. UK Edition ECCS - European Convention for Constructional Steelwork, John Wiley & Sons and SCI – Steel Construction Institute, 2014.

Simões da Silva L., Tankova T., Marques L., Rebelo C. (2016). *Safety assessment of EC3 stability design rules for flexural buckling of columns*, Advanced Steel Construction – an International Journal, 2016, 12(3), pp. 328-358.

Simões da Silva L., Marques L., Tankova T., Rebelo C., Kuhlmann U., Kleiner A., Spiegler J., Snijder H.H., Dekker R., Dehan V., Haremza C., Taras A., Cajot L.G., Vassart O., Popa N. (2017). *SAFEBRICTILE: Standardization of Safety Assessment Procedures across Brittle to Ductile Failure Modes*, 2017, RFSR-CT-2013-00023, Final Report.

Simões da Silva L., Tankova T., Marques L, Rebelo C., Taras A. (2019). *Safety assessment of Eurocode 3 stability design rules for the lateral-torsional buckling of beams,* In: Advanced Steel Construction – an International Journal, 15(1).

Snijder H.H., Hoenderkamp J.C.D. (2007). *Buckling curves for lateral torsional buckling of unrestrained beams*, Rene Maquoi 65th birthday anniversary, 2007, Liège Belguim.

Snijder H.H., Cajot L.G, Popa N., Spoorenberg R.C. (2014). *Buckling curves for heavy wide flange steel columns*. In: Romanian Journal of Technical Sciences, Applied Mechanics, 59(1/2), pp. 178-204.

Spoorenberg R.C., Snijder H.H., Hoenderkamp J.C.D. (2010). *Experimental investigation of residual stresses in roller bent wide flange steel sections,* In: Journal of Constructional Steel Research, 66, pp. 737-747.

Strating J., Vos H. (1973). *Simulation sur Ordinateur de la Coubre C.E.E.M de Flambement á l'aide de la Méthode de Monte-Carlo*, In: Construction Métallique, no.2, pp. 23-39

Subramanian L.P., Jeong W.Y., Yellepeddi R., White D.W., (2016). *Assessment of I-Section Member LTB Resistances Considering Experimental Tests and Practical Inelastic Buckling Solutions,* Structural Engineering, Mechanics and Materials Report No.110, School of Civil and Environmental Engineering, Georgia Institute of Technology, Atlanta, GA.

Subramanian L.P., White, D.W. (2017). *Resolving the Disconnect between Lateral Torsional Buckling Experimental Tests and Tests Simulations, and Design Strength Equations*, In: Journal of Constructional Steel Research, 128, pp. 321-334.

Szalai J., Papp F. (2010). *On the theoretical background of the generalization of Ayrton- Perry type resistance formulas*. In: Journal of Constructional Steel Research 66.5, pp. 670-679.

Szalai J. (2017). *Complete generalization of the Ayrton-Perry formula for beam-column buckling problems.* In: Engineering Structures, 153, pp. 205-223.

Szalai J., Papp F. (2017). *Reforming the "General method". Overall Stability Design Method OSDM – the Hungarian proposal.* ECCS TC8 – Stability, Document TC8-2017-10-009.

Tankova T., Simões da Silva L., Marques L., Rebelo C., Taras A. (2014). *Towards a standardized procedure for the safety assessment of stability design rules*, In: Journal of Constructional Steel Research, 103, pp. 290-302.

Tankova T., Marques L., Simões da Silva L., Andrade A. (2017). *Development of a consistent methodology for the out-of-plane buckling resistance of prismatic beam-columns,* In*:* Journal of Constructional Steel Research, 128, pp. 839-852.

Taras A., Greiner R. (2010). *New design curves for lateral–torsional buckling—Proposal based on a consistent derivation*. In: Journal of Constructional Steel Research, 66, pp. 648-663.

Taras A. (2010). *Contribution to the development of consistent stability design rules for steel members*" PhD Thesis, Technical University of Graz, Graz, Austria, 2010

Taras A., Dehan V., Simões da Silva L., Marques L., Tankova T. (2017). *Guideline for the Safety Assessment of Design Rules for Steel Structures in Line with EN 1990*, Deliverable D1.1, SAFEBRICTILE RFSR-CT-2013-00023.

Tebedge N., Alpsten G., Tall L. (1973). *Residual-stress measurement by the Sectioning Method*, In: Experimental Mechanics, pp. 88-96.

Timoshenko S.P. (1953). *Theory of bending, torsion and buckling of thin-walled members of open cross-section*. In: Collected Papers of Stephen P. Timoshenko, McGraw-Hill, New York, pp. 559-609.

Timoshenko S.P., Gere J.M. (1961). *Theory of Elastic Stability*, 2nd Edition, New York: McGraw-Hill.

Vlasov V.Z. (1961). *Thin-Walled Elastic Beams.* In: 2nd Edition, Israel Program for Scientific Translation, Jerusalem.

von Karman T. (1910). *Untersuchungen uber Knickfestigkeit. Forschungsarbeiten*, No. 81, Berlin.

Vrouwenvelder, A.C.W.M. (2002), *Developments towards full probabilistic design codes,* Structural Safety, 24, pp. 417- 432.

Yang Y.B., Yau, J.D. (1987). *Stability of Beams with Tapered I-Sections*. In: Journal of Structural Division, ASCE, 113, Issue 9, pp. 1337-1357.

Yang B., Nie S., Xiong G., Hu Y., Bai J., Zhang W., Dai G. (2016). *Residual stresses in welded I-shaped sections fabricated from Q460GJ structural steel plates*, In: Journal of Constructional Steel Research, 122, pp. 261-273.

Young B.W., Robinson K.W. (1975). *Buckling of axially loaded welded steel columns*, In: The Structural Engineer, 53, pp. 203-207.

Wagner H. (1936). *Verdrehung und Knickung von offenen Profilen (Torsion and buckling of open sections)*. NACA Technical Memorandum No. 807.

Wang Y.B., Li G. Q., Chen S.W. (2012). *Residual stresses in welded flame-cut high strength steel H-sections*, In: Journal of Constructional Steel Research, 79, pp. 101-114.

Ziemian R.D. (2010). *Guide to Stability Design Criteria for Metal Structures, Sixth Edition*. John Wiley & Sons Inc.

NOTATIONS

Lowercase Latin letters

a_0, a, b, c, d	Class indexes for buckling curves according to EC3-1-1
b	Cross-section width/ Retrogression coefficient
e_0	Maximum amplitude of a member imperfection
f_y	Yield stress
h	Cross-section height
h_{max}	Maximum cross section height
h_{min}	Minimum cross section height
$h_{xc}^{II}{}_{,lim}$	Cross-section height at $x_{c,lim}^{II}$
$k_{yy}, k_{zy}, k_{yz}, k_{zz}$	Interaction factors dependent of the phenomena of instability and plasticity involved
n	Number of cases
r_0	Polar radius of gyration
r_e	Experimental resistance
r_t	Theoretical resistance
t_f	Flange thickness
t_w	Web thickness

$v(x)$	Transverse displacement along z-axis
$v_0(x)$	Initial transverse displacement along z-axis
$v_{cr}(x)$	Transverse displacement component of the mode shape along z-axis
$w(x)$	Transverse displacement along y-axis
$w_0(x)$	Initial transverse displacement along y-axis
$w_{cr}(x)$	Transverse displacement component of the mode shape along y-axis
$x_{c,lim}^{II}$	Second order failure cross section for a high slenderness level
$x_{c,N}^{j}, x_{c,M}^{j}, x_{c,MN}^{j}$	Denomination of the failure cross section (to differentiate from the type of loading it refers to): N – do to axial force only; M – due to bending moment only; MN – due to the combined action of bending moment and axial force
x_c^{I}	First order failure cross section
x_c^{II}	Second order failure cross section
x_{min}	Location corresponding to the smallest cross section
x-x	Axis along the member
y-y	Cross-section axis parallel to the flanges
z-z	Cross-section axis perpendicular to the flanges

244 |

Uppercase Latin letters

A	Cross-section area
A_g	Gross cross-section area
A_{min}	Cross-section area of the smallest cross section in of a tapered member
C_b	Lateral-torsional buckling modification factor
C_m	Equivalent moment factor according to clause 6.3.3

C_{mS}	Equivalent moment factor
C_{ii}, C_{ji}	Plasticity factors according to clause 6.3.3
C_w	Warping constant
E	Modulus of elasticity
E_d	Design value of the actions
F_e	Elastic critical stress
F_y	Specified minimum yield stress
G	Shear modulus
I_t	Torsional moment
I_y	Moment of inertia y-axis
I_z	Moment of inertia z-axis
J	Torsional constant
L	Member length
L_b	Length between points that are either braced against lateral displacement of the compression flange or braced against twist of the cross section
L_p	Limiting length
L_r	Limiting length
M	Bending moment
$M_{b,Rd}$	Design buckling resistance moment
M_{cr}	Elastic critical moment
$M_{c,x}$	Factored buckling strength about x-x axis
$M_{c,y}$	Factored buckling strength about y-y axis
M_{Ed}	Design bending moment

M_n	Nominal flexural strength
M_p	Plastic bending moment
$M_{r,x}$	Maximum bending moment design value about x-x axis
$M_{r,x}$	Maximum bending moment design value about y-y axis
$M_{pl,y,Rd}$	Design value of the plastic resistance to bending moments about y-y axis
M_y	Bending moments, y-y axis
$M_{y,Ed}$	Design bending moment, y-y axis
$M_{pl,z,Rd}$	Design value of the plastic resistance to bending moments about z-z axis
M_z	Bending moments, z-z axis
$M_{z,Ed}$	Design bending moment, z-z axis
N	Normal force
N_{cr}	Elastic critical force
$N_{cr,x}$	Elastic critical force for torsional buckling
$N_{cr,y}$	Elastic critical force for in-plane buckling
$N_{cr,z}$	Elastic critical force for out-of-plane buckling
N_{Ed}	Design normal force
N_{pl}	Plastic resistance to normal force at a given cross section
$N_{pl,Rd}$	Design plastic resistance to normal forces of the gross cross section
P_c	Factored buckling strength
P_f	Probability of failure
P_n	Nominal buckling strength
P_r	Maximum axial design values acting on the member
R_d	Design value of the resistance

S_x Elastic section modulus about the x-axis

W_w Elastic warping modulus

$W_{y,el}$ Elastic section modulus y-y axis

$W_{y,pl}$ Plastic section modulus y-y axis

$W_{z,el}$ Elastic section modulus z-z axis

$W_{z,pl}$ Plastic section modulus z-z axis

Z_x Plastic section modulus about the x-axis

Uppercase Greek letters

Φ Cumulative distribution function (CDF) for the standard normal distribution

Lowercase Greek letters

α Angle of taper

α_E FORM (First Order Reliability Method) sensitivity factor for effects of actions

α_R FORM (First Order Reliability Method) sensitivity factor for resistance

α, α_{EC3} Imperfection factor according to EC3-1-1

$\alpha_b^{(Method)}$ Load multiplier which leads to the resistance for a given method

α_{cr} Load multiplier which leads to the elastic critical resistance

$\alpha_{cr,op}$ Minimum amplifier for the in-plane design loads to reach the elastic critical resistance with regard to lateral or lateral-torsional buckling

α_{pl}^{M} Load amplifier defined with respect to the plastic cross section bending Moment

α_{pl}^N	Load amplifier defined with respect to the plastic cross section axial force
$\alpha_{ult,k}$	Minimum load amplifier of the design loads to reach the characteristic resistance of the most critical cross section
β	Reliability index
γ_{M0}	Partial factor for resistance associated with cross-section checks
γ_{M1}	Partial factor for resistance of members to instability assessed by member checks
γ_F	Partial factor for actions, also accounting for model uncertainties and dimensional variations
γ_f	Partial factor for actions, which takes account of the possibility of unfavorable deviations of the action values from the representative values
γ_{Sd}	Partial factor associated with the uncertainty of the action and/or action effect model
γ_M	Partial safety factor for a material property also accounting for model uncertainties and model variations
γ_m	Partial factor for a material property
γ_{Rd}	Partial factor associated with the uncertainty of the resistance model;
δ_0	General displacement of the imperfect shape
δ_{cr}	General displacement of the critical mode
ε	Utilization ratio at a given cross section
ε_M^I	Utilization ratio regarding first order bending moment M
ε_M^{II}	Utilization ratio regarding the second order bending moment
ε_N	Utilization ratio regarding the axial force N
η	Generalized imperfection
η_{LT}	Generalized imperfection for lateral-torsional buckling

η_{tot}	Total generalized imperfection
η_y	Generalized imperfection for flexural buckling, y-y axis
η_z	Generalized imperfection for flexural buckling, z-z axis
$\bar{\lambda}_{op}$	Global non-dimensional slenderness of a structural component for out-of-plane buckling according to the general method of clause 6.3.4
$\bar{\lambda}$	Non-dimensional slenderness
$\bar{\lambda}(x)$	Non-dimensional slenderness at a given position
$\bar{\lambda}_{ip}$	Non-dimensional slenderness for in-plane flexural buckling
$\bar{\lambda}_y$	Non-dimensional slenderness for flexural buckling, y-y axis
$\bar{\lambda}_z$	Non-dimensional slenderness for flexural buckling, z-z axis
$\bar{\lambda}_{LT}$	Non-dimensional slenderness for lateral-torsional buckling
$\bar{\lambda}_{LT,0}$	Plateau length of the lateral torsional buckling curves for rolled sections
$\bar{\lambda}_0$	Plateau relative slenderness
φ	Over-strength factor
ϕ	Ratio between $\alpha_{pl}{}^M$ and $\alpha_{pl}{}^N$
ρ	Cross-section factor
σ	Standard deviation
$\theta(x)$	Twist rotation
$\theta_0(x)$	Initial twist rotation
$\theta_{cr}(x)$	Twist rotation component of the mode shape
χ	Reduction factor

χ_{LT}	Reduction factor due to lateral-torsional buckling
χ_{num}	Reduction factor (numerical)
χ_{op}	Reduction factor for the non-dimensional slenderness $\overline{\lambda}_{op}$
χ_y	Reduction factor due to flexural buckling, y-y axis
χ_z	Reduction factor due to flexural buckling, z-z axis
ψ	Ratio between the maximum and minimum bending moment, for a linear bending moment distribution

ACRONYMS AND ABBREVIATIONS

CoV   Coefficient of variation

FB   Flexural buckling

FB y-y   Flexural buckling about the major axis

FB z-z   Flexural buckling about the minor axis

FEM   Finite Element Method

FORM   First Order Reliability Method

FTB   Flexural-torsional buckling

GF   General formulation

GM   General Method

GMNIA   Geometrical and Material Non-linear Analysis with Imperfections

LBA   Linear Buckling Analysis

LTB   Lateral Torsional-Buckling

SORM   Second Order Reliability Method

TB   Torsional buckling

UDL   Uniformly distributed loading